

**Fuel Spray, Engine Deposit and Real Driving Emissions
Analysis of Heavy Duty Trucks Using Used Cooking Oil as a
Fuel**

Buland Ibraheem Azeez Dizayi

Submitted in accordance with the requirements for the degree of
PhD

The University of Leeds
Energy Research Institute
School of Chemical and Production Engineering

March, 2016

The candidate confirms that the work submitted is his own and that appropriate credit has been given where reference has been made to the work of others.

This copy has been supplied on the understanding that it is copyright material and that no quotation from the thesis may be published without proper acknowledgement.

Assertion of moral rights:

The right of Buland Ibraheem Azeez Dizayi to be identified as Author of this work has been asserted by <him/her> in accordance with the Copyright, Designs and Patents Act 1988.

© 2016 The University of Leeds and Buland Ibraheem Azeez Dizayi.

Acknowledgements

I would like to thank Dr. Hu Li for his invaluable counselling and knowledge transfer throughout the course of the research.

I also would like to thank the UK Department for Transport and Technology Strategy Board for supporting the research element within the project “Environmental and Performance Impact of Direct use of Used Cooking Oil in 44 tonne Trucks under Real World Driving Conditions” which is part of the Low Carbon Truck Demonstration Trial.” Thanks go to United Biscuits Midlands Distribution Centre for the provision of a truck and general support and collaboration in field tests. Thanks also go to Bioltec System GmbH for advice and permission to use some technical information and Convert2Green for the provision of C2G UBF for the tests.

Dedicated to

The memory of my father Ibraheem Azeez Dizayi.

My mother J. H. Shamdeen, my two brothers Dr Mand and Lawand Dizayi
and my wife Ronak.

Abstract

The current project represents the first attempt to test the environmental performance of the direct utilisation of purified used cooking oil as a fuel in a heavy goods vehicle under real world driving conditions. The properties of the used cooking oil were different from those of petroleum diesel (PD) standards however, its heat value, carbon footprint reduction potential and low cost were the key incentives driving its use as a fuel.

The current research was a collaborative project between Convert to Green (C2G), the fuel provider, the United Biscuits Midlands Distribution Centre, the heavy goods vehicle provider and the University of Leeds as the scientific consultant and research executor.

The brand of used cooking oil was Convert to Green Ultra-biofuel (C2G UBF) tested on a Mercedes-Benz EURO 5 emissions standard compliant 44 tonne articulate heavy goods vehicle (HGV). The HGV was modified for on-board UBF heating and mixing with PD. UBF was heated by heat recovery from the engine cooling system.

The results showed that the UBF/PD blending ratio was 0.845 as a journey average for the entire test series. However, the HGV was recorded to run on 100% UBF at steady high speed on the M1 motorway in the Midlands region of the UK. There were no discernible deficiencies in the HGV's performance or its traction effort. Nevertheless a slight increase in specific fuel consumption (SFC) was detected for the blended fuel. Engine durability, combustion chamber deposits and maintenance frequency were not affected by the UBF content in the fuel.

Although the engine technology was designed to suppress particulate matter (PM) within the combustion process, the use of blended UBF further reduced the tailpipe PM emissions compared to the use of PD. Carbon monoxide emissions decreased when using the blended fuel, while nitrogen oxides, total hydrocarbons and carbon dioxide increased compared to PD emissions.

The benefits of UBF utilisation as a fuel lie in the huge carbon savings and reduced PM emissions when compared to the use of PD as well as its use in providing a cost effective fuel supply and waste management technique.

Table of Contents

Acknowledgements	iii
Abstract	i
Table of Contents	iii
List of Tables	xi
List of Figures	xv
List of Acronyms	xxv
Chapter 1 Introduction	1
1.1 Factors affecting the fuel spray, combustion process and emissions	3
1.2 Pollution mitigation strategies.....	6
1.3 Motivation for research.....	8
1.4 Overall aims and objectives of the project.....	10
Chapter 2 Literature Survey	13
2.1 World energy demand and the need for renewable fuels in the transport sector	13
2.2 The fuel: used cooking oil (UCO)	14
2.2.1 The increasing interest in UCO for transportation	16
2.2.2 The life cycle assessment of UCO and the life cycle energy demand	17
2.3 General properties of UCO in comparison to petroleum diesel and biodiesels	20
2.3.1 Cetane number	21
2.3.2 Ignition delay (ID)	21
2.3.3 Fuel properties affecting the physical delay	23
Kinematic viscosity	23
Density	23
Surface tension	24
Fuel volatility	24
2.4 Diesel technology	25
2.5 The vehicle: heavy goods vehicle (HGV) and real world driving conditions (RWDC)	26
2.5.1 The capacity of HGVs and their usage in the UK and their contribution in pollution.....	26
2.5.2 Real world testing conditions.....	29

2.5.2.1	Vehicle specific power	31
2.5.2.2	Vehicle speed, acceleration and road gradient	32
2.6	The impact of renewable fuels on engine components and performance	33
2.6.1	The impact of renewable fuels on engine components	33
2.6.2	The impact of UCO on engine performance	35
2.6.3	The fuel injection system in CI engines	36
2.6.4	Fuel spray characteristics	38
2.6.4.1	Fuel jet penetration length	38
2.6.4.2	Fuel mean droplet size	39
2.6.4.3	Fuel spray cone angle	40
2.6.4.4	Fuel jet velocity	40
2.6.5	Deposit formation mechanisms in and around the injector nozzle	40
2.6.6	The impact of UCO on the fuel injection system and process	41
2.7	CI engines emissions and their control, and the impact of fuelling with UCO	43
2.7.1	Particulate matter (PM)	43
2.7.2	Particulate matter formation mechanisms	44
2.7.2.1	PM formation in the combustion chamber	45
2.7.2.2	PM formation in the exhaust pipe	47
2.7.3	Factors affecting PM formation and survival	48
2.7.3.1	The fuel	48
2.7.3.2	Combustion chamber environment	51
2.7.3.3	Engine operational conditions	53
2.7.3.4	Engine design and accessories	54
2.7.3.5	Fuel injection	56
2.7.4	The impact of UCO presence on PM emissions	60
2.7.5	PM emissions mitigation	61
2.7.5.1	In cylinder PM mitigation	61
2.7.5.2	Diesel particulate filter (DPF)	61
2.7.6	Primary gaseous emissions from CI engines	63
2.7.6.1	Carbon monoxide	63
2.7.6.2	Nitrogen oxides	64

2.7.6.3	Volatile organic compounds.....	66
2.7.6.4	The impact of UCO presence in the fuel on gaseous emissions.....	67
2.7.7	Gaseous emissions mitigation.....	69
2.7.7.1	In cylinder gaseous mitigation.....	69
2.7.7.2	Selective catalytic reduction (SCR) and urea injection.....	70
2.7.7.3	The impact of UCO on emissions after treatment facilities	71
2.8	Modifications needed for fuelling CI engines with UCO	74
2.8.1	Fuel tank and lines heating through heat recovery from the engine	74
2.8.2	Combustion chamber insulation and configuration.....	77
2.8.3	CI engine aspiration system enhancement	77
2.9	Novel strategies for emission mitigation	79
2.9.1	Novel fuel injection strategies.....	79
2.9.2	Novel combustion strategies	80
2.10	Conclusion	83

Chapter 3

	Experimental and Methodology	87
3.1	The test-vehicle and its technical specifications.....	90
3.2	Modifications to HGV for surrogate fuel adaptation.....	92
3.3	Real world test journey description	94
3.4	On-board apparatus layout and power supply.....	97
3.5	PM emissions collection and measurement	100
3.5.1	Cumulative PM _{2.5} collection and measurement by a single stage filtration unit.....	102
3.5.1.1	The apparatus and on-board test procedure description.....	102
3.5.1.2	Gravimetric and thermo-gravimetric analysis for PM _{2.5} samples	103
3.5.2	PM ₁₀ size distribution determination by Andersen impactor	105
3.5.2.1	Apparatus and on-board test procedure description.....	105
3.5.2.2	Gravimetric and thermo-gravimetric analysis	107

3.6	Characterisation and quantification of error sources in PM data	107
3.6.1	Systematic error	107
3.6.2	Random error	107
3.6.3	PM data processing and conversion for comparison purposes	108
3.7	Gaseous emissions measurements	110
3.7.1	NO _x measurement by zirconia solid electrolyte	111
3.7.1.1	Zirconia sensor description and apparatus layout	111
3.7.2	Exhaust gas speciation and measurement by FTIR spectroscopy	112
3.7.2.1	FTIR Apparatus and test procedure description	112
3.8	FTIR data validation	113
3.8.1	NO accuracy	113
3.8.2	THC accuracy	114
3.8.3	CO and CO ₂ accuracy	114
3.8.4	Data repeatability	114
3.8.5	FTIR data calculation and conversion for comparison purposes	115
3.9	HGV dynamics and road analysis	117
3.10	Heavy goods vehicle fuel consumption measurement	118
3.11	Apparatus time alignment.....	120
3.12	In vitro fuel analyses.....	120
3.12.1	C2G UBF sample preparation for analysis	121
3.12.2	Fuel density	121
3.12.3	Fuel viscosity.....	122
3.12.4	Fuel surface tension	123
3.12.5	Fuel CHNS analysis	124
3.12.6	Fuel GC-FID analysis	125
3.12.7	Inductively coupled plasma (ICP) spectroscopic technique for inorganic elements measurement.....	127
3.13	Fuel spray characteristics.....	129
3.14	Fuel injector inspection.....	130
3.14.1	Fuel injector collection plan	130

3.14.2 Fuel injector inspection by the scanning electron microscope (SEM) and energy dispersive x-ray (EDX)	131
---	-----

Chapter 4 The effects of C2G UBF on vehicle specific power and specific fuel consumption under real world driving conditions . 133

4.1 Fuel type, blending ratio and delivery control effects on engine performance	135
4.2 Vehicle specific power (VSP)	138
4.2.1 Vehicle specific power for the entire test series	138
4.2.2 The effect of fuel type on VSP in selected road sections throughout the HGV journey.....	139
4.2.2.1 Steady high speed HGV travel on M1 motorway...	139
4.2.2.2 High torque performance on the ramp to M1.....	140
4.3 Specific fuel consumption (SFC)	141
4.3.1 The effect of fuel type on specific fuel consumption for the entire journey	141
4.3.2 The effect of fuel type on specific fuel consumption for HGV travel under steady high speed conditions.	143
4.3.3 The effect of fuel type on specific fuel consumption for a HGV travel under high torque conditions.	144
4.4 Engine-out temperature	145
4.4.1 The effect of BL fuel on engine-out temperature during the entire test series.....	147
4.4.2 The effect of using the BL fuel on engine-out temperature under steady high speed travel on the M1 motorway.....	147
4.4.3 The effect of using the BL fuel on the engine-out temperature under high torque performance.....	148
4.5 Statistical analysis	149
4.5.1 Statistical analysis for the entire test series data.....	149
4.5.2 Statistical analysis for the steady high speed HGV travel data	153
4.5.3 Multi-regression analysis for the steady high speed HGV travel.....	154
4.5.4 Statistical analysis for the vehicle performance under high torque performance	157
4.6 Conclusions.....	159

Chapter 5

Evaluation of fuel physical and chemical properties and their effect on fuel injection characteristics, fuel consumption and engine deposits..... 162

5.1	Analysis of fuel properties affecting its precombustion behaviour	162
5.1.1	General	162
5.1.2	Fuel density.....	164
5.1.3	Fuel viscosity.....	166
5.1.4	Fuel surface tension.....	168
5.1.5	UBF chemical structure.....	168
5.2	Analysis of fuel properties affecting the combustion process and emissions	169
5.2.1	Fuel heating value.....	169
5.2.2	CHNS-O analysis	170
5.2.3	Determination of metals in the fuel.....	170
5.2.4	Thermo-gravimetric analysis for the fuel	171
5.3	Fuel injection characteristics	172
5.3.1	Fuel jet length.....	172
5.3.2	Fuel mean droplet size	174
5.3.3	Fuel Spray Cone Angle	176
5.3.4	Fuel jet velocity	178
5.4	Effect of the fuel properties on combustion chamber deposits..	180
5.4.1	Visual comparison between fuel injectors operated on PD and UBF	180
5.4.2	Visual comparison for the effect of engine operation duration on deposit accumulation from different fuels	182
5.4.3	Visual comparison for the combustion chamber deposits in two identical engines	184
5.4.4	Chemical analysis by energy dispersive x-ray (EDX).....	184
5.5	Conclusions.....	186

Chapter 6 Quantitative and qualitative comparison for HGV PM emissions produced from C2G UBF and its blends with PD to PD obtained under real world driving conditions 189

6.1	Quantitative analysis for PM collected cumulatively by filtration..	190
6.2	Qualitative analysis for PM _{2.5} emissions from the combustion of PD and BL fuel in HGV (Thermo-gravimetric analysis)	194

6.3 Statistical analysis	202
6.3.1 Analysis of variances.....	202
6.3.2 Multi-regression analysis.....	203
6.4 Particle size distribution by inertial impaction	206
6.5 Thermo-gravimetric analysis for PM _{0.4}	213
6.6 Conclusions.....	216
Chapter 7 Quantitative and qualitative comparison for engine gaseous emissions produced from the utilisation of C2G UBF as a surrogate to PD	219
7.1 Gaseous emissions from the HGV during the whole journey	221
7.1.1 Physical analysis for the observed variations in HGV emissions and performance caused by switching from PD to the BL fuel.....	221
7.1.2 Statistical analysis for the observed variations in HGV emissions and performance caused by the BL fuel in comparison to PD.....	223
7.1.3 Analysis for the correlations suggested by the multi-regression models and their effect on HGV emissions.....	228
7.2 Gaseous emissions from the HGV travelling at steady-high speed on M1 motorway	234
7.2.1 Physical analysis of the observed variations in HGV emissions caused by switching from PD to the BL fuel during steady-high speed HGV travel	234
7.2.2 Statistical analysis for the observed exhaust emissions caused by UBF and PD combustion during steady-high speed HGV travel on the M1 motorway	239
7.2.3 Analysis for the correlations suggested by the multi-regression models and their effect on HGV emissions throughout the steady-high speed HGV test	244
7.3 Gaseous emissions from the HGV under high torque performance	247
7.3.1 Physical analysis for the observed variations in HGV emissions caused by high torque performance; A comparison between PD and the BL fuel	248
7.3.2 Statistical analysis for the observed variations in HGV emissions caused by the BL fuel under high torque engine performance	249
7.3.3 Analysis for the factors suggested by the predictive models and their effect on HGV emissions under high torque performance.....	255

7.4 Conclusions.....	260
7.4.1 Engine-out NO _x emission status.....	260
7.4.2 NO _x downstream to SCR emissions status	261
7.4.3 Carbon monoxide emissions status.....	261
7.4.4 Carbon dioxide emissions status.....	261
7.4.5 Total hydrocarbon emissions status.....	262
7.4.6 The overall variations in gaseous emissions from fuelling the HGV with BL fuel in comparison to PD.	263
Chapter 8	
Final conclusions and recommendations for future work.....	265
8.1 The conclusions	265
8.2 Recommendations for future work	267
8.3 Proposed strategies for further HGVs emissions mitigation using non-esterified UCO.....	268
List of References	269

List of Tables

Table 2.1 The annual growth in UCO dependence for road transport in the UK (Millions of Litres).	16
Table 2.2 UCO contribution in biodiesel production, total diesel fuel required for road transport and in GHG savings in the UK.	17
Table 2.3 UCO properties in comparison to UCOME, palm oil and No.2 PD	20
Table 3.1 Engine technical specifications.....	91
Table 3.2 Major vehicle positions between Ashby De La Zouch and Wigston	96
Table 3.3 TGA apparatus program for GF/F filters.	105
Table 3.4 PM size distribution across Andersen’s impactor stages.....	106
Table 3.5 Fuel injectors deposit inspection plan.....	130
Table 4.1 Multi-regression analysis and ANOVA results to predict VSP throughout the entire test series.....	150
Table 4.2 Multi-regression analysis and ANOVA results to predict SFC throughout the whole journey.	152
Table 4.3 Multi-regression analysis and ANOVA results to predict EoT throughout the whole journey.	152
Table 4.4 Statistical analysis showing the effect of fuel type on the group of engine performance factors under steady high speed conditions.	153
Table 4.5 Independent samples test. The effect of fuel type on vehicle performance factors under steady high speed HGV travel.....	154
Table 4.6 Multi-regression analysis and ANOVA results for the prediction of VSP under steady high speed HGV travel.	155
Table 4.7 Multi-regression analysis and ANOVA results for SFC as the dependent variable in a steady high speed HGV travel.	156
Table 4.8 Multi-regression analysis and ANOVA results for EoT as the dependent variable in the steady high speed HGV travel on M1 motorway.....	157
Table 4.9 Multi-regression analysis and ANOVA results to predict the effect of fuel type and other performance variables on vehicle specific power. High torque condition.....	158
Table 4.10 Multi-regression analysis results to predict the effect of fuel type and other performance variables on HGV LF. High torque condition.....	159
Table 5.1 Calculated gas pressure, temperature and density through 360° crankshaft rotation of the HGV engine under maximum torque speed using diesel dual cycle. Data for UBF combustion.	163

Table 5.2 GC-FID analysis of C2G UBF.....	167
Table 5.3 GC-FID analysis for C2G UBF data averaged for two samples.....	169
Table 5. 4 Comparison between HHV and LHV for PD and UBF on mass and volumetric bases. Data obtained from four fuel samples. .	169
Table 5.5 CHNS-O analysis for the C2G UBF and PD as a base fuel.	170
Table 5.6 ICP test results for C2G UBF	171
Table 5.7 Variation of fuel jet characteristics per 10% increase in UBF content in the BL fuel	187
Table 6.1 Percentage of PM components from the BL fuel and PD at different payloads and road loads. Data based on TGA for samples obtained from 30 real world trips.....	196
Table 6.2 Variation of PM _{2.5} emissions and its components from the combustion of the BL fuel in comparison to those of PD in HGV at different Payloads and road loads.....	197
Table 6.3 The effect of using C2G UBF in the BL fuel on PM _{2.5} emission components from HGV under different loads.	202
Table 6.4 Analysis of variance for PM EF obtained from HGV operation on PD and BL fuel. The units are in (g/kWh).....	202
Table 6.5 Levene's test for equality of variances and t-test for the equality of means for PM EF and its components. The units are in (g/kWh).....	203
Table 6.6 Multi-regression analysis for PM _{2.5} . VOF is the dependent variable.....	204
Table 6.7 PM regression analysis. EC as the dependent variable.	204
Table 6.8 PM regression analysis. Ash as a dependent variable.	205
Table 6.9 PM regression analysis, total PM as a dependent variable.	206
Table 6.10 PM ₁₀ size segregation for BL fuel and PD emissions and the % variation PM EF at each impactor stage as the BL fuel substitutes PD.	211
Table 6.11 Variation of PM _{0.4} components as BL fuel substitutes PD at different HGV loads.....	215
Table 6.12 In-vitro analysis for C2G UBF and PD chemical structure and thermal properties.	217
Table 7.1 Analysis of variance for BL fuel and PD and their effects on gaseous emissions.(The whole journey is considered). [g/kWh].....	223
Table 7.2 t-test for equality of means for the effect of fuel type, BL fuel compared to PD, on gaseous emissions (g/kWh) through the entire test series.....	224

Table 7.3 Multi-regression analysis and ANOVA for the effect of fuel type and other performance parameters on engine-out NO _x across the entire test series. Data based on 32 trips.	225
Table 7.4 Multi-regression analysis and ANOVA for the effect of fuel type and HGV performance parameters on NO _x downstream to SCR through the entire test series. Data based on 32 trips.	226
Table 7.5 Multi-regression analysis and ANOVA for the effect of fuel type and HGV performance variables on CO emissions throughout the entire test series. Data based on 32 trips.	226
Table 7.6 Multi-regression analysis and ANOVA for the effect of fuel type and HGV performance parameters on CO ₂ emissions throughout the entire test series. Data based on 32 trips.	227
Table 7.7 Multi-regression analysis and ANOVA for the effect of fuel type and HGV performance parameters on THC emissions during the entire test series. Data are based on 32 trips.	228
Table 7.8 Analysis of variance for UBF and PD and their effects on gaseous emissions.(Steady-high speed HGV travel on M1 Motorway). Analysis base on 32 vehicle trips. Data units are in [g/kWh].	240
Table 7.9 t-test for equality of means for the effect of fuel type on gaseous emissions (Steady-high speed HGV travel on M1). Data units are in [g/kWh].	240
Table 7.10 Regression analysis for the effect of fuel type and other performance parameters on engine-out NO _x . (Data exclusively represent the steady high speed HGV travel).	241
Table 7.11 Regression analysis for the effect of fuel type and other performance parameters on NO _x downstream to SCR. (Data exclusively represent the steady state vehicle travel).....	242
Table 7.12 Multi-regression analysis for the effect of fuel type and other variables on CO ₂ emissions. (Data exclusively represent the steady-high speed HGV travel).	242
Table 7.13 Regression analysis for the effect of fuel type and other performance parameters on THC. (Data exclusively represent the steady high speed performance).....	243
Table 7.14 Analysis of variance for BL fuel and PD and their effects on gaseous emissions from a HGV under high torque conditions. Data in [g/kWh].....	249
Table 7.15 Levene’s test for equality of variance and t-test for equality of means for the effect of fuel type on gaseous emissions from HGV under high torque operation. Data units in [g/kWh].....	250
Table 7.16 Multi-regression analysis for the effect of fuel type and other performance variables on engine-out NO _x . (Data exclusively represent high torque engine performance).	251

Table 7.17 Multi-regression analysis for the effect of fuel type and other performance variables on NO _x downstream to SCR. (Data exclusively represent high torque engine performance).....	252
Table 7.18 Multi-regression analysis for the effect of fuel type and other performance variables on CO. (Data exclusively represent high torque engine performance).....	253
Table 7.19 Multi-regression analysis for the effect of fuel type and other performance variables on CO ₂ . (Data for HGV at high torque performance).....	254
Table 7.20 Multi-regression analysis for the effect of fuel type and other performance variables on THC. (Data for HGV under high torque operation).....	255
Table 7.21 The overall variations in gaseous emissions from the utilization of BL fuel in a HGV (84.5% UBF) compared to PD.	263

List of Figures

Figure 2.1 Comparison between distillation curves of PD and rapeseed oil. Reproduced from [19].	24
Figure 2.2 The number of licenced HGV and LGV in the UK 1994-2015.[60]	27
Figure 2.3 Goods moved and vehicle kilometres, annual, 1990 – 2014.[61]	27
Figure 2.4 Fuel consumption by HGV travelling fully loaded or with an empty trailer in Great Britain, 1993 – 2014 [62].	27
Figure 2.5 Gaseous emissions from HGV 1999-2013. [63, 64]	28
Figure 2.6 PM emissions from HGVs in the UK 2000-2013.[64]	28
Figure 2.7 Diesel fuel jet development, flame types and emissions [93].	46
Figure 2.8 Sketch of the Leaner Lifted- Flame Combustion (LLFC) strategy. H is the lift-off length, LL fuel jet penetration length and Φ_H is the equivalence ratio at jet centreline at (H) [121].	57
Figure 2.9 Diesel particulate filter monolith.	62
Figure 2.10 NO _x , HC and CO variation with ϕ . Reproduced from [1].	65
Figure 2.11 Typical diesel after treatment installation showing the urea SCR system.	70
Figure 2.12 Dual fuel system used as an on-board fuel heating and mixing facility	75
Figure 2.13 Equivalence ratio versus combustion temperature for conventional diesel engines showing soot and NO _x formation zones and the PCCI and HCCI operation zones.	80
Figure 3.1 Zirconia solid electrolyte NO _x sensor and K-type thermocouple position on the exhaust manifold.	88
Figure 3.2 The tractor, Mercedes-Benz AXOR-C 2543 LS. The dimensions are in mm. Source www.mercedes-benz.co.uk .	90
Figure 3.3 The engine OM 457 LA EURO 5	90
Figure 3.4 the fuel injection system layout of the test vehicle.	92
Figure 3.5 The modified fuel storage system.	93
Figure 3.6 the Bioltec fuel mixer and transfer to the injection pump.	93
Figure 3.7 Bioltec control unit.	94
Figure 3.8 Road profile, HGV position and the routine vehicle commute path. All the main positions are described in table 3.2 below.	95
Figure 3.9 Emissions measurement apparatus, vehicle dynamics and power supply units installed on the driver's bed.	97

Figure 3.10 Schematic diagram for the apparatus layout for gaseous emissions, fuel consumption and vehicle dynamics measurements installed inside the driver's cabin.....	98
Figure 3.11 Schematic diagram for the PM emissions collection apparatus layout inside the driver's cabin.	99
Figure 3.13 PM ₁₀ size distribution and PM _{2.5} collection assembly with flowmeters and vacuum pumps.....	102
Figure 3.14 Shimadzu 50 thermo-gravimetric analyser.	104
Figure 3.15 Andersen impactor and its principle of operation [158].	106
Figure 3.16 The location of zirconia sensor and exhaust gas temperature measurement probe.	111
Figure 3.17 Racelogic Vbox II, vehicle positioner allocator and speed calculator.....	117
Figure 3.18 Bioltec system controller with communication unit and software.....	119
Figure 3.19 Micrometrics AccuPyc 1330.	121
Figure 3.20 Bohlin rheometer.	123
Figure 3.21 CAM 2008, KSV instruments, for surface tension analysis. ...	124
Figure 3.22 Flash 2000 CHNS analyser.....	125
Figure 3.23 Perkin Elmer Clarus 500 GC-FID apparatus.	126
Figure 3.24 Surface scanning electron microscopy.....	132
Figure 4.1 Bioltec system response to C2G UBF temperature. A cold start from Ashby towards Wigston.....	136
Figure 4.2 Bioltec system response to C2G UBF temperature. A hot start from Wigston towards Ashby.....	136
Figure 4.3 Rate of fuel consumption for C2G UBF and PD for the HGV journey in fig.4.1.....	137
Figure 4.4 Rate of fuel consumption for C2G UBF and PD for the HGV journey in fig.4.2.....	138
Figure 4.5 The effect of vehicle payload and road load on VSP during the entire journey. Data based on 32 trips. ET and LT are empty trailer and loaded trailer respectively. A2W and W2A are the HGV direction from Ashby to Wigston and Wigston to Ashby respectively.	139
Figure 4.6 The effect of vehicle payload and road load on VSP. Steady high speed HGV travel on the M1. Data based on 32 trips. ET and LT are empty trailer and loaded trailer respectively. A2W and W2A are the HGV direction from Ashby to Wigston and Wigston to Ashby respectively.	140

Figure 4.7 VSP for HGV performing under high torque conditions using BL fuel and pure PD. Data based on 16 test trips.	140
Figure 4.8 Specific fuel consumption for a HGV operated on different fuels, BL fuel and PD, under different payloads and road loads. The plots are based on 32 trips. ET and LT are empty trailer and loaded trailer respectively. A2W and W2A are the HGV direction from Ashby to Wigston and Wigston to Ashby respectively.....	141
Figure 4.9 Vehicle SFC vs power demand for the HGV operated on different fuels, BL fuel and PD separately. Data based on 32 vehicle trips.	142
Figure 4.10 Specific fuel consumption for the HGV travelling at steady high speed on M1 motorway using BL fuel and PD separately. The plot is based on data analysis from 32 trips. ET and LT are empty trailer and loaded trailer respectively. A2W and W2A are the HGV direction from Ashby to Wigston and Wigston to Ashby respectively.	143
Figure 4.11 Specific fuel consumption vs vehicle power demand for the HGV traveling at steady high speed on M1 motorway. The plots are based on data from 32 trips.	143
Figure 4.12 Specific fuel consumption for the HGV at high torque performance using BL fuel and PD separately. The plot is based on data analysis from 16 trips.	144
Figure 4.13 Specific fuel consumption vs vehicle power demand for the HGV under high torque travel using BL fuel and pure PD separately. The plots are based on data from 16 trips.	145
Figure 4.14 Engine-out temperature correlation with engine load factor, and the rate of fuel consumption during an example outbound journey of the HGV.....	146
Figure 4.15 Engine-out temperature correlation with engine load factor, and the rate of fuel consumption during an example inbound journey of the HGV.....	146
Figure 4.16 A comparison between engine-out temperatures for the vehicle operated on BL fuel and PD at different loads through the entire test series. Results are based on 32 trips. ET and LT are empty trailer and loaded trailer respectively. A2W and W2A are the HGV direction from Ashby to Wigston and Wigston to Ashby respectively.	147
Figure 4.17 Engine-out temperature for the HGV operated on BL fuel in comparison to PD at different loads under steady high speed travel. Results are based on 32 trips. ET and LT are empty trailer and loaded trailer respectively. A2W and W2A are the HGV direction from Ashby to Wigston and Wigston to Ashby respectively.	148

Figure 4.18 Engine-out temperature for the HGV under high torque performance. A comparison between BL fuel and PD. The plots are based on 16 tests with STERROR $\pm 11^{\circ}\text{C}$	149
Figure 5.1 P-V diagram for the test HGV DICl engine at maximum torque; A comparison between UBF and PD combustion. (1) start of compression stroke, (i) start of injection, (2) end of compression stroke, (x) end of constant volume combustion and start of constant pressure combustion, (3) end of constant pressure combustion, (4) end of power stroke and (5) start of suction stroke. The properties of the events are explained in table 5.1 below.....	163
Figure 5.2 Fuel density variation with temperature, C2G UBF from different seasonal batches in comparison to PD and rape seed oil...	165
Figure 5.3 Fuel density variation with temperature. Comparison among C2G UBF and its blends to PD. Data are based on three samples and five dilutions for each sample.	165
Figure 5.4 Variation C2G UBF kinematic viscosity with temperature. A comparison between C2G UBF collected at different seasons to PD.	166
Figure 5.5 Variation of C2G UBF kinematic viscosity with temperature and UBF content in the blend compared to PD.....	167
Figure 5.6 Variation of surface tension with blending ratio and temperature. A comparison between C2G UBF and PD. Data averaged for three fuel samples.....	168
Figure 5.7 TGA analysis for C2G UBF. Data are averaged for four samples.....	171
Figure 5.8 Fuel jet length as a function of crank angle. A comparison among UBF and its 80% blend with PD to pure PD. Fuel temperature and engine speed the controlling factors.	172
Figure 5.9 Fuel jet penetration as a function of jet Reynolds number for UBF at different engine speeds.....	173
Figure 5.10 Variation of fuel jet penetration with UBF content in the blend at different engine speeds and temperatures.	173
Figure 5.11 Variation of fuel SMD with injection timing and duration at different fuel temperatures and engine speeds.	174
Figure 5.12 Fuel SMD as a function of UBF content in the blend at various fuel temperatures and engine speed.	175
Figure 5.13 Fuel spray cone angle variation with crank angle at different engine speeds, fuel temperature and mixing ratios for UBF and PD.	177
Figure 5.14 fuel spray cone angle variation with UBF content in the blend at various temperatures and engine speeds.....	178

Figure 5.15 variation of fuel spray cone angle with Reynolds number for various fuel temperatures and engine speeds.	178
Figure 5.16 variation of fuel jet velocity with crank angle for different fuel temperatures and at different engine speeds.	179
Figure 5.17 SEM electron images for fuel injectors being operated on different fuels.....	180
Figure 5.18 SEM images for the needles of the fuel injectors operated on different fuel.	181
Figure 5.19 SEM images for injector holes operated on UBF on the same engine for different durations.	182
Figure 5.20 a & b SEM images for a fuel injector shoulder	183
Figure 5.21 SEM images for two injectors operated on UBF, running for nearly the same distance on two identical engines	184
Figure 5.22 EDX analysis for the deposits on the injector shoulder.	185
Figure 6. 1 Visual inspection of GF/F filters showing PM collected from HGV exhaust in real world driving under different loads. The upper two were taken from HGV operated on PD while the lower two from HGV operated on BL fuel.	191
Figure 6.2 PM emission factor for the combustion of BL fuel and PD under different operational conditions. ET and LT are empty trailer and loaded trailer respectively. A2W and W2A are the HGV direction from Ashby to Wigston and Wigston to Ashby respectively. The data are the average of 20 trips for the BL fuel, 5 per trip category, and 14 trips for PD, 2~5 trips per category. SE ± 0.001253	192
Figure 6.3 Vehicle PM EF versus VSP. A comparison between PM emissions from PD and BL fuel at different HGV performance conditions. The data are averages for 14 and 20 trips for the PD and BL fuels respectively. SE ± 0.001253	193
Figure 6.4 PM EF versus SFC. A comparison between conventional PD emissions and C2G UBF. The data are averages for 14 and 20 trips for the PD and UBF respectively. SE ± 0.001253	194
Figure 6.5 Thermo-gravimetric analysis (TGA) for PM _{2.5} collected on GF/F filters. A comparison between BL fuel and PD PM components for an empty trailer HGV trip.	195
Figure 6.6 Thermo-gravimetric analysis (TGA) for PM _{2.5} collected on GF/F filters. A comparison between BL fuel and PD PM components for a loaded trailer HGV trip.	195

Figure 6.7 VOF EF obtained from a HGV operated on PD and BL fuel under different operational conditions. ET and LT are empty trailer and loaded trailer respectively. A2W and W2A are the HGV direction from Ashby to Wigston and Wigston to Ashby respectively. The data are the average of 20 trips for the BL fuel, 5 trips per category, and 14 trips for PD, 2-5 trips per category. SE $\pm 1.69E-04$	196
Figure 6.8 VOF EF as a function of VSP for PD and BL fuel. The data are averages for 14 and 20 trips for the PD and BL fuel respectively. SE $\pm 1.69E-04$	198
Figure 6.9 VOF as a function of engine-out temperature. The data are averages for 14 and 20 trips for the PD and BL fuel respectively. SE $\pm 1.69E-04$	198
Figure 6.10 VOF EF as a function of SFC for PD and BL fuel. The data are averages for 14 and 20 trips for the PD and BL fuel respectively. SE $\pm 1.69E-04$	199
Figure 6.11 Elemental carbon (EC) emission factor, a comparison between BL fuel and PD under different vehicle operational conditions. ET and LT are empty trailer and loaded trailer respectively. A2W and W2A are the HGV direction from Ashby to Wigston and Wigston to Ashby respectively. The data are the averages for 20 trips for the BL fuel, 5 per trip category, and 14 trips for PD, 2-5 trips per category.	199
Figure 6.12 EC EF versus VSP from PD and BL fuel PM emissions. The data are averages for 14 and 20 trips for the PD and UBF respectively. SE $\pm 2.84E-05$	200
Figure 6.13 EC EF as a function of SFC for a HGV operated on PD and UBF. The data are averages for 14 and 20 trips for the PD and UBF respectively. SE $\pm 2.84E-05$	200
Figure 6.14 Ash emission factor, a comparison between BL fuel and PD under different vehicle operational conditions. ET and LT are empty trailer and loaded trailer respectively. A2W and W2A are the HGV direction from Ashby to Wigston and Wigston to Ashby respectively. The data are the average of 20 trips for the BL fuel, 5 per trip category, and 14 trips for PD, 2-5 trips per category. SE $\pm 1.46E-05$	201
Figure 6.15 Visual comparison for PM collected at different stages of Andersen's impactor. The HGV was operated on PD and travelling with empty trailer.....	207
Figure 6.16 Visual comparison for PM collected at different stages of Andersen's impactor. The HGV was running on BL fuel and travelling with empty trailer.....	208

Figure 6.17 Size distribution for PM ₁₀ EF for PD and BL fuel obtained from a HGV traveling with an empty trailer. The data are averaged for (6) round trip journeys. SE±3.366E-5.....	209
Figure 6.18 Size distribution for PM ₁₀ EF from PD and BL fuel obtained from a HGV traveling with loaded trailer. The data are averaged for (7) round trip journeys. SE±3.366E-5.....	209
Figure 6.19 PM EF for three PM size ranges obtained from HGV operated on PD and C2G UBF at different operational conditions. ET and LT are empty trailer and loaded trailer respectively. The data are averaged from 13 round trip journeys. SE±3.366E-4.	210
Figure 6.20 Effect of load increase on selected PM sizes from PD and BL fuel combustion. Data averaged for 13 round trip journeys.....	211
Figure 6.21 Reduction in selected PM sizes as BL fuel substitutes PD. Data are the averages of 13 round trip journeys.	212
Figure 6.22 TGA test results for PM _{0.4} collected on Andersen's back-up filter. The plots show the effect of fuel type on PM emissions under different HGV load conditions. The data are averages of 3 round trip journeys per category. SE±0.0364	213
Figure 6.23 TGA test results for PM _{0.4} collected on Andersen's back-up filter. The plots show the effect of load on PM emissions from HGV operation on PD and BL fuel. The data are averages of 3 round trip journeys per category. SE±0.0364.	214
Figure 6.24 a comparison for PM _{0.4} and its components emitted from the combustion of the BL fuel and PD in a HGV under different loads. ET and LT are the empty and loaded trailer respectively. The data are the average of 9 round trip journeys.	215
Figure 7.1 NO _x downstream SCR emissions, engine-out temperature, road elevation and HGV speed during a real world journey from Ashby de la Zouch towards Wigston. The vehicle payload is 31 tonnes. 86.5% of the journey's fuel is C2G UBF.	222
Figure 7.2 NO _x downstream to SCR emissions vs the amount of fuel consumed during a real world journey from Ashby De La Zouch to Wigston. The vehicle payload is 31 tonnes and 86.5% of the journeys fuel is C2G UBF.....	223
Figure 7.3 NO _x EF at the tailpipe of a HGV fuelled with BL fuel and PD. Data based on 32 real world trips. ET and LT are the HGV empty trailer and loaded trailer respectively. A2W is the outbound journey from Ashby to Wigston while W2A is the inbound journey....	229
Figure 7.4 Tailpipe NO _x emission factor vs vehicle power demand obtained from real world HGV tests. The graphs compare between NO _x EF from BL fuel and PD. Data based on 32 real world trips.....	229

Figure 7.5 NO _x emission factor vs vehicle specific fuel consumption obtained from real world HGV tests. The graphs compare between NO _x EF from BL fuel and PD.	230
Figure 7.6 CO ₂ EF from real world tests of a HGV fuelled by BL fuel and the PD. Data based on 32 real world trips. ET and LT are the HGV empty trailer and loaded trailer respectively. A2W is the outbound journey from Ashby to Wigston while W2A is the inbound journey.....	232
Figure 7.7 CO ₂ EF vs vehicle SFC obtained from real world HGV tests. The graphs compare between CO ₂ EF from BL fuel and PD.	232
Figure 7.8 THC EF from real world tests of a HGV fuelled by BL fuel and the PD. Data are based on 32 trips. ET and LT are the HGV empty trailer and loaded trailer respectively. A2W is the outbound journey from Ashby to Wigston while W2A is the inbound journey....	233
Figure 7.9 THC EF vs SFC obtained from real world HGV tests. The graphs compare between THC EF from BL fuel and PD. Data are based on 32 real world trips.	233
Figure 7.10 NO _x downstream to SCR variation with temperature, vehicle speed and road gradient. Steady-high speed HGV travel on M1 motorway.....	234
Figure 7.11 NO _x EI downstream to SCR in correlation to the rate of UBF and PD consumption. A HGV moving on M1 motorway at steady-high speed.	235
Figure 7.12 NO _x EI downstream to SCR in correlation to the rate of PD consumption. A HGV moving on M1 motorway at steady high-speed.	235
Figure 7.13 Comparison between real world CO EI from (A) UBF and (B) PD from a HGV traveling at steady-high speed on M1 motorway.....	236
Figure 7.14 Comparison between real world CO ₂ EI from (A) UBF and (B) PD from a HGV traveling at steady-high speed on M1 motorway.....	237
Figure 7.15 Comparison between real world THC EI from (A) UBF and (B) PD from a HGV traveling at steady-high speed on M1 motorway.....	237
Figure 7.16 HGV gaseous emissions related to engine performance and road load. A sample journey (18032014-A2W-1140-PD-LT).....	238
Figure 7.17 Tailpipe NO _x EF from real world tests of a HGV fuelled with UBF and the PD travelling at steady high speed. ET and LT are the HGV empty trailer and loaded trailer respectively. A2W is the outbound journey from Ashby to Wigston while W2A is the inbound journey. Data based on 32 real world trips.	244

Figure 7.18 Tailpipe NO _x EF vs vehicle power demand obtained from steady high speed HGV travel in real world test. The graphs compare between NO _x EF from UBF and PD. Data based on 32 trips.	245
Figure 7.19 Tailpipe NO _x EF as a function of SFC for a HGV travelling at high steady speed. Data base on 32 real world trips.....	245
Figure 7.20 CO ₂ EF from real world tests of a HGV fuelled with UBF and the PD travelling at steady high speed. ET and LT are the HGV empty trailer and loaded trailer respectively. A2W is the outbound journey from Ashby to Wigston while W2A is the inbound journey. Data based on 32 real world trips.	246
Figure 7.21 CO ₂ EF as a function of SFC for a HGV travelling at high steady speed. Data base on 32 real world trips.	246
Figure 7.22 THC EF from real world tests of a HGV fuelled with UBF and the PD travelling at steady high-speed. ET and LT are the HGV empty trailer and loaded trailer respectively. A2W is the outbound journey from Ashby to Wigston while W2A is the inbound journey. Data based on 32 real world trips.	247
Figure 7.23 NO _x EI downstream to SCR in correlation to temperature, road gradient and speed. The engine is operated under high torque conditions. The loaded HGV is accelerating on a 240m long ramp.	248
Figure 7.24 NO _x EI downstream to SCR correlated to the amount of UBF consumption under high torque performance. The GVW is 31 tonnes and the HGV is accelerating on an inclined ramp to merge on M1 motorway.....	249
Figure 7.25 Tailpipe NO _x EF obtained from a HGV under high torque performance using two different fuels; BL fuel (84.6 % UBF on average) and PD. Data based on 16 real world trips.....	256
Figure 7.26 NO _x EF as a function of SFC for a HGV under high torque conditions using two different fuels; BL fuel and PD. Data based on 16 trips.	257
Figure 7.27 CO EF obtained from a HGV under high torque performance using two different fuels; BL fuel and PD. Data based on 16 trips	257
Figure 7.28 CO ₂ EF obtained from a HGV under high torque performance using two different fuels; BL fuel and PD. Data based on 16 trips.	258
Figure 7.29 CO ₂ EF as a function of SFC obtained from a HGV in a high torque performance using two different fuels; BL fuel and PD. Data based on 16 trips.	258

Figure 7.30 THC EF obtained from a HGV in a high torque performance using two different fuels; BL fuel and PD. Data based on 16 trips.	259
Figure 7.31 THC EF obtained from a HGV in a transition and fuelled with two different fuels; BL fuel(84.6% UBF on average) and PD. Data based on 16 trips.	259
Figure 7.32 variation in HGV emissions tested under real world conditions due to the utilisation of different fuels under specified operational conditions. The values are percentages of pollutant EF	264

List of Acronyms

a	Vehicle acceleration
A/F	Air to fuel ratio
A2W	Ashby De La Zouch to Wigston
AF _{st}	Stoichiometric air to fuel ratio
Ah	Ampere hour
AL	Aluminium
ANOVA	Analysis of variance
ASTM	American Standard for Testing Materials
a _t	Instantaneous acceleration
aTDC	After top dead centre
B20	20% biodiesel in the blend with petroleum diesel
bbf	Blue barrel
BDC	Bottom dead centre
bg _y	Billion gallons per year
BL	Blended fuel
BOD	Biochemical oxygen demand
bTDC	Before top dead centre
C	Carbon
C	Concentration
C2G	Convert to green
CA	Crank angle
CARB	California Air Resources Board
C _d	Coefficient of discharge
CFD	Computational fluid dynamics
CI	Compression ignition
Cl	Chlorine
CN	Cetane number
CO	Carbon monoxide
CO ₂	Carbon dioxide
Cu	Copper
CV	Calorific value
d	Distance
DEF	Diesel exhaust fluid
df	Degrees of freedom
DICI	Direct injection compression ignition
d _o	Nozzle orifice diameter
DOC	Diesel oxidation catalyst
D _p	Particle diameter
DPF	Diesel particulate filter
e	Exponent

EC	Elemental carbon
ECU	Engine control unit
EDX	Energy dispersive x-ray
EF	Emission factor
E_{ff}	Fossil energy
EGR	Exhaust gas recirculation
EI	Emission index
ELCA	Exergetic life cycle assessment
EOI	End of injection
EoT	Engine-out temperature
E_p	Primary energy
EPA	Environmental Protection Agency
ET	Empty trailer
EU	European Union
F	Variance to error ratio
FCO	Fresh cooking oil
Fe	Iron
FER	Fossil energy ratio
FID	Flame ionisation detection
FLL	Flame lift-off length
FTIR	Fourier transform infra-red
g	Gravitational acceleration
GC	Gas chromatography
GEMIS	Global Emission Model for Integrated Systems
GF/A	Glass fibre type A
GF/F	Glass fibre type F
GHG	Greenhouse Gas
GPS	Global positioning system
GVW	Gross vehicle weight
h	Height
H	Hydrogen
h	Hour
H/C	Hydrogen to carbon ratio
HCCI	Homogeneous charge compression ignition
HGV	Heavy goods vehicle
HHV	Higher heat value
HPCR	High pressure common rail
HySEE	Hydrogenated soy ethyl ester
Hz	Hertz
I	Moment of inertia
ICE	Internal combustion engines
ID	Ignition delay
ISF	Insoluble fraction

K_{gas}	Molecular ratio of the pollutant gas to exhaust gas
k_{pm}	Constant, reciprocal of gas density
L	Angular momentum
LC	Life cycle
LCA	Life cycle assessment
LF	Load factor
LGV	Light goods vehicle
LII	Laser-induced incandescence
LLFC	Leaner Lifted Flame Combustion
L_o	Experimental lift-off length
LT	Loaded trailer
LTC	Low temperature combustion
m	mass
MCT	Mercury cadmium telluride
\dot{m}_f	Fuel mass flowrate
MK	Modulated Kinetics (Nissan)
MoO_3	Molbedium trioxide
mpg	Miles per gallon
N	Number of cases
N_2O	Nitrous oxide
n_c	Number of carbon atoms
n_H	Number of hydrogen atoms
NH_3	Ammonia
NO	Nitrogen oxide
n_o	Number of oxygen atoms
NO_2	Nitrogen dioxide
NO_x	Nitrogen oxides
NTE	Not-to-Exceed
OC	Organic carbon
OH	Hydroxyl radical
Pa	Pascal
PAH	Poly-cyclic aromatic hydrocarbons
PCB	Polychlorinated hydrocarbons
PCCI	Premixed Charge Compression Ignition
PD	Petroleum diesel
PLIF	Planar laser-induced florescence
PM	Particulate matter
ppm	Part per million
Q	Exhaust gas volumetric flowrate
Q_f	Fuel volumetric flowrate

r	Radius
Re	Reynolds number
RED	Renewable Energy Directive
RES	Renewable Fuel Standard
RHR	Rate of heat release
RTFO	Renewable Transport Fuel Obligation
RWDC	Real world driving conditions
S	Fuel jet penetration length
SCR	Selective catalytic reduction
SEM	Scanning electron microscope
SFC	Specific fuel consumption
SHU	Sample handling unit
SI	Spark ignition
SMD	Sauter mean diameter
SN	Swirl number
SOC	Start of combustion
SOF	Soluble organic fraction
SOI	Start of injection
SUV	Sport utility vehicle
SV	Space velocity
SVO	Straight vegetable oil
t	Time
T	Temperature
T2W	tank to wheel
TDC	Top Dead Centre
TEOM	Tapered element oscillating microbalance
T_{eq}	Equilibrium temperature
TGA	Thermo-gravimetric analysis
THC	Total hydrocarbons
TiO ₂	Anatase
TN	Tumble number
ToF	Type of fuel
TRCC	Toroidal re-entrant combustion chamber
UBF	Ultra-biofuel
UCO	Used cooking oil
UCOME	Used cooking oil methyl ester
UNIBUS	Uniform Bulky Combustion System (Toyota)
V	Catalyst volume
V ₂ O ₅	Vanadium oxide
V _{act}	Actual fuel velocity
VGT	Variable geometry turbocharger
VHS	Very high significant

VIF	Variance inflation factor
VOF	Volatile organic fraction
VSP	Vehicle specific power
VSP _t	Instantaneous vehicle specific power
V _t	Instantaneous velocity
V _{th}	Theoretical fuel velocity
VVT	Variable valve train
W2A	Wigston to Ashby De La Zouch
W2T	Well to tank
W2W	Well to wheel
WO ₃	Tungsten trioxide
x	Characteristic length scale for fuel jet
XRD	X-ray diffraction
ZSE (ZrO ₂)	Zirconia solid electrolyte

Greek letters

η_{LC}	Life cycle energy efficiency
ν_f	Fuel kinematic viscosity
α	Fuel jet cone angle
Δd_h	Horizontal distance between two points
Δh	Change in height
Δt	Time increment
ζ_{st}	Percent stoichiometric air
θ	Road gradient
ρ_f	Fuel density
ρ_g	Gas density
σ	Standard deviation
ϕ	Equivalence ratio
Ω	Oxygen ratio
ω_{swirl}	Swirl angular velocity

Chapter 1

Introduction

Known as the black gold, petroleum is one of the major discoveries in human history. In addition to its energy content, its ingredients are useable to the last droplet. Our lives became so dependent on petroleum that there has been increasing recent concern about the depletion of its resources. However, the engineering and geological estimations revealed by British Petroleum (BP) in 2012 showed a growth in global oil reserves since the 1980's [2].

World energy demand is progressively increasing due to the high rates of population growth, welfare and prosperity. This has led to petroleum witnessing some periods of high prices and others of high production rates. The petroleum industry created a verity of businesses ranging from the huge petrochemical industries down to smaller family size businesses.

Its high energy density, ease of storage and transfer, availability and stability, and a vehicle range of a few hundred kilometres per tank, promoted the reliability of petroleum as a fuel for transportation. Nowadays, there are several types of engines which are designed to work on different cuts of petroleum products. The spark ignition engine (SI), the compression ignition engine (CI) (known as the diesel engine), and the gas turbine are the most common examples. There was always a mutual interaction between the fuel refining industry and the engine production industry. Engine manufacturing research labs always demanded petroleum fuel of premium quality. Therefore, each type of fuel possesses a different set of properties which make it behave differently during the combustion process. Engines manufacturers design their engines to the available market fuel specifications.

The transportation sector is a major consumer of petroleum as a fuel and of its by-products. In the United States the daily fuel consumption is around 19 million blue barrels (bbl) of fuel from which 95% is used in the transport sector. The United Kingdom's daily petroleum diesel (PD) consumption is 470,000 bbl in the transport sector [2]. These figures of fuel consumption are increasing due to progressive increases in usage and an increase in the number of transportation means. Among the transportation means, road transport is probably the highest consumer of petroleum fuel and its by-products. The US General Motors, Toyota of Japan and VW are in competition to exceed 10 million vehicles production per year. The vast majority of vehicles produced

worldwide are on-road vehicles and some off-roads. Therefore, millions of kilometres of roads were paved by petroleum products such as asphalt and bitumen to carry these huge numbers of vehicles.

The huge growth in the number of transportation units made the world more connected, and seemingly smaller and easier to live in. However, it deteriorated both local and global air quality to levels that threaten our lives. The transport sector was identified as the major contributor to the global carbon foot print and the greenhouse effect [3], lead, zinc and asbestos poisoning, photochemical smog, particulate pollution and noise. There are estimated to be five thousand mortalities each year related to automotive emissions in the UK [4]. These problems have motivated scientists and engineers to concentrate their endeavours towards pollution mitigation. This comprises innovations in engine technology and fuel refining processes as well as the search for alternative, low carbon renewable fuels.

The current project aims to carbon footprint reduction caused by the HGVs. The negative consequences of global warming and the future expectations led the international organisations to take precautionary measures for pollution mitigation. Therefore, the European target for fuel consumption in passenger cars was set to 5.6 and 4.9 Litres/100 km by 2015 for gasoline and diesel cars respectively and CO₂ emissions was set to 130 g/km. These were promoted to a new target of 4.1 and 3.6 Litres/100 km and CO₂ emissions to 95 g/km for gasoline and diesel cars respectively in 2021 [5].

The United Nations Framework Convention on Climate Change (UNFCCC) in its 16th session has set a target of 2°C or less average temperature rise compared to the pre-industrial levels. This could be achieved by 50% cut in global emissions by 2050. In fact the scenarios show that the reduction in global emissions could take place after their peak in 2020 [3].

The non-mandatory EU directive (2009/29/EC) launched a scheme to increase the biofuel content in conventional petroleum fuel to 10% by 2018. To avoid any controversy about the utilisation of edible oils as a fuel, used cooking oil (UCO) became a very competitive fuel for use in diesel engines. To comply with existing diesel engine technology, UCO derived biodiesel was produced. Biodiesel, with the existing blending ratios, has performed satisfactorily so far in diesel engines. However, environmental impact assessments of the biodiesel have revealed relatively high costs of production and around 10% material loss and energy loss during biodiesel processing.

Added to that, the energy spent in biodiesel processing reduced its renewability level and its life cycle efficiency. Due to its oxygen content, slightly higher NO_x emissions and other pollutants were indicated from the use of biodiesel compared to petroleum diesel at different rates depending on the engine technology.

In order to maintain high GHG saving levels in the UCO and to reduce its cost, some heavy goods vehicle (HGV) fleet operators have decided to use the UCO directly in their HGVs. In fact, the high heat content of UCO and its resiliency to changes in its properties to become compatible to petroleum diesel (PD) by heating made the idea applicable. Very little is known however, about the tailpipe emissions that may result from the use of UCO within HGVs in the real world and this is a key focus of the current work.

1.1 Factors affecting the fuel spray, combustion process and emissions

Engine technology development is one solution for emission mitigation. Understanding all the events taking place from the start of fuel injection to the start of combustion all the way to the end of the combustion process is a key factor in combustion optimisation for higher power outputs and lower emission levels. The most challenging issue is the limited time frame, which is a matter of a few milliseconds, to fit all the events in a high timing precision. It is the history of fuel droplet conversion into energy and by-products throughout the combustion process.

Fuel injection systems play a major role in the fuel journey as it converts to energy. The high injection pressures achieved recently, about 200 MPa, are very much controlling the fuel mean droplet size, the spray cone angle and the penetration length throughout the combustion chamber [6-8]. The high pressure common rail (HPCR) fuel injection system offers a constant high pressure available very close to the fuel injectors. This prevents any time delays for the pressure wave to reach the nozzle and eliminates pressure wave attenuation due to fuel pipe elasticity [9]. The availability of fuel at very high pressures in the vicinity of the combustion chamber with an electronic actuation of the injectors facilitated the multi-injection process. A few consecutive injections of different amplitudes and durations per cycle became achievable [10]. Accordingly, a very wide range of different combustion

scenarios became applicable. To reduce the ignition delay (ID) period and emissions formation, pilot injections were introduced 4 ms before the main injection, to undergo the preflame reactions for the main injection.

The pump-line-injector is also improved by installing individual pumps very close to the injector. This fuel system layout is less expensive and it provides the same high pressures as the common rail system. The fuel pressure varies directly with the engine output power [11]. The injector needle is electronically actuated to control injection timing and duration. This pressure-load variation affects the fuel spray characteristics at different engine operational conditions. Finer fuel spherules with wider spray cone angle and shorter penetration are the characteristics of the fuel injection under high loads.

The mean droplet size is very much related to the injection pressure. The higher the injection pressure the smaller the mean droplet size [12]. The droplet size distribution is very important in the mechanism and speed at which the fuel droplets convert from the liquid phase to the gaseous phase. The smaller the droplet size distribution the larger the fuel-air contact area. Fuel is usually injected at temperatures around 100°C into hot air at temperatures higher than 500°C [13, 14]. Larger fuel droplets absorb more heat due to the larger temperature difference between their surface and centre. Once their temperature reaches the self-ignition temperature they suddenly burnout. In other words, they resist the combustion at the beginning to burn suddenly causing a very high rate of heat release. Although they possess high inertia, their large cross-sectional area impedes their travel. Smaller droplets have less inertia but they experience many cycles of heating, evaporation and cooling. Therefore, they might over take the larger droplets and produce a vapour cone in their wake. The intervention of these wakes produce the flame front in the premixed flame zone. At this stage fuel volatility play a decisive role in the liquid to vapour conversion speed [9]. In fact the higher the speed of conversion the shorter is the ID period. A shorter ID leads to a higher rate of heat release and pressure rise. This results in a very high peaks of pressure rise and temperatures in the vicinity of the top dead centre (TDC) [15].

The in-cylinder global environment is shown to affect the fuel spray configuration and the combustion process. Engine compression ratio controls the properties of the air confined in the combustion chamber prior to the fuel injection. The higher the compression ratio the higher the pressure, temperature and density of the air in the combustion chamber [8]. These

severe in cylinder conditions affect the fuel-air mixing process. The higher air density restricts the fuel spray propagation and deep penetration. However, it increases the fuel spray cone angle [7]. This results in increasing fuel spherule separation as they move deeper in the combustion chamber. It also reduces the possibility of spherule collision and provides more hot air around the fuel spherules to enhance the evaporation process [16]. On the other hand the high gas pressure reduces the flame lift-off length to restrict the amount of air entrainment into the fuel spray [17]. The higher air temperature enhances the fuel evaporation process to contribute in the ID period reduction.

Most of the recently manufactured moderate and high speed diesel engines are direct injection (DI) engines. The position of the fuel injector, the number and direction of the fuel jets and their penetration length are very crucial factors in the combustion process. The number, size and lift height of the inlet and exhaust valves in conjunction with inlet manifold attachment to the cylinder head all work together to provide the required swirl and turbulence during the intake and compression strokes. The bowl shaped piston crowns work to force air, confined between the cylinder head and the flat rim of the piston crown, to flow towards the centre of the combustion chamber as the piston approaches its upper dwell. This improves the air swirl before and through the injection process. It is a counter-flow against the fuel spray.

Fuel properties on the other hand play a decisive role in fuel atomisation, evaporation and mixing with air. The fuel physical properties like viscosity, density and surface tension control the spray droplet mean size, spray cone angle and penetration length [18]. Higher fuel volatility speeds up the evaporation process [19]. Fuel density affects the speed of pressure wave movement in the fuel system. Increases in fuel density cause advanced fuel injector opening for a longer duration. The fuel viscosity impedes the fuel flow in the fuel system. A higher injection pressure is required to achieve the same injection characteristics from a less viscous fuel. Higher fuel viscosity results in a larger mean droplet size and a narrower spray cone angle. However, it might increase the flame lift-off length letting more air entrainment into the fuel spray. The net effect is a prolonged physical ID period. The surface tension of the fuel preserves the droplet shape and structure. It actually works against the pressure difference between inside and outside the droplet which increases at higher droplet speed leading to a premature droplet collapse [20, 21].

The fuel properties analysis were considered as one of the major components of the current research. Knowing the variations in UBF properties under temperatures and blending ratios similar to those encountered within the fuel injection system have a key role in the determination of fuel jet characteristics. In fact the fuel jet characteristics in conjunction with the combustion chamber configuration paved the way to predict the possible combustion scenarios under different operational conditions. All these results were directed to expect the reasons for the variations in the measured emissions between PD and the BL fuel.

As the environmental consequences of diesel engine emissions became a real threat, mandatory emissions standards forced engine manufacturers to include emissions mitigation as a priority in their designs. In fact in addition to carbon dioxide (CO₂), four emissions were regulated. These include carbon monoxide (CO), total hydrocarbons (THC), nitrogen oxides (NO_x the sum of NO and NO₂) and particulate matter (PM).

1.2 Pollution mitigation strategies

The emissions were divided under high temperature combustion and low combustion temperatures. NO_x is mostly increased by high combustion temperatures. It is usually formed in the diffusion flame at the flame periphery. At temperatures higher than 1600°C, oxygen and nitrogen react in series of reactions to produce NO. Maximum NO_x formation takes place at equivalence ratios close to unity [1, 22]. Therefore, low combustion temperature could mitigate NO_x. This could be achieved by a retarded fuel injection process in which most of the combustion process takes place during the power stroke under lower pressures and temperatures [1]. Unfortunately this action sacrifices engine power and fuel economy. Fuels with short IDs experience irradiative near adiabatic premixed flames. Therefore, most of the heat is released rapidly within the diffusion flame zone, thus increasing NO_x emissions.

The other alternative technique for NO_x reduction, is to introduce controlled amounts of exhaust gas into the intake air. This mechanism is called exhaust gas recirculation (EGR). The idea is to utilise the high heat capacity of the exhaust gas as a heat sink to achieve cooler combustion [23].

The aforementioned high temperature combustion conditions are exactly the ones needed for PM mitigation. This trade-off between NO_x and PM emissions

makes the pollution mitigation situation more complicated to be solve by the traditional combustion strategies [24].

PM is produced within fuel rich mixture packets. These packets are usually formed in poorly atomised fuels with low air entrainment and poor mixing qualities. Low oxygen contribution lead to fuel pyrolysis and the formation of poly-cyclic aromatic hydrocarbons (PAH). These are the soot precursors which could be eliminated within high temperature and high oxygen diffusion flames [25]. Soot might survive if the diffusion flame is quenched by the relatively cooler cylinder walls. Adjacent flames interception could also provide a passage for soot escape [1]. Increasing the fuel injection pressure and reducing the air pressure increases the flame lift-off length. This increases air entrainment for a leaner premixed flame with radicals formed to react with PAH and reduce soot formation. Carbon monoxide and THC also result from low temperature, rich incomplete combustion.

Within this context, it is the designers choice in terms of which of the emissions to mitigate inside the combustion chamber leaving the others for the exhaust aftertreatment systems. High temperature combustion reduces the CO, THC and PM to very low levels while leaving the NO_x to be treated by the NO_x aftertreatment facilities; probably selective catalytic reduction (SCR). By selecting low temperature combustion, NO_x will be reduced satisfactorily throughout the combustion process. However, a diesel particulate filter (DPF) and diesel oxidation catalyst (DOC) will be a mandatory measure for PM, CO and THC mitigation.

The fuel itself could also be modified to achieve the same objectives. In warm weathers, advanced fuel injection of low cetane number (CN) fuels increases the ID period. This results in a better fuel evaporation and enhanced homogeneity of the mixture. This will offer a lean low temperature combustion which targets NO_x and PM at the same time. The higher CO and THC could be reduced more easily with low cost oxidation catalysts.

Carbon dioxide is related to the amount of fuel consumed. 21% of GHG emissions is from the transport sector and a quarter of that amount is from HGVs [3]. Downsized turbocharged engines reduce fuel consumption and therefore CO₂ emissions. Otherwise, the number of transportation means should be reduced.

The other alternative for reducing CO₂ emissions from the transport sector is by using renewable oxygenated fuels. These fuels are usually derived from agricultural origins. The idea is carbon saving by using renewable fuels which

re-absorb carbon during a short growing cycle, in contrast to burning fossil fuels which releases extra carbon to atmosphere which has been fixed in the fossil fuel reservoir for millions of years [26].

1.3 Motivation for research

The current research is part of the UK's national efforts to reduce carbon footprint and other regulated diesel emissions. The project is a collaborative work between Convert to Green, the renewable fuel supplier, United Biscuits Midlands Distribution Centre, the heavy goods vehicle (HGV) fleet operator and test HGV supplier and the University of Leeds as the scientific consultant and research performer.

The proposed fuel is used cooking oil (UCO) known as convert to green ultra-biofuel (C2G UBF) after the fuel provider company. It is a non-esterified used cooking oil collected locally or imported and prepared for use as a fuel by filtration. The transesterification process reduces the renewability level of the fuel and its lifecycle efficiency. The renewability level means the amount of energy consumed to prepare a defined fuel mass. Since only filtration is used in processing the UCO, its renewability level is high compared to bio-diesel which involves transesterification. Lifecycle efficiency means the amount of energy which remains in the final product compared to the raw material [26]. This is also higher for UCO compared to bio-diesel. However, these savings also come at a price in terms of fuel properties. In vitro analysis reveals huge differences between the physical and chemical properties of C2G UBF and market petroleum diesel (PD) [18], whereas the same may not be said for bio-diesel. The only encouraging property is its heat content which is comparable with that of PD on volumetric bases (see table 6.12). A key aim of the project was therefore to explore the impact of these differences in fuel properties and whether heating the UBF is able to reduce the huge gap in properties compared to PD to reasonable limits.

The HGV used within the real world emissions tests as part of this work was a EURO 5 emissions standard compliant vehicle. The vehicle was a Mercedes-Benz Axor-C 2543, A 44 tonne articulated tractor-trailer powered by Mercedes-Benz OM 457 LA six-cylinder inline turbocharged direct injection compression ignition (DICI) engine. The maximum fuel injection pressure was 180 MPa. The engine output was 315 kW at 1900 rpm and the maximum torque was 2100 Nm at 1100 rpm. The compression ratio was 18.5:1. The intake air temperature was set not to exceed 55°C. The combustion chamber

configuration was an inverted mushroom shaped combustion chamber carved in the piston crown. In fact these are the major specifications which made the combustion of C2G UBF easier (see table 3.1).

It was decided to test the C2G UBF on this particular vehicle in the real world to get realistic results. Added to that some chassis dynamometer tests failed to give the precise emissions due to the engine control unit (ECU) interference. The ECU changes engine operation mode when tested for emissions by injection retardation for a cooler low NO_x combustion while sacrificing the fuel economy and power [27].

The study comprises the effect of C2G UBF on the vehicle performance, specifically the HGV output power and fuel consumption. Engine durability was also taken into consideration by periodical fuel injector inspections for any damage and deposits (see chapter 5). The engine maintenance record was also checked-out with the technical team of the United Biscuits Midlands Distribution Centre repair and maintenance garage. The fuel consumption for PD and UBF were obtained from the Biotec system. This was an extra mechanism used for mixing UBF with PD at different proportions whenever is needed. This mixing process took place automatically depending on the UBF temperature and the preloaded engine performance maps. UBF was heated by heat recovery from the engine cooling system at no cost and extra load to the engine.

PM emission measurement was cumulatively achieved by collecting the PM on filter papers through two heated PM sampling lines. The PM measurements include gravitational analysis and size segregation. The tests went deeper to analyse the major components of the PM by thermo-gravimetric analysis (TGA) (see chapter 3).

Gaseous emissions measurements were performed through two systems. The first one was installed on the exhaust pipe upstream to the SCR to measure the engine-out NO_x using zirconia solid electrolyte sensor and OBD 1000 analyser. The second system was installed at the tailpipe at the exit of the SCR system. Gas sample was taken continuously through a heated line to the Fourier-Transform Infra-Red (FTIR) apparatus. Data for THC, CO, CO₂ and NO_x were recorded at 0.5 Hz for later analyses.

HGV dynamics including vehicle velocity, position and elevation were continuously recorded at 5 Hz using Racelogic 2 Vbox. These data were used to calculate the vehicle specific power (VSP) and HGV power demand.

UBF and PD density and viscosity were tested in the lab at different temperatures from 15°C~100°C. UBF and PD surface tension and heat value tests were also performed.

1.4 Overall aims and objectives of the project

The current research aims to study the environmental performance of direct utilisation of used cooking oil in HGVs under real world driving conditions. It comprises the environmental impacts represented by the quantitative and qualitative analyses of the combustion emissions. A high priority is given to the carbon footprint reduction for used cooking oil (UCO) and the amount of CO₂ savings in comparison to PD and biodiesel to legitimise UCO utilisation as a fuel. Nevertheless other regulated gaseous and particulate emissions from the combustion of UCO are also included in this research. The HGV performance as it travels in real world journeys between two designated places is another area to be covered. The HGV performance is the way the HGV engine behaves under real world road resistances as it runs on UCO compared to PD. It is the capability of the UCO fuelled HGV to achieve the same pay loads designated by the manufacturer. The study also engulfs engine durability as it runs for extended periods of time on UCO. This could be achieved by monitoring engine deterioration and its performance attenuation as it runs for extended periods on UCO.

In order to achieve the aforementioned objectives, a roadmap is implemented to connect the properties of the UCO to the final combustion products passing through the engine technology and the expected combustion scenario. Therefore the first task is to study the fluidity of UCO as it flows through the fuel system. UCO heating and mixing with PD were recommended in the literature. However, knowing the extent of heating and mixing for this particular product is a challenge. Moreover the heating and mixing had to be accomplished automatically on board. Therefore the fuel system is modified by incorporating the Bioltec system between the fuel tanks and the high pressure pump to control the mixing process. This necessitates the study and analysis of the Bioltec system behaviour.

It is also realised that none of the environmental impacts and vehicle performance could be explained without detailed analyses of the fuel injection process comparatively between UCO and PD. This could only be achieved by merging the fuel injection dynamics into the engine operation cycle to obtain the real in-cylinder environment at which the fuel is injected.

Testing the HGV under real world driving conditions elevated the complexity of the performance analyses. Unlike in-vitro chassis-dynamometer tests, the engine performance had to be measured from the road resistances exerted on the HGV. These resistances include air drag and friction, HGV rolling resistance, acceleration resistance and gradient resistance. All these resistances work collectively on the engine. The power delivered by the engine to overcome these resistances is referred to as the vehicle specific power (VSP). The continuous fluctuations in the VSP affects the amount of fuel consumption through the driver's reaction. This made the specific fuel consumption (SFC) a major performance criterion.

Engine durability is a crucial objective, since more frequent needs for engine maintenance and failure during goods transport could reduce the reliability of UCO as a fuel. Therefore a thorough investigation for the combustion chamber configuration became essential to facilitate the main objectives. This could be achieved by investigating the sectional drawings of the engine and engine parts dimensions. In fact this kind of analyses also enables the observer to predict the probable causes and position of deposit morphology. Once the decision is taken, the related engine parts could be studied for the quantity and quality of the deposits according to a pre-planned time schedule. Scanning electron microscopy (SEM) and energy dispersive x-ray (EDX) could be one option to detect the possible causes of engine deposit formation and engine failure.

The environmental impact of the direct utilisation of UCO as a surrogate to PD could be obtained by measuring tailpipe emissions. The gravimetric analysis of the particulate matter (PM) obtained from the combustion of UCO and PM size distribution provide sufficient data for comparison to those of PD. Thermogravimetric analysis for the PM facilitates the determination of OC/EC ratio and how it is compared to PD. The trade-off between PM and NO_x

emissions is another objective to be studied in par with CO, THC and CO₂ emissions. The HGV is equipped with a selective catalytic reduction (SCR) system as the only exhaust aftertreatment system to tackle NO_x emissions. Therefore NO_x measurement upstream (engine-out) and downstream (tailpipe) to the SCR is taken into consideration.

It is decided to test the UCO on one of the fleet HGVs to eliminate any inconsistency that might emerge from the differences between the engine technologies or lab conditions. The real world tests spontaneously incorporate some extra variables which are unachievable in the simulated lab tests, such as the driver's behaviour, the interaction between the road profile and the payload, and the variations in weather conditions during a particular journey. The tests will be performed as the HGV travels on one of its routine routes between Ashby De La Zouch to Wigston in the Midlands. The journey comprehensively includes urban, rural and motorway driving sections.

Chapter 2

Literature Survey

2.1 World energy demand and the need for renewable fuels in the transport sector

The world daily oil consumption, as per 2010 statistics, was 87 million blue barrels (bbl) on average [2]. 20-23% of this amount is consumed in the United States from which 95% is consumed in the transport sector. The figure is expected to increase to 100 million bbl/day in the year 2035 [2]. In the United Kingdom, 74.433 million litres is the daily consumption of petroleum diesel (PD) in the transport sector as per the 2014-2015 Renewable Transport Fuel Obligation (RTFO) report [28]. High concerns about CO₂ emissions in the EU region and NO_x in North America led the environmental bodies to announce mandatory legislations to merge renewable fuels in the transport sector. The EU (2009/28/EC) Renewable Energy Directive (RED) set the target of 10% renewable fuel in road transport to substitute petroleum fuel by 2020. To achieve that goal, the UK's 2009 RTFO legislation obligated the fossil fuel suppliers to include a certain percentage of renewable fuels from a sustainable resource in their supplies.

The US Environmental Protection Agency (EPA) launched the Renewable Fuel Standard (RFS) in 2005 to blend 7.5 billion gallons per year (bgy) of renewable fuel with gasoline in 2012. This was amended by the RFS2 to raise the stake to 15.2 bgy in 2012 and set 36 bgy as a target for 2022 [2].

One of the main advantages of biofuels lie in the energy density they possess. It is quite comparable to PD. Vehicle refuelling is quite easy and a journey of several hundred kilometres is achievable with one tank filling. Moreover, For the low blending wall of (10% biofuel), no vehicle modifications are needed.

Probably the main drawback lies in the type of feedstock and the scale of production. According to UK RTFO reports biofuel supplied to the market covers only 3.29% (4.578 million litres per day) of the total annual UK demand by the transport sector. Biodiesel comprises 50% of supplied biofuel [28]. In 2010 with the cutting edge, by then, biofuel production technologies, 40% of the US corn crop was used to provide only 6% transport fuel demand. Crops are different for their amount of biofuel yield and the amount of energy required in their production (energy ratio). In Brazil, as hydro-electric power is a main contributor in the national energy production, the cost of biofuel is relatively low.

There is a very serious debate about land exploitation for biofuel production especially from edible crops. Therefore the feedstock might be limited to non-edible plants or waste materials. As a result, used cooking oil (UCO) merged into biodiesel production during the last decade. Since then its contribution to biodiesel production increased to reach 88.5% in the year 2011~2012 [28].

The other drawback is the energy conversion efficiency of the internal combustion engine (ICE) which is quite low meaning that very much of the biofuel energy is dissipated in the ICE.

From the aforementioned data, it is arguably believed that biofuels could act as a transient fuel working side by side with PD and existing engine technologies. Vehicle electrification could be a more promising scenario in long term transport strategies.

This chapter is a demonstration for the eligibility of used cooking oil as a material and a quantity to be used as a renewable fuel. The chapter is mainly trying to answer some key questions about its eligibility for usage as a fuel, such as: are there any global or local interests in its usage? Are there any public objections or environmental precautions about its storage and handling as a fuel? How does UCO behave in the engine? Do the differences with PD properties require special treatment or expensive vehicle modifications? How does UCO compete with biodiesel? How does the fuel interact with the fuel system and what is its effect on engine durability? What are the combustion products compared to PD?

2.2 The fuel: used cooking oil (UCO)

Used cooking oil is a waste material, in a solid or liquid state. In fact it hasn't been classified as a solid or liquid waste yet and is even not considered as a hazardous substance or a recyclable material. Therefore it's disposal hasn't been legislated or regulated under solid waste disposal guidelines [29]. Used cooking oil was always considered as a problematic refuse that burdens municipalities and sewage treatment plants. Unlike solid wastes, as a liquid, it was very difficult to implement a certain strategy for its storage and handling for collection at residential and commercial levels. Therefore it was much easier to spill it into the sewers [30]. In some developing countries, due to profit making and poor government supervision for UCO recycling, millions of tonnes of UCO flow back to the dining table again [31]. It was medically proven that a repeated usage in the fryers would certainly turn it into a carcinogenic material [30]. However, no health hazards from frequent skin or eye contact

for extended exposures are expected unless a large amount of UCO vapour is inhaled [32]. Its utilisation as nutrient for livestock feeding was banned due to concerns of build-up through the food chain up to mankind [33]. Therefore billions of litres were produced yearly to be disposed-of somehow. In fact burning it was probably the most appropriate alternative way of disposal or at least size reduction. UCO disposal by incineration was an option since its emissions and residues were not considered as a real threat to the environment. They eventually degrade and merge into a certain life cycle. In the occasion of accidental spillage it is much less toxic than PD to human and to the aquatic life. Micro-organisms in the soil and water are very keen to decompose UCO into primary elements. However the continuous drainage to water bodies could increase the biochemical oxygen demand (BOD) and reduce the dissolved oxygen (DO) in the receiving water body below threshold levels of 4mg/l. This will result in a dead section in flowing streams or eutrophication in lakes [34].

Being a nonedible food waste with a high heat content encouraged the idea of incineration but as a fuel for industrial heating. In fact it was its physical properties that hindered its usage as a fuel in the transportation sector.

The highly sophisticated engine designs used nowadays were specifically designed to operate on petroleum products. A very narrow tolerance is left to account for fuel property variation throughout the seasons. Unfortunately, the physical properties of UCO were outside of these tolerances. The need for renewable energy resources created the biofuels side by side to wind and solar energies. Biodiesel was designed in the labs to act as a surrogate for petroleum diesel. However, the ethical debate about the utilisation of edible vegetable oils as a fuel increased the UCO chances to play a key role in diesel engines.

To be enlisted as a fuel for diesel engines, it was necessary to bring its physical properties to be comparable to those of PD. This started at an industrial level by UCO conversion to biodiesel through trans-esterification. However the fall in global oil prices and the amount of fossil energy consumed in the trans-esterification process made the fuel relatively expensive and less environmental friendly [35]. Laboratory analysis showed that UCO physical properties could be comparable to those of the PD by moderate heating [19, 36, 37]. This heat is actually obtainable for no extra cost or load on the engine. Engine rejected-heat recovery is quite sufficient to prepare the UCO for combustion [38]. Actually this opened a new horizon in on-board UCO

treatment and utilisation as a fuel in the transport sector. To this point UCO was proven to be cost effective and environmental friendly. However, question still arise about the combustion, engine performance and engine compliance to environmental standards. These questions will be addressed throughout this research. On the other hand what level of people awareness and incentives are needed to ensure the continuity of UCO flow in sufficient amounts to potential purification centres? Probably “Biofuel for UCO” is the answer for the incentive part.

2.2.1 The increasing interest in UCO for transportation

The EU Renewable Energy Directive (RED Dir. 2009/28/EC) set a mandatory target to achieve 20% petroleum fuel replacement by biofuels by 2020 [39]. This includes 17% replacement in heating and cooling, 26% replacement in electricity and 6% replacement in all kinds of transportation means. The UK ministry of transport reported an increasing interest in biodiesel production where UCO and other feedstock were used in the production.

Table 2.1 The annual growth in UCO dependence for road transport in the UK (Millions of Litres).

Obligation year	UCO			Other feedstock			Biodiesel	Diesel
	Produced in the UK	Imported	Total	Produced in the UK	Imported	Total		
Year 1 (2008/2009)	35.90	3.60	39.50	31.50	986.70	1018.20	1057.70	N/A
Year 2 (2009/2010)	29.90	13.10	43.00	71.60	998.70	1070.30	1113.30	24,371
Year 3 (2010/2011)	106.40	352.80	459.20	36.00	403.90	439.90	899.10	24,959
Year 4 (2011/2012)	155.90	667.50	823.40	25.40	81.15	106.55	930.00	25,567
Year 5 (2012/2013)	139.00	242.00	381.00	34.00	73.00	107.00	488.00	25,833
Year 6 (2013/2014)	143.00	465.00	608.00	57.00	194.00	251.00	859.00	26,333
Year 7 (2014/2015)	161.00	402.00	563.00	81.00	193.00	274.00	837.00	27,168

Source: Approved annual Renewable Transport Fuel Obligation reports 2008-2016.[28, 40-45]

Table 2.1 shows summarised data obtained from the Renewable Transport Fuel Obligation (RTFO) throughout the years 2008~2015. It is indicated that the amount of UCO collected locally increased 4.5 fold and the amount imported increased by more than 110 fold during the aforementioned period.

Table 2.2 reveals that UCO contribution in biodiesel production increased from 3.7% to more than 67% and biodiesel consumption in road transport increased from 0.18% to 3.08%. Although a drop in the industry demand occurred in the year 2012, the demand pace restored its high rate again in the next year.

Table 2.2 UCO contribution in biodiesel production, total diesel fuel required for road transport and in GHG savings in the UK.

Obligation year	UCO contribution to total biodiesel production %			BD consumption in road transport %			% GHG savings compared to PD
	Produced in the UK	Imported	Total	Produced in the UK	Imported	Total	
Year 1 (2008/2009)	3.40	0.34	3.73	N/A	N/A	N/A	85
Year 2 (2009/2010)	2.68	1.18	3.86	0.12	0.05	0.18	85
Year 3 (2010/2011)	11.80	39.20	51.00	0.43	1.41	1.84	84
Year 4 (2011/2012)	16.76	71.77	88.54	0.71	2.93	3.64	83
Year 5 (2012/2013)	28.48	49.60	78.07	0.67	1.22	1.89	80
Year 6 (2013/2014)	16.64	54.13	70.78	0.76	2.50	3.26	78
Year 7 (2014/2015)	19.23	48.03	67.26	0.71	2.29	3.08	78

Source: Approved annual Renewable Transport Fuel Obligation reports 2008-2016. [28, 40-45]

2.2.2 The life cycle assessment of UCO and the life cycle energy demand

Life cycle assessment (LCA) had been recently used to indicate the degree of renewability of surrogate fuels. The assessment comprises the impact of the fuel at different stages of production. These impacts might include the global warming potential, eutrophication potential, ozone depletion potential in the stratosphere, photochemical ozone creation potential in the troposphere, acidification potential and other environmental concerns. Therefore factors like fertilisers, pesticides were included to assess the amount of nitrous oxide N₂O emitted [46] from which 10% is NO_x, or the amount of polychlorinated hydrocarbons (PCBs) leachate to the ground waters or phosphate flow to the receiving surface water bodies [47]. Fossil energy consumed is another crucial issue in the LCA analysis. Petroleum diesel (PD) used in land cultivation, harvesting, irrigation and crop transportation could really affect the energy

efficiency of the surrogate fuel. Special software packages had been developed for certain fuels derived from agricultural origins. The final decisions on the degree of renewability for a certain crop is based on the balance between the amount of energy gained and the fossil energy consumed at different stages of the fuel production.

Sheehan et al.[26] elucidated that the imbalance between the duration of carbon release and sequestration causes the greenhouse effect. This time difference could take ages for the combustion of PD while the carbon release from the combustion of biofuels is used somewhere else by plants by photosynthesis.

They suggested the fossil energy ratio (FER) as a means to indicate the degree of renewability of a particular resource.

$$\mathbf{FER} = \mathbf{CV/E_{ff}} \quad \dots\dots\dots 2.1$$

where

CV is the calorific value for the renewable fuel [MJ/kg].

E_{ff} is the amount of fossil energy required to convert a defined mass of raw material to a renewable fuel [MJ/kg].

Therefore a fuel is considered as non-renewable if FER is less than unity, while a highly renewable fuel possesses a FER of infinity.

It is of great importance to indicate the amount of energy remained in the fuel product throughout the conversion process from the feedstock. This was referred to as the life cycle energy efficiency, defined as

$$\mathbf{\eta_{LC}} = \mathbf{CV/E_p} \quad \dots\dots\dots 2.2$$

where E_p is the total primary energy contained in the feedstock [MJ/kg].

In fact the UCO under investigation is expected to possess a very high η_{LC}. The fuel is keeping its potential energy since it undergoes purification by filtration, no matter is removed or energy dissipated.

Talens et al.[48] used the exergetic life cycle assessment ELCA approach to evaluate the environmental impacts of UCO as a fuel. The approach also accounts for the energies utilised in the production processes from natural resources other than the PD. Obviously hydroelectric or nuclear power in the fuel production significantly reduces the production cost and promotes the FER. They concluded that UCO is originally a waste and a scarce amount of energy is consumed to convert to fuel. Any further processing (trans-

esterification) using fossil fuels reduces its degree of renewability and increases the environmental impacts by 68%.

Fontaras et al. [49] researched the LCA for four crops, their products and by-products as potential raw materials for renewable fuel production as straight vegetable oil (SVO) or BD. They collected data from different production stages starting from the crop cultivation, irrigation, fertilization, protection, harvesting to the transportation, seed separation, oil extraction, drying, oil refinement and transesterification to process by the Global Emission Model for Integrated Systems (GEMIS) software. The fuels were also tested on a diesel passenger car for their performance and emissions acceptability. They concluded that SVO is more renewable and sustainable in terms of the GHG saving potential than biodiesel. Sunflower obtained the first position with a GHG saving of 58~71% followed by rapeseed oil with 48~62%, soya bean oil with 47-60% and cottonseed oil with 35~47%. The higher extremes are for the SVO. This was attributed to lower expenses and fossil fuel consumption as the sunflower SVO is rain irrigated and non-esterified. The minimum threshold for GHG saving for a biofuel is set to 35% aiming to 60% target by 2018 according to EU legislations. It is true that UCO is originally a SVO produced for food processing not as a fuel. However after frying it becomes a waste material. Therefore to use it as fuel its life cycle starts after the fryer.

As part of the current research, Li et al. [50] used LCA to determine the carbon saving by using purified used cooking oil (UCO) as a fuel in HGVs in comparison to UCO derived biodiesel and PD. Their analysis covered fuel production processes from well to wheel (W2W) which they professionally split to well to tank (W2T) and tank to wheel (T2W) respectively. The UK carbon calculator package, as a tool to meet the requirements of the Renewable Transport Fuel Obligation (RTFO), was used to facilitate the analysis. The researcher concluded that the direct usage of UCO in diesel engines reduces the carbon footprint by 54% compared to UCO-biodiesel and 98% compared to PD. Actually the huge CO₂ saving in the renewable surrogate lies in the (T2W) part which was set to zero for the renewables. This is because the amount of CO₂ produced from the combustion process is sequestered by plant photosynthesis, while PD combustion is releasing CO₂ which had been stored underground for long periods. Between the purified UCO and the transesterified UCO, the amount of CO₂ released from the trans-esterification process is nearly comparable to that released from the whole UCO production process. In addition there is a 10% reduction in the total yield of the biodiesel due to glycerol removal as a by-product. It could be inferred that a huge CO₂

saving is achievable by the direct usage of purified UCO with a little investment in HGV fuel system modification.

In fact a better CO₂ saving could be achieved if the amount of energy consumed in UCO waste management like sewer cleaning and waste water clarification before disposal or reuse was accounted for.

2.3 General properties of UCO in comparison to petroleum diesel and biodiesels

Annand et al. [51] compared the properties of non-esterified UCO to those of non-esterified palm oil, UCO driven biodiesel (UCOME) and PD as shown in table 2.3. Among the potential advantages of UCO properties are the cetane number and the heating value which are comparable to those of PD.

Table 2.3 UCO properties in comparison to UCOME, palm oil and No.2 PD

Property	Units	ASTM		Petroleum Diesel PD	Palm Oil	UCO	UCOME
		Standard	PD Limits				
Density @15°C	kg/m ³	D 1298	860-900	828.1	914.7	918.4	877.7
Kinematic Viscosity @40°C	cSt	D 445	1.9-6.0	2.417	39.49	45.34	4.731
Cetane Number	-	D 613	≥ 47	51	60	53	61
Calorific Value	MJ/kg	D 240	-	42.11	37.41	35.82	38.034
Cloud Point	°C	D 2500	-	0	22	24	20
Pour Point	°C	D 97	-15 to 10	-6	9	9	9
Flash Point	°C	D 93	>130	49	305	305	170
Fire Point	°C	D 93	-	55	310	345	190
Iodine Value	g I ₂ /100g	D 5554	120	-	56.74	92.5	64.32
Acid Value	mg KOH/g	D 664	≤ 0.80	-	7.24	2.896	0.38
Saponification	mg KOH/g oil	D 5558	-	-	205.63	195.48	182.78
Copper Strip Corrosion-3 hr, 100°C	-	-	Class 3	-	1(a)	1(a)	1(a)
Sulphur Content	% wt	D 5453	0.05	0.0492	0	0	0
Conradson Carbon Residue	% wt	D 189	0.2	0.002	0.004	0.01	0.002

Source: Anand et al. [51]

The high flash point and fire point are other advantages from the fire risk point of view. The zero sulphur content eliminates one of the PM precursors and exhaust after treatment poisoning. The disadvantages were mainly in the physical properties of UCO. Its density at 15°C is about 11% higher than that of PD and the kinematic viscosity at 40°C is 7.5 fold greater than the upper allowable limit of the American Standard for Testing Materials (ASTM) for PD and around 19 times higher than typical market PD specifications. The higher pour point and cloud point are very problematic in terms of fuel filter clogging and fuel transfer and pumping.

Winfield et al. [52] described UCO collected from the food industry, stored and blended with other waste oils, as very inconsistent. In addition to feedstock diversity, the impurities from frying different kinds of food consist of free fatty acids, polymers, chlorides and phospholipids, which cannot be adequately removed through the cleansing process. They strongly recommended UCO conversion to biodiesel through trans-esterification before usage as a fuel. This act purifies the methyl-ester and leaves the impurities within the glycerine fraction. It also reduces its viscosity and change the molecular structure. Additives like antifoaming agents, preservers and useful-life stretchers added to straight vegetable oils will certainly increase the diversity of UCO from place to place.

2.3.1 Cetane number

The cetane number could be defined as the measure of diesel fuel ignitability. Ignitability or auto-ignition is the start and the speed at which the heat is released. In conventional diesel combustion, cetane number covers the physical and chemical parts of auto-ignition. The physical part incorporates fuel atomisation, evaporation and mixing with air while the chemical part is the fuel reactivity[9]. In new diesel combustion strategies, the physical part is very much reduced mainly by the high injection pressure characteristics and the combustion chamber configuration. In addition to the high thermal and mechanical stress applied to the fuel spray the chemical delay is influenced by the fuel characteristics. Cetane number is related to the ignition delay property of the fuel. The larger the cetane number the shorter is the ignition delay. It has been detected that branched unsaturated hydrocarbons possess lower cetane number and poor ignition delay [53].

2.3.2 Ignition delay (ID)

Kalghatgi [1] defines the ID as the time interval between the start of injection (SOI) and the start of combustion (SOC). It reflects the resistance to

autoignition. The SOI could be determined by the moment at which the injector needle started to leave its seat. In optically accessible engines, the time of first appearance of the fuel from the injector hole is the SOI. The SOC is realised from the heat release history in the combustion chamber. As the fuel is injected, the atomised fuel droplets start to evaporate by the heat gain from the hot compressed air, which is in fact a negative heat release. As the evaporated fuel mixes with air it produces a combustible mixture and starts to ignite, which is considered as a positive heat release. A visual inspection for the heat release trace or when the derivative of heat release is changed from negative to positive is the SOC [9].

The ID is a matter of a physical and a chemical delays taking place in parallel. The fuel spray disperses conically in the combustion chamber which reduces the chances of droplet collision and build up in droplet size. Hence smaller droplets experience cycles of evaporation a cooling until they vanish. These droplets leave a conical vapour in the wake to interfere with those of other adjacent droplets. As this cloud of vapour ignites it is called the flame front. Larger droplets absorb the heat due to the temperature gradient between the surface and the centre of the droplet. Their high inertia make them overtake the smaller ones for a sudden explosion with a deeper penetration in the combustion chamber [9].

In fact the physical delay ends as the fuel air mixture becomes ignitable but the start of the chemical delay is difficult to predict.

During the chemical delay, larger fuel molecules degrade to smaller ones and with the presence of the oxygen, radicals are formed. The rate of chemical reactions increases exponentially with the increase in the amount of radicals formed and the mixture is said to be auto-ignitable [15].

The physical delay is controlled by the proper engine and fuel injection system design, while the chemical delay is influenced by the working gas characteristics, the reactivity and chemical characteristics of the fuel.

The HGV under investigation is powered by an engine in which the fuel injection pressure reaches 180 MPa. The fuel issues from seven 0.2 mm diameter orifices. This high pressure produces very fine fuel spherules, increases the spray cone angle and reduce fuel penetration. This will certainly reduce the physical ID especially at high power demands. Combustion chamber configuration, an inverted mushroom shaped void carved in the piston crown, keeps the atomised fuel at high temperatures. In addition, air inlet and exhaust ports are designed to produce high swirl and tumble in the

combustion chamber to provide better air-fuel mixing. The high engine compression ratio (18.5:1) which is high enough to bring the working gas to very high pressures and temperatures to assist the evaporation process and reduce the ID period.

2.3.3 Fuel properties affecting the physical delay

Kinematic viscosity

Kinematic viscosity is a measure of fluid resistance to flow. A Newtonian fluid flowing in a pipe under laminar conditions behave like a bundle of concentric cylinders flowing in the same direction with a velocity gradient. The one at the centre possesses the highest velocity and the outer cylinder retains zero velocity.

Hribernik and Kegl [33] compared the viscosity of UCO to that of type 2 PD. They reported 10 times higher UCO viscosity. However, heating the UCO up to 100°C reduces its viscosity 7 times. Blending the UCO with PD is another way for viscosity control. A 70% by 30% UCO/PD blend reduces the pure UCO viscosity by 50%. Triglycerides are diagnosed as the cause of the higher viscosities which had a direct effect on UCO atomisation and evaporation in the combustion chamber [53].

During the current research both of the strategies are implemented to tackle the high viscosity of UCO. On-board heating of the UCO and mixing with PD. Heat recovery from the engine coolant is used for UCO warming. Therefore the engine is made to start with PD to warm-up to the design temperature. As soon as the coolant circulation thermostat opens hot coolant passes through a heat-exchanger located in the UCO storage tank. The two fuels start to mix at different proportions according UCO temperature. The higher the UCO temperature the larger its content in the fuel blend. The high injection pressure is another factor to mitigate the viscosity effects.

Density

Density is the amount of matter contained in a unit volume. As explained earlier, the density of UCO is much higher than that of PD. This will primarily affect the injection process and the fuel dynamics in the combustion chamber. Denser fuels require higher injection pressures to perform the same as PD. Denser fuels possess higher inertia to penetrate deeper in the combustion chamber with a smaller spray angle [6, 54]. This will limit the mixture formation and increases the fuel-wall collision.

On-board UCO heating and the high fuel injection pressure of the HGV under investigation are expected to mitigate the adverse effects of high UCO density.

Surface tension

The surface tension is the force in the liquid-gas interaction surface. It holds the liquid configuration, as a spherule, against the internal and external pressure differences. Therefore a higher surface tension maintains the fuel droplet for a longer time before being collapsed especially at high droplet speeds [20]. Surface tension is inversely proportional to temperature [21].

In the current project, UCO surface tension is also controlled by the high fuel injection pressure, high combustion chamber temperature and mixing with PD at low UCO temperatures.

Fuel volatility

A volatile fuel is more ready to evaporate at lower temperatures. Diesel fuel consists of a range of components of different volatilities. During the fuel distillation process, fuel components of high volatility require lower distillation temperatures to evaporate leaving the less volatile components to evaporate at higher temperatures. Therefore, the distillation characteristics of the fuel shows how readily given percentages of the fuel volatilize [9]. For instance, T95 is the temperature at which 95% of the fuel evaporates. The higher the T95 the lower is the volatility characteristic of the fuel. SVO possess a higher distillation temperature for all its fractions up to T80 at which it coincides with that of PD as shown in fig.2.1. Above T80 the distillation temperature of PD become higher than that of SVO [19].

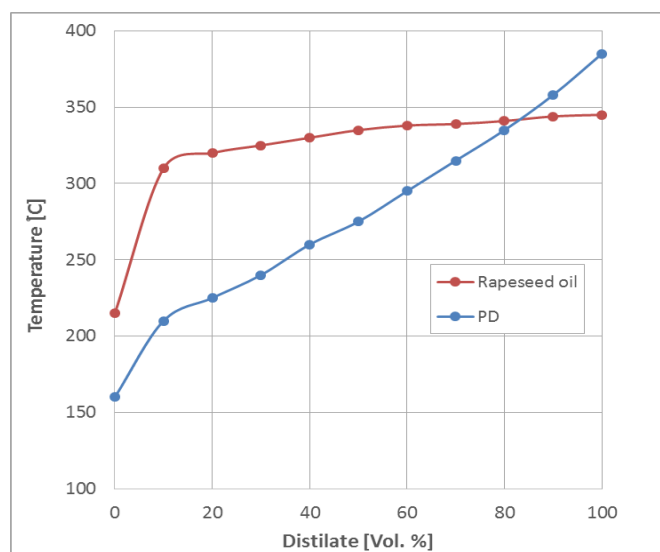


Figure 2.1 Comparison between distillation curves of PD and rapeseed oil. Reproduced from [19].

In fact, the volatility property of the fuel affects the physical delay part of ID and thereby the fuel jet characteristics. High pressure fuel injection systems are quite successful in minimising the mean droplet size ready for evaporation, however it is the fuel volatility that play the leading role in fuel evaporation thereafter. In that context, low volatile fuels droplets might evaporate later or continue to flow until they reach the relatively colder cylinder walls and accumulate. Incomplete combustion and higher HC emissions is witnessed as the T95 increases especially in HGV [55].

In the current research, the compression ratio of the engine under investigation is 18.5:1 which is high enough to increase the compressed air temperature to very high levels suitable for UCO evaporation.

2.4 Diesel technology

Modern diesel engines are predominantly four stroke engines. Their thermodynamic principle is based on the air-standard cycle or the diesel dual cycle. The fuel is injected late in the compression stroke and spontaneously ignited under high compression pressures. This is where the diesel engine acquired its name as a compression ignition (CI) engine. These engines usually possess high compression ratios up to (23:1) which describes the number of volume reductions as the piston moves from the bottom dead centre (BDC) to the top dead centre (TDC). This requires a longer stroke length and a larger crank arm. During the suction stroke, air flows to fill the vacuum produced as the piston travels away from its upper dwell at TDC. At the end of the compression stroke, as the piston is close to its upper dwell, fuel is injected as a spray under a very high pressure up to (200 MPa). Unlike the petrol engine, the amount of fuel injected controls the engine output not air throttling which adversely affects the performance under partial throttle operation. The main conundrum in diesel operation is the limited time for mixture formation before the start of combustion (SOC). To mix means to bring the fuel to the gaseous phase, the same as the air. This is partially solved by the high injection pressure for a very fine atomisation of the fuel. The high in-cylinder global temperature and fuel volatility do the rest. The time interval between the start of injection (SOI) and the start of combustion (SOC) is called the ignition delay (ID). The fuel injection pressure might vary according to the load and speed, which leads to different fuel spray characteristics at different operational conditions. Combustion chamber design and configuration play a major role in the fuel handling and the degree of mixture homogeneity. Higher

combustion efficiencies can be facilitated by preventing fuel-wall impingement and enhanced air swirls and tumbles. Again the long piston travel throughout the power stroke provides a longer residence time and exhaust gas cooling. The exhaust gases are forced to leave the cylinder by the scavenging action of the piston and exhaust valve opening. The amount of exhaust gas entrapped in the cylinder as a gas residue depends mainly on the number of exhaust valves, exhaust back pressure and engine speed. From the point of fuel injection on going, every single action plays a crucial role in engine performance and emissions [56-59].

The HGV under investigation is a EURO 5 emissions standard compliant vehicle. It is powered by Mercedes-Benz OM 457 LA engine. The engine is a 6-cylinder inline, four stroke, turbocharged DICl engine. A list of engine specifications is demonstrated in table 3.1. These specifications combined with combustion chamber configuration and the high pressure fuel injection system are expected to deliver a high performance operation with relatively low emissions especially the particulate matter PM (as explained in chapter 6). It is also expected that the HGV under investigation will tolerate the use of fuels other than PD. In order to facilitate the use of UCO as a fuel, Bioltec system is fitted to the fuel system to deliver UCO and PD blends to the engine. The fuel blending ratio depends on UCO temperature and the electronic commands from the engine control unit (ECU). These commands are based on preloaded engine performance maps.

2.5 The vehicle: heavy goods vehicle (HGV) and real world driving conditions (RWDC)

2.5.1 The capacity of HGVs and their usage in the UK and their contribution in pollution

According to the UK ministry of transport the number of the HGVs increased by 63 thousand vehicles during the last two decades [60]. The total number of HGVs became 483.77 thousand in the third quarter of 2015. Fig.2.2 illustrates that the number of light goods vehicles (LGVs) increased dramatically during the same period to reach 3.623 million vehicles with an increase of 1.486 million vehicles during the last two decades.

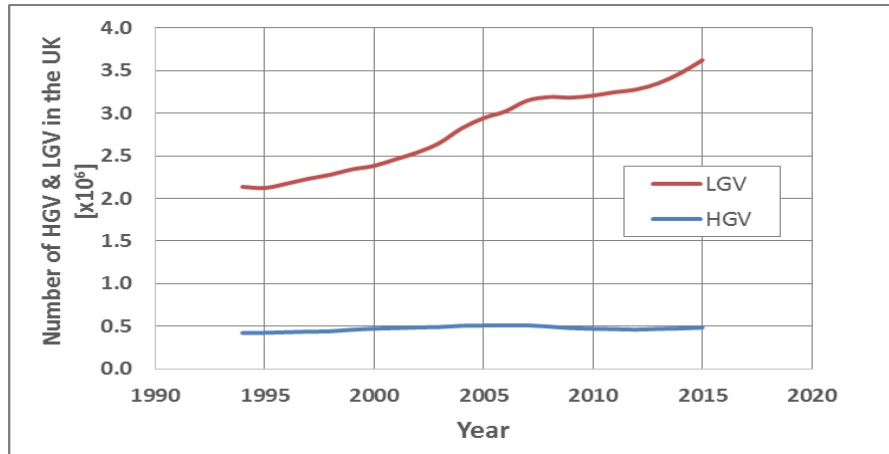


Figure 2.2 The number of licenced HGV and LGV in the UK 1994-2015.[60]

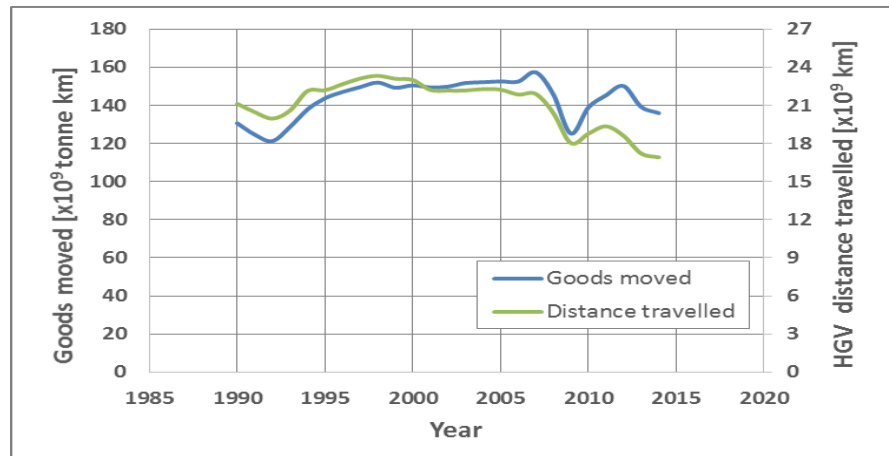


Figure 2.3 Goods moved and vehicle kilometres, annual, 1990 – 2014.[61]

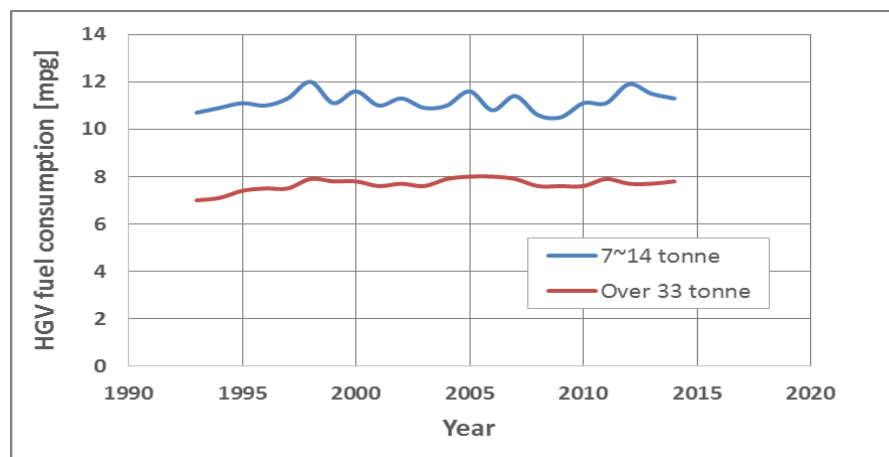


Figure 2.4 Fuel consumption by HGV travelling fully loaded or with an empty trailer in Great Britain, 1993 – 2014 [62]

Fig.2.3 depicts the annual amount of goods moved in billion tonne km and the distance travelled by HGVs during the period 1990-2014. The typical mileage recorded for HGVs running loaded or empty is illustrated in fig.2.4. The data were built on the fleet operator records of fuel consumption or the amount of fuel used from their own fuel supplies.

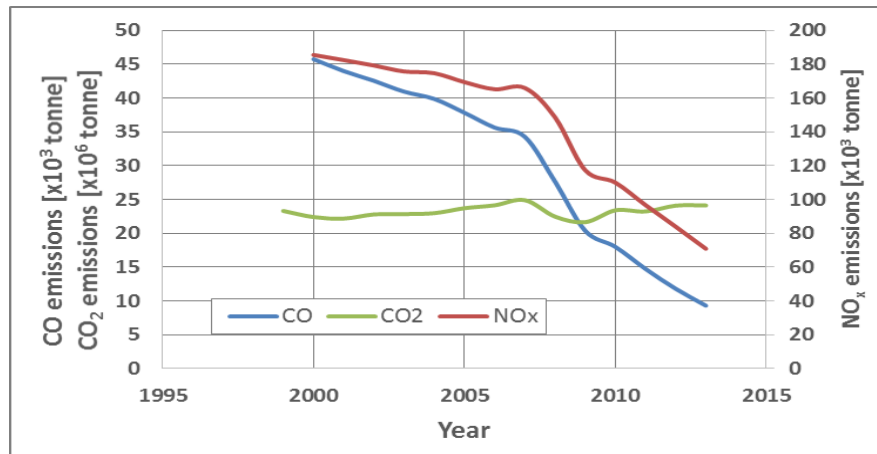


Figure 2.5 Gaseous emissions from HGV 1999-2013. [63, 64]

Despite the numerous increases in the road transport in the UK during time interval between 1999-2013, the pollution indicators from HGVs are quite optimistic [64]. Fig.2.5 shows that CO emissions dropped from 46 thousand tonnes per annum to just 9 thousand tonnes per annum or an 80.43% reduction. NO_x declined from 186 thousand tonnes per annum to 71 thousand tonnes which represents a 61.8% decrease. In contrast, the increase in the number HGVs inevitably results in CO₂ increases. The figure shows that CO₂ emissions increased from 23.3 million tonnes per annum to 24.1 million tonnes per annum in the time interval between 1999~2013 [63].

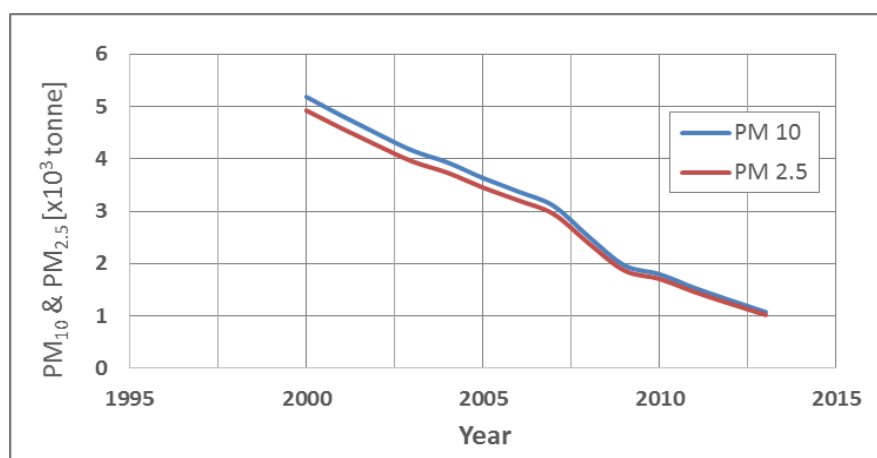


Figure 2.6 PM emissions from HGVs in the UK 2000-2013.[64]

Particulate matter from HGVs had been mitigated by 80% between 2000-2013 [64] as shown in fig.2.6. In fact the drastic progress in engine and exhaust aftertreatment technologies with a slight support of the biofuels were the driving force behind the aforementioned pollution mitigation. Nevertheless this wasn't the case for CO₂ as it depends mainly on the amount of fuel consumed and the increase in the number of vehicles.

The HGV under investigation is a EURO 5 emissions standard compliant vehicle. According to the manufacturer, the engine is designed to suppress PM within the combustion process and to tackle gaseous emissions through exhaust aftertreatment facilities. In fact the high combustion temperature reduces CO and THC emissions, however it increases NO_x emissions. The engine manufacturer selected the selective catalytic reduction (SCR) as an exhaust aftertreatment facility to tackle NO_x emissions.

2.5.2 Real world testing conditions

Laboratory tests are usually designed to simulate the real world conditions. Steady state cycles are designed to simulate vehicle travel at constant speed, which could be high or low speed on an elevated road. Transient cycles simulate vehicle acceleration and deceleration. These tests can be performed at different loads. The particularity of real world tests lies in bringing more realistic factors into vehicle operation and performance. Driver's behaviour as he/she interacts with speed limits and traffic regulations that affect vehicle performance are not accounted for in the lab tests. Similarly, sudden variations in ambient temperature and humidity at different road segments in conjunction with road gradient throughout the journey are not easy to provide in the lab. There is one more engine operation which is unachievable in the lab or test rigs. It is the case of a loaded vehicle moving downhill. The increase in load in this particular case is increasing the vehicle kinetic energy rather than hindering the vehicle motion.

As road emissions standards are increasingly becoming more stringent, and since the combustion process is controlled by the ECU to provide different operational modes. These modes compromise between fuel economy, power and emissions. Some engine manufacturers used specially designed algorithms and electronic circuits to change the combustion mode during the lab tests. During in-vitro emissions checks, the ECU automatically sacrifices fuel economy for lower emissions [27]. This can be accomplished by retarding the fuel injection timing for a few crank angle degrees automatically by the

ECU. Eventually the vehicle brand survives the emissions tests without meeting the specified standards.

HGV engine emission certification tests are usually performed by in vitro engine-dynamometer tests. The engine is tested according to a specially designed real world simulated test cycles. Incorporating the engine control unit (ECU), for a better engine performance management at multi-operational modes, increases the difficulty of engine emissions rate measurements. To achieve the best fuel economy rates, the ECU allows engine emissions to exceed the certification standards. However, during the engine emission test it turns the engine operation to the low emission mode [27]. This was the main motivation for the environmental bodies like the Environmental Protection Agency (EPA) and California Air Resources Board (CARB) to adopt the on-road diesel engine emissions tests at Not-to-Exceed (NTE) engine operation zone.

Engines are usually built and calibrated to meet specified applications. The operational ranges at which the engines run are different from one application to another. LGVs, HGVs, urban buses and off-road machinery perform differently. These application needs special design and calibration requirements. Therefore even in real world tests, the specified vehicle should be tested in its design range called NTE [65].

Emissions measurement in confined places like tunnels are applicable to measure the amount of pollution load exerted by a known number of vehicles traveling through the tunnel. The results don't reflect the emissions from a targeted vehicle type at different operational modes. The diversity of the vehicle using the tunnel, their engines, type of fuel used and the unique vehicle operation mode, limited the capabilities of this method [66].

Road-side remote sensing is an automatic and accurate instantaneous emissions measurement technique. These are usually stationary units located at per-specified locations to be monitored. It could give a good indication of the effects of road transport on emission in that area. It is quite difficult to install them in congested commercial places in the city centre. Therefore, vehicle testing using portable emissions measurement (PEM) under real world driving conditions could be the most appropriate technique for emissions and fuel consumption measurement. A vehicle of a specified load category and compliance to emissions standards could be tested with different types of fuels or fuel blends. The tests might incorporate vehicle rolling resistance, acceleration resistance, gradient resistance, payload, different weather

conditions, spontaneous variation in the driving modes and driver's behaviour if needed [66].

2.5.2.1 Vehicle specific power

It is quite appropriate to use ECU broadcasted data in HGV real world tests. Engine speed fuel mileage and engine torque and power developed to withstand the road load is accessible. Moynahan et al.[67] developed a vehicle road load model to verify vehicle ECU power broadcast obtained from real world driving conditions. Although the broadcasted data do not account for the gearbox and final drive efficiencies, they declared that the data were still reliable and could be corrected for the missing efficiencies.

In the current project, engine load factor (LF) which is actually a measure in percentage for the amount of external load exerted on the engine. This was the only engine broadcast data accessible in the tests. It was accompanied by the Bioltec fuel mixing system data (explained in chapters 3 and 5).

Alternatively, the road load can be calculated using the vehicle specific power (VSP). The VSP is defined as the instantaneous vehicle power normalised to its mass in a third-order polynomial of vehicle velocity that incorporates the rolling, aerodynamic, acceleration and road gradient resistances. Koupal et al. [68] developed a VSP general model that accounts for all the aforementioned resistances. The model is resilient and modifiable to apply to all vehicle categories by changing the coefficients of the resistance terms. These coefficients vary with the vehicle payload.

$$VSP_t = 0.0661V_t + \left[\frac{2.89 \cdot 10^{-3}}{m} + 4.2 \cdot 10^{-5} \right] V_t^3 + V_t a_t + g V_t \sin \theta_t \quad \dots\dots 2.3$$

where

VSP_t is the instantaneous vehicle specific power [kW/tonne]

V_t is the HGV instantaneous velocity [m/s]

m is the HGV mass [tonne]

a_t is the HGV instantaneous acceleration [m/s^2]

g is the gravitational acceleration [m/s^2]

θ is the road gradient [rad].

2.5.2.2 Vehicle speed, acceleration and road gradient

Moynahan et al.[67] used the vehicle ECU data as one source for vehicle velocity measurement. The ECU actually collects the vehicle velocity from a speed pick-up sensor that measures the rotational speed on the main transmission shaft in the vehicle gearbox. The ECU is calibrated to convert the rotational velocity to vehicle velocity. A GPS with an antenna fitted on the vehicle roof was also used for ECU velocity data verification. The GPS used the satellite to define the vehicle position, height and speed. Using a data acquisition unit, the velocity data were recorded at 1 Hz then converted to 5 Hz through a specific software. To smooth-out the noise in GPS data, they used vehicle maximum possible acceleration of 4.4 m/s². If the speed difference between any two consecutive velocity readings resulted in an acceleration higher than 4.4 m/s² the velocity reading was changed by the previous reading.

Kinsey et al.[69] used the diesel emissions aerosol laboratory (DEAL) on-board a diesel powered tractor-trailer to measure both the HGV exhaust emissions and the road emissions back-ground. The project was evaluating the differences in engine emissions from petroleum diesel and B20 biodiesel.

In addition to ECU velocity data, they used the (Datron DLS1) instrument for HGV velocity measurement. The instrument is an optical system used to measure the speed of objects moving across its illuminated field of vision. The instrument was fixed to the HGV chassis facing the pavement to detect road irregularities as moving objects. The output was a voltage signal proportional to HGV velocity.

Racelogic II (Vbov) (explained in detail in chapter 3) is the instrument used to measure HGV velocity in the current research. The instrument is a GPS that receives signals from the satellites through its roof mounted antenna. The signals are amplified and logged to laptop a computer through the Daqview data logger. In addition to the velocity, HGV position, elevation and heading against the north direction was obtained.

Moynahan et al.[67] proposed a five point central difference numerical differential as a means for vehicle velocity correction as follows:

$$\mathbf{a} = \frac{-\mathbf{V}_{i+2} + 8\mathbf{V}_{i+1} - 8\mathbf{V}_{i-1} + \mathbf{V}_{i-2}}{12\Delta t} \dots\dots\dots 2.4$$

where

a is the vehicle acceleration at time t [m/s²]

V is the velocity reading [m/s]

Δt is the time increment between two velocity readings in [s]

For velocities less than 16km/h, the researchers set vehicle acceleration equal to zero to avoid the noise in the high resolution velocity readings.

The corrected vehicle velocity data were used to calculate the distance travelled by the vehicle as follows:

$$d_i = d_{i-1} + V_i * \Delta t \quad \dots\dots\dots 2.5$$

where

d is the distance travelled by the vehicle, along the road, at time Δt in [m].

The road gradient was found by the inclination angle θ

$$\theta = \tan^{-1} \frac{\Delta h}{\Delta d_h} \quad \dots\dots\dots 2.6$$

where

Δh is the change in height between two points at the bottom and top of an inclination [m]

Δd_h is the horizontal distance between the selected Δh points [m].

The change in height (Δh) could either be measured by the GPS or a micro piezometer with corrections for the any pressure errors obtained from vehicle movement at high velocities [69].

The same procedure was adopted in the current research to calculate the HGV dynamics and VSP (as explained in chapter 3).

2.6 The impact of renewable fuels on engine components and performance

2.6.1 The impact of renewable fuels on engine components

Fraer et al.[70] investigated the effect of biodiesel B20 on different engine parts through a comparative research. Eight trucks from the United States Postal Services (USPS) were investigated. Four 1993 Ford 9-tonne cargo vans each powered by a 6 cylinder 7.8 litre engine and four 1996 Mack

articulated trucks each powered by a 6 cylinder 12 litre engine. Two of each group were operated on B20 and the others on PD. The study was a four year program between 2000~2004 during which the vehicles ran on B20 for 960,000 km accumulated distance. The engines and fuel systems were removed, disassembled, and inspected. They reported no discernible differences in engine part wear, except sludge build up on the valves deck around the rocker assemblies was seen. This was attributed to out-of-specification B20 fuel batches in one of the Mack trucks as biodiesels contain relatively high concentrations of sodium from the transesterification process. A PD fuelled Ford truck had big end and main bearings failure due to unidentified improper lubrication.

Chase et al.[71] ran durability and performance tests on two heavy duty Caterpillar engines with rated power output of 435 hp. They used hydrogenated soy ethyl ester (HySEE) 1:1 blends with type-2 PD. The first engine was conditioned and bench tested for pollution investigation, while the second was mounted on a Kenworth heavy duty truck. The test vehicle consumed 70,379 litres of HySEE and a total of 145,746 litres of fuel and ran for 326,235 km. Their results showed that using the arctic package and vehicle indoor parking allowed the vehicle to operate in all weather conditions. Engine teardown showed no accelerated engine degradation and the vehicle was expected to run for more than 1.6 million km.

Nishimura et al.[72] examined the impact of UCO-BD on engine lubricating oil performance in a fleet of seven cargo vehicles. They focused on engine wear and high temperature corrosion. The results were compared to those obtained from their bench tests. They concluded that engines fitted with a diesel particulate filter (DPF) exhibited higher oil viscosity reduction and more lubrication oil dilution by the fuel. This was attributed to the increase in back-pressure due to prolonged post injection period for DPF regeneration. The higher back-pressure enhances the blow-by process and as the UCO-BD possesses a higher boiling point than PD, it tends to remain for extended periods of time in the oil sump. They also observed a steady state lubrication oil level in the sump for the vehicles fuelled with UCO-BD. This was related to the equilibrium between the higher lubrication oil dilution and consumption. Laboratory tests for anti-wear characteristics using the four-ball machine revealed that a combination of UCO-BD with fresh lubrication oil showed minimum wear scar or the highest anti-wear performance. They concluded that UCO-BD has an anti-wear effect which counteracts oil degradation due to dilution with fuel. Copper and lead corrosion were higher in a mixture of

20% UCO biodiesel and fresh lubrication oil compared to an analogous mixture with used lubrication oil. This was attributed to the formation of the carboxylic acids from the degradation of the UCO and the oil which was higher in the case of the mixture with used oil.

Fazal et al.[73] studied the effect of palm oil derived biodiesel on the degradation of metal parts of the engine and compared the results to those of PD. The study was conducted on four metals namely, copper, brass, aluminium, and cast iron. The metals were immersed in the fuels for 2880 hours at 25~27°C then examined by X-ray diffraction (XRD) and scanning electron microscopy (SEM/EDS). They concluded that BD is more corrosive than the PD. The metals showed different responses to the BD. Their response from the most affected was Cu, BS, Al, and Fe respectively. Different metal compounds were found on the exposed surfaces and the biofuel degraded at different levels while embracing the metals. The response of BD from the worst to the less affected was Cu, BS, Al, and Fe respectively.

Shahid and Jamal [74] concluded in their review the suitability of vegetable oils derived biodiesel as alternative fuels. They stated that more care and periodic services are required for the engines operated with BD's due to the higher carbon deposits in the combustion chamber and particularly on nozzle tips. Fraer et al [70] found no differences in fuel injection pump wear and performance with the exception of Mack trucks fuelled with the B20. They were more susceptible to fuel injector and fuel filter replacements because of the out-of-specification fuel batches, the biological contamination of the fuel and the larger amounts of fuel circulation in the fuel system.

In the current research, a thorough investigation for the combustion chamber configuration, revealed that it is hard for the fuel to reach the cylinder walls or piston rings to result in any deposits or damage. Therefore engine deterioration and deposit accumulation was planned to be inspected periodically through fuel injector inspection. A couple of fuel injectors from different cylinders were removed for inspection to indicate the effect of deposit aging at different HGV mileages (as explained in Chapters 3 and 5).

2.6.2 The impact of UCO on engine performance

Hribernik and Kegl.[75] installed a piezoelectric pressure probe in the pre-chamber and an inductive sensor to produce an indicated pressure and injector-needle lift histories respectively. With the aid of LabVIEW software,

they were able to measure the pressure-time history to predict the rate of heat release (RHR). They studied the combustion of UCO in a four cylinder, four stroke, 1.6 litre, indirect injection (IDI) diesel engine. PD was the base fuel. Blended fuels from UCO and PD were prepared. Namely a 50% UCO by 50% PD called UCO50 and a 75% UCO by 25% PD called UCO75. They stated that even though the fuel nozzles open faster with the increase of the amount of UCO in the blend, the pre-chamber pressure rise started at the same time for the three fuels. This was attributed to the longer ignition delay periods which were directly proportional to the increase of the amount of the UCO in the blend. This was followed by a poor fuel atomisation and evaporation due to the higher viscosities of the fuels with higher UCO content. As the combustion process proceeded in the main chamber they observed increased oscillation amplitudes with the increase in UCO content in the blends 7J/°CA and 12J/°CA for UCO50 and UCO75 respectively while the oscillation frequency remained constant at 2000 Hz. The oscillation amplitude did not affect the duration of combustion but it adversely affected the combustion stability. The higher the oscillation amplitude was, the greater the degree of combustion instability. They also believed that these oscillation amplitudes adversely affected the efficiency of combustion and increased HC and CO emissions. Their results also showed that the output power was identical for the fuels even though the CV of UCO was 13% lower than that of the PD. This was attributed to the higher density of the UCO (12.5% higher than PD) being injected per cycle and a larger quantity as well due to the higher pressures and prolonged duration of the injection of UCO. The engine delivered higher torques at low speeds. The study also revealed a faster decrease in torque and power due to the way the fuel interacted with the fuel injection pump. The fuel injection pump governor starts to reduce fuel delivery to the engine faster than the case with the PD.

In fact the effect of fuel property differences between UCO and PD in the current research is minimised by the on-board UCO heating process. Therefore UCO is heated prior to its mixing with PD and delivery to the fuel injection pump. Engine design and the extremely high injection pressures were expected to improve fuel injection properties and the combustion process.

2.6.3 The fuel injection system in CI engines

Fuel injection systems used in diesel engines could be classified as the individual injection system and the common-rail system. In both cases a low

pressure transfer pump transfers the fuel from the fuel tank through the filter to the fuel injection pump. In the individual injection system a separate pumping and metering unit is allocated for each cylinder. In early designs for small applications, the pumping and metering units were held together in an inline arrangement in a block. The pumping action was performed by reciprocating plungers, actuated by a camshaft incorporated in the same block, and retaining spring. The metering was performed by a rack connected to the accelerator and a pinion for each plunger. To avoid any sudden fuel cut, the rack position was controlled by a centrifugal governor. For larger applications, these pumping and metering units were fitted to each cylinder separately. Fuel under high pressure was delivered to the injectors which were installed in one per cylinder. In other designs, the pumping and metering units were held together in a cylindrical configuration called the rotary pump actuated by a ring cam. The individual pump system was also known as the pump-line-nozzle. The material, thickness and length of the lines became very problematic as the demand for higher injection pressures increased. Pressure surges and variations in pressure intensity and timing were witnessed from cylinder to cylinder and cycle to cycle. The differences in line lengths and the continuous pressure build-up and release per cycle were behind these variations. Therefore more stiff, smaller and shorter fuel lines were the remedy. To facilitate this kind of arrangement individual fuel pumps were installed separately in the cylinder block and actuated by the engine camshaft, while the fuel metering was achieved by electromagnetically controlled fuel injectors. This is the design adopted by Mercedes-Benz in the current test vehicle. The maximum injection pressure is 180 MPa produced by each individual fuel injection pump (see fig.3.3). Therefore these individual pumps should be calibrated to deliver the same amount of fuel at the same timing and pressure. The injector nozzle comprises seven 0.2 mm diameter holes. The injector is centrally positioned in the cylinder-head to face the piston-crown carved combustion chamber. The fuel system needs a special adaptation to protect the fuel injection system and maintain the high engine performance as UCO is directly used as a fuel. Therefore, Bioltec system is fitted to the HGV under investigation prior to the fuel injection pump. A heat exchanger is also placed in the UCO storage tank to warm-up the UCO. Properly mixed fuel blends, in different proportions according to UCO temperature and engine demand, are delivered to the fuel injection pump.

In order to eliminate the pipelines, the individual pumps and injectors were put together as one unit on the cylinder head and actuated by a camshaft. This

design is called the unit-injector. The injection pressure increases with engine speed, a high pressure fuel injection system could produce a pressure of 25 MPa at idle speed, 135 MPa at normal speeds and 160 MPa at high speeds. The mean fuel droplets become smaller as the injection pressure increases. Therefore a better fuel atomisation is expected at higher speeds [76].

The common rail system, known as high pressure common rail (HPCR) was profoundly designed to tackle the pressure variations and surges [9]. Fuel at pressures as high as the injection pressure, is produced by a high pressure pump, which could be the rotary type with one outlet, and delivered to the common rail. The common rail is a thick-walled small diameter cylinder connected to the fuel injectors through short pipes. As the high pressure pump is in continuous operation, there is a stand by fuel in the common rail at the injection pressure. In fact this system configuration with the aid of electronically operated fuel injectors provides the advantage of multi-injection strategy [10]. To reduce the ID period and emissions formation pilot injections were introduced, 4 ms before the main injection, to undergo the preflame reactions for the main injection [11]. Multi-main injections are also possible with the HPCR system [77].

2.6.4 Fuel spray characteristics

The fuel spray configuration is a decisive factor in compression ignition (CI) engine operation. It mainly depends on the fuel characteristics and in-cylinder global environment. Undoubtedly the design of the fuel injection system is based on PD characteristics. However, due to some extreme weather conditions auxiliary units are fitted to work in conjunction to the fuel injection system to rectify the combustion conditions to the normal diesel operation.

2.6.4.1 Fuel jet penetration length

The fuel jet penetration length could be defined as the maximum distance reached by the fuel jet before wall collision. Wakuri et al.[54] developed a fuel jet model based on the momentum theory with the negligence of the relative motion between the fuel droplets and the surrounding air.

$$S = 1.189 C_d^{0.25} \left[\frac{\Delta P}{\rho_g} \right]^{0.25} \left[\frac{d_o t}{\tan \alpha} \right]^{0.5} \dots\dots\dots 2.7$$

where

ΔP is the pressure drop across the nozzle opening [Pa].

d_o is the nozzle hole outlet diameter [m].

ρ_g is the gas density [kg/m³].

α is the fuel jet cone angle [Deg.].

t is the time measured from the start of injection [μ s].

C_d is the coefficient of discharge for the nozzle opening which could be found by the following equation proposed by Dernette et al.[6]

$$C_d = 1 - 5.26 v_f^{-0.06} \cdot \Delta P^{-0.73} - \left[\frac{-400 v_f^{-0.74} \cdot \Delta P^{-0.51}}{Re^{0.54}} \right] \dots\dots\dots 2.8$$

where

Re is the Reynolds number for the flowing fuel.

ΔP is the pressure drop across the nozzle opening [MPa].

v_f is the fuel kinematic viscosity [cSt]

$$Re = \frac{V_{th} \cdot d_o}{v_f} \dots\dots\dots 2.9$$

V_{th} is the theoretical fuel velocity issuing from the nozzle opening [m/s].

$$V_{th} = \left[\frac{2 \Delta P}{\rho_f} \right]^{0.5} \dots\dots\dots 2.10$$

Where

ρ_f is the fuel density [kg/m³]

Martinez et al.[78] reported that C_d has a very limited effect on the jet penetration length, they mentioned a variation of 3% in the penetration length for C_d variation between 0.58 to 0.87. However it affects the cavitation phenomenon in the nozzle. They also found a strong direct proportion between the jet penetration length and the nozzle diameter.

2.6.4.2 Fuel mean droplet size

Sauter mean diameter (SMD) is defined as the mean diameter of the fuel droplets that have the same surface area to volume ratio. It is a crucial indicator for the fuel atomisation and mixing with air. The smaller the droplet

size the better the mixing process. Equation 2.11 is a model proposed by Dernette et al.[6] for SMD determination under high injection pressures.

$$\text{SMD} = 9.57 \cdot V_{\text{act}}^{-0.37} \cdot \rho_g^{0.21} \cdot \rho_f^{0.28} \cdot e^{0.03v_f} \quad \dots\dots\dots 2.11$$

Where

e is the exponent of kinematic viscosity

2.6.4.3 Fuel spray cone angle

Agarwal and Chaudhury [79] defined the spray cone angle as the largest angle formed by two straight lines from the nozzle hole to the spray boundary. A model proposed by Dernette et al.[6] was used for spray cone angle determination.

$$\tan \frac{\alpha}{2} = 0.24 \left[\frac{\rho_g}{\rho_f} \right]^{0.24} \cdot \Delta P^{0.08} \cdot e^{-0.24 \Delta P^{-0.58}} \cdot v_f \quad \dots\dots\dots 2.12$$

2.6.4.4 Fuel jet velocity

V_{act} is the actual initial fuel velocity issuing from the nozzle opening. Fuel jet velocity decreases as the jet penetration increases due to the high frictional shear and aerodynamic drag which increases the jet cross-sectional area.

$$V_{\text{act}} = C_d V_{\text{th}} \quad \dots\dots\dots 2.13$$

2.6.5 Deposit formation mechanisms in and around the injector nozzle

Lüft et al.[80] studied the effect of different nozzle geometries on the combustion and emissions of a single cylinder turbocharged diesel engine with a fuel pressure up to 1800 bar. They concluded that relatively large and un-tapered nozzle holes improve the combustion of rapeseed oil biodiesel. This was related to the higher kinematic viscosity and surface tension of the biodiesel which wets the injector surface and holes and the high cetane number results in a faster combustion process to increase the intensity of heat near the nozzles. The net result would be fuel coking and injector clogging. In

comparison to PD, they declared a reduction in almost all the emissions except NO_x. This was attributed to the extra amount of oxygen in the biodiesel which on the other hand reduced smoke emissions.

Goosen et al.[81] referred to the higher bulk modulus of elasticity of the biodiesels which results in earlier nozzle opening and advanced ignition timing. This effect combined with the higher cetane number of the biodiesel could cause higher heat intensity in the vicinity of the injectors and more possibility of coking. High intensity combustion peak pressure and engine knocking is more likely to take place leading to lower power output.

Kalam and Masjuki [82] investigated the emissions and combustion chamber deposits resulting from the combustion of preheated crude palm oil, as an SVO, and its emulsions with 1%, 2% and 3% water in comparison to PD. The tests were accomplished in 100 hours for each kind of fuel then the engine was dismantled to find out the nature and amount of the deposits. The engine was a four stroke water cooled single cylinder DI diesel engine. The tests were conducted at a constant speed of 2700 rpm and 5.5 Nm load. They concluded that the physicochemical properties of preheated SVO are similar to those of the PD therefore it is suitable for long term engine runs. Lower CO and HC emissions were witnessed and lower fixed carbon deposits were found in the combustion chamber compared to SVO emulsions and the PD as well. They also stated that preheating the SVO increases the NO_x compared to the SVO emulsions due to water presence in the emulsions which reduced the combustion temperature.

In the current research, fuel injector deposits and deposit aging were inspected periodically according to a HGV mileage schedule. The injector nozzle and needle were inspected by scanning electron microscopy (SEM) for size and geometrical and morphological analysis. Energy dispersive x-ray (EDX) was also used for deposit material analysis. The results are demonstrated in chapter 5.

2.6.6 The impact of UCO on the fuel injection system and process

Rosca et al.[83] used UCO derived biodiesel in a DI diesel engine. They observed an earlier start of combustion which increased the rate of emissions, decreased the peak mean effective pressure (mep), the rate of pressure rise and engine output. Therefore they suggested higher injector pressure and

precise injection timing for the reduction of the emissions and engine performance enhancement. Fuel injection timing retardation for a few crank angle CA degrees was recommended as a remedy, because it compensated for the reduced ignition delay period and high heat release near the injectors.

Dernotte et al.[12] conducted an experimental study on the effect of the variation of fuel viscosity and density on the flow characteristics through nozzle orifices. Their experiments were carried out on three conical convergent orifices using nine fuels. Their study revealed that increasing the fuel kinematic viscosity ν_f from 0.6–7.0 mm²/s reduces the discharge coefficient C_d by 10% for a pressure drop ΔP across the orifice of 25 MPa and reduces C_d by 2% for ΔP of 55 MPa. No tangible effect of viscosity was observed for higher ΔP up to 180 MPa. They also found that fuel density ρ_f does not affect the discharge coefficient.

Hribernik and Kegl [75] examined the injector needle lift timing and duration and the pressure–time history for the injection system. The study revealed 10% volumetric increase in the amount of UCO75 injected in comparison to PD especially at high speeds. A longer injection duration for the UCO75 was also witnessed at all engine speeds and an injection advancement was observed at low engine speeds. These might be related to the higher Bulk modulus of elasticity of the UCO which resulted in injection advancement. Although the injection pressure-time history for the two fuels had the same profile, a 13% higher maximum injection pressure was observed for the UCO75. A 0.5°CA earlier nozzle opening and 1°CA later nozzle closer than the PD was observed.

Winfried et al.[84] explained the effect of impurities, un-dissolvable matter and organic compounds containing high nitrogen can plug up the nozzles and cause carbon deposits in the combustion chamber and the outlets. Non-esterified free fatty acids and different kind of salts can cause corrosion in the engine and catalyse the oxidation processes.

Fraer et al.[70] found no differences in fuel injection pump wear and performance with the exception of Mack trucks fuelled with the B20. They were more susceptible to fuel injector and fuel filter replacements because of the out-of-specification fuel batches, the biological contamination of the fuel and the larger amounts of fuel circulation in the fuel system. Chase et al.[71] observed that the fuel injectors and the whole fuel system were quite clean after a vehicle road test for 326,235 km on HySEE fuel.

In the current research, the UCO is industrially purified to minimise any adverse effects on the HGV fuel system. On-board UCO heating is another effective treatment for UCO preparation for injection. Eventually the high injection pressure tackles the fuel atomisation process. However, slight differences with PD properties still exists which are expected to affect the combustion process and emissions.

2.7 CI engines emissions and their control, and the impact of fuelling with UCO

2.7.1 Particulate matter (PM)

Andrews et al.[85] defined particulate matter (PM) as any material collected on a filter paper of defined pore size in atmospheric air quality sampling. Gravimetric analysis for the filter papers is the most reliable measurement method. However, many automatic real-time measurement apparatus were invented but gravimetrically calibrated.

Maricq [86] and Tobias et al.[87] classified diesel particulate emissions into two categories. Firstly, Individual agglomerates of ultrafine elemental carbon (EC) and metallic ash particles of 15~30 nm diameter covered by heavy end organic compounds and sulphate. Secondly, nucleation particles composed of condensed hydrocarbons and sulphates from lube oil and heavy end fuel components.

Pi-qiang et al.[88] explained that diesel particulate matter (PM) could take the solid phase and/or the liquid phase. It is composed of an insoluble fraction (ISF) and a soluble organic fraction (SOF). The ISF consists of soot, a solid matter formed from the nucleation of unburned fuel vapours, small amounts of sulphates and nitrates. The SOF is composed of unburned fuel, engine lube oil and their pyrolysis half products.

Soot

Tree and Svensson [25] defined soot as unburnt vapours usually formed in a fuel rich area in the combustion chamber at elevated temperatures. Carbon to hydrogen ratio in the soot increases through the nucleation process from 1:1 to 8:1. The soot density is $1.84 \pm 0.1 \text{ g/cm}^3$ and it represents more than 50% of diesel particulate emissions. Kittleson [89] noted that a $0.03 \text{ }\mu\text{m}$ diameter carbon sphere has a specific surface area of $100 \text{ m}^2/\text{g}$. This will have a key role in volatile organic fraction (VOF) adsorption.

2.7.2 Particulate matter formation mechanisms

PM evolution

Tree and Svensson [25] and Kayes and Hochgreb [90] described the genesis, growth and diminution of the PM as follows:

The Genesis of PM

Pyrolysis

Hydrocarbons under high temperatures, perhaps with the presence of small amounts of oxygen, change their molecular structure to produce soot precursors. These include polycyclic aromatic hydrocarbons (PAH), unsaturated hydrocarbons, polyacetylenes, and the hydroxyl radical (OH) which plays an important role in fuel and precursor oxidation processes especially at high temperatures. Pyrolysis is counteracted by oxidation and the latter dominates at higher temperatures. Therefore premixed flames soot less than diffusion flames at high temperatures.

Nucleation

Gaseous hydrocarbons might be converted to very tiny particles of 1.5-2 nm diameters in a temperature range of 1000~1300°C. During this process, cyclic and straight hydrocarbons are restructured to new dehydrogenated cyclised structures called the PAH. The growth of PAH creates the particle nuclei with large hydrogen content. These particle nuclei are formed in the very reactive zone at the premixed flame front due to the presence of high concentrations of radicals and ions at high temperatures [25, 91].

Superficial growth

Tiny readily nucleated particles in the primary reaction zone increase their size and mass by the accumulation of hydrocarbon layers on their hot and radical surfaces. The rate of particle growth is in direct proportion to the residence time albeit it is inversely proportional to ambient temperature and particle size. Therefore particles far from the primary reaction zone grow faster due to the increased adsorption and absorption processes. Similarly smaller particles grow faster since their surfaces are more reactive than the larger coated particles. Most of the particulate mass is gained from the surface growth process, therefore extended residence time increases the particle mass. Most of the researchers showed that particle size range at this particular stage could be between 20-50 nm. Lee et al.[92] stated that PM size distribution

decreases from 34.4 nm to 28.5 nm as the engine speed and load increase. They related their results to the higher temperatures for soot oxidation and shorter residence time.

Coagulation and agglomeration

The collision of individual particles could result in new shapes and structures. During these processes the total mass of the particles remains constant while the gross number of particle decrease. The process is said to be coagulation if the collision of the two individuals resulted in a new bigger and heavier particle. Agglomeration takes place as the particle collision results in a cluster or a fractal chain of sticking particles which is more likely to take place in diesel engine emissions. The particle size range might increase to 100 nm ~2 μm .

The Diminution of PM

Oxidation

During the oxidation process most of the carbon in the fuel or soot could be converted to carbon dioxide at any stage of the PM formation history. Soot oxidation takes place at high temperatures around 1100°C and at fuel lean environments, at the flame periphery, by O₂ and OH radicals, through direct contact with the charge air or within the flame due to the presence of the OH.

2.7.2.1 PM formation in the combustion chamber

During fuel injection

Dec [93] illustrated DICI engine combustion in fig.2.7. The figure shows from left, start of injection (SOI), fuel jet penetration, flame lift-off, fuel rich premixed flame, and stoichiometric diffusion flame which confines the whole combustion zone.

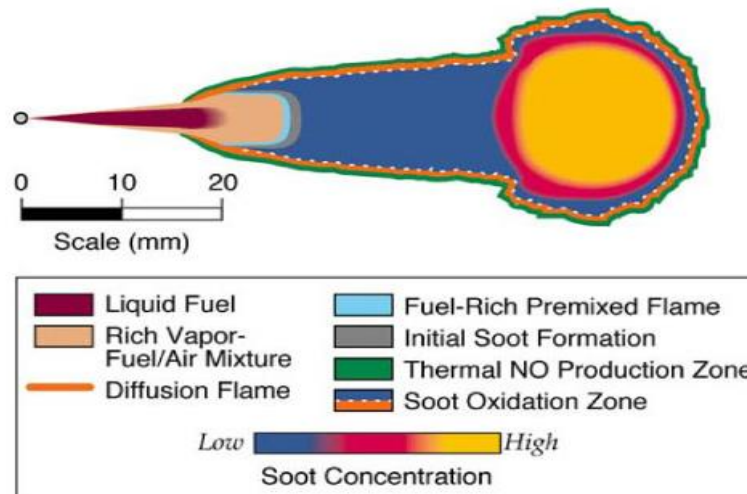


Figure 2.7 Diesel fuel jet development, flame types and emissions [93].

Laser jet imaging was used to identify soot, NO and OH radicals. Simultaneous images, for soot by planar laser-induced incandescence (LII) and images for OH by planar laser-induced fluorescence (PLIF) enabled him to distinguish soot formation at the fuel rich premixed flame area followed by soot accumulation and growth within the flame. No soot could be observed outside the flame zone because of its oxidation by the OH in the high temperature diffusion flame zone at the flame periphery. However, soot survival is possible as the flame length extends to hit the combustion chamber walls or laterally hit the adjacent flame. A small amount of soot might impinge on the walls or deposit by the thermophoresis mechanism, while the majority leave the combustion chamber with the exhaust gases.

At the end of injection

At the end of the injection process, the injection pressure decreases and the fuel jet elimination rate depends on the fuel injector design. However the fuel jet continues to flow, but under decreasing pressure which shortens the jet and perhaps to end with dribbling. Due to poor fuel atomisation, larger soot particles could form along the jet axis during jet contraction.

At the end of combustion process

At this stage, fuel rich mixture pockets collapse to even smaller pockets due to the high in-cylinder temperature. As the temperature decreases along the expansion stroke, only the highly reactive and unstable fuel fractions would burn and oxidise. Soot and the stable fraction of the mixture would be left un-

oxidised and cooled to even lower temperatures. These circumstances are quite suitable for the absorption of intermediate products by the fine soot particles to increase their size and mass.

2.7.2.2 PM formation in the exhaust pipe

PM regulations mostly deal with particulate mass, a criteria which was met by most of the engine manufacturers. However Kittleson [89] declared in his review that diesel particulates represent the accumulation mode which are mainly carbonaceous soot formed directly from the combustion process and their size range is 50 nm ~1000 nm. Smaller particles $D_p < 50$ nm are called nanoparticles. They are hydrocarbons or sulphates formed by nucleation during dilution and cooling of the exhaust. This size range has a negligible mass but dominated most of the engine-out PM emissions in terms of number. More than 90% of the particle number could be found in the nucleation mode while it possesses only 20% of the PM mass. Many recently produced engines comply with mass based regulations; nevertheless they emit even larger numbers of nanoparticles. It is believed that new particle number based regulations are mandatory to eradicate PM effects. Kittleson [89] argued that unlike the mass, particle number is un-conserved due to the nucleation and coagulation which makes it very difficult to design and impose number based regulations.

Kittleson et al.[94] investigated PM size distribution through their on-road and laboratory experimental study for four heavy duty diesel vehicles. They concluded that nanoparticles are formed either by the nucleation of low volatility species like sulphuric acid and water, or perhaps by the nucleation of non-volatile species of metallic or carbonaceous origins. Then they undergo growth by the accumulation of high molecular weight unburned hydrocarbons from fuel or lubrication oil. The presence of solid carbonaceous agglomerates attracts volatile hydrocarbons with their high absorption capacity to enhance the accumulation mode and suppress the nanoparticles. Therefore fuels and engine technologies play a substantial role in PM mode identification. The authors also stressed on particle loss during the sampling process. They stated that particles smaller than 20 nm are significantly susceptible to loss and wall deposition by dilution and cooling.

2.7.3 Factors affecting PM formation and survival

2.7.3.1 The fuel

C/H ratio

Barry et al.[95] stated that fuel composition affects soot quantity and its formation mechanisms, but fuel components play different roles in soot formation. Therefore higher carbon content fuels tends to produce more soot since part of the carbon might survive the combustion and is not converted to CO. Higher oxygen and hydrogen concentrations in fuel molecules reduces soot formation at different levels. This could be attributed to the improved oxidation process and higher combustion temperatures.

Tree and Svensson [25] concluded in their review that most of the researchers agree that soot formation is correlated to fuel structure in diffusion flames but not premixed flames. Normal and saturated fuel structures tend to soot less while the increase in carbon to carbon bonds increases the fuel tendency to soot because they have a higher C/H ratio. Compact isomers and branched chain molecules soot more in diffusion flames. Miyamoto et al.[96] declared that C/H ratio is the governing factor in PM formation at a given ignition delay and equivalence ratio. They also stressed on the insignificance of fuel structure on PM emissions.

Oxygen content

Oxygenated fuels soot less. This might be attributed to the higher temperatures obtained in the premixed flames in association with a reduction in carbon to carbon bonds. Miyamoto et al.[97] used four fuels of different oxygen content as pure fuels and blended with PD. Their experiments were conducted on two single cylinder DI diesel engines. Their results showed that soot emissions were inversely proportional to fuel oxygen content and soot could be totally eliminated if the fuel oxygen content reaches 30% by weight. Cheng et al.[98] found that PM reduction characteristic of the oxygenated fuels are more apparent in higher loads. They also observed a slight increase in PM emissions for the oxygenated fuels at low engine loads. Their investigation revealed that oxygenated fuels tend to reduce soot precursor formation in the rich premixed combustion zone, while the PAH growth was impeded through aromatics oxidation by OH radicals. Mueller et al.[99] applied the oxygen ratio (Ω) to diesel engines. It represents the ratio of the total oxygen content in the reactants of the mixture to the amount of oxygen required for a stoichiometric combustion.

$$\Omega = \frac{n_o}{2n_c + 0.5n_H} \dots\dots\dots 2.14$$

where n_o , n_c , and n_H are the number of oxygen, carbon and hydrogen atoms in the mixture respectively.

In the current research fuel elemental analysis is quite important to reveal the amount of oxygen content in the UCO which doesn't exist in PD. On the other hand, gravimetric and thermos-gravimetric analysis (TGA) for the PM collected on filter papers will provide the answer for the quantity and quality of the UCO PM compared to that of PD.

Sulphur content

Bardasz et al.[100] stated that high sulphur content in some diesel fuels and lubricants lead to higher PM emissions. These fuels have destructive effects on diesel oxidation catalyst (DOC) by poisoning from the high sulphur content. A DOC converts SO_2 to sulphate particulates. Very high levels of sulphur oxides, SO_2 and smaller amounts of SO_3 which readily react with water vapour to produce sulphuric acid are also witnessed in the emissions. The higher the sulphur content in the fuel the higher the sulphur based PM emissions. Kweon et al.[101] indicated that 10% higher PM emissions were measured as the fuel sulphur content increases from 10~400 ppm. Goswami et al.[102] stated that reducing fuel sulphur content from 350-5 ppm could reduce PM emissions by 7~8% and soot by 15~18%.

Polycyclic aromatic hydrocarbons PAH

Riddle et al.[103] stated that the contribution of PAH in PM emissions depends mainly on their molecular weight. Light molecular weight PAH fractions of the fuel contribute into gaseous emissions while heavy weight PAH fractions contribute in PM emissions. Engine load controls the status of the intermediate range of PAHs. At high loads, this fraction of PAH is more likely to produce PM and vice versa. Alander et al.[104] stated that reformulated fuels with 45% lower aromatics and 94% lower sulphur content might decrease PM emissions up to 40%. Ullman et al.[105] found in their studies on a heavy duty diesel engine fuelled by different petroleum and synthetic fuels. They found a very weak correlation between the fuel cetane number and its aromatics content with particulate formation. Oxygen and sulphur content in the fuel have the most efficacy on PM emissions.

Ladommatos et al.[106] investigated the effect of aromatic content variation on engine PM emissions at constant engine calibration and operational conditions. They concluded that only the EC component of PM increases with aromatics increase. They considered the aromatics as a combustion retardant.

Fuel cetane number

Kook and Pickett.[107] confirmed that fuels with high cetane number usually possess shorter ignition delay periods. The ignition delay could be even shorter at higher temperatures. Therefore the combustion of relatively lower cetane fuels at LTC will increase the ignition delay period. This will end up with longer flame lift-off length, more air entrainment and less soot formation. The authors also stressed on the effect of fuel chemical structure on soot formation. Aromatics and cyclo-paraffins have a higher propensity to soot. Yet these small amounts of soot might survive and escape the engine due to the delayed combustion process. Pickett et al.[108] observed that prolonged ignition delay periods could reduce the controllability of the combustion process through injection timing and rate. Therefore oxygenated fuels with shorter ignition delays are recommended.

Ash

Maricq [86] stated in his review that metallic ash is considered as a problematic material for aftertreatment facilities as it accumulates in the diesel particulate filter (DPF) and do not burn out during regeneration. It also has very detrimental health effects when the fine ash particles escape the after treatment facilities. Nevertheless, the presence of ash reduces soot activation energy from 162~116 kJ/mol to enhance soot oxidation and DPF regeneration.

Equivalence ratio φ

Li et al.[109] emphasized that the trade-off between soot and NO_x emissions is unavoidable in diesel engine operation. Soot oxidation could be achieved at high temperatures with sufficient amounts of oxygen. These conditions favour NO_x formation. Therefore reducing engine-out of any of these two emissions needs exhaust after-treatment for the other one to comply with the

emission standards. They suggested a simultaneous method to reduce engine-out of the two emissions. Reducing NO_x formation by low temperature combustion (LTC) assisted by moderate exhaust gas recirculation (EGR). Suppressing soot formation by air pressure boosting rather than burning at elevated temperatures with excess oxygen could be the solution. Finally controlling soot particle size which is a function of its surface area is another factor to burn out the soot at lower temperatures. Königsson et al.[110] observed that increasing the swirl number (SN) from 0.5 to 6.5 would increase the heat transfer to the coolant by 50% associated with improved combustion efficiency and uniform heat distribution in the combustion chamber. The improved mixing would reduce the locally rich or lean mixtures and their consequences on the entire combustion process. Eventually a uniform LTC was achieved.

Kalghatgi [1] described the effect of the equivalence ratio on soot formation. He stated that soot is firstly formed in a fuel rich premixed flame zone at the fuel jet periphery with an equivalence ratio of $\phi = 4$. This was followed by soot oxidation and burn out with the presence of oxidants in the diffusion flame at higher temperatures. This could be seen close to the cylindrical exposed surface of the jet but not the tip. At the jet tip soot oxidation is nearly negligible as the flames completely cover the combustion products including soot precursors from oxidation therefore more soot is formed. Eventually, no soot escapes the diffusion flame surrounding the combustion products unless it extinguished or deformed by the combustion chamber walls or adjacent fuel jets. He suggested that soot minimisation at relatively moderate temperature combustion requires equivalence ratios of $\phi < 2$. Alternatively, he expected that low soot and NO_x combustion is achievable by using low autoignition fuels. Although this strategy is associated by a higher CO and HC emissions due to the lower combustion temperatures (LTC), he advised that CO and HC removal by an oxidation catalyst is much easier than the NO_x and soot after treatment facilities.

2.7.3.2 Combustion chamber environment

Ambient temperature

Glassman [91] stated that soot formation in premixed flames could reach the peak in a temperature range of 1200~1400°C after which it decreases. However, soot oxidation in diffusion flames varies directly with temperature increase. Siebers et al.[111] attributed soot formation enhancement in the

premixed zone to the decreased flame lift-off length which shields the fuel vapour from air at this particular temperature range then higher temperatures would improve the evaporation and activation of the atomised fuel. Richards [9] showed that low combustion chamber temperatures impede the evaporation of low volatile fuel cuts. This will increase the fuel jet penetration length with a higher chance of wall collision. Maricq [86] indicated that, cold start of a light duty diesel vehicle showed a considerable increase of the SOF nucleation mode while the solid particulates were not affected by the cold start.

Ambient pressure

Tree and Svensson [25] showed in their review that soot formation is encouraged by pressure increases in the premixed flame zone. Nevertheless, it is hindered in the diffusion flame zone as the pressure increases. This was attributed to variations in the charged air density, fuel jet cone angle and penetration length, fuel droplet size and speed, air and fuel mixing and thermal diffusivity [112-114].

In the current research, the HGV under investigation is powered by a turbocharged high compression ratio diesel engine. The compression ratio is 18.5:1 which is assisted by a very efficient turbocharging action to keep the engine at a very high volumetric efficiency at all operational conditions. Keeping in mind that the engine is designed to deliver its maximum power at 1900 rpm, which is considered as a low speed compared to LGVs and passenger cars. All these features enhance the working gas pressure. Therefore the compression pressure is expected to be high at the SOI to increase the spray cone angle and exert a high shear to fuel droplets. This might result in droplet superficial disintegration and collapse.

Ambient oxygen content

Higher oxygen presence in the combustion chamber is usually associated with elevated combustion temperatures. However, the increase of oxygen enhances the oxidation process as well and the net effect is a reduction in soot emissions but higher NO_x release [25]. Payri et al.[115] studied the effect of charge air oxygen content on PM mass emissions under different temperatures and inlet pressures. They concluded that controlling PM emissions could be achieved by reducing PM formation or improving PM oxidation. They observed O₂ content in the charge air to play a key role in supporting these mechanisms. A peak PM emission could be observed for a certain oxygen concentration. Higher or lower levels of oxygen could reduce

the PM mass emissions either due to PM oxidation enhancement by the higher combustion temperatures or intrinsically reduced PM formation as O₂ in the charge air decreases. But the lower intake O₂ content consistently increased PM number emissions.

In the current research, the engine under investigation is turbocharged and the maximum intake air flowrate reaches 26.3 m³/min. in the same way, the exhaust flowrate is high to reach 56 m³/min. These flowrate are sufficient enough to keep the engine at a high volumetric efficiency for an improved combustion process. These high flowrates are only achievable when the inlet and outlet ports are properly designed with a sufficient number of valves and a proper valve timing. The high turbocharging efficiency assisted by the intercooler deliver sufficient air at a relatively low temperature of 55°C to maintain the inlet air at a high density.

2.7.3.3 Engine operational conditions

Pi-qiang et al.[88] bench tested a euro1 emission compliant heavy duty diesel engine and concluded that the variation in engine load directly affected the PM emissions and their ingredients. Their observations showed that the PM emissions are directly proportional to load increase at a given speed which is mostly due to the increase in ISF content while the SOF content of the PM decreased. Kweon et al.[101] observed a trade-off between EC and OC emissions as engine load and speeds changed. They found an 80% increase in EC with load and speed increase while OC decreased by 70%. Shah et al.[116] observed exactly the opposite trend in PM emissions with respect to engine load and speed. The study included a fleet of eleven HGVs operated on CARB transient cycle. They observed a decrease in both EC and OC emissions as the load and speed elevated from low to high (creep to cruise mode) but at different rates. Accordingly OC decrease was 4 times greater than EC decrease.

Kweon et al.[101] believed that the effect of speed and load on diesel PM emissions is related to the time available for air-fuel mixture formation and rate of activation and the efficiency of combustion. Therefore higher OC emissions are expected at low speed and load operation. This could be attributed to lower combustion efficiency at lower temperatures which results in higher unburnt hydrocarbons from fuel and lube oil. Therefore higher OC emissions prevail from the premixed combustion zone. At high speeds, the higher combustion frequency increases the combustion chamber temperature but

reduces the time required for fuel mixing and activation. At higher loads, the higher combustion temperature is related to the amount of fuel delivered to the engine. The net effect is a longer ignition delay and more EC emissions from the diffusion flame.

In the current research, the HGV is tested under real world driving conditions in a well-defined route that comprises urban, steady-high speed and high torque vehicle travels. Therefore, engine performance and emissions are analysed at these particular conditions separately to have a better understanding of engine outcome while operated on UCO compared to PD. The load applied to the HGV is the pay load, represented as gross vehicle weight (GVW), and the road load which comprises the rolling, acceleration and air resistances.

2.7.3.4 Engine design and accessories

Air swirl

Dembinski and Angstrom [117] studied the mutual interaction between the fuel jet and charged air swirl on the combustion process using computational fluid dynamics (CFD) simulation. They found that fuel injection at high pressures changes the air swirl behaviour from the rigid body rotation pattern to the vortex motion pattern after the fuel injection. Although the angular momentum decreases with fuel injection, the total kinetic energy of the mixture increases. As a result, the swirl angular velocity decreases at the bowl wall, while the redirected high energy flames increase the angular velocity at the cylinder centreline. The advantage is to keep the high concentration of unburned fuel droplets and vapours away from the combustion chamber walls and provide sufficient air for a complete combustion. This will reduce soot formation and improve its oxidation during the power stroke. The authors calculated the swirl angular velocity from the CFD results.

$$\omega_{\text{swirl}} = \frac{L}{I} \quad \dots\dots\dots 2.15$$

where

$$L = \sum_{i=1}^n ((m_i \cdot r_i^2) \cdot \omega_i) \quad \dots\dots\dots 2.16$$

$$I = \sum_{i=1}^n m_i \cdot r_i^2 \quad \dots\dots\dots 2.17$$

L is the angular momentum [kg.m².rad/s]

I is the total moment of inertial [$\text{kg}\cdot\text{m}^2$]

m_i is the mass of an arbitrary element volume in the swirl [kg]

r_i is the radius of rotation for m_i from the centre of rotation [m]

Königsson et al.[110] studied the effects of charge-air swirl and tumble on soot and HC emissions. The test engine was a single cylinder Scania EURO 5 compliant engine with variable valve train (VVT) mechanism. They concluded that a higher swirl number could be obtained by using a low valve lift strategy and following a trapezoidal valve lift profile in order to accomplish the highest gas inlet velocity that coincides with the maximum piston speed during the suction stroke. Although they used the diesel fuel as a pilot fuel injected into a premixed diesel-methane blend, they observed 85% soot reduction as the swirl number (SN) increases from 0.5 to 7. They also found that at low to moderate SN, the increase in tumble number (TN) might increase soot emissions. However, during the combustion process, tumbles tend to disintegrate to smaller turbulent eddies to enhance the mixing process. Swirls also tend to improve the oxidation of HC entrapped in the piston crevices after being released during the power stroke. They observed a 20% HC emission decrease as the SN increases from 0.4 to 3. Therefore lower HC emissions were observed.

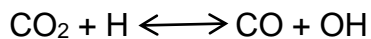
Jazair et al.[118] used neat UCO as a fuel in a DI diesel engine. They observed that high turbulence combustion effectively reduced PM emission at all operational loads due to better fuel jet evaporation, reduced wall collisions and higher speed of combustion.

The HGV under investigation in the current research is turbocharged and the inlet and exhaust port configuration are designed to provide the required air swirl. The swirls take place during valve overlap period to extend throughout the suction and compression strokes. At the end of compression stroke as the piston reaches its upper dwell, the squish action forces the air to flow towards the centre of the combustion chamber. The inverted mushroom shaped combustion chamber carved in the piston crown deliberately forces the incoming air to make tumbles and mix with the fuel.

EGR

Siebers et al.[17] investigated the effect of EGR on soot emissions. They found that using high rates of EGR displaces the natural amount of oxygen in the charged air and it reduces flame reactivity. The increase in flame lift-off

length (FLL) would compensate for the oxygen shortage. Dec and Kelly [119] showed that high rate of EGR might result in flame extinction and impede soot oxidation due to the dilution effect and reduced reactivity of the oxidation radicals. Kook et al.[23] concluded that EGR increases the heat capacity of the diluted charged air, thus a reduced adiabatic flame temperature is obtained associated by lower NO_x emissions. Li et al.[120] used argon, carbon dioxide and nitrogen as charge air diluents to simulate an EGR system. They concluded that smokeless combustion requires a high heat capacity dilution gas, and the higher the O₂ presence the higher heat capacity content of the dilution gas is needed. Their investigation of the sensitivity coefficient and reaction rates of the H and OH radicals showed that OH is more effective in soot oxidation. Therefore endothermic dissociation of CO₂ at higher combustion temperatures improved soot oxidation.



Their investigations also revealed that reducing O₂ content in the charge air to 16% by any dilution gas will achieve a NO_x free exhaust. Eventually NO_x emissions could be reduced by reducing combustion temperature under the effect of reduced oxygen content, higher heat capacity of the dilution gas and the endothermic dissociation of CO₂. Goswami et al.[102] found that increasing the rate of EGR at high loads resulted in an exponential increase in soot emissions due to the reduced air excess ratio at high load operation. However, soot emission was much lower at low loads when the rate of EGR increased.

The vehicle under investigation is not provided by an EGR system. However, the mathematical analysis showed that using UCO as a fuel might lead to higher exhaust gas residual in the cylinder than PD. This could be attributed to the lower combustion pressure in the case of UCO.

2.7.3.5 Fuel injection

Flame lift-off length

Siebers and Higgins [111] defined the flame lift-off length (FLL) as the axial distance between the injector orifice and the start of the stabilised flame as illustrated in fig.2.8. The longer the FLL the larger the amount of air entrained into the hot vaporised fuel for a better mixture oxidation in the premixed combustion zone and less soot formation. They also stated that soot might completely vanish if the Percent Stoichiometric Air (ζ_{st}), which is the ratio of

the actual air entrained to the stoichiometric air required for a complete burning of the injected fuel, is in the range of 40~50%.

$$\zeta_{st}\% = 100 * [(\sqrt{1 + 16(\frac{L_o}{x})^2} - 1)/2AF_{st}] \quad \dots\dots\dots 2.18$$

$$x = d_o \sqrt{C_d \frac{\rho_f}{\rho_a} / [0.75 * \tan(\frac{\alpha}{2})]} \quad \dots\dots\dots 2.19$$

where

ζ_{st} is the percent stoichiometric air [%]

L_o is the experimental lift off length [mm]

AF_{st} is the stoichiometric air to fuel ratio by mass

x is the characteristics length scale for the fuel jet [mm]

C_d is the orifice discharge coefficient

d_o is the injector orifice diameter [mm]

ρ_f is the fuel density [kg/m³]

ρ_a is the air density [kg/m³]

α is fuel jet cone angle [deg.]

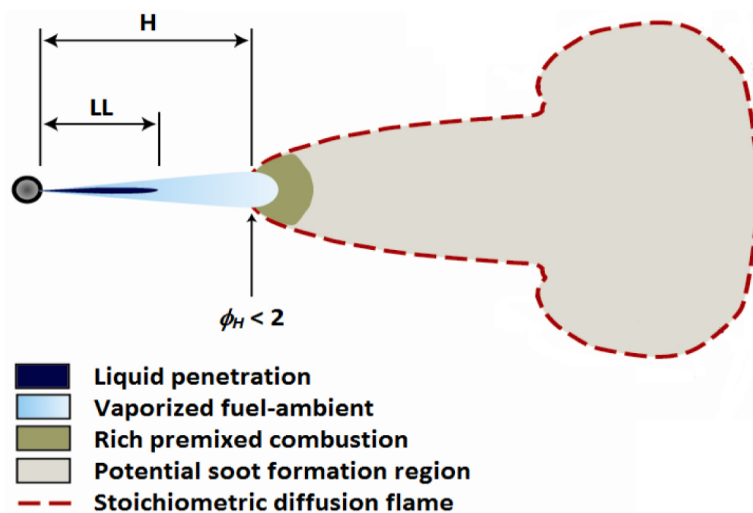


Figure 2.8 Sketch of the Leaner Lifted- Flame Combustion (LLFC) strategy. H is the lift-off length, LL fuel jet penetration length and Φ_H is the equivalence ratio at jet centreline at (H) [121].

Conventional fuel jet patterns exhibited liquid fuel jet covered by a very rich vapour zone which was completely engulfed by the flame. Recent diesel

combustion strategies are based on low temperature combustion LTC at relatively lower compression ratios and much higher injection pressures. The lower combustion temperature and air density would increase the FLL as they control the thermal diffusivity and laminar flame speed. The high injection pressure provides a higher internal energy to the fuel jet to enhance fuel atomisation and eventually better evaporation and mixing with air. Although the smaller nozzle orifices inversely affect the FLL, it will be compensated by the higher injection pressure which improves fuel atomisation and increases the fuel jet cone angle. Ultimately the fuel jet will be shorter with a smaller amount of fuel being injected and a longer FLL for a higher (ζ_{st}).

The fuel injection strategy in the engine under investigation is based on a very high injection pressure up to 180 MPa in par with a high compression pressure. The high injection pressure produces finer fuel droplets to improve fuel atomisation. It also works with the high density air entrapped in the combustion chamber to reduce the spray penetration and increase spray cone angle. In fact this action increases the ratio of the distance between adjacent fuel droplets to their mean diameter. Therefore no collisions are expected and a higher fuel evaporation is expected due to the presence of excess air in the vicinity of individual droplets. Bearing in mind that a fuel of finer droplets possess a larger surface area for heat transfer and evaporation.

Injection pressure

Dec [93] in his description of the propagation of DI fuel jet in the combustion chamber. The author stated that, the high injection pressure delivers higher energy to the smaller droplets formed for faster evaporation. The high injection pressure increases the fuel jet cone angle and reduces the fuel jet penetration length hence a better fuel atomisation. Tree and Svensson [25] related the decrease in soot morphology to the fact that, higher injection pressure increases fuel jet velocity which in turn increases the flame lift-off length and the percent stoichiometric air. More air entrainment is expected. The overall effect is improved mixture homogeneity. Homogenous mixtures lead towards a better combustion completion with minimised intermediate products.

Injection timing

Dec et al.[119] found that late fuel injection of prolonged ignition delay fuels would lead to an extended combustion process through the expansion stroke. The relatively cool environment with early exhaust valve opening might impede the soot burn-out process which could result in higher soot emissions. An early ending of the combustion process could result in soot oxidation at

high in-cylinder temperatures. Ladommatos et al.[122] during their investigation of the influence of piston crown temperature on emissions. They found a linear relationship between injection timing advancement and piston temperature. They announced an increase of 0.9~1.9°C in piston temperature per crank angle degree injection advancement. However 1.8°C/CAD was recorded at the jet impingement spots in the piston bowl. They also found an increase of piston temperature in the range of 0.3~0.6°C per 1°C increase in cylinder block temperature while steadily holding the cylinder head temperature and injection timing at 90°C and 1deg bTDC respectively. Raising the piston temperature from 189~227°C reduced HC emissions by 27% and smoke emission was increased by 25%. NO_x emissions were not affected by this temperature increase but apparently increased by injection advancement.

The higher density and bulk modulus of elasticity of UCO in the current project is expected to affect the injection timing with a slight advancement and possibly a longer injection duration. Meanwhile, the lower calorific value of UCO will lead to a cooler combustion process. Therefore a different fuel injection timing and duration and combustion chamber temperature are expected between UCO and PD combustion.

Injector orifice size, number and orientation

A smaller amount of fuel would be injected per time from the smaller size orifice at a constant injection pressure. This would increase the percent stoichiometric air leading to less soot. However this would be counteracted by a slightly reduced flame lift-off length [25]. Hottenbach et al.[123] investigated the effect of cluster nozzle technique on soot morphology. They replaced each orifice on the injector tip by a cluster of two orifices. The diameters of Cluster orifices were selected to produce the same flow number as the single orifice and they were oriented to direct the fuel jets at 10° and 20° separation angle. They concluded that soot was reduced due to the decrease of fuel jet at the centre of the flame where most of the soot formed and nucleated especially for the 10° separation cluster and a shorter fuel jet penetration length was observed in case of the clusters specifically the 20° one. A slightly longer flame lift-off length was indicated for the cluster orifices compared to the conventional nozzle. The 10° orifice cluster showed superiority because the jet core was thinner and the flame took the mushroom shape to allow better soot oxidation.

In the current research the fuel injector possesses seven 0.2 mm diameter orifices. The central position of the fuel injector directs the fuel spray radially to the piston crown cavity which represents the combustion chamber of this particular engine. The injection pressure that reaches a maximum of 180 MPa is a crucial factor that governs fuel atomisation i.e. mean droplet size, spray cone angle and the penetration length. It also increases the fuel/air contact area and provide a larger air volume around the spherules for improved heat transfer and evaporation. The net effect is shorter physical ID period.

2.7.4 The impact of UCO presence on PM emissions

Jazair et al.[118] studied the effects of using UCO as a surrogate to PD on engine performance and emissions. The bed test for a DI diesel engine revealed that engine operation with UCO at high loads produced lower PM emissions, predominantly as soot, compared to PD. Low and intermediate load operation showed higher PM emissions from UCO mostly in the form of SOF. This was attributed to the long chain triglyceride hydrocarbons in UCO and its high kinematic viscosity and lower volatility. Both soot and SOF were reduced by blending UCO with PD which improved the evaporation of the mixture and reduced its kinematic viscosity.

Hribernik and Kegl [75] installed a piezoelectric pressure probe in the pre-chamber and an inductive sensor to produce an indicated pressure and injector-needle lift histories respectively. With the aid of LabVIEW software, they were able to measure the pressure-time history to predict the rate of heat release (RHR). They observed that PM emissions from the combustion of UCO blends with PD remained unchanged compared to those of the pure PD. Their tests were carried out on an IDI diesel engine. Chase et al [71] showed 50% reduction in PM emissions in the steady state engine test fuelled by pure HySEE and reduction of 35% for the 50/50 blend with PD compared to the pure PD. During the transient test PM emissions of HySEE were 50% higher than that of the PD.

In the current research, UCO is automatically mixed with PD after being heated to the desired temperature. the presence of PD decreases as the temperature of UCO increases. This kind of on-board treatment is inevitable to reduce UCO's high viscosity and density to be comparable to PD. The high injection pressure (180 MPa maximum pressure), combustion chamber configuration and the global in-cylinder temperature at the SOI (447°C~598°C theoretically calculated) are quite sufficient for efficient fuel atomisation. The

calculated combustion temperatures for UCO and PD are 2650°C~2900°C respectively. This high diffusion flame temperature assisted by the OH radicals engraves soot and reduces the VOF.

2.7.5 PM emissions mitigation

2.7.5.1 In cylinder PM mitigation

Soot is formed in a fuel rich premixed flame when the equivalence ratio (ϕ) is higher than 2 [1, 93, 109]. Therefore the fuel mixture should be kept lean if the combustion strategy is to suppress engine-out soot. But in conventional diesel engines it is impossible to achieve lean combustion because of the high CN fuel required especially in cold weathers. In fact it is the high CN that makes the fuel auto-ignite early before the end of injection (EOI) especially at higher loads. Early auto-ignition results in rich mixture packets that produce soot. In that context, it is quite important to keep the combustion temperature high enough in order to burn the soot at the diffusion flame periphery in abundant presence of oxygen [1].

The high temperature also prevents the VOF condensation throughout the long expansion stroke. This will reduce the total engine-out particulates.

Mechanically, the very high fuel injection pressures reduce the ID period by producing very tiny fuel spherules that evaporate promptly and spread out widely across the combustion chamber to improve the mixing process. This is very important especially for the heavy components of the fuel which need extra heat to evaporate. Otherwise, using fuels of lower CN will result in a more homogeneous mixture and leaner combustion but higher HC and CO is expected.

2.7.5.2 Diesel particulate filter (DPF)

For engines designed to suppress NO_x emissions within the combustion chamber, the presence of PM removal units in the exhaust aftertreatment become inevitable. Diesel particulate filters (DPF) are surface filters which are designed to collect the PM on their upstream surface due to their tiny porous structure. This process is called wall-flow [124]. Collecting the PM will increase the pressure drop across the DPF which will produce a high back-pressure on the engine. Therefore it's a design mandate to build filters with large surface area to volume ratios [9]. The typical design is a monolith block, as shown in

fig. 2.9, that incorporates a number of parallel channels along the long side of the monolith. In order to achieve the maximum surface area, some of the channels are plugged from the upstream side while the adjacent one is plugged at the downstream side. The size of the inlet and outlets might be different and usually the inlets are made larger. PM loaded exhaust gas is forced to pass through the longitudinal walls leaving the PM on the upstream side. A proper design and configuration of the monolith might reduce the engine noise to desirable levels to replace the muffler. Cordierite is the most reliable monolith material since it has been used extensively in the catalytic converters and is heat resistant [125].

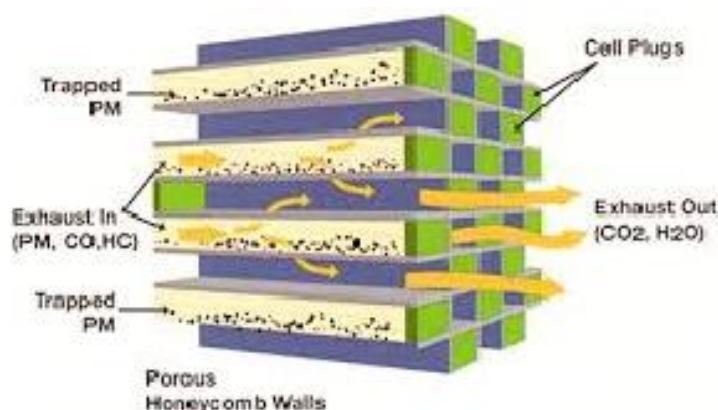


Figure 2.9 Diesel particulate filter monolith.

The DPF should be cleaned periodically to reduce the back-pressure on the engine and to reduce fuel consumption. A fully loaded DPF might stall the engine. The cleaning process is called filter regeneration through which the accumulated soot is burned. Soot burning needs high temperature, time and an oxidant. As a lean combustion, diesel exhaust contains sufficient oxygen but the exhaust gas temperatures reaching the filter are in the range of 200~500°C might not be enough for a fast and complete burning. Therefore fuel-borne catalysts (FBC) are added to the fuel which survive the combustion process to penetrate through soot layer and enable its burning.

NO₂ is a faster oxidant than the O₂, to help increase the NO₂, diesel oxidation catalyst (DOC) is installed upstream to DPF to oxidise NO to NO₂. In other designs, using high pressure common rail fuel injection (HPCR) systems, occasional extra injections are performed. The extra injection takes place late in the power stroke to increase the temperature of the exhaust gas. Part of the unburnt fuel is further oxidised on the DOC to raise the exhaust gas temperature for a faster soot burning in the presence of the FBC.

Thermal regeneration could be achieved by heating the exhaust gas to the PM ignition temperature T_{ign} using electrical elements or a burner. The frequency of regeneration should be calibrated for the most efficient fuel economy. An open loop control for a known distance or duration might be suitable for vehicles operated with a known duty-cycle. A closed loop control is more efficient, in which the frequency of regeneration could be optimised by fuel economy and the heat generated from engine loading rather than the artificial heating. A more sophisticated design called aerodynamic regeneration uses compressed air to flush out the filter and collect the soot in a separate chamber for burning. It is a less heat dependent process therefore the DPF could be installed further downstream to offer more time for SOF condensation and removal [22].

2.7.6 Primary gaseous emissions from CI engines

Primary pollutants are those released immediately from the tail pipe to the ambient air. They contribute to air quality aggravation and damage to human health and property. Their emission per vehicle has been progressively decreasing due to the technological improvements in engine hardware and calibration, but a growing number of the vehicles are impeding the pollution mitigation programs.

2.7.6.1 Carbon monoxide

Eastwood [22] stated that CO is formed from oxygen-deficient combustion of carbonaceous materials. Although diesel engines operate on lean mixtures or there is always sufficient air in the combustion chamber, the heterogeneous property of the mixture resulted in localised CO formation due to insufficient oxygen in these locations. Cold starts lessen the mixing process from which more CO is expected. Transient operation associated to acceleration, deceleration and gear changes where the driver demands sudden high power output also produces high CO emissions otherwise a very sluggish operation is expected from the engine. Secondary oxidation during the expansion and exhaust strokes might take place if the temperatures are maintained high and mixing mechanisms push the combustion process towards more completion.

Ferguson [57] explained the effect of exhaust gas cooling on higher CO emissions. He mentioned that mixtures burned at the beginning of the combustion process and first exhausted into a lower temperature exhaust manifold produce higher CO emissions than those exhausted late to a higher

temperature exhaust manifold. Diesel engines produce less CO emissions since they are operated with lean mixtures and it is observed that DI engines produce more CO than IDI engines. This could be attributed to the higher speeds and limited duration of combustion in DI engines.

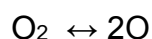
The engine for the HGV under investigation, is very much depending on its high compression ratio and injection pressure to improve the air/fuel mixing process. The aim is, to achieve a short adiabatic premixed flame leading to a high temperature diffusion flame that to oxidise CO. Added to that the relatively low engine speed (maximum 1900 rpm) offers sufficient time for a complete combustion.

2.7.6.2 Nitrogen oxides

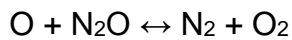
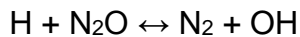
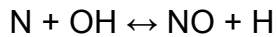
Eastwood [22] stated that NO_x are formed in the combustion chamber due to the presence of atmospheric N_2 and O_2 which are involved in chain reactions under elevated temperatures up to 1600°C . NO_x are mainly formed in the diffusion flame area on the flame periphery with a small portion formed in the premixed flame area. Advanced fuel injection and early burning during the compression stroke result in higher NO_x concentrations due to the higher temperatures. However combustion on the power stroke produces less NO_x emissions. Hsu [59] stated that 90% of NO_x formed in the combustion chamber is nitrogen oxide (NO). NO is stable at high temperatures but it oxidises rapidly at room temperature to NO_2 . There are three scenarios for NO formation as follows:

- i The Zeldovich mechanism or thermal NO formation. During the combustion process, oxygen molecules in the cylinder dissociate at temperatures higher than 1000°C to oxygen atoms which attack nitrogen molecules to produce NO. At temperatures higher than 1300°C the rate of NO formation doubles for every 100°C temperature increase. The rate of NO formation is maximum at lean AF ratios near stoichiometric value to secure sufficient amount of oxygen as shown in fig.2.10. Leaner mixtures reduce combustion temperature and reduce NO formation.

Benson and Whitehouse [56] and Mueller et al.[16] summarised Zeldovich chain reactions as follows:



The modified Zeldovich reactions are:



And the complementary reactions are:

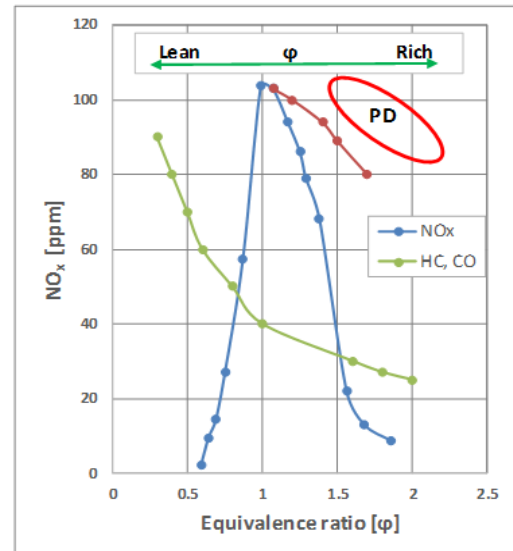
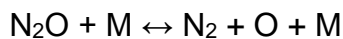
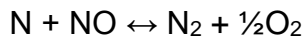


Figure 2.10 NO_x, HC and CO variation with ϕ . Reproduced from [1].

- ii The Fenimore mechanism or prompt NO formation. It occurs for fuel rich flames as carbon and hydrogen radicals attack nitrogen to form cyanide HCN. It is followed by the oxidation of HCN to form NO. This theory is temperature independent.
- iii The oxidation of nitrogen in the diesel fuel. Nitrogen content in PD is less than 0.01% by weight, even though only a small portion is converted to NO and a little amount is released as N₂.

Mueller et al.[16] related the higher NO_x formation from biodiesels to the higher oxygen content in biodiesel which reduces in-cylinder soot formation. Reduced soot means less radiative flame or a higher adiabatic diffusion flame temperature is expected from biodiesel combustion compared to PD. Eventually the higher diffusion flame temperature leads to higher NO_x formation from biodiesel combustion.

Hellier et al.[126] found a linear correlation between ignition delay and NO_x formation in a single cylinder DI common rail diesel engine under constant injection timing and constant ignition timing. They declared that a 10% increase in ignition delay resulted in 14% and 10% increase in NO_x emissions at constant injection and constant ignition timing respectively. This was attributed to higher maximum in-cylinder temperature and higher rate of heat release due to the extended premixed combustion.

Ferguson [57] summarised NO_x formation in diesel engines as follows:

- NO_x are maximum for slightly lean mixtures.

- Reduced combustion duration and heat loss due to high engine speed increases NO_x formation.
- Higher coolant temperatures and increased deposit accumulation in the combustion chamber decreases the heat loss which results in higher NO_x formation.
- Charge dilution by residual gas through EGR or throttling (deceleration) or increased humidity of inlet air decreases NO_x formation.
- Injection timing strongly affect NO_x formation, the earlier the injection timing the higher is the NO_x emission.
- NO_x concentration is directly proportional to engine brake mean effective pressure (bmep) in DI engines.
- In IDI engines, peak NO_x concentration is observed at loads slightly lower than the peak load.

The engine for the HGV under investigation in the current research is designed to mitigate PM within the combustion process as explained earlier in section 2.7.5. The high combustion temperature, low engine speed and extended combustion process throughout the power stroke are expected to produce high levels of NO_x. It is also expected that UCO to be the higher NO_x producer, compared to PD, in spite of its lower combustion temperature. The effect of high oxygen content in UCO could be the major factor behind high NO_x emissions.

2.7.6.3 Volatile organic compounds

The main compounds embraced by the VOC are the alkynes, alkenes, alkanes, and the aromatics. The latter is the building block for the Poly (cyclic)-Aromatic Hydrocarbons (PAH). The quantity of unburned hydrocarbon emissions is affected by the availability of oxygen in the combustion chamber. Recent diesel engines are low HC emitters because of the lean characteristic of diesel combustion where the air-fuel ratio ranges from 17:1 to 70:1, higher injection pressure and higher combustion temperature. The heterogeneous nature of the mixture indicates areas of rich mixtures, lean mixtures and no fuel at all. There are many factors contributing in HC formation related to engine design or tuning as follows [22, 57]:

- Crevices: Flame extinction before it enters crevices like piston rings or air chambers.
- The quench layer: worn and rough walls have a quenching effect on the approaching flames.

- Porous deposits: mixtures in the voids of deposits are unreached by the flame.
- Absorption by the oil: the thin film of lubricating oil on the cylinder walls might absorb the hydrocarbons during the compression stroke and desorb them during the expansion stroke. It mainly depending on the solubility, vapour pressure and the diffusion rate of HC in oil.
- Late burning: fuels introduced at the end of the injection process have more chance to survive the combustion late in the expansion stroke as the flame extinguishes due to chilling effects.
- Injector effects: in certain injector designs a little portion of fuel might remain in the nozzle opening (sac) after the injection. This fuel might enter the combustion chamber as vapour. Unwanted secondary injections caused nozzle reopening under the effect of pressure wave pulsation resulting in unburned HC's.
- Increased engine wear increases the clearance between the piston and cylinder. This will result in an incremental increase in HC emissions due to the quenching action of the walls surrounding the confined gases. This behaviour exists to certain wear limits after which HC emissions reduce suddenly as the engine wear increases.

The engine for the HGV under investigation is designed to operate at high combustion temperatures. The fuel is injected into the combustion chamber which in this case carved in the piston crown. This combustion chamber configuration eliminates any contact of the fuel with cylinder walls or to hide in the crevices. Turbulence and swirls enhance the finely atomised fuel to mix with air. However, due to the physical and chemical properties of UCO, which are quite different from those of PD, differences in VOC emissions are expected with UCO producing more.

2.7.6.4 The impact of UCO presence in the fuel on gaseous emissions

Li et al.[127] used fresh cooking oil (FCO) as a fuel in a 6 cylinder heavy duty Perkins Phaser DI diesel engine. They observed higher CO emissions from FCO, compared to PD, due to incomplete atomisation and evaporation of the fuel jet which resulted in poor combustion quality. They also witnessed 25% higher NO_x emissions from FCO combustion at high load operation. Hossain et al.[128] used UCO derived biodiesel in a three cylinder IDI Lister Petter

diesel engine. Their results showed 3% increase in CO₂, 4% reduction in NO_x and 15 fold reduction in CO at full load compared to PD.

Sidibé et al.[129] stated in their review that the CO concentration profile of SVO/PD blends is the same as that of the pure SVO with minimum values obtained at moderate loads between 60~80%. CO emissions increased as the SVO share in the blend increased. CO₂ emissions from the blends were comparable to or higher than that of the PD which was attributed to the higher oxygen O₂ content in the SVO. They also stated that all the authors agreed upon the decrease in NO_x emissions from the blends compared to that of the PD as a result of the lower combustion temperatures obtained from the blends due to their higher viscosities.

Saravanan et al.[130] stated that molecular atmospheric nitrogen is the dominant source of NO_x emissions. Exhaust gas treatment is one solution for NO_x reduction, however reduced combustion temperature and reducing oxygen availability in the combustion chamber are more effective and economical techniques for NO_x formation control. Practically this could be achieved by increasing the rate of EGR and or by injection timing retardation. EGR replaces O₂ by the inert exhaust which has a higher specific heat capacity. Injection retardation reduces the rate of pressure rise and the peak pressure which will lead to a lower combustion temperature, a reduced contact between O₂ from air with N₂ from the fuel and producing a fuel rich zone to reduce NO_x to N₂. Biodiesels and SVO possess higher density and viscosity therefore they have a longer ignition delay. This will increase the rate of pressure rise and peak pressure and temperature. Therefore a higher NO_x is expected.

Hribernik and Kegl [75] stated that higher combustion-pressure oscillation-amplitudes caused by the larger amounts of UCO content in the blend, adversely affected the stability of combustion which in turn increased the HC and CO emissions. No fuel injection advancement is required since the increase in ignition delay is compensated by injection advancement due to the higher bulk modulus of elasticity of UCO. Injection advancement reduces HC and CO emissions nevertheless it increases the NO_x emissions. They also stated that fuel preheating is essential for higher UCO content fuel blends.

In fact this is what is expected to happen in the vehicle under investigation perhaps at different extents depending on detailed differences between the two engines.

Chase et al.[71] studied the effect of hydrogenated soy oil ethyl ester HySEE and its 50/50 blend with PD on the emissions from a heavy duty Caterpillar engine. Compared to the PD the pure HySEE showed 5% increase in NO_x while the 50/50 blend showed only 2.8% increase. Transient emissions from on-road engine test showed 6.4% and 4.8% increase in NO_x for the PD and the HySEE respectively. This was related to engine tuning by injection retardation and decreased injection pressure. It wasn't related to the fuel itself.

From the aforementioned analysis, it could be inferred that the high injection pressure is the key factor for improved fuel atomisation and mixing with air. The high combustion temperature controls the amount and type of emissions. It reduces PM, THC and CO while NO_x increases and vice versa. The high compression ratio increases air temperature and pressure prior to the SOI. Turbocharging increases the volumetric efficiency and working gas density for higher power output and improved combustion. Swirls, turbulences and piston squish action offer better mixing. Fuel injector position and the combustion chamber configuration play a key role in controlling fuel jet trajectory within a controlled volume.

There is no doubt that the high viscosity of UCO will adversely affect the injection process to a certain extent which could be defined by the injection pressure. The high UCO density could compensate for its lower calorific value. The higher bulk modulus of elasticity of UCO might lead to fuel injection advancement and extended for a longer period of time. The heat release rate might be affected by the UCO CN and viscosity which will affect the emissions.

2.7.7 Gaseous emissions mitigation

2.7.7.1 In cylinder gaseous mitigation

If low NO_x emission combustion is the objective, a lean homogeneous mixture is required provided the combustion temperature shouldn't exceed 1900°C. This is actually the premixed compression ignition (PCI) approach. Low CN fuels with advanced injection provide sufficient time for fuel evaporation and mixing before the SOC. Alternatively, exhaust gas recirculation (EGR) could reduce the combustion temperature by the high specific heat capacity of the exhaust gases. In this process a controlled amount of exhaust gases is recirculated and mixed with the induction air [1]. The main drawback of the low temperature combustion is high PM, HC and CO emissions which require exhaust aftertreatment facilities fitted to the exhaust system.

2.7.7.2 Selective catalytic reduction (SCR) and urea injection

Heavy duty diesel vehicles adopted lately the selective catalytic reduction SCR to reduce NO_x emissions. The most recent units use urea injection to convert NO to elemental nitrogen and water vapour. Each unit consists of a stainless steel casing in which a monolith or many plates are embedded. A commercially produced Urea, known as diesel exhaust fluid (DEF), which is the source of NH₃, is injected into the exhaust gas upstream to the SCR unit as shown in fig 2.11.

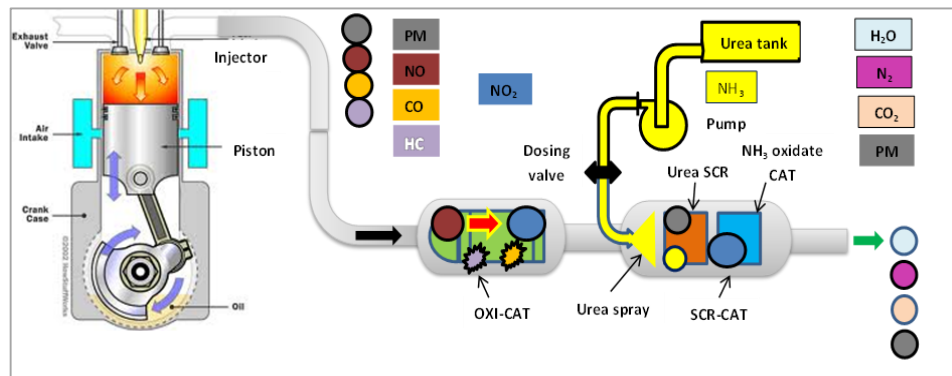


Figure 2.11 Typical diesel after treatment installation showing the urea SCR system.

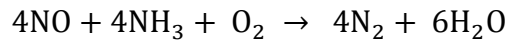
El-behery et al.[131] described the SCR system fitted to HGVs as follows:

Urea tank: it is a high density polyethylene container. It is about 30 litres in capacity to hold enough fluid between two successive vehicle fuellings. The tank has a drain valve at the bottom and a strainer and vent holes in the filler cap.

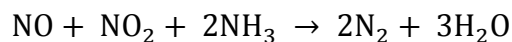
Urea injection system: it is a steel box containing the metering pump, electronic control unit ECU, safety and diagnostic valves and sensors. Urea is injected under a pneumatic pressure in to the exhaust pipe.

Catalytic SCR muffler: in this unit the exhaust gases flow through a diesel oxidation catalyst (DOC) to increase the NO₂/NO_x ratio to 50% by the oxidation of NO to NO₂ reducing HC content. The DOC is followed by a urea injection nozzle from which a spray of urea water solution is injected on two consecutive SCR ceramic monoliths. The first one for temperatures higher than 350°C while the second for temperatures less than 350°C. This arrangement enables NO_x removal at a wide range of temperatures (180°-550°C). The rear catalyst incorporates a Platinum oxidation catalyst on the outlet side to prevent ammonia slippage [132].

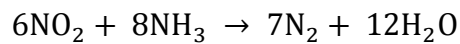
Gao et al.[133] and Clarebout et al.[134] stated that the monolith encompasses anatase TiO₂ as a supporting material, vanadium oxide V₂O₅ as the main active component which is very active even in low temperatures, silicates as mechanical promoters and tungsten trioxide WO₃ combined with MoO₃ as active additive agents. The standard catalytic conversion is as follows:



A faster reaction might take place as the quantity of NO₂ increases. This reaction does not involve oxygen as follows



A slow SCR reaction is also possible as represented below



On board storage, control and injection facilities could achieve NO_x reduction by 90%. To avoid any drop in NO_x reduction efficiency and the escape of NH₃ with exhaust gases, the operational temperature, which depends on the bed ingredients and the components of the exhaust gases, should be controlled. Ideally the stoichiometric value for NH₃ to NO_x reaction is unity therefore closed loop control systems are essential to keep the process as efficient as possible since the process is sensitive to the fluctuations in NO_x concentration. Durability tests of the SCR showed a relatively small drop in reduction efficiency after a relatively short period of operation which is attributed to the reduced porosity due to void blockage by impurities. Thereafter, the reduction efficiency stabilises then it gradually deteriorates.

The SCR system of the HGV under investigation is explained in chapter 3. In order to make sure that ammonia is spread-out over the SCR monolith, the manufacturer installed the urea injector immediately behind the turbocharger. The high exhaust temperature and long detention time ensures urea evaporation to thoroughly cover the monolith and prevent ammonia spillage. Urea injection control was not based on the SCR NO_x removal efficiency, instead it was controlled by the ECU, which was receiving feedback signals about the engine load or temperature.

2.7.7.3 The impact of UCO on emissions after treatment facilities

Li et al.[127] concluded that a diesel oxidation catalyst DOC worked most efficiently with fresh cooking oil (FCO) compared to PD at all loads and

temperatures. They affiliated these results to the higher VOF content in the FCO. Cosseron et al.[135] described the effect of PM₁₀ emitted from the combustion of biodiesel derived from UCO and soy bean oil on the 4-way catalytic converter fitted to the exhaust system of a single cylinder diesel engine. The 4-way catalytic converter showed remarkable removal efficiency for the fine particles of less than 1µm aerodynamic diameter. The use of a 20% soybean BD blend with PD significantly reduced the emission factor without changing the number size distribution. However a 20% UCO BD blend with PD shifted the number size distribution to the larger particles. They also reported that the 4-way catalytic converter increased carbonyl compounds, formaldehydes, and acetaldehyde concentrations at its output. This was affiliated to the larger particulate size distribution especially for the soluble organic fraction SOF.

Keuper et al.[136] elucidated the factors affecting SCR performance as follows:

Urea injection nozzle allocation

It is strongly recommended to ensure a complete mixing between urea and the exhaust gases to avoid ammonia slippage. A proper allocation of the urea nozzle and the use of baffles will avoid wall contact of urea spray which minimises urea crystallisation and decreases the minimal dosing release temperature.

NO₂/NO_x ratio

Experimental results reveal that NO₂/NO_x ratio of 50% resulted in highest NO_x reduction efficiency. A DOC is usually installed before SCR to oxidise NO to NO₂ and to reduce HC and CO emissions. However, this ratio is un-achievable at low and high temperatures. At low temperatures, during engine warm-up DOC is less efficient in NO oxidation to NO₂ which could be improved by adding more platinum to the DOC to help generate NO₂ earlier. At high temperatures NO₂ is unstable and might dissociate.

Space velocity (SV)

Monolith volume as well as residence time are important factors as they extend the contact between the reactants. Space velocity is defined by Ardanese et al.[137] as:

$$SV = \frac{Q}{V} \dots\dots\dots 2.20$$

where

Q is the exhaust gas volumetric flowrate [L/min]

V is the catalyst volume [L]

A space velocity exceeding 40×10^3 [1/hr] is unacceptable for low speed operation.

Temperature

Since there are many reactions taking place in the SCR, catalysts of wide operational temperatures are required. Actually it is difficult to find catalysts working efficiently to cover the wide range of temperatures. Ferric zeolite is stable at high temperatures while copper based zeolite is more efficient at low temperatures.

Naseri et al.[138] tested an advanced layout for diesel aftertreatment systems. They tested a combination of diesel oxidation catalyst and diesel particulate filter coated by selective catalytic reduction as an integrated unit and a selective catalytic reduction unit with urea injection before the integrated unit (DOC + SCR-DPF + SCR).

This system was operated while EGR system was switched-off to allow higher engine NO_x emissions which allows higher NO oxidation to NO_2 in the DOC or higher NO_2/NO ratio at the SCR-DPF. Although urea injection reduces soot burning and increases soot accumulation in the DPF, the higher NO_2 increases the soot burning and the net effect is higher soot burning. This behaviour leads to a more efficient passive regeneration process which reduces the frequencies of active regenerations of DPF and consequently more fuel economy. Finally they witnessed higher NO_x removal efficiency as the exhaust gases flow through the SCR unit this was attributed to the larger total SCR volume.

Mizushima et al.[139] studied the effect of BD derived from UCO on the performance of urea-SCR diesel aftertreatment. In the course of their work, they compared B100 with PD and concluded that urea-SCR performance deteriorated as they used the B100. This was firstly attributed to the higher engine-out NO_x due to higher combustion temperatures and secondly due to lower NO_2/NO_x ratio for the B100 at the inlet of urea-SCR. Engines operated by B100 produce more NO than NO_2 . This NO_2/NO_x decrease was affiliated to the slight decrease in exhaust temperature for the B100 at the DOC inlet. Since the DOC is very sensitive to temperature changes therefore lower NO_2 is produced. The other possible reason for lower NO_2 is higher SOF formation from the B100 combustion due to poor BD atomisation and evaporation. This

will increase SOF accumulation in the DOC which hinders NO oxidation to NO₂.

Brookshear et al.[140] investigated the effects of Na contaminated B20 on two different diesel aftertreatment layouts particularly

DOC + SCR + DPF for LGV's

DOC + DPF + SCR for HGV's

They concluded that the NO_x reduction efficiency of the copper-zeolite SCR was the worst compared to other SCR materials during their exposure to Na contaminated exhaust gases. They also stated that SCR efficiency largely depends on its position in the diesel aftertreatment arrangement. The SCR of the LGV configuration was severely affected by Na contamination especially when the SCR was subjected to pure NO while no impact on HGV arrangement was observed. The cordierite DPF of HGV configuration was deeply penetrated by Na and it works as a shield for SCR protection. This leads to 20% reduction in surface area of the entire DPF.

2.8 Modifications needed for fuelling CI engines with UCO

2.8.1 Fuel tank and lines heating through heat recovery from the engine

The higher viscosity, density and bulk modulus of elasticity of UCO compared to PD necessitates UCO property change to approach those of PD. These properties are inversely proportional to temperature. Therefore on-board UCO temperature control prior to its injection in to the cylinder is a key solution. Blending UCO with PD is a complimentary solution for more flexibility in operation especially during cold starts as UCO is very viscous and dense. Practically this could be achieved by on-board UCO heating by heat recovery from the engine coolant. Fuel mixing and metering is controlled by an engine control unit (ECU) to fulfil engine demand. It is inevitable to switch back to 100% PD before engine shutdown to flush out the fuel injection system by PD and be ready for the next cold start with PD as shown in fig.2.12. In this system only the PD is recirculated to PD tank while the UCO is recirculated back to the fuel injection pump. During fuel system flush-out process, only PD flows through the system to clean out the fuel injection pump and injectors and the excess PD flow cleans the fuel filters then drained to the UCO tank.

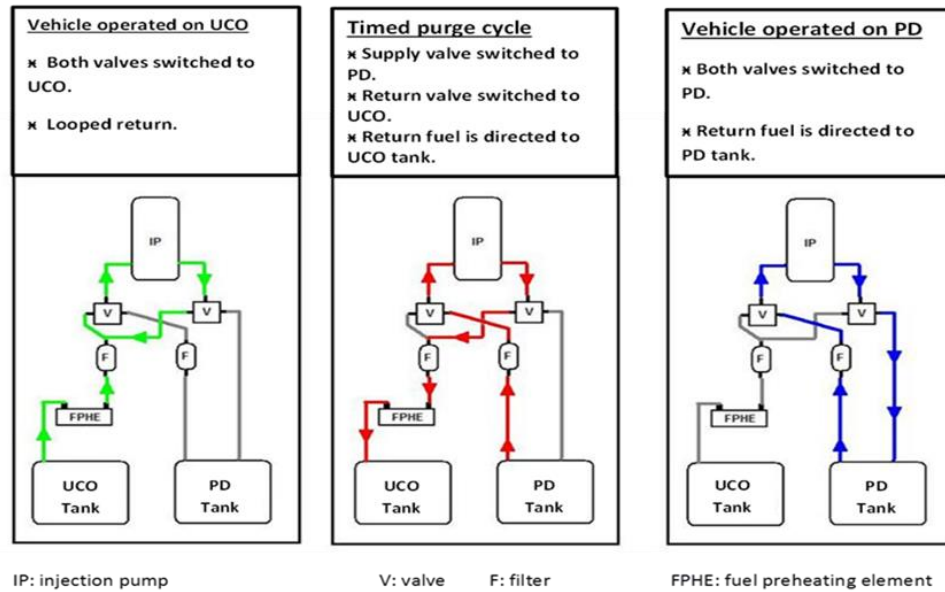


Figure 2.12 Dual fuel system used as an on-board fuel heating and mixing facility

The engine of the HGV under investigation is fitted with the same flush-out system. However, the Bioltec system delivers fuel blends at different proportions depending on UCO temperature. UCO heating is accomplished by the heat recovered from the coolant through a heat exchanger placed in the UCO compartment of the storage tank.

Obert [141] defined the multi-fuel capacity of the diesel engine as it complies to the following characteristics:

- The ability to operate on type-2 PD fuel oil and a number of other fuels including special gasoline without adjustments, and with power variations arising only from differences in density and pumping characteristics.
- Low fuel consumption and clear exhaust on all fuels.
- The ability to start satisfactorily at -31.6°C with any of the fuels without external aids.

Dorn and Zahoransky [38] studied the operation of three different diesel engines fuelled with four non-esterified plant oils (virgin vegetable oil VVO). They recommended VVO heating to 90°C as a mandatory practice prior to the fuel injection. This will enhance the atomisation of the injected fuel and control the fuel jet configuration to imitate those of PD.

Pugazhvadivu and Jeyachandran [37] investigated the effect of UCO preheating on the performance and emissions of a single cylinder diesel engine and compared the results with the PD. UCO was introduced to the

engine at three different temperatures, 30°C, 75°C and 135°C respectively. They found that UCO shows higher bsfc than PD at all loads and speeds. The lower calorific value of UCO with its higher viscosity, density, and surface tension were the main reasons. UCO preheating reduces this deviation. The maximum thermal efficiency was improved from 21.6% to 25.8% as UCO was heated from 30°C to 135°C respectively.

Pugazhvadivu and Jeyachandran [37] examined the properties of the UCO particularly the viscosity. They found that the viscosity of UCO at 135°C coincides with that of the PD at 30°C. They concluded that although UCO produces higher CO emissions than the PD, the increase of preheating temperature reduced the gap. UCO preheating is directly proportional to NO_x emissions but they were still lower than that of PD. Preheating of the UCO reduces bsfc to certain values which are very close to that of PD.

Wu et al.[142] studied the impact of using BDs and their oxygenated additives on CI engine performance and emissions. They announced reduced engine power by 9%~12% and an increase in bsfc by 13%~15% in comparison to PD. This was affiliated to the low calorific values of the oxygenated additives.

UCO was used as a fuel in a six cylinder diesel Mercedes-Benz car and a V-8 Chevrolet Suburban SUV in real world tests. UCO preheating to 70°C as an optimum temperature for long term engine operation was recommended. Heating was achieved by circulating UCO feed pipes around the engine before injection [29].

Vojtišek-Lom et al.[36] concluded that heating the SVO past 55°C and additional electrical heating of the high pressure injection lines does not improve the combustion timing or exhaust emissions. They also reported that at higher engine loads the fuel temperatures would increase from 40°C at the pump inlet to 70°C at the injector inlet. This will reduce the need for the artificial SVO heating.

On-board heating of UCO in the HGV under investigation is achieved at no extra cost or engine power consumption. It is done by heat recovery from the cooling system. The Bioltec system works to produce fuel blends suitable for the injection process. In fact this depends on UCO temperature and the ECU preloaded engine performance maps. The driver has the choice to run the HGV on pure PD or the BL fuel which is predominantly UCO as its temperature is above 70°C at the Bioltec outlet to reach 90~100°C at the injector nozzle [13, 14].

2.8.2 Combustion chamber insulation and configuration

Işcan and Aydin.[143] studied the effect of combustion chamber insulation on corn oil biodiesel blends with PD usability, performance ratings and engine emissions. The test was carried out on a single cylinder air cooled DI diesel engine. The cylinder head, valves and piston crown were coated with ZrO_2 for an adiabatic combustion process. They concluded that the combustion chamber coating was durable after extended periods of operation (100 Hours). The performance ratings of the coated engine with the biodiesel were improved and the bsfc was almost the same to the uncoated engine with PD fuel. The coated diesel engine operated with the biodiesel exhibited lower CO and HC emissions while the NO_x emissions were higher compared with the conventional diesel engine operated with the PD due to the adiabatic conditions and higher oxygen content of the BD. Aydin [144] achieved the same results on his study on the same engine while using SVO like pure inedible cottonseed oil and sunflower oil blends with PD at different ratios up to B35. He also reported lower smoke emissions from the SVO in both coated and uncoated engines.

Jaichandar et al.[145] studied the effect of combustion chamber geometry and the injection timing on the performance and emissions of a single cylinder DI diesel engine. The engine was fuelled with ultra-low sulphur diesel ULSD as the base fuel and compared with the B20 pongamia BD. Keeping the compression ratio unchanged; two combustion chamber geometries were used. A conventional hemispherical open combustion chamber and a modified toroidal re-entrant combustion chamber (TRCC) were tested. They reported a 5.64% gain in brake thermal efficiency, 4.6% reduction in bsfc with a considerable reduction of CO and HC and an increase of 11% of NO_x in the modified engine operated with B20 pongamia BD even though the BD was 14.5% more viscous and 2.3% lower calorific value. This was attributed to the better homogeneity of the mixture, higher combustion temperatures and higher oxygen content and cetane number of the BD. The injection timing retardation improved then deteriorated the performance and optimised at 23° bTDC.

2.8.3 CI engine aspiration system enhancement

Conventional diesel vehicles used to soot apparently during transitions. These are a stepwise or pulse stimulations in the operational conditions like, gear shifts and acceleration and change to higher loads. The sudden increase in

the amount of fuel injected is the stimulus which increases the speed followed by a higher air demand. At the very beginning the increased fuel injection would increase the equivalence ratio. A very rich combustion with limited oxidation would certainly lead to increased emissions. Meanwhile there would be an instantaneous demand for air due to the sudden increase in engine speed.

Unfortunately there is a time lag between the fuel and air induction systems due to the simultaneous increase in air flow resistance. This will result in a sudden drop of the volumetric efficiency and in cylinder air density. A deeper fuel jet penetration would result in flame or even fuel impingement to the cylinder walls. More soot precursors and recently formed particles won't be oxidised due to the collapse in flame structure. They will escape the diffusion flame, and will be wall deposited or emitted through exhaust port.

Turbochargers convert the high enthalpy of exhaust gas to high speed shaft work. The air compressor would be actuated by the exhaust gas turbine. The total time lag from the fuel injection to compressor actuation is called the turbo lag. Variable geometry turbocharger (VGT) assisted by exhaust bypasses are recently fitted to new engines to help reduce turbo lag effects.

Stoffels et al.[146] studied the transient acceleration performance and suggested a low backpressure behind the turbine assisted by an efficient intercooler will significantly improve the charged air density and engine performance through transients under severe environmental conditions. They also suggested a linear rate of boost pressure for smoother vehicle acceleration.

Cieslar et al.[147] proposed a novel strategy through air injection into the exhaust manifold to help accelerate the compressor as a means for turbo lag management. The tests were carried out on a four cylinder, 2 litre, variable geometry turbocharged (VGT) EURO5 compliant engine. The tests showed 60% reduction in time to torque at the 3rd gear braking and tip-in manoeuver. Arnold et al [26] elucidated the electrically assisted turbocharging system. They stated a 1.6 kW electric energy for only 2 seconds is quite sufficient to reduce the time to torque by more than 60% as the 1600 kg vehicle was accelerated from idle speed on the 4th gear.

Rao and Mohan [148] studied in their experimental work the effect of supercharging on the performance of a DI diesel engine fuelled by a non-processed pure cotton seed oil SVO. They concluded that; increasing the injection pressure (IP) to values higher than the specified ones does not

improve the performance of the naturally aspirated and supercharged engine operated by the SVO. They also reported that a gradual improvement in performance is associated with the increase of the supercharging pressure at the recommended injection pressure. They observed a 15% reduction in bsfc when the supercharging pressure was 0.4 bar(g) higher compared to the naturally aspirated engine where both were being operated by SVO. Smoke density varied inversely with the increase of supercharging pressure for the SVO operated engine.

2.9 Novel strategies for emission mitigation

2.9.1 Novel fuel injection strategies

Mueller et al.[149] studied the effect of advanced injection strategy and dual injection strategy on the combustion process and the attenuation of soot and NO emissions. The study was carried out on a single cylinder version of a caterpillar C-10 engine. The engine was modified for optical injection and flame observation. Their observations on the advanced injection strategy indicated poor combustion efficiency due to longer fuel jet penetration and wall impingement. The combustion starts with cool flame reactions due to mixture stratification followed by higher combustion temperature. Eventually the combustion was characterised as HCCI like combustion with low soot and negligible NO emissions.

The dual injection strategy was designed to produce a pre-injection at 44°bTDC while the main injection was studied at 5°bTDC and 13°aTDC respectively. They observed different injector lags for the pre and main injections. During the pre-injection process, doubling the speed from 900~1800 rpm delayed the pre-injection by 3 CAD which equals 63% decrease in ignition delay period. This resulted in shorter combustion duration with a higher heat release rate. The expected pre-combustion condition would be a shorter oxidation time for a richer mixture. A different ignition delay was observed for the main injection process. Therefore doubling the engine speed decreased the ignition delay by 9 CAD which equals 30% decrease in time due to a 1 CAD injector lag. The rate of heat release decreases to one fourth as the speed doubles and the duration of combustion increases as the speed increases.

A 50% improvement in combustion efficiency was observed for the dual injection process because the high efficiency main combustion burned out the unburnt premixed mixture left-over from the early combustion process. NO

emission was also reduced by an order of magnitude compared with the conventional single injection especially for the retarded main injection (13°aTDC) as the combustion took place at a lower temperature during the expansion stroke.

2.9.2 Novel combustion strategies

Tree and Svensson [25] elucidated, in their review, emissions formation in conventional diesel engines. According to fig.2.13 richer mixtures produce more soot and the highest soot concentration could be obtained at moderate temperatures (1900~2100°K). These are exactly the conditions at the rich premixed flame at the downstream zone ahead the fuel jet.

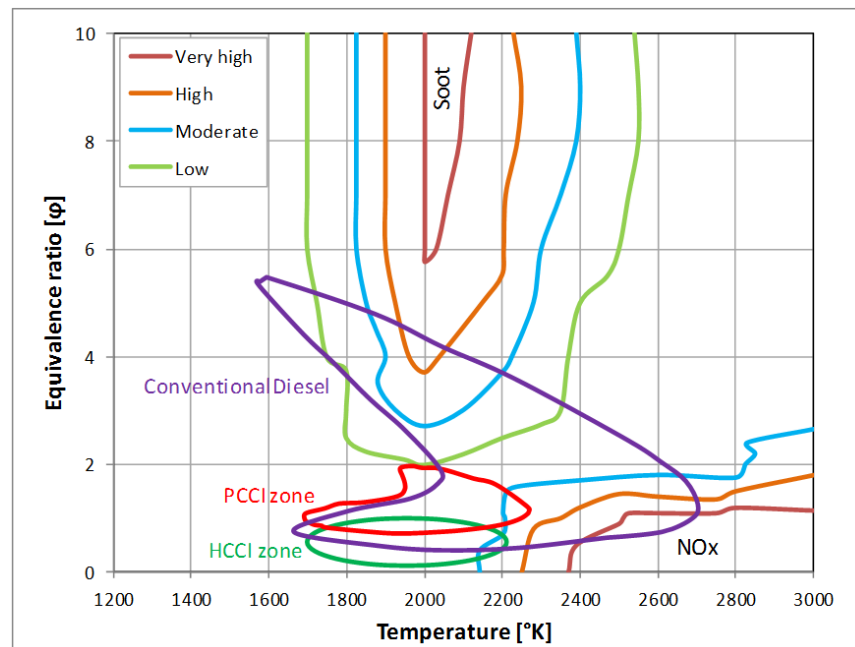


Figure 2.13 Equivalence ratio versus combustion temperature for conventional diesel engines showing soot and NO_x formation zones and the PCCI and HCCI operation zones.

Reproduced from Li et al [109].

As the temperature increases, soot concentration decreases with the presence of the oxidants in the diffusion flame. At the diffusion flame where the temperatures are very high and the ambient oxygen is sufficient, higher NO formation is observed. Increasing ϕ at these circumstances could reduce NO to N₂. They concluded that low emission CI combustion could be achieved by keeping the combustion conditions confined by the lower left corner of the ϕ vs T diagram with an exponentially decaying relationship line between ϕ

and T. Two promising combustion approaches are under investigation in this particular area namely; the Premixed Charge Compression Ignition (PCCI) and the Homogeneous Charge Compression Ignition (HCCI) which are explained in the following paragraphs.

Pickett et al.[150] in their endeavour to achieve a soot free mixing controlled combustion with negligible NO_x emissions, they concluded that the aforementioned results could be achieved by any one of the following conditions:

- Downsizing the injector orifice to 50 μm to inject type 2 diesel fuel in an EGR diluted charge environment to achieve 10% oxygen content. The ambient temperature was kept around 1000°K. A well-mixed lean mixture was developed which resulted in an extended flame lift-off length and a lower soot formation. This was only achievable by the lower ambient oxygen and a smaller amount of fuel being injected from the smaller orifice. Although the lower ambient oxygen adversely affect soot oxidation in the diffusion flame as the temperature decreases, it significantly reduces the amount of NO_x formed as well.
- Downsizing the injector orifice to 50 μm to inject type 2 diesel fuel into a cooler environment at 850°K without EGR to preserve oxygen content in the charged air at 21%. The combined effect of the shorter jet penetration length and higher oxygen content produce a lean mixture and extend the flame-lift-off length therefore a soot free combustion will take place and the low ambient temperature cooled down the diffusion flame for a very low NO_x formation.
- The utilisation of a 180 μm injector orifice to inject an oxygenated fuel into a hot (1000°K) and very dense (30 kg/m^3) environment. This procedure required a very high EGR levels to keep the oxygen content in the charged air in the range of 5~8%. The relatively larger orifice will increase the fuel jet penetration length and the higher ambient temperature would certainly reduce the flame-lift-off length. Albeit the high oxygen content in the fuel at the elevated temperature would activate the reactants towards soot-less complete combustion. The higher ambient temperature is counteracted by the lower ambient oxygen. This combination would minimise NO_x formation at the diffusion flame zone.

A few applications were developed to achieve the aforementioned goals. HCCI engines are considered as environment friendly engines at low load operation. They satisfy the LTC ($T < 1350^\circ\text{C}$) and low ϕ ($\phi < 0.3$) conditions together. Their principle is to develop a lean homogeneous fuel-air mixture by

injecting the fuel into the induction manifold to provide sufficient time and turbulence for a homogeneous mixture to form prior to combustion. Fang et al.[151] stated that under HCCI conditions, premixed flame combustion dominates and the diffusion flame is eliminated. Eventually, a soot free combustion that doesn't encourage NO_x formation later on is achieved. Unfortunately HCCI principle is still inefficient in large scale high load engines where richer mixtures are required. Pidol et al.[152] used ethanol based fuels to expand the operating range of the HCCI engine. They concluded that low aromatic content and high oxygen in these fuels reduced soot precursor formation and improved soot oxidation at the premixed flame zone. The lower cetane number extended the ignition delay period for better mixture homogeneity to maintain the soot-free property. They also suggested a lower injection pressure to overcome the high noise associated with HCCI operation at high loads.

In practice Modulated Kinetics (MK) engines were built. The MK is accomplished by increasing the injection pressure, retarding the injection timing, increasing the EGR rates with enhanced air movement.

For moderate loads, Fang et al.[151] recommended the Uniform Bulky Combustion System mode (UNIBUS) which produces a uniform lean mixture by early in-cylinder fuel injection as short pulses from a pintle type injector at a high injection pressure.

The PCCI engine is a combustion strategy in which SOI takes place early at the end of suction stroke or the beginning of the compression stroke. Although, an overall lean mixture is obtained from the stratified premixed charge, some local rich fuel-vapour air zones around the fuel jet also produced. Therefore it is a LTC of a heterogeneous mixture which covers the high load domain of engine operation.

Manin et al.[121] suggested the Leaner Lifted Flame Combustion (LLFC) as a novel combustion strategy to reduce both soot and NO_x emissions. Unlike the LTC, the heat release in this technique is controllable by the injection process rather than by the chemical kinetics. Moreover, the combustion process is more quite at the range of operational loads and speeds. Polonowski et al.[153] indicated the principle of LLFC is to achieve a low combustion temperature at equivalence ratios less than or equal to two ($\phi \leq 2$) on the fuel jet centreline. This means a well-mixed lean mixture with short ignition delay to be burned at low temperatures with sufficient amounts of oxygen delivered within the fuel. This could be achieved by reducing the

amount of fuel being injected through smaller orifices under higher injection pressures to increase the FLL and decrease ϕ . A moderate EGR rate to reduce the chemical kinetics of the mixture therefore increase the ignition delay period and extended the FLL. The oxygen present within the oxygenated fuel reduces ϕ at the fuel jet centreline to enhance the completion of the premixed flame to produce a soot free combustion. Eventually, the cooler diffusion combustion achieved could detrimentally affect soot oxidation, however it will reduce NO_x formation as well. Polonowski et al.[153] stated that LLFC could be achieved but not sustained. Flame and fuel jet, from adjacent orifices, interference could affect the sustainability of LLFC through reducing the FLL. Therefore reducing the number of orifices to five or less is recommended.

2.10 Conclusion

A scarce amount of data was found about the direct usage of pure UCO in diesel engines. Probably nothing was performed under the real world test conditions. In fact, due to the un-clarity in the data, some of the following items became the starting points for this research.

1. The global production of UCO is high with low levels of exploitation.
2. The energy density is comparable to PD.
3. Mature UCO production technology as a biofuel.
4. No health hazards in case of long term usage and exposure.
5. Huge difference in the physical properties compared to PD. That's why most of the work was performed on the UCO derived biodiesel rather than the refined UCO.
6. Many contradiction in research findings due the differences in the original feedstock, the fuel injection system and engine technology and test strategy.

The current research is basically part of the national efforts to reduce carbon foot print in the UK [28]. The main approach is to test used cooking oil (UCO) in a heavy goods vehicle (HGV) under real world driving conditions (RWDC). In fact UCO is a waste material abundantly produced worldwide[37, 154]. Using UCO as fuel in diesel engines could arguably be the best waste management technique. It incorporates waste collection, treatment and degradation to natural elements after extracting its stored energy in a record time. Given that UCO possesses a calorific value quite comparable to that of

petroleum diesel (PD), and in order to maintain its high level of renewability and energy efficiency, it was decided to be used directly in diesel engines.

UCO is characterised by its high density and viscosity compared to the pump PD at ambient temperatures [53]. These property differences are large enough to impede its usage in a low performance diesel engine which intrinsically designed to work on PD [33]. The UCO density is about 7.7% higher than that of PD at 20°C. The kinematic viscosity of UCO is 16 fold higher than that of PD at 20°C. On the other hand, the oxygen content of UCO and its chemical structure play a key role in the combustion process and emissions.

To bridge the gap between the two fuels, UCO heating become a mandatory practice [36, 37, 83]. An on-board fuel heating and mixing facility is installed and connected to the fuel system for this purpose. This unit is called the Bioltec system. UCO heating to 70°C, by heat recovery from the engine cooling system is sufficient enough to flow freely without mixing through the fuel pipes down to the fuel injectors. At the fuel injector its temperature is promoted to 90~100°C [13, 14]. After this particular point, fuel atomisation, evaporation and mixing with air depend mainly on engine design and specifications.

The test vehicle is a 44 tonne articulate HGV. The tractor is Mercedes-Benz Axor-C 2543. It is powered by 315 kW six cylinder in-line DICl engine as demonstrated in table 3.1. The engine is turbocharged and equipped with a high performance fuel injection system which is capable to inject the fuel at 180 MPa from seven 0.2 mm orifices. The compression ratio is 18.5:1 and the bore to stroke ratio is 0.825. The combustion chamber is shaped like an inverted mushroom carved in the piston crown. The engine is designed to deliver its maximum power at 1900 rpm which is considered as a moderate speed. All these properties worked together to make the UCO combustion possible.

As the fuel is injected under high pressure a spray of fine spherules is produced. The mean diameter of the spherules depend on engine load and injection pressure [6]. The higher the injection pressure the smaller the spherules are [79, 155]. The spray cone angle is also directly proportional to the injection pressure and the in-cylinder air pressure[155]. The higher the compression ratio the wider the spray cone angle is. In fact these high pressures limit the fuel penetration length. The produced spherules will certainly have different sizes. The large spherules absorb heat for a longer

period of time until they burn suddenly. The smaller ones have less inertia but they experience a number of heating, evaporation and cooling cycles until they vanish. They might overtake the larger ones [133]. The very large spray cone angle increases the distance between the adjacent spherules to have more air-fuel contact. This increases the rate of fuel evaporation due to less air saturation with fuel vapour [149]. The fuel vapour in the wake of the evaporating spherules produces the flame front of the premixed flame. At this particular stage, the higher kinematic viscosity of UCO offers a narrower spray cone angle and larger mean droplet size [18]. The distillation curve of SVO shows that most of the distillation cuts become volatile at temperatures between 320~340°C. PD components distillate gradually as the temperature increases [19]. These differences in fuel properties increase the physical ignition delay period of UCO but it decreases its chemical delay. Therefore it is expected that the UCO combustion will be slightly delayed but the rate of heat release will be much higher [33]. Added to that the oxygen content of UCO accelerates the premixed combustion [53]. This high rate premixed combustion approaches the adiabatic conditions due to less heat dissipation in radiation. Hence a very high diffusion flame temperature is expected in the case of UCO [99].

The physical properties of UCO could probably reduce its flame lift-off length [17]. This will adversely affect the AF ratio towards a richer premixed combustion of UCO [121]. However, the oxygen contained within the UCO is sufficient for a lean premixed combustion close to the PCCI approach [1]. The oxygen content and the high rates of radicals (OH) produced, react with soot precursors in the premixed flame and oxidise soot and CO at the higher diffusion flame temperatures [98]. The sudden high rate of heat release of UCO combustion leads to a shorter combustion throughout the power stroke and a cooler environment for the exhaust gases to enable VOF condensation. Hence larger particulates are expected from UCO combustion.

The properties of UCO and the nature of its combustion process lead to its propensity to produce less soot, CO and THC but higher NO_x. In fact the lower CV of UCO controls the overall combustion temperature and prevents the NO_x emissions to be even higher.

The tests were planned to carry out under RWDC. That is to avoid any interference of the ECU which might alter the operational mode of the engine [27] and the emissions as a consequence. It was also the fleet operator and the fuel provider's will to test the UCO on their own HGVs to avoid any doubts

arising from the differences between the laboratory engine and the one fitted to the HGV. There are also some differences in the way of engine loading which are expected to affect the engine performance and the emissions.

Chapter 3

Experimental and Methodology

The utilisation of renewable fuels is a key element of the UK's national transport policy for carbon footprint reduction. Fuel suppliers and fleet operators struggle to achieve the 10% target of petroleum fuel substitution with renewable fuels by 2020. The trans-esterification process successfully produced the biodiesels which were very comparable to petroleum diesel (PD). However there were some drawbacks such as the cost of production, the amount of energy used and the amount of matter and energy wasted in the trans-esterification process. It was these drawbacks which led the fuel suppliers and the fleet operators to adopt alternative feedstocks and processing techniques. One of the alternatives is the direct utilisation of used cooking oil (UCO) in heavy goods vehicles (HGV). The idea is on-board mixing of UCO with PD in different proportions after being heated by engine coolant.

The current project is profoundly to examine the eligibility of UCO as a fuel and its direct utilisation in HGVs. The eligibility comprehensively includes the environmental impacts, the HGV performance and durability. It is actually a comparative study between UCO and PD. A project of this kind requires a collaborative work between the interested parties represented by Convert 2 Green (C2G) as the fuel supplier and the United Biscuits Midlands Distribution Centre (UBMDC) as the fleet operator and the test HGV provider and the University of Leeds, on the other hand, as the research performer.

In that context, the practical part of the project was divided into field work for data collection from the real world driving tests, and laboratory tests for the fuels and collected samples. This was preceded by investigations for the HGV specifications and its exhaust aftertreatment system.

The real world journey was carefully selected for data sufficiency and the diversity of driving conditions. Added to that, mandatory health and safety measures were followed very strictly to avoid any damage to the people involved, the work environment and the facilities. These investigations played a key role in decisions upon the major performance variables to be investigated and the relevant type of equipment to be used for each variable. Decision making about the type of test instrumentation to be installed on board, the amount of space required and instrument layout, were made after deep discussions. Providing a sufficient source of power for apparatus commissioning was accounted for and implemented. Some of these decisions were reached after a few preliminary real world tests. Accordingly, the sleep

bed in the driver's cabin behind the driver's seat was utilized as the safest and sufficient space for equipment installation. All the test equipment were strap fixed in position to avoid any movement during the normal HGV travel or any possible traffic accidents which might threaten the drive and researcher safety. The required power demand for the test equipment was calculated and accordingly two 12 V 120 Ah batteries were selected. Prior to each journey the batteries were fully charged, however due to the relatively long journey duration, especially during congestions, a power backup line was provided from the HGV electrical system. The two batteries were connected in series and a power inverter was used to provide the 240 V alternating current required by the testing instruments. All the sampling pipe and wires between the test apparatus and the sampling probes were passed through openings made in a plastic replacement for the back window of the driver's cabin.

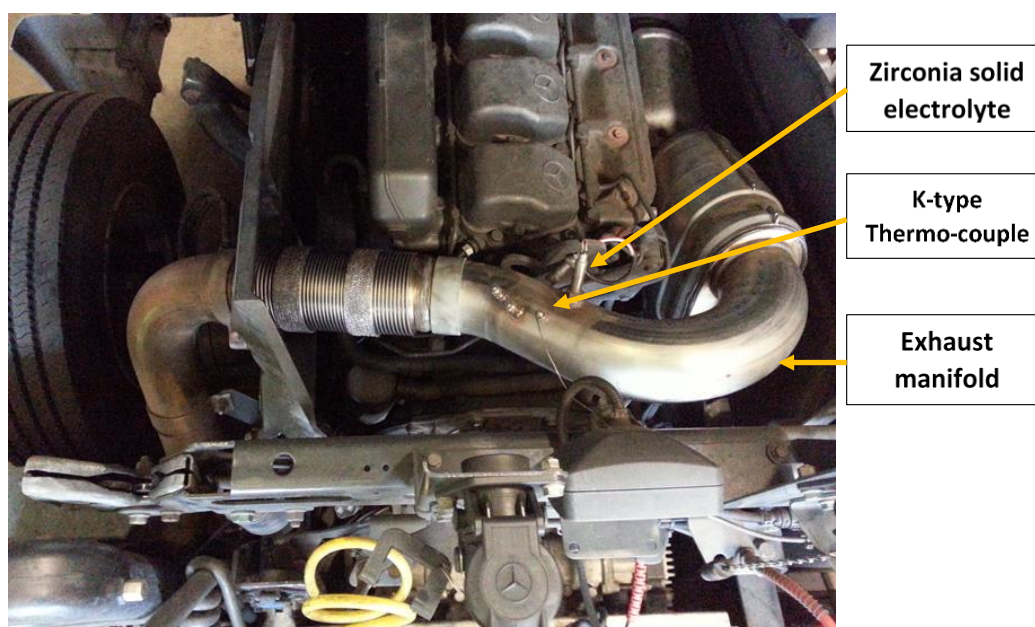


Figure 3.1 Zirconia solid electrolyte NO_x sensor and K-type thermo-couple position on the exhaust manifold.

The study plan branched to, (i) engine-out emissions where the direct effects of the new fuel were investigated, and (ii) tailpipe emissions where the final emission concentrations, as released to the receiving environment, were investigated and compared to the related standards. However, engine-out PM sampling was impossible because the urea injector was situated directly behind the turbocharger. PM samples taken in this particular section of the exhaust manifold, during the preliminary tests, showed huge amounts of ammonium nitrate collected on the filter papers. Since the selective catalytic

reduction (SCR) unit does not affect PM concentration, PM collection probes were located at the tailpipe.

The Fourier Transform Infra-Red (FTIR) sampling probe and the two PM sampling probes, were 6.25 mm stainless steel pipes, securely fixed by a specially designed triple holder fixed in the tailpipe at the SCR outlet. A K-type temperature sensor was also positioned at the same place to measure SCR operational temperature.

To measure the engine-out gaseous emissions and temperature, a Zirconia solid electrolyte (ZSE) sensor and a K-type temperature sensor were installed on the upstream side of the SCR as shown in fig.3.1.

The surrogate fuel, which is merely a purified used cooking oil named C2G UBF after the producer company, Convert to Green, and a complimentary part to be distinguished from biodiesel was called “Ultra Biofuel”. Samples from C2G UBF were taken periodically for lab analysis to study the physical, chemical and thermal properties of the UBF. The fuel samples were also used to watch any possible seasonal variations in its properties due to temperature variations and feedstock.

An engine durability test plan was established to investigate any detrimental effect the surrogate fuel might have compared to PD during the two years of project life. A total of twelve fuel injector samples were taken for in-vitro analysis. These injectors were taken at specified HGV mileages some working on PD and others on blended fuel (BL).

Vehicle speed, heading, position and road profile were measured by the Racelogic global positioning system (GPS) called the Vbox II as explained in section 3.9. These variables were used to determine the sum of the vehicle resistances such as, rolling resistance, air resistance (drag and friction) and gradient resistance. The role of HGV payload and road load were considered individually in the analysis. Vehicle mileage and the time were recorded at the beginning and the end of each journey.

The amount of fuel consumed, whether PD or BL fuel was also taken in consideration. The test HGV was fitted with a Bioltec system, which works as a fuel metering system and a fuel blender. It is the driver's option whether to run the HGV on PD or the BL fuel, however the Bioltec system controls the status of the fuel delivered to the HGV's fuel injection system. The Bioltec system uses the preloaded engine performance maps and C2G UBF temperature to control the surrogate fuel delivery and the mixing ratio with PD.

The average journey mile per gallon (mpg) was also recorded at the end of each journey. The weather conditions were also recorded in each side of the journey. These include, the temperature, pressure, humidity, wind speed and direction.

3.1 The test-vehicle and its technical specifications

The United Biscuits Midlands Distribution Centre uses a fleet of articulated vehicles. Heavy good vehicles have different classifications. The one provided as a test vehicle carries the registration plates FN11 SVC. The tractor was a 6x2 Mercedes-Benz Axor-C 2543 LS powered by a six cylinder in-line direct injection compression ignition (DICl) engine compliant to EURO V emissions standards. The gross vehicle weight (GVW) was 44 tonnes.

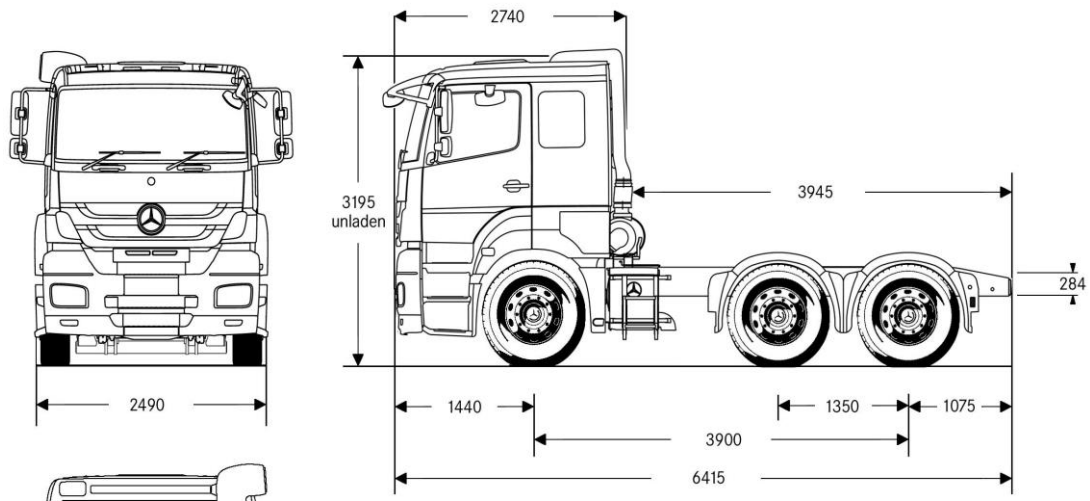


Figure 3.2 The tractor, Mercedes-Benz AXOR-C 2543 LS. The dimensions are in mm. Source www.mercedes-benz.co.uk.

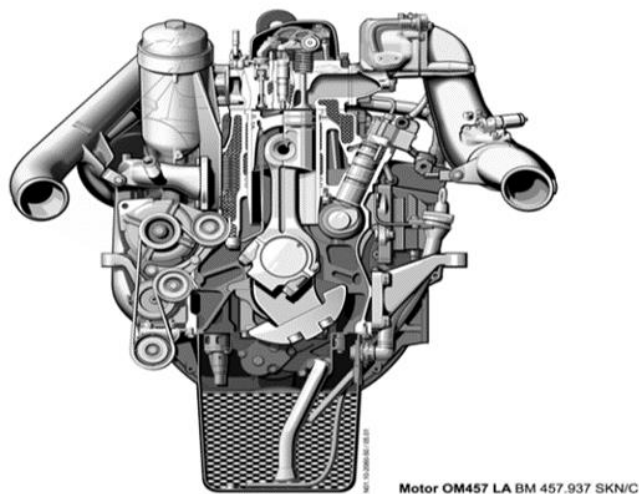


Figure 3.3 The engine OM 457 LA EURO 5.

Fig.3.2 exhibits the front and side view of the tractor and their dimensions. The vehicle is powered a six-cylinder in-line turbo-charged engine as shown in fig.3.3. The technical specifications of the engine are summarised in table 3.1.

Table 3.1 Engine technical specifications

Engine parameter or physical quantity	Units	Value
Engine model	OM 457 LA EURO 5	
No of cylinders		6 in line
Firing order		1-5-3-6-2-4
Displacement	Litre	11.97
Bore	mm	128
Stroke	mm	155
Connecting rod length	mm	≈250
Piston crown cavity volume	cm ³	93.6
Compression ratio		18.5
Engine compartment temperature(max permissible)	°C	100
Rated power	kW	315 at 1900 rpm
Maximum torque	Nm	2100 at 1100 rpm
Low idle speed, standard	rpm	560
Mean effective pressure at maximum torque	bar	22.05
Mean effective pressure at rated power	bar	16.62
Cooling system thermostat start to open at	°C	83
Cooling system thermostat fully opened at	°C	95
Charge air pressure after turbocharger at rated power	bar	1.9
Charge air pressure after turbocharger max.	bar	1.9
Charge air temperature before engine	°C	41
Fuel injectors	6 Electronic controlled unit injectors centrally positioned in the cylinder head	
Injection pumps	6 single injection pumps integrated in the cylinder block	
Maximum injection pressure	bar	1800
Number of injection holes	-	7
Injector hole diameter	µm	200
Maximum permissible fuel jet length	mm	≈48
Fuel consumption at rated power	g/kWh	202
Fuel consumption at full load	g/kWh	185
Intake air volumetric flow rate at rated power	m ³ /min	26.3
Intake air volumetric flow rate (max.)	m ³ /min	26.4
Maximum permissible air temp at rated power	°C	55
Exhaust gas mass flow rate at rated power	g/s	530
Exhaust gas volumetric flow rate at rated power	m ³ /min	56
Exhaust gas temperature at rated power	°C	430
Exhaust gas temperature (max.)	°C	530

The fuel injection system is a pump-line-injector system, in which an individual fuel injection pump was built in the cylinder block. Each pump is directly connected through a short steel pipe to a designated injector. The injectors are centrally positioned for a direct in-cylinder injection. The fuel injectors are electronically controlled by the engine control unit (ECU) as presented in fig.3.4.

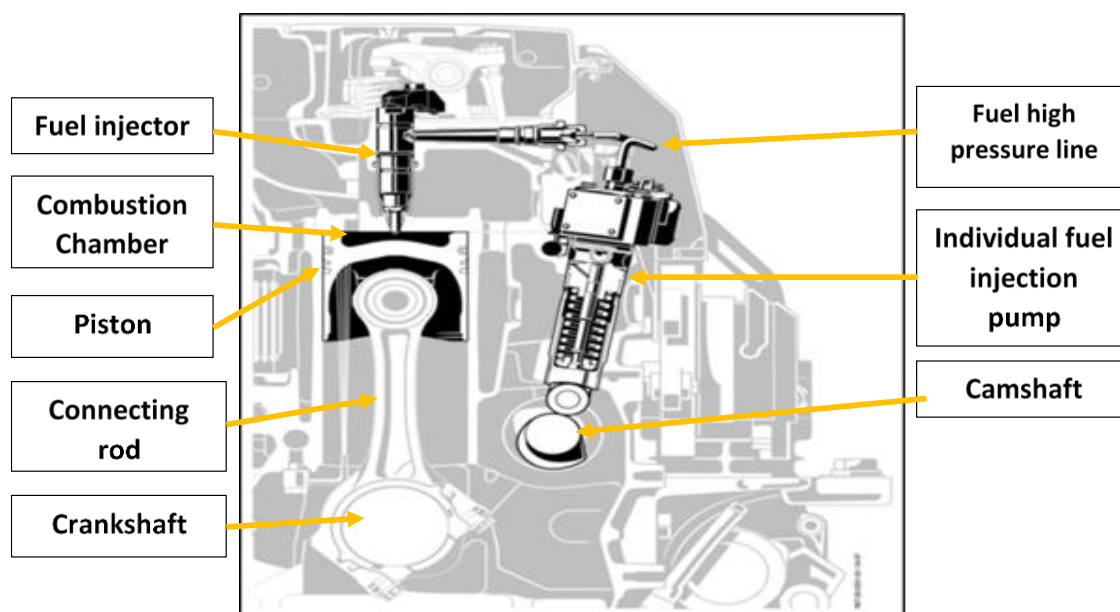


Figure 3.4 the fuel injection system layout of the test vehicle.

3.2 Modifications to HGV for surrogate fuel adaptation

Vehicle adaptation for the surrogate fuel requires special modifications for the fuel system prior to the fuel injection pump. Fig. 3.5 shows the modification in the fuel storage tank. The retrofitted tank consisted of two separated compartments, one for PD with 160 lit capacity and the second of 300 lit capacity for the UBF. It is quite obvious that a heat exchanger is submersed in the UBF compartment exclusively. The two fittings at the top of the tank are connected to the engine cooling system to reuse the heat rejected to the coolant. The hot coolant warms up the UBF to the target temperatures between (45~80°C). The higher the UBF temperature the higher its contribution in the fuel blend. Therefore the HGV starts with PD for a while, depending on the ambient temperature, to the point at which the UBF gets warm enough to be delivered by the Bioltec system.



Figure 3.5 The modified fuel storage system.

At the end of each journey, in which the blended fuel is selected by the driver, it is mandatory for the driver to flush out the fuel system with PD before engine shut down. This is a precautionary measure to ensure a prompt next engine cold start by avoiding UBF thickening and coagulation and fuel system closure.



Figure 3.6 the Bioltec fuel mixer and transfer to the injection pump.

Fig.3.6 shows the fuel line fitted Bioltec hardware. The unit has its own filter and an inlet and outlet for PD and UBF. The control unit shown in fig.3.7 enables the driver to select the type of journey fuel and do the system flushing

with PD prior to engine shut down. The display gives the driver the Bioltec system status and the temperature of the flowing fuel and the mixing ratio.

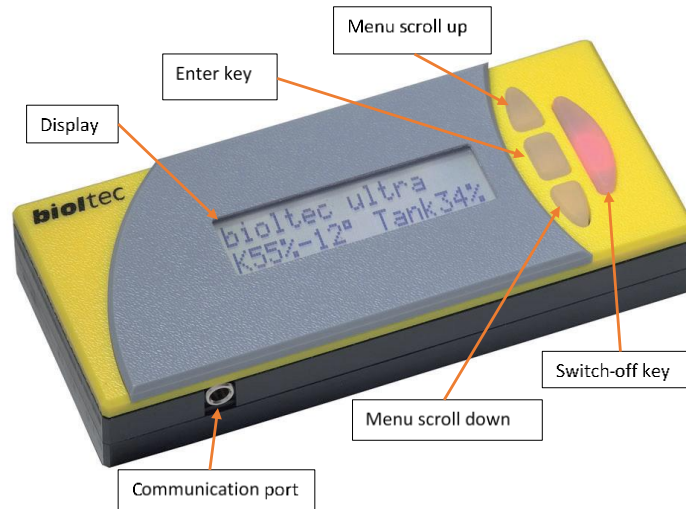


Figure 3.7 Bioltec control unit.

(Courtesy of Bioltec systems GmbH. www.bioltec.de)

The Bioltec system delivers 10 ml of fuel at a time. It starts with the PD by default even if the auto mode (BL fuel) is manually selected. On the auto mode, the system automatically switches to UBF depending on the UBF temperature. The higher the UBF temperature the more its content in the blend to the point where the HGV runs on 100% UBF with occasional PD contribution at sudden changes in vehicle performance. The communication between the Bioltec system and the engine ECU, which is preloaded with engine performance maps, facilitates the amount of fuel to be delivered and its mixing ratio. Having the Bioltec software installed on the laptop computer, various data were logged in such as, fuel tank temperature, flowing fuel temperature, fuel mixing ratio, engine load factor, PD consumption, UBF consumption.

3.3 Real world test journey description

The selected real world journey is actually one of the United Biscuits Midlands Distribution Centre's routine vehicles journeys. V box data analysis show that the journey starts from Ashby De La Zouch, 65 Resolution road (52.75 Latitude, -1.454 Longitude and 138m above sea level). The journey ends at Wigston, 59 Canal Street (52.57 Latitude, -1.1323 Longitude and 78m above sea level). The length of the journey is 34.641 km and the overall change in

height potential is – 60 m. Although the vehicle travelled on the same route, the return journey is 443 m shorter and the vehicle used to travel mostly uphill. The journey comprises steady state and transitional driving conditions.

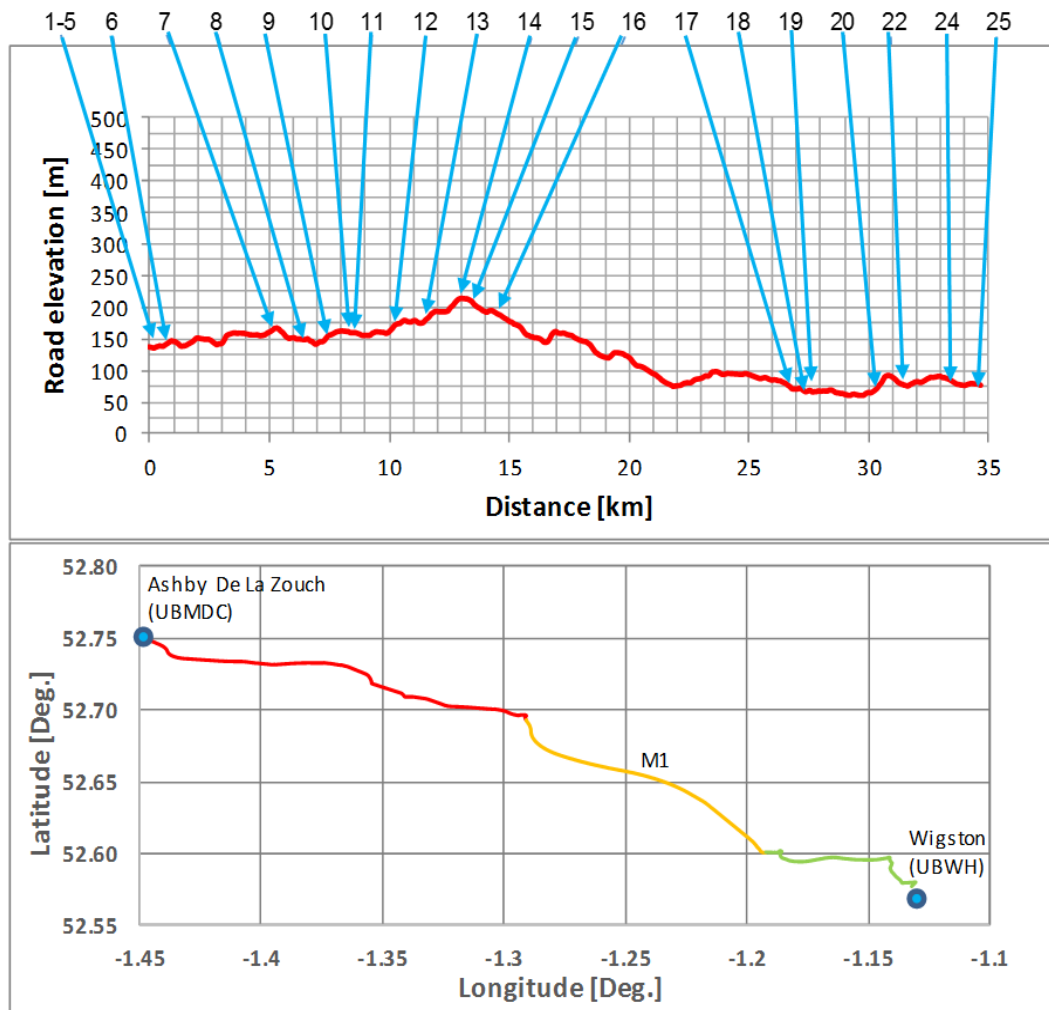


Figure 3.8 Road profile, HGV position and the routine vehicle commute path. All the main positions are described in table 3.2 below.

Fig.3.8 shows the road profile and vehicle elevation during the journey, while table 3.2 describes the position of the major stationary points on the journey path between the two destinations. Fig.3.8 also shows the top view for the road between Ashby de la Zouch and Wigston.

The major steady state driving section is travelling on M1 motorway for 12.3 km. This part has a 110 m elevation difference between its two ends and it is a downhill travel in the outbound journey and exactly the opposite during the inbound journey. This particular road segment is selected to characterise the effects of using C2G UBF, as a surrogate to PD, on vehicle emissions and engine performance under steady state driving conditions.

The journey also included urban and suburban sections. The traffic was controlled by traffic lights, traffic calming and many roundabouts were encountered as shown in table 3.2. Among all the vehicle transitional operations, the ramp to merge on M1 on the outbound journey was selected. This road segment is a straight and inclined path. It is characterised by its 240 m length and a 3% gradient. It immediately starts after a roundabout under the M1 overpass.

Table 3.2 Major vehicle positions between Ashby De La Zouch and Wigston

Distance from start km	Position No.	Vehicle location
0.002	1	Start, 65 Resolution road, Ashby De La Zouch (UBMDC)
0.071	2	TESCO entrance (1st round-about)
0.216	3	TESCO outlet (2nd round-about)
0.223	4	Nottingham road (Traffic lights to enter)
0.378	5	Large round-about to A511 (1st on A511)
0.729	6	Large round-about and overpass on A42 to A511 (2nd on A511)
5.365	7	Round-about to Stephenson way A511 (3rd Round about)
6.737	8	Round-about to stay on Stephenson way(4th on A511)
7.256	9	Round-about to stay on Stephenson way (5th on A511)
8.525	10	Traffic lights
8.939	11	Round-about on to Bardon road (the quarries) (6th on A511)
10.355	12	Round-about stay on Bardon road A511 (7th on A511)
11.694	13	Round-about on to Shaw lane (8th on A511)
13.060	14	Round-about onto Little Shaw lane (9th on A511)
13.910	15	Round-about underpass to M1 ramp (10th on A511)
14.601	16	M1
26.902	17	Junction 21 leave M1
27.202	18	Turn left on to the overpass to merge onto A5460
27.651	19	Merge onto A563 via ramp to ring road
30.279	20	Round about
30.283	21	Leave the round-about to Soar Valley way A563
31.567	22	Pork pie round-about
31.569	23	Exit from Pork pie round about to Saffron Ln B5366
33.582	24	T junction to St Thomas road (Traffic lights turn left)
34.484	25	59 Canal road (UBWH)

The vehicle enters the ramp at very low velocity and starts to accelerate to reach a steady speed of 82~90 km/h (depending on the driver's behaviour) on an inclined road. It is considered as severe engine operation. The road profile

is used as one of the major factors in the determination of vehicle specific power (VSP) in collaboration with vehicle speed and acceleration.

3.4 On-board apparatus layout and power supply

The main objectives of the project were the environmental and performance impacts of UBF as a surrogate to petroleum diesel PD under real world driving conditions. It was decided to control exhaust gas emissions sampling and perform PM sampling from the driver's cabin. Emissions sampling and performing on board experiments are quite different from laboratory environments. In fact there were many challenging obstacles to overcome. These obstacles and limitations were concluded as follows which became the major design requirements for the on-board apparatus selection.

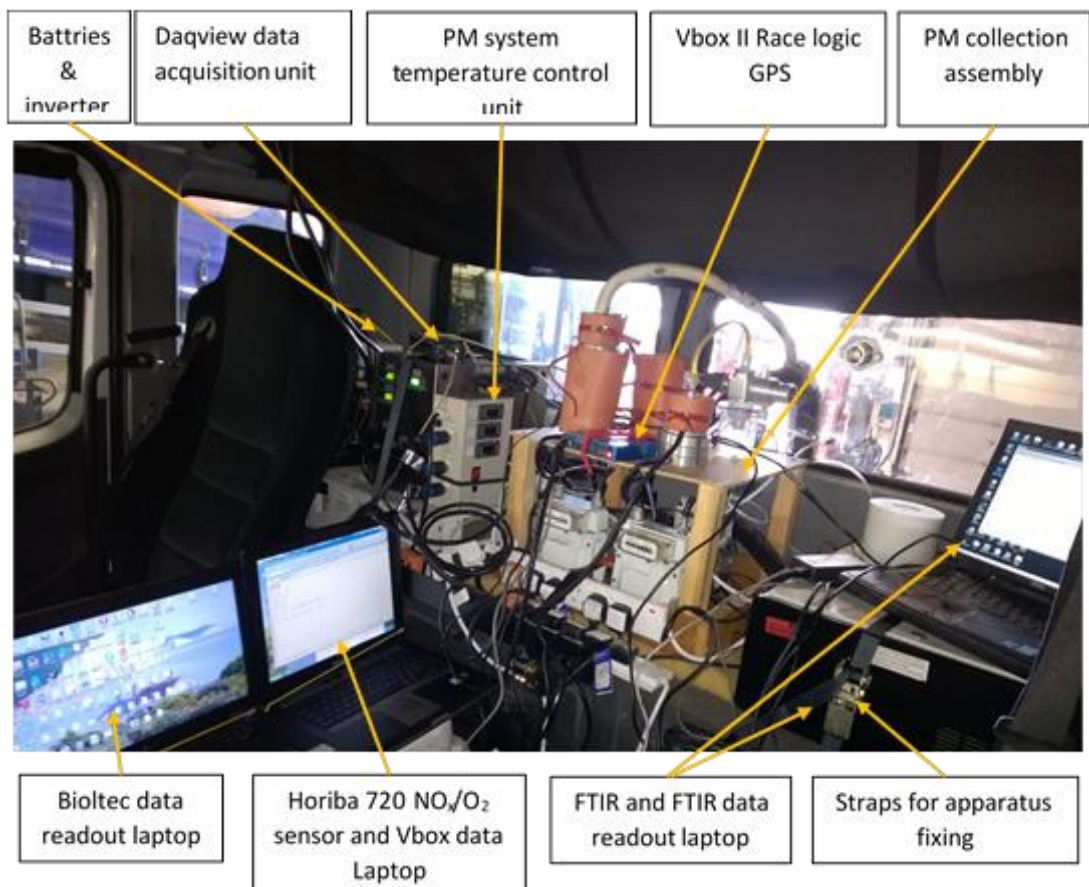


Figure 3.9 Emissions measurement apparatus, vehicle dynamics and power supply units installed on the driver's bed.

- The health and safety issues especially those related to driver distraction such as high temperature, noise, the risk of loose equipment parts and apparatus exhaust. Therefore all the apparatus were fixed in position individually by heavy duty straps. Three hole in the replaced back window were fitted with Swagelok fittings for apparatus exhaust. The heat emitted from the equipment were quite sufficient to switch off the cabin heating system. The only unavoidable nuisance was the 45 db noise level from the two vacuum pumps.
- Vehicle vibrations and biaxial tilting, which might adversely affect the sampling process especially PM sampling. This was a crucial factor in apparatus selection due to their robustness to vibrations.
- The limited space inside the driver's cabin to accommodate the apparatus. Actually, the driver's bed (2 m x 0.9 m) was utilised for apparatus installation added to that the area between the driver and passenger's seats was used for laptop installation as shown in Fig.3.9.

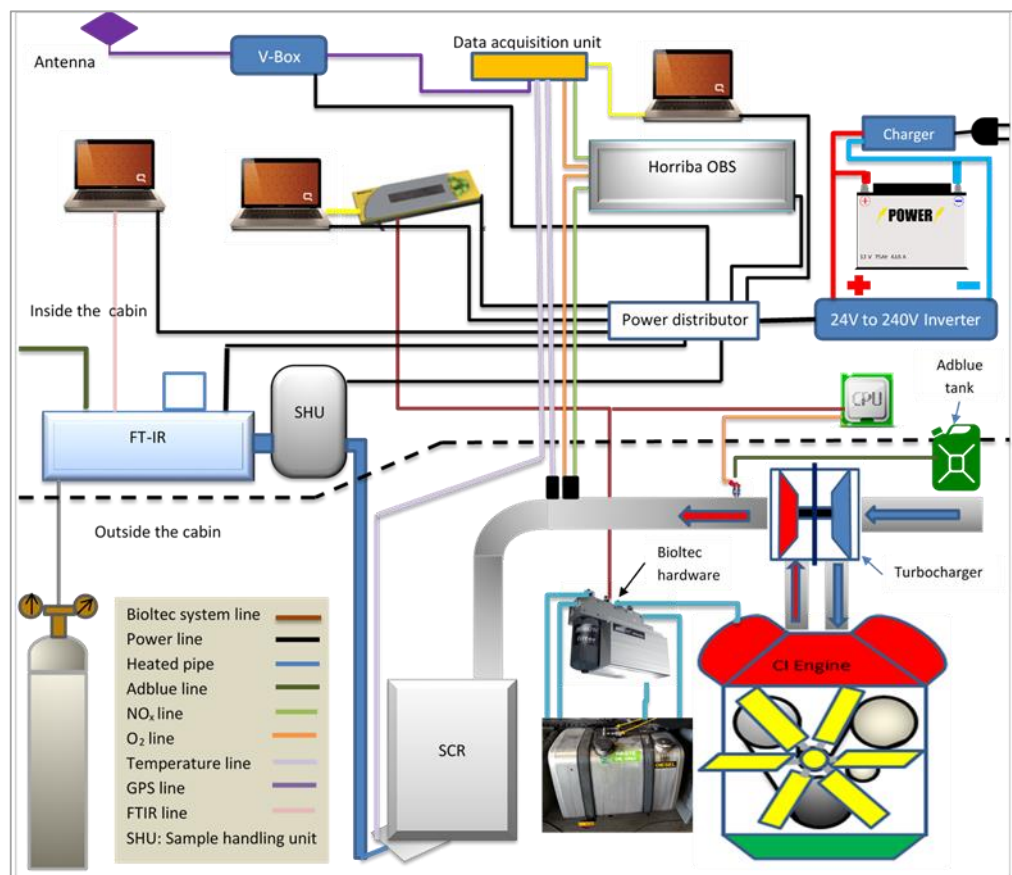


Figure 3.10 Schematic diagram for the apparatus layout for gaseous emissions, fuel consumption and vehicle dynamics measurements installed inside the driver's cabin.

- Apparatus power supply. According to the estimated power demand for the apparatus, two 12V 120 Ah batteries were connected in series to provide 24 V. These batteries were fully charged from the mains prior to each journey. A power inverter was used to convert the battery output to 240 V ac. Furthermore, and as a precautionary measure, two power leads were taken from the vehicle electric system to recharge the batteries for extended journey durations especially due to congestion.
- HGV aftertreatment technology limited the PM sampling probe to the tailpipe due to urea injection behind the turbocharger as shown in fig.3.11. The designer took the advantage of high engine-out temperature and retention time for better urea evaporation and more evenly distribution on the SCR catalyst.

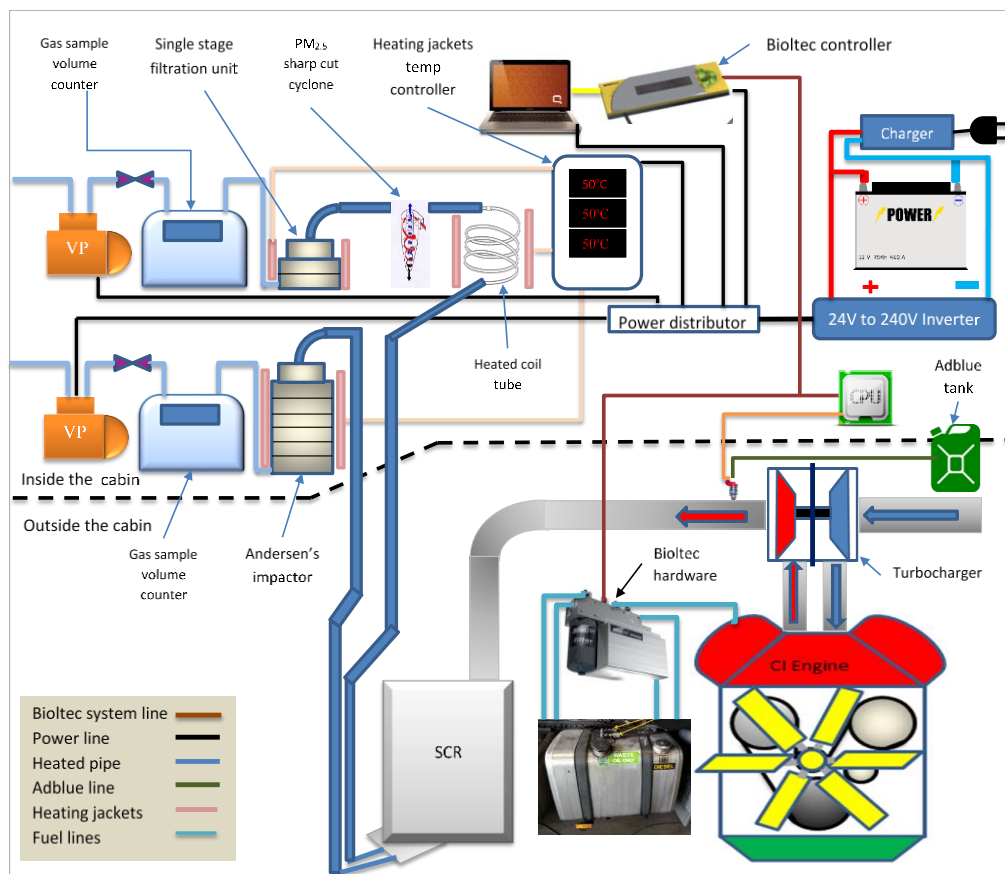


Figure 3.11 Schematic diagram for the PM emissions collection apparatus layout inside the driver's cabin.

- In order to follow up the precise details of engine out emissions which are substantially related to certain road event, the apparatus response should be as high as possible.
- Condensation of vaporous emissions in the sampling lines could lead to material loss and incorrect readings. Water soluble gaseous emissions might not reach the analyser in the lines.

The flexibility in decision making upon the right apparatus which could possibly be used on board became very limited to the ones shown in fig.3.9 and explained in the schematic view in fig.3.10 for gaseous emission measurement and fig.3.11 for PM emission collection.

3.5 PM emissions collection and measurement

The history of PM travel between the combustion chamber to the tailpipe tremendously affects its composition and physical properties [89]. Added to that, exhaust flowrate fluctuates in accordance to the driver's assessment for the road circumstances including traffic legislations and vehicular or mobile object interventions. Therefore, isokinetic sampling became inapplicable under these circumstances. Moreover, vehicle vibration and biaxial tilting limited the PM collection strategy to the cumulative mode rather than the continuous time dependent measurement. It was quite important to take the sample from the centre of the tailpipe at the SCR outlet. The sampling flowrates were kept constant across the journey to the values specified by the manufacturer of the PM sampling apparatus.

Two PM sampling lines were taken alongside with the FTIR heated line. The combination of the three sampling lines were coaxially covered by a 13 mm wall thick foam insulator as shown in fig.3.12. The two PM lines have to maintain a temperature of 50°C, all the way to the collection point, to enhance nucleation of the volatiles and prevent water vapour condensation on the system especially on filter papers [156]. Using new Teflon tubes, 6.25 mm diameter, as PM sampling lines could result in PM loss on the inner surface of the tubes [85]. Therefore, dummy tests were performed to ensure complete inner wall coverage with PM.

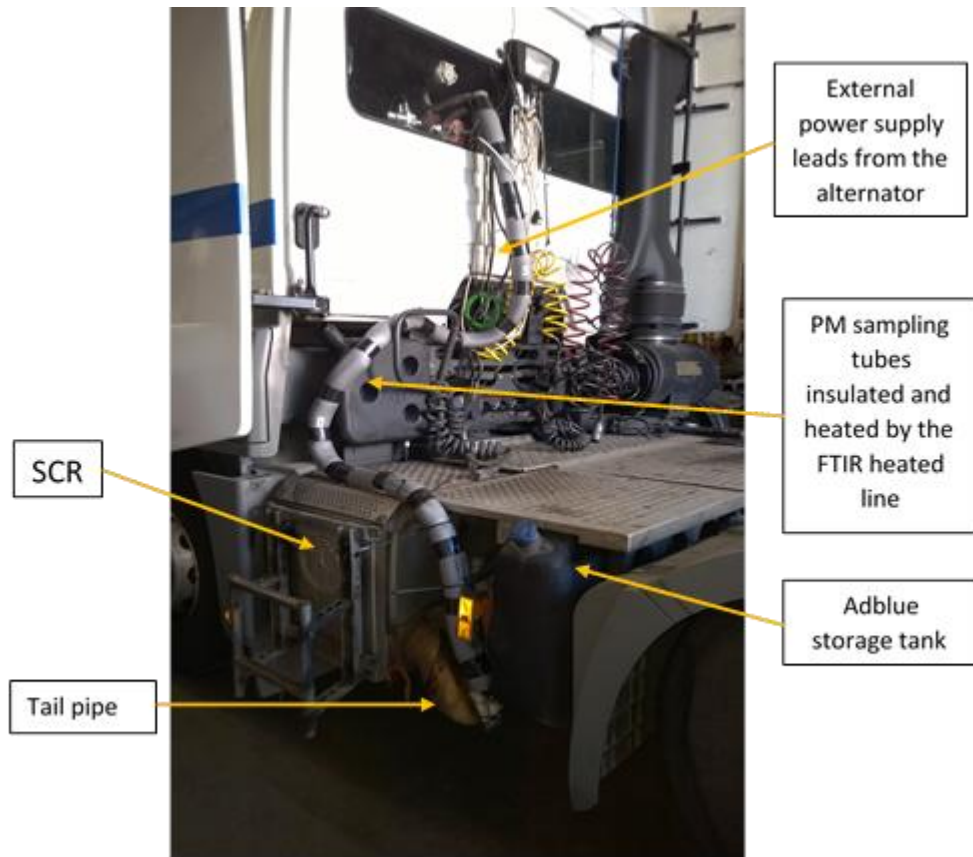


Figure 3.12 FTIR heated line and the two PM sampling lines all wrapped by a cylindrical insulator from the tailpipe to the cabin.

Inside the cabin, the lines were kept warm by passing the exhaust sample through a 4.5 m coiled stainless steel heated lines and the sampling apparatus were also heated by specially designed heating jackets to prevent any water vapour condensation on the filter papers. The temperatures of the heating jackets were controlled and kept constant at 50°C by a specially designed controller for this particular purpose.

The PM sampling and collection systems were designed and arranged in a wooden frame as shown in fig.3.13 to analyse the PM on gravimetric and particle size bases. The two fuels were tested in the HGV under the same conditions and the same test procedure was applied. The results from the two fuels were eventually compared to the steady state and transient EURO 5 emission standards.

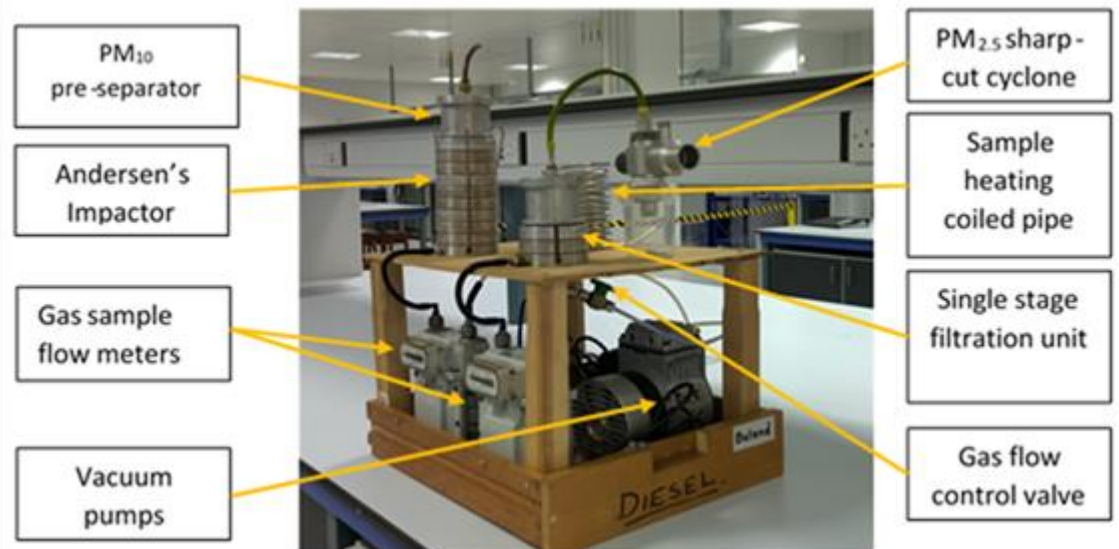


Figure 3.13 PM₁₀ size distribution and PM_{2.5} collection assembly with flowmeters and vacuum pumps.

3.5.1 Cumulative PM_{2.5} collection and measurement by a single stage filtration unit

The cumulative PM sampling and collection system was designed to examine the differences between PM emissions from the two fuels quantitatively and qualitatively. This system targets PM_{2.5} cumulatively collected throughout each direction of the journey from Ashby De La Zouch to Wigston or the other way around.

3.5.1.1 The apparatus and on-board test procedure description

The PM_{2.5} collection system consisted of a few elements connected in series as demonstrated in the schematic diagram at the top left part of fig.3.10 and fig.3.13. The first element is a coiled stainless steel pipe of 4.5 m length by 6.25 mm inside diameter surrounded by an aluminium foil to cover the whole unit as a cylinder. This unit was wrapped by a heating jacket to keep the flow temperature maintained at 50°C along the journey. As PM_{2.5} was the objective, a PM_{2.5} sharp-cut cyclone was used before the filtration unit. Gas sample flowrate was maintained at 16.67 lit/min. In fact this flowrate was specified for the sharp-cut cyclone which was originally designed for a tapered-element oscillating-microbalance TEOM system and adapted for this project. As a result, the retention time throughout the heating-coil was 0.5 s. The sample flow was directed to the single stage filtration unit, which was

actually the last stage of a second Andersen's impactor to embrace the back-up filter. This unit holds the filter paper on its perforated base and is fixed in position with the aid of a rubber O-ring.

The filter media was Whatman's [157] glass fiber (GF/F) grade 1825-090 filter paper. Its thickness was 420 μm , diameter was 90 mm with basis weight of 75 $\text{g}\cdot\text{m}^{-2}$. Filter material was simply a wire-mesh of low ash content 100% borosilicate glass.

The sample flowrate was measured by a gas counter which was connected in series to a control valve before the vacuum pump and then discharged to the atmosphere. The sample exhaust tube was fastened through Swagelok to the rear window of the cabin as demonstrated in fig.3.9 and 3.12. The flowrate was calibrated while the engine was running by measuring the time for a given volume of gas sample to pass the counter. It was also checked throughout the journey especially at high speed sections of the journey to tackle the effect of negative pressure in the wake zone behind the cabin.

3.5.1.2 Gravimetric and thermo-gravimetric analysis for PM_{2.5} samples

Prior to any gravimetric analysis, filter papers needed to be prepared and conditioned. First of all the filter needed to be trimmed to 81 mm diameter to fit the filter holder. This was accomplished in a clean dry environment with an 81 mm inside diameter stainless steel cutter. This was followed by filter paper numbering on its periphery using a pencil. It is recommended to keep the numbered side of the filter facing the downstream side of the sample flow to keep the filter identity for further analyses. Numbered filters were conditioned in a desiccator for 24 hours using silica gel as a drying agent [127]. Moisture removal could reduce the sources of error in filter mass. Gravimetric analyses were achieved by a high accuracy, 0.005 mg, Mettler Toledo electronic balance. The balance pan is merely a cage where the filter is placed by tweezers. A record of all the filter numbers and weights were saved for comparison with the after sampling filter weighing. It is recommended to have three blank filters which are not going to be involved in the filtration process. These blanks could indicate the effect of filter aging, between the two weighings, on its weight which will be used in the error analysis. All the filters should be kept securely in the desiccator ready for the sampling process.

At the beginning of each trip, a clean filter was taken carefully by tweezers and placed on the perforated filter holder then secured by the O-ring. After

replacing the pre-separator, the whole unit was embraced by the heating jacket and kept at 50°C.

Prior to the journey start, the sample gas counter reading was recorded then the vacuum pump and the stopwatch were started simultaneously as the vehicle start to move. At the end of each test the filtration unit was disassembled and the O-ring removed very carefully, with tweezers, to avoid any damage to the filtrate. The loaded filter was taken from its clean periphery, saved in a petri-dish, labelled and wrapped with a plastic bag then refrigerated.

Before weighing the loaded filters, they were desiccated for 24 h to stabilise. Filter mass difference, before and after the journey is the amount of PM collected during that particular journey. However any reduction in the blank filters weight should be averaged and added to PM mass.

Thermo-gravimetric analysis (TGA) for PM collected on filter papers were performed to determine the amount of volatile organic compounds (VOC), elemental carbon (EC), and metallic residues of minerals. Results obtained from TGA of the two fuels were eventually compared and will be presented in section 6.2.

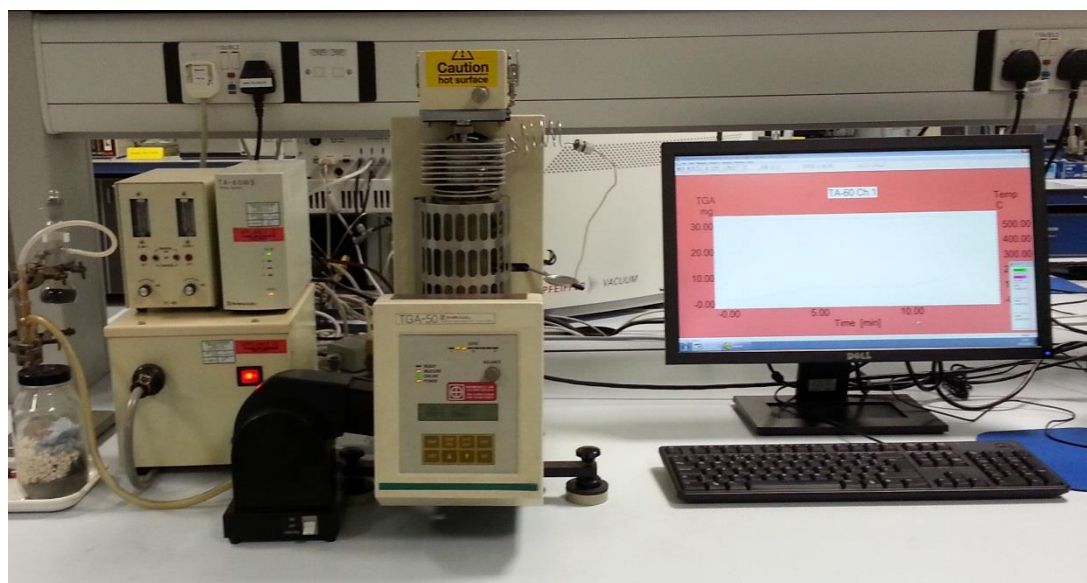


Figure 3.14 Shimadzu 50 thermo-gravimetric analyser.

The apparatus used for filter paper TGA was (Shimadzu 50, Japan) as shown in fig.3.14. Before the test, the loaded filter had to be folded and wrapped by a thin platinum wire and hooked to the main spindle of the TGA instrument to replace the crucible. However, since the volume of the folded filter paper is large and would certainly touch the adjacent thermocouple, only one eighth of

the filter paper was used. It is quite important to cut a representative portion from the filter paper in terms of PM distribution. A 28.5 mm circular cutter was designed and manufactured for this purpose.

In a test procedure developed by Li et al.[127], the machine was programmed to heat the loaded filter portion as shown in table 3.3. The program targets the moisture first by heating the filter in a nitrogen environment. Light volatiles, heavy volatiles were also removed by evaporation. The machine automatically switches to air at 550°C to burn the elemental carbon while the remaining weight is merely ash. The same test procedure was performed on three blank GF/F filters to determine filter material loss at each stage of the experiment in order to be averaged and subtracted from their counterparts obtained from the loaded filters. Randomly, some of the tests were repeated by taking another portion from the original filter. Fortunately the same results were obtained.

Table 3.3 TGA apparatus program for GF/F filters.

Gas	Pace rate [°C/min]	Maximum temperature [°C]	Hold time [min.]
N ₂	20	100	5
N ₂	20	550	10
Air	10	560	10

3.5.2 PM₁₀ size distribution determination by Andersen impactor

The second PM sampling line taken from the tailpipe to the driver's cabin ends at the PM₁₀ size distribution system as shown in fig.3.11. Understanding the differences between the PM size distribution for the two fuels in conjunction to their constituents would be very useful from the environmental and health point of view.

3.5.2.1 Apparatus and on-board test procedure description

The Andersen impactor is a vertically installed cascade impactor as shown in fig.3.15. There are eight consecutive impaction stages preceded by a pre-separator where particulates larger than 10 µm were removed. At the lower end of the impactor, a back-up filter holder exists to remove PM less than 0.4 µm. By maintaining the sample flowrate at 28.5 lit/min, as specified by the manufacturer, PM size distribution throughout the impaction stages takes the form exhibited in table 3.4. The PM size collected on each stage represents

the stage cut-off diameter known as D50, which is the PM size at 50% collection efficiency for that particular stage.

Table 3.4 PM size distribution across Andersen's impactor stages.

Impactor stage	0	1	2	3	4	5	6	7	Back Filter
PM size range [μm]	≥ 9.0	9.0-5.8	5.8-4.7	4.7-3.3	3.3-2.1	2.1-1.1	1.1-0.7	0.7-0.4	0.4-0.0

The filter papers used in the impaction stages are glass fibre type A (GF/A) grade 1820-6537, paper thickness is 260 μm , the diameter is 81 mm with a basis weight of 53 g.m^{-2} . Filter material was simply a wire-mesh of low ash content 100% borosilicate glass. The diameter of the GF/A filter exactly coincides with the impactor plate diameter, therefore the papers were placed into the concaved side of the plates. In fact the plates hinders the air flow through the filter papers therefore no filtration is actually taking place.

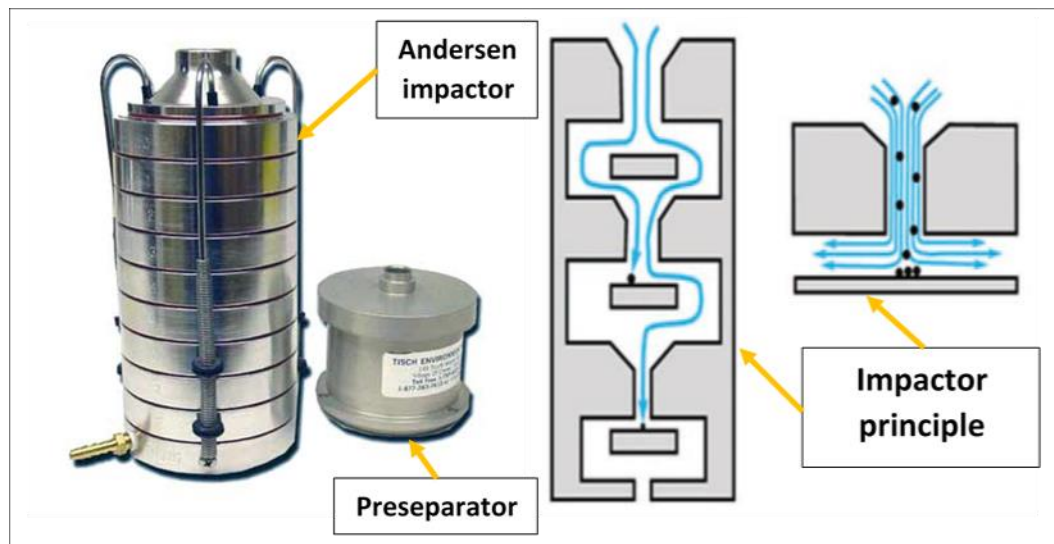


Figure 3.15 Andersen impactor and its principle of operation [158].

Air flows axially through a huge number of jets towards the filter papers but the streamlines are forced to change their direction at 90° towards the plate periphery as shown in fig.3.15. Coarse particulates possess higher inertia than the smaller ones, they leave the gas stream as they fail to follow the streamlines. Eventually coarse particulate would be captured on the filter surface and some might rebound or scour back to the gas stream especially when the filter surface is overloaded and dark radial lines appear on the filter surface. The size of the jets get smaller but their number increases as the gas moves downstream. These jets are merely axial holes in each impactor stage

parallel to its longitudinal axis. The gas jet speed continues to increase all the way down to the last stage of the impactor. That's why the captured PM sizes are successively smaller down to the lower stages. Particulate smaller than 0.4 μm are collected by the backup filter which is merely a GF/F filter.

3.5.2.2 Gravimetric and thermo-gravimetric analysis

The same previously explained steps of filter numbering, conditioning and weighing were followed as for the GF/F filters keeping in mind the importance of the blank filter in error calculation.

During PM₁₀ tests, the impactor was loaded with a set of eight GF/A filters plus one GF/F filter at the backup stage. This should be done carefully by keeping the numbered side facing the downstream side and any mixing between the paper sequences should be avoided. Due to the small amount of the PM collected on the impactor stages, the filters were kept in position for the round trip journey. The precision in time recording from switching-on the vacuum pumps to switch-off at the end of the journey is very important for gas flowrate measurement.

The amount of PM collected on the various impactor stages were not quite enough to perform TGA. Therefore, TGA was performed for the backup filters only and the results were compared to those obtained from the single stage filtration unit for the two fuels. The same TGA apparatus programming was applied.

3.6 Characterisation and quantification of error sources in PM data

3.6.1 Systematic error

Systematic errors are the errors that affect the accuracy of the data [159]. In the PM analysis, the systematic error is exclusively confined to the sample weighing process or the balance accuracy. It equals to one decimal fraction of the balance display. In digital balances, unless specified by the manufacturer, this value is divided by two. Therefore the systematic error for the Metler Toledo balance is 0.005 mg.

3.6.2 Random error

Random errors are the errors which usually affect the precision or repeatability of the data [159]. This kind of error is actually related to the way and the

conditions at which the filters were handled. Also, the nature of the experiments encountered are very decisive in the amount of error. In order to evaluate these two sources of error, blank filters were used.

Filter weight loss due to its aging in the time interval confined between the two filter weighing processes was calculated from the change in the blank filter mass. The weight loss for the three blank filters of each category were averaged as follows:

Random error from filter aging

For GF/F filters = -0.1167 ± 0.0208 mg

For GF/A filters = -0.0276 ± 0.0115 mg

Since the research required TGA for a portion of GF/F filters. It was expected that part of the filter material was evaporated or burnt under the high oven temperatures. Doing TGA for the blank GF/F filters revealed the amount of filter material lost at each stage of the TGA procedure. These errors were calculated as follows

Random error for VOF = -0.4038 ± 0.0197 mg

Random error for C = -0.0027 ± 0.0033 mg

Random error for Ash = -0.0017 ± 0.0017 mg

Random error for PM = -0.4083 ± 0.0156 mg

The combined random error for GF/F filters are

$$\begin{aligned} \text{Random error} &= 0.1167 - (8 \times 0.4083) + (\pm 0.0208) + (\pm 8 \times 0.0156) \\ &= -3.1497 \pm 0.1456 \text{ mg} \end{aligned}$$

The first term is the amount to be subtracted while the second term represents the deviation from the mean.

3.6.3 PM data processing and conversion for comparison purposes

PM mass results obtained from the gravitational analysis were corrected by adding the amount of weight loss obtained from the blank filters after being averaged. If there are any differences in the HGV load in the same load category, the PM mass should be corrected by multiplying by a load correction factor. The results were divided by the sample flowrate to obtain PM

concentration in mg/m³. PM emission index (EI) was found through the following equation suggested by Langton et al [160].

$$\mathbf{PM\ EI = k_{PM} * C * 10^{-3}[1 + (A/F)]} \quad \dots\dots\dots 3.1$$

Where

PM EI is particulate matter emission index in [g/kg_{fuel}]

k_{PM} is the reciprocal of exhaust gas density = 0.8474 m³/kg

C is the PM concentration in [mg/m³]

A/F is the trip average air to fuel ratio obtained from Chan's formula [161, 162]

In order to compare to the HGV standards in [g/kWh], PM EI was converted to PM EF as follows

$$\mathbf{PM\ EF = PM\ EI * SFC} \quad \dots\dots\dots 3.2$$

Where

PM EF is the particulate matter emission factor in [g/kWh]

SFC is the trip averaged specific fuel consumption in [kg_{fuel}/kWh]

Dealing with the PM mass from the TGA required a thorough understanding of the whole process in order to envisage the way PM EF was calculated.

Before doing the TGA for the loaded filter portion, it was quite important to record the filter to portion mass ratio. After performing the TGA for the filter portion and in order to obtain the mass evaporated and/or burnt in the time series throughout the TGA test, the final mass of the what is remaining from the filter portion was deducted from every single reading in the mass time series as follows:

$$\mathbf{mass\ removed_t = Filter\ portion\ mass_t - Filter\ portion\ mass_{final} \dots 3.3}$$

where

mass removed_t is the mass evaporated or burnt from the PM and filter material at any time during the TGA test.

The same mathematical operation was applied to the blank filters and an averaged time series was obtained. This was followed by subtracting the average blank portion TGA time series from the loaded filter portion TGA time series to obtain the pure PM mass freed from the filter material as follows

$$PM_t = \text{mass removed from loaded filter portion}_t - \text{average mass removed from blank filters}_t \quad \dots\dots\dots 3.4$$

Eventually, the final PM results were plotted against time then the values of PM components were obtained as follows

Moisture mass content was calculated and excluded from the PM results since it is not considered as PM. This was achieved by subtracting PM mass at the end of the steady state 100°C period from the $PM_{t=0}$ value.

Volatile organic compounds (VOC) or the organic carbon content was obtained in the time interval between the start of temperature rise after 100°C up to 553°C.

Elemental carbon (C) was obtained as the temperature exceeds 553°C or when the machine shifts to air to the point at which the TGA plot began to flatten.

Ash was obtained by subtracting the sum of moisture, VOC and C from $PM_{t=0}$.

The values for the PM components were thereafter corrected to the original filter size by multiplying by filter to portion mass ratio. They were then corrected for load and the PM EF obtained for each component the same way as explained for the whole filter.

3.7 Gaseous emissions measurements

One of the main objectives of the project is the evaluation of the environmental impact of gaseous emissions, particularly the regulated gaseous emissions and CO₂. The comparison between the gaseous emissions of the two fuels and the EURO 5 standards could be very crucial in the final decisions as to whether the surrogate fuel could be considered as a renewable environmentally friendly fuel. Two sampling probes were installed, the first one was installed upstream to the SCR to particularly measure engine-out NO_x and O₂ by zirconia solid electrolyte. The second probe was located in the tailpipe precisely at the SCR exit for gas speciation and to focus on NO_x, CO, THC and CO₂ emissions.

3.7.1 NO_x measurement by zirconia solid electrolyte

Although the HGV was fitted with a state of the art NO_x after treatment system, it was very important to measure what comes out from the combustion chamber in terms of NO_x. Fig.3.16 illustrates the position of the zirconia sensor and the thermocouple on the exhaust manifold.

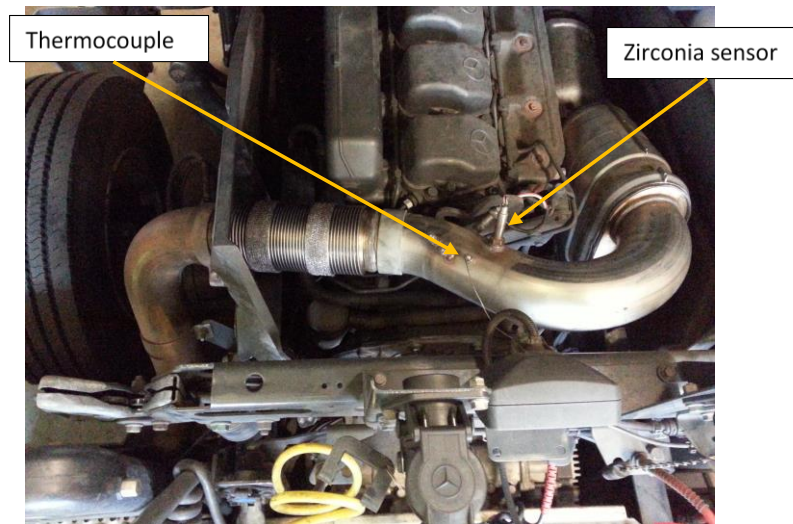


Figure 3.16 The location of zirconia sensor and exhaust gas temperature measurement probe.

3.7.1.1 Zirconia sensor description and apparatus layout

The zirconia solid electrolyte (ZrO₂) generates an electromotive force when it is placed between two compartments of different O₂ potentials. If this phenomena is inverted by applying a small voltage difference across the zirconia sides, O₂ will be generated. Practically, the zirconia sensor consists of two compartments. The sample gas enters the first compartment, through a diffusion hole, where NO₂ gets deoxygenated. The oxygen is pumped out and the NO rich sample gas enters the second compartment where the NO is deoxygenated to N₂ and O₂ and the oxygen is pumped out. Therefore the total electromotive force generated is proportional to NO_x and O₂ concentrations in the sample gas.

A brand new, factory calibrated zirconia solid electrolyte (ZSE) was used. The generated signal was amplified in a Horiba MEXA 720 NO_x analyser and logged into the laptop through Daqview interface as illustrated in fig.3.10. The data were processed by a special software and displayed in excel format in a

time response of 0.2 s increments. Data collection by the ZSE sensor is very much representative in terms of the event timing because of the high speed signal travel from the sensor to the analyser.

3.7.2 Exhaust gas speciation and measurement by FTIR spectroscopy

Gaseous emissions from the HGV tailpipe to the receiving environment are the ones concerning the research collaborative parties. These emissions were measured by the Fourier Transform Infra-Red (FTIR) apparatus. Emissions like CO, CO₂, THC and NO, NO₂ and NO_x were detected. However, NO_x was under scrutiny for two reasons. The first is related to the trade-off between NO_x and PM, and the manufacturer selected to treat PM through the combustion process rather than NO_x. The second is the role of SCR performance in emissions. Therefore it was quite interesting to understand the SCR behaviour and its effect on NO_x emissions.

3.7.2.1 FTIR Apparatus and test procedure description

Theoretically, FTIR is built upon the shape of spectra obtained as a substance is subjected to infrared rays. The difference in spectrum of different substances is the result of their absorbance capacity of infrared. The absorbance, according to Lambert-Beer's law, is directly proportional to the target substance concentration and the light path length. Therefore any chemical compound could be easily analysed to know its components and their concentrations. To help collect all the spectrum continuously and promptly, the system uses Fourier transform technique in a specially designed software.

Practically, the instrument used was the Temet Gaset CR 2000, Temet instruments Oy, Finland. A light source produces an infrared ray that is converted by an interferometer to an interference beam. The beam passes through a number of lenses and reflectors on its way to pass through the sample cell. The gas sample flows continuously through the sample cell. After being absorbed by the gas sample components, part of the beam reaches the infrared detector to produce the interferogram. Fourier transformation analysis of the interferogram develops a power spectrum as a transmittance. The absorbance spectra could be calculated from the difference between the power spectrum and a preloaded spectra of reference substances. The FTIR has the capability to process 65 components at a very high frequency of 0.5 Hz. The apparatus detector is a mercury cadmium telluride (MCT) with the

capacity to scan 10 spectra per second and it detects emission concentrations as low as 0.5-3 ppm [163].

Working on the FTIR apparatus requires some complimentary units. Heated sample lines were used to keep the sample at 180°C to avoid water condensation which might affect the concentration of the water soluble gases. Also, high boiling point gases might condensate as well. A temperature controller is used for this purpose which is integrated with the sample handling unit. The latter is a sample delivery pump used to transfer the sample to the FTIR at 2~10 lit/min. To avoid any PM deposition in the gas detection cell, the sample handling unit is fitted with a cylindrical disposable filter of 2 µm aperture. After being analysed, the gas sample is exhausted outside the driver's cabin by a Swagelok fitted to the rear window of the cabin.

At the beginning of the test, a warm-up period of 45 minutes is recommended by the manufacturer. The instrument and the heated lines were switched-on. The instrument status could be monitored through a laptop computer on which the calcmnet software was installed. About 500 ml of liquid nitrogen was poured carefully to bring the infrared generator temperature to 196°C sub-zero. All the health and safety measures were followed precisely. A pure nitrogen gas bottle was connected to the sample handling unit (SHU) for zero setting of the instrument.

By turning the sample valve on the SHU to the Zero gas position, the nitrogen purges out the air and the machine zero reading was checked from the laptop screen. A zero gas measurement was inspected by the spectra displayed on the laptop. If satisfied the gas sample valve was turned to the sampling position and the nitrogen gas bottle shut-down, otherwise the apparatus zeroing function was selected to bring it to zero reading.

3.8 FTIR data validation

3.8.1 NO accuracy

FTIR NO data accuracy was checked comparatively with the Horiba Mexa 7100-D chemiluminescence system. An 818 ppm certified NO gas bottle in conjunction with a certified N₂ gas bottle, from BOC gas supplier, were used in the comparison. First the Horiba Mexa 7100-D zero reading was calibrated by a pure nitrogen gas, then the span reading was calibrated with the certified NO gas. To compare NO readings between FTIR and Horiba

chemiluminescence system, a gas divider was used. The zero gas bottle (certified N₂) and span gas bottle (certified NO) were connected to the gas divider. In the gas divider the two gases were mixed at different percentages controlled by the operator. An equal gas pressure was maintained for the two gases and the output mixture flow rate was maintained at 2 lit/min. Each time the gas mixture selector was changed, the gas pressure control valves were regulated to keep the gas pressure balance indicator at the zero position. The gas divider outlet was divided by a T-junction Swagelok connection to supply the Horiba and FTIR simultaneously with the desired NO concentration. Ten FTIR measurements of 20 s each was recorded at each concentration and the corresponding Horiba reading was recorded.

3.8.2 THC accuracy

The way that Horiba 7100 D detects the THC is by using the flame ionisation detection FID technique. Accordingly, a comprehensive detection for the sum of nearly 160 HC species, present in the vehicle exhaust, is performed in a very high response. The FTIR is set to detect around 30 HC species individually. Therefore about one third of THC is detected [163].

3.8.3 CO and CO₂ accuracy

A previous study performed by Daham et al.[163] revealed a good correlation between FTIR and Horiba 7100 D outputs especially for CO. There was a slight underestimate of the FTIR results which was attributed to the slower response of FTIR which made the machine to miss some of the sudden high emission peaks. According to the manufacturer recommendations no apparatus calibration is required unless a major hardware part is changed. In this particular case the machine should be calibrated at the manufacturer facilities under special conditions of high pressures and temperatures.

3.8.4 Data repeatability

In terms of data precision and repeatability, the machine showed a very high repeatability as it has been subjected to the same changes in events [163].

The total weight of the power supply and sampling apparatus including the three laptop computers were negligible to the vehicle power output capabilities 315 kW.

3.8.5 FTIR data calculation and conversion for comparison purposes

Results obtained after FTIR data processing are volumetric presented in ppm or percentages. To prepare the data in a better way for comparison to the standards or emissions from other vehicles of the same class, the data were converted to mass basis output usually referred to as emission index (EI) in g/kg_{fuel}. This could be achieved by calculating the air fuel ratio (A/F) on a mass basis. Before that, oxygen concentration in the exhaust gas was determined because FTIR is unable to measure O₂.

Many formulae were suggested for A/F determination depending on the volumetric emissions analysis especially CO, CO₂ and THC. In the course of this research, Chan's formula was used because it explicitly included air humidity and the unburnt HC as well [161]. The formula was tested against experimental data and the results satisfactorily matched between the model and the experiment [162]. Considering a fuel with the following formula C_αH_βO_γN_δ, the air to fuel ratio A/F is

$$A/F = \frac{138}{12.011\alpha + 1.008\beta + 15.999\gamma + 14.007\delta} \times \frac{A_1\beta - A_2 + 2\alpha A_3 A_4 - 2\gamma(A_4 + A_5)}{2(2.0028)(A_1 + A_5) - 0.0014 \times 2A_3 A_4} \quad \dots\dots\dots 3.5$$

Where

$$A_1 = [\text{CO}] + [\text{CO}_2] + [\text{HC}] \quad \dots\dots\dots 3.6$$

$$A_2 = x[\text{HC}] \quad \dots\dots\dots 3.7$$

$$A_3 = [\text{CO}] + 2[\text{CO}_2] + 2[\text{O}_2] + [\text{NO}] + [\text{NO}_2] \quad \dots\dots\dots 3.8$$

$$A_4 = 1 + [\text{CO}]/([\text{CO}_2][\text{K}]) \quad \dots\dots\dots 3.9$$

$$A_5 = [\text{CO}]/([\text{CO}_2][\text{K}]) \quad \dots\dots\dots 3.10$$

$$K = e^{[2.743 - \frac{1.761}{0.001T_{eq}} - \frac{1.611}{(0.01T_{eq})^2} + \frac{0.2083}{(0.01T_{eq})^3}] } \quad \dots\dots\dots 3.11$$

T_{eq} is the equilibrium temperature which varies between (1738°K~1814°K)

K is a function of T_{eq} and it takes the values (3.5 and 3.8)

x is the hydrogen to carbon ratio (H/C) of the specified fuel. For C2G UBF the derived fuel formula is C₁₈H₃₄O₂ while for PD C₁₂H₂₃ therefore x values of 1.89 and 1.92 were used respectively.

CO, CO₂ and HC are the concentrations in percentages.

It is recommended to demonstrate gaseous emissions as mass based per unit mass of fuel consumed. This is called emission index (EI) which is a better way in emissions comparison between different engines of the same category. A conversion equation proposed by Li et al.[164] and Andrews et al.[165] was used to find the EI for the relevant pollutants

$$\text{Gas EI} = k_{(\text{gas})} * C * 1000 * [1 + (A/F)] \quad \dots\dots\dots 3.12$$

where

Gas EI is the emission index of a particular gaseous pollutant in [g/kg_{fuel}]

k_(gas) is the gaseous pollutant to exhaust gas molecular weight ratio as follows

k_{CO} = 0.971 , k_{CO₂} = 1.526 , k_{THC} = 0.555 methane eq. and k_{NO_x} = 1.595 NO₂ eq.

C is the concentration of the gaseous pollutant which might be in ppm or percentage. Therefore the EI equation should be multiplied by 10⁻⁶ if ppm is substituted or 10⁻² if the emissions are in percentages.

A/F is the mass based air to fuel ratio obtained from Chan's formula (shown above).

To be comparable to the emissions standards, the emissions were further converted to emission factor in [g/kWh] or distance specific emission factor in [g/km]. as follows

$$\text{Gas EF} = \text{Gas EI} * \text{SFC} \quad \dots\dots\dots 3.13$$

where

Gas EF is the emission factor for a particular gaseous pollutant in [g/kWh]

SFC is the HGV specific fuel consumption in [kg_{fuel}/kWh].

3.9 HGV dynamics and road analysis

In the real world tests, the measured emissions should be related to on road events. Vehicle speed, acceleration and power demand to overcome the rolling, gradient and air resistances are related to the measured emissions. In fact the amount and type of load exerted on the engine could be a crucial factor for the amount and type of emissions. However payload could be constant throughout the journey while the road load fluctuates with every acceleration and deceleration and as road gradient changes. The driver's behaviour, if not trained according to a certain policy, is expected to affect the quality and quantity of emissions.

The aforementioned vehicle dynamic variables were measured by Vbox II, Race Logic, UK. As shown in fig.3.17. This unit is a compact box that works as GPS to determine the vehicle position, speed and elevation. The vehicle position is interpreted as a longitude, latitude coordinates, while the speed is given in km/h. Vehicle direction with respect to the north direction is also provided in degrees. The elevation, from which the road profile is derived, is given in meters height from sea level.

Several sources of error were identified. They were generated as the Vbox leaves one satellite to engage another one. This was repeatedly encountered throughout the journey. The accuracy of the satellite to define the vehicle position and speed and/or the differences in their orbits resulted in these error readings.

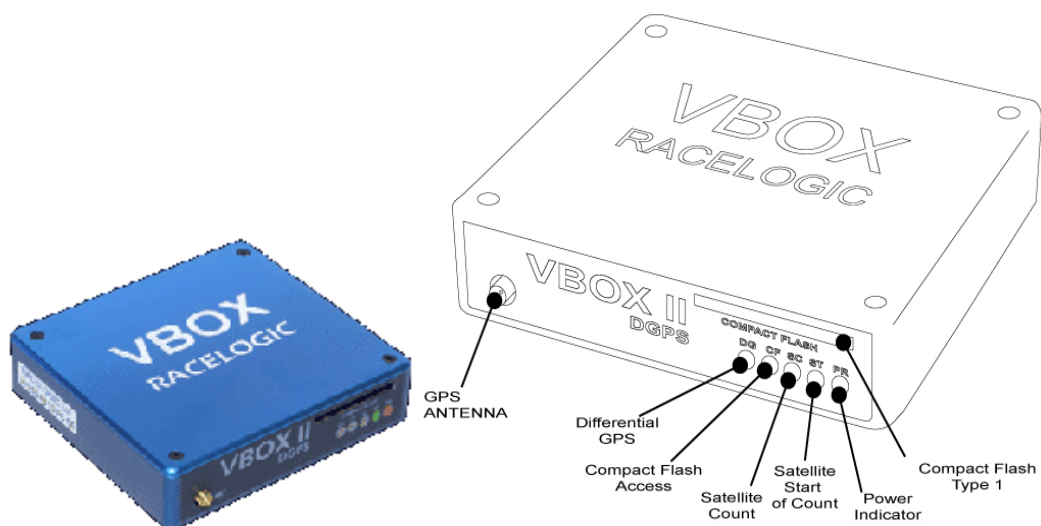


Figure 3.17 Racelogic Vbox II, vehicle positioner allocator and speed calculator.

(Courtesy of Racelogic, UK)

To tackle this dilemma, the road profile was smoothed out by comparison to the data obtained from google maps [166] which accurately defined the road characteristics. The vehicle speed was corrected by checking the pre and post speeds to the error position.

The Vbox system records the data on a removable SD chip to be downloaded later on to a computer. For a better coverage of the on road events especially at high HGV speeds, the data collection frequency was set to 5 Hz.

The Vbox was connected to a laptop computer through a data acquisition system, DAQP-12, Quatech, Inc Ohio, USA. Velocity data were simultaneously merged with NO_x and O₂ obtained from the ZSE sensor and the engine-out and tailpipe temperatures from the thermocouples to achieve a time alignment among these variables. Actually the HGV speed was presented in voltage units therefore a conversion factor of 25.5 was applied to represent the real velocity in km/h.

Data from the Vbox were substituted in a special formula suggested by MOVES [68] for HGV to determine the instantaneous vehicle specific power (VSP_t). The vehicle output power in kW per tonne of payload was calculated as a time series to sum in all the road loads exerted on the engine every 0.2 seconds throughout the journey. The MOVES VSP_t formula for a HGV with GVW >15 tonne is demonstrated in chapter 2 eq.2.3.

3.10 Heavy goods vehicle fuel consumption measurement

Bioltec data were displayed on the controller screen, and were also logged in a laptop computer through a communication unit and specially designed software as presented in fig.3.18. The software saves the data in csv files every three minutes and 14 seconds.

The physical quantities recorded in each file are, fuel flow temperature, fuel mixing ratio, fuel tank temperature, PD and UBF consumption as a counter of the number of deliveries of 10 ml each and engine load factor. Each one of these quantities were recorded at a different time series. Therefore, Bioltec data processing starts from collecting all the data in a single file that belong to a certain HGV trip. The data of each physical quantity were converted using [=VALUE(TRIM(CLEAN('spread sheet name'! First square in the column)))] function and copied in an excel spread sheet. Since the time interval between two consecutive data points was about 6 s, the gaps between these points

needed to be filled in order to match other time series obtained from the ZSE, Vbox and FTIR. This was achieved through (R) a special statistical software.

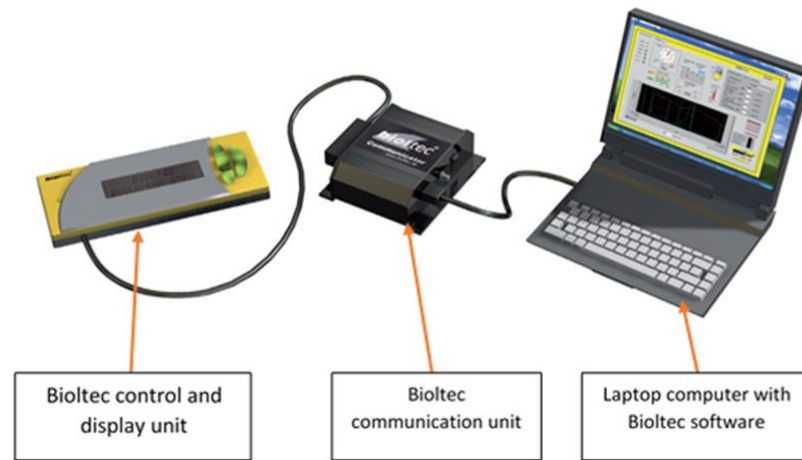


Figure 3.18 Bioltec system controller with communication unit and software.

The fuel consumption for each fuel was calculated as follows

$$Q_f = \left[\frac{V_{n+1} + V_n}{2} \right] / [t_{n+1} - t_n] \quad \dots\dots\dots 3.14$$

where

Q_f is the volumetric rate of fuel consumption in [ml/s]

V_{n+1} and V_n are the fuel volume consumed in two consecutive time intervals in [ml]

t is the time in [s].

to convert to mass basis

$$\dot{m}_f = Q_f * \rho_f \quad \dots\dots\dots 3.15$$

Where

\dot{m}_f is the mass rate of fuel consumption in [g/s]

ρ_f is the fuel density at 90°C (fuel injection temperature) in [g/ml]

The specific fuel consumption was calculated by

$$SFC = 3.6 * \frac{\dot{m}_f}{VSP * GVW} \quad \dots\dots\dots 3.16$$

Where

SFC is the specific fuel consumption in [kg/kWh]

GVW is the gross vehicle weight in [tonne]

VSP is the vehicle specific power in [kW/tonne]

3.11 Apparatus time alignment

It was very important to set the time on the three laptop computers and give the same file name to the measured variables on the same trip. At the trip start, all the measurements should start together for an easier time alignment in the subsequent analysis. Eventually and after finalising data processing from each apparatus, all the results related to particular trip were collected in one spreadsheet in a time aligned format using the indirect function (=INDIRECT("spreadsheet name! column" & \$Factor's column)). The factor's column is calculated to bring the data, from the secondary spreadsheet to the master spreadsheet, that match the time increments in the master spreadsheet after rounding-up the decimals.

Prior to the data transfer to the master spreadsheet, it was very important to find out the engine start time to align the emissions with vehicle position and dynamics. This was achieved by checking any sharp change in CO, NO_x from the FTIR data to match with the sudden changes in NO_x in ZSE data which is linked to the vehicle speed. Knowing the vehicle speed helps to match the data with the Vbox data including the vehicle coordinates and level on the map.

3.12 In vitro fuel analyses

The specifications of market petroleum diesel PD are usually standard nationwide with a limited tolerance left for differences due to the seasonal temperature extremes or location. In contrast, the specifications of used cooking oil are also affected by the feedstock. Therefore, it was of extreme importance to perform in vitro analysis for the C2G UBF fuel and compare the results with those of the PD. The analyses included the physical, chemical and thermodynamic properties of the surrogate fuel. The physical analyses were performed to clarify the fuel behaviour in the fuel lines and throughout the injection process. The chemical analysis revealed the structure of the fuel and how this could affect its physical properties and emissions. The thermal properties revealed the heat content of the fuel and the chemical structure of the fuel. A simulation for the target engine in operation was performed to

understand the behaviour of the injected fuel and its effect on the combustion process.

3.12.1 C2G UBF sample preparation for analysis

Convert to green ultra-biofuel samples were taken directly from the fuel storage tank at the United Biscuits Midlands Distribution Centre. The samples were collected on monthly basis but seasonally classified. These UBF samples were volumetrically diluted with PD in 20% increments from 0% UBF (pure PD) to 100% UBF (pure UBF).

3.12.2 Fuel density

The density of the fuel represents the amount of matter contained in a unit volume. Fuel metering, to fulfil engine demand at different operational conditions, is volumetrically controlled [167]. Therefore, the denser the fuel the more matter will be introduced to the combustion chamber. The fuel density also affects the injection characteristic and ultimately the combustion process and emissions as discussed in Dizayi et al.[18].



Figure 3.19 Micrometrics AccuPyc 1330.

The UBF density was measured by an AccuPyc 1330, Micrometrics, gas displacement pycnometer as shown in fig.3.19. The procedure is to pour a known mass (about 6 g) of the fuel in the instrument's container. The container should be covered and placed back in the instrument. The measured fuel mass should be entered into the instruments software. Nitrogen gas flows into the container and the amount of volume displaced by the fuel is automatically

measured. Eventually the instrument displays the density at room temperature which was 21°C.

The fuel density at the range of operational temperatures of 45°C to 90°C was also determined by weighing a known volume of fuel at different temperatures.

A 50 ml clean glass pycnometer was weighed empty (35.1273 g) but covered by its own glass cap. Then the pycnometer was filled with the fuel sample and recapped. A capillary passage in the cap enables the entrapped air and excess fuel to escape. The external surface of pycnometer was thoroughly cleaned. A water bath was set to the desired temperature and the pycnometer was placed in the water bath. Water temperature was inspected to reach a stable temperature. The pycnometer was taken to measure its mass again. The difference in mass reading is the mass of the 50 ml of fuel. The test was repeated in 10°C increments from 15°C to a maximum temperature of 100°C. The upper limit represents the approximate temperature at which the fuel is injected in to the combustion chamber as indicated from the Bioltec data and according to Pickett et al.[168]. Laboratory temperature was recorded at 23°C.

3.12.3 Fuel viscosity

The dynamic viscosity of the fuel was measured by a Bohlin rheometer, Malvern instruments, at a temperature range of 15°C to 110°C. The machine shown in fig.3.20 is built on the principle of fluid resistance to the relative rotation between two flat plates. About 3 ml of fuel was placed on the lower stationary flat plate, by a disposable graduated transfer pipet, vwr.com, while the upper plate, 40 mm diameter disc, was pre-set to leave a 150 µm gap with the lower plate during the test. The temperature of the lower plate was automatically controlled by water flowing underneath the lower plate. The rate of temperature increase was 0.27°C/s and the machine returns a record every 10~15 seconds. The spindle rotation speed was set to 50 rpm. To avoid fuel spillage, the two plates were kept confined in two half-cylindrical shells.

The same machine was used to determine the instantaneous viscosity of the fuels at a constant temperature of 40°C. The principle is to apply shear stress (in Pascals) on the fuel located between the two plates and measure the strain in the fuel. The stress was set to increase at a rate of 6.17% and the corresponding strain was recorded in (1/s).



Figure 3.20 Bohlin rheometer.

3.12.4 Fuel surface tension

Extremely high injection pressures tend to increase the amount of atomised fuel. In other words, more spherically shaped fuel droplets rather than a cylindrical jet is the aim. The fuel holds anyone of these structures by its surface tension. It is simply the kind of interaction among the liquid, the surrounding gas and any contact with a solid surface. Surface tension acts against the pressure difference between inside the liquid body and the outer environment. Therefore the structure collapses as the pressure difference exceeds surface tension.

The surface tension of UBF and PD were tested by CAM 2008 ,KSV instruments, as shown in fig.3.21. As the liquid-gas interaction was of interest, the pendent drop test was performed. Principally, the machine uses the shape of a pendent drop from a syringe to measure its surface tension. A high speed camera takes 10~20 frames per second to send it to a computer. The lower 2/3 part of the image, which is not deformed by the syringe, is used by the software for surface tension calculation.

According to the manufacture it is recommended to calibrate the machine prior to the test, especially when any of the major parts of the machine are removed. These parts include the sample platform, the syringe holder and the camera itself. The calibration is achieved by a standard 4 mm stainless steel ball provided by the manufacturer. An image of the standard ball with its real diameter were fed to the software according to the existing position of the

camera and zooming capacity. The software saves the new setting for comparison throughout the test.

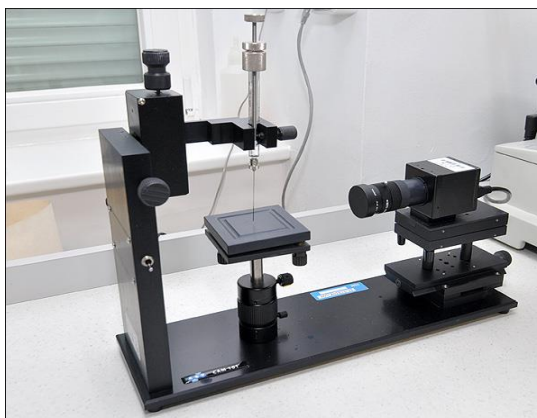


Figure 3.21 CAM 2008, KSV instruments, for surface tension analysis.

Practically, a fuel sample was pumped in and out of the syringe, several times, to get rid of any air bubbles present in the syringe. Holding the syringe vertically with its tip at top, the tip should be wiped and a new 0.7 mm dia. syringe needle is to be fitted on the syringe tip. Air should be discharged from the needle by carefully pushing the plunger. The next step is to fix the syringe, upside down, by the syringe clamp on the machine. The plunger was gently pushed to allow a single droplet to hang on the needle tip on the verge of falling. Before using the software to take the photo of the droplet, data about the test, sample name and fuel density should be loaded to the software. In this particular test the image interval is 1 second and number of frames taken is 20. To avoid fuel contamination, a new 2 ml syringe, Terumo syringe with needle, was used.

3.12.5 Fuel CHNS analysis

Doing elemental analysis for the PD and UBF was of utmost importance to measure the mass percentage of the components of these fuels and to quantify the difference in these components. Knowing the C/H is a key factor that affects the combustion process and PM formation. Nitrogen content slightly affects NO_x formation. Sulphur content works as a PM seed and it also causes exhaust aftertreatment poisoning. Therefore CHNS analysis was performed. The apparatus was a Flash 2000, thermo-scientific as shown in fig.3.22. Approximately 3 mg of each fuel sample is placed in tin capsules.

The capsules were placed in the auto-sampler. The samples were fed to the machine to be heated to 900°C to 1000°C in the oxidation/reduction reactor. Oxygen is introduced to the sample at a precise timing and amount to ensure complete combustion. At these high temperatures, oxygen reacts with the tin capsule to result in an exothermic reaction which increases the temperature to 1800°C for a short interval. All the fuel components change to gases and are separated in a chromatographic column to be detected and measured according to their thermal conductivity.



Figure 3.22 Flash 2000 CHNS analyser.

3.12.6 Fuel GC-FID analysis

Gas chromatography (GC) is a technique used for gas component separation to be furtherly detected by different indicators depending on the type of the released compounds. A gas sample is injected into the system and transported by a carrier gas. The two gases should pass through a column located in an oven to control the interaction between the sample gas and the column material. A proper selection of the right column for a particular test is very important. Columns are either packed or coated with a preselected material called the stationary phase. Moreover, column length and diameter play a key role in the interactions with the stationary phase. Different sample gas components possess different retention times in the column depending on their adsorption and desorption properties with the stationary material in the column. Accordingly different batches of sample gas components leave the column to be detected separately [169].

Flame ionisation detection (FID) is a method for hydrocarbon (HC) determination in a sample gas. The principle is briefly the combustion of the sample gas in a hydrogen flame to produce HC ions from which the instrument indicates the number of carbon atoms contained in the gas sample. In practice, a fuel gas, a mixture of 40% hydrogen with an inert gas like nitrogen or helium, is mixed with the sample gas and fed to the combustor through a nozzle. The mixture of fuel gas and sample gas burn in the presence of atmospheric air. To collect the HC ions generated from the combustion of the sample gas, an electric gradient between the nozzle and the collector should be applied. As a result, an electric current is produced in proportion to HC concentration in the sample gas. The tiny electric current needs to be amplified. Nevertheless, the instrument output depends on its sensitivity to each HC in the sample gas. Therefore a response factor is used for each HC component which is merely a relative sensitivity compared to propane, the calibration gas [169].

To ensure a resilient transfer of the sample through the apparatus and avoid any damage to the GC-FID apparatus, the C2G UBF samples were transesterified to UBF-biodiesel, UBF fatty acid methyl ester, (UBF-FAME). A mixture of 9:1 ratio methanol to UBF was prepared and mixed with 1.5% catalyst. The three components of the mixture were steadily stirred for three hours under optimal test conditions of 75°C.

The GC apparatus used in the analysis was Perkin Elmer Clarus 500, shown in fig.3.23, in conjunction with flame ionisation detection.



Figure 3.23 Perkin Elmer Clarus 500 GC-FID apparatus.

The data were logged to a laptop computer on which Totalchrom software was installed for machine control and data processing. Using a GC method developed by Jenny Wilson of Infineum UK Ltd, the initial oven temperature was held at 140 °C for 5 minutes then ramped at a pace rate of 4°C/min up to 240°C for a second retention time of 15 minutes. The selected GC column was a capillary tube of 100 m x 0.5 mm coated with a 0.2 µm thick fused silica, SP-2380 Supelco. A 1 mm³ solution of 2% v/v UBF-FAME with toluene was automatically injected into the GC apparatus.

Different batches of HC leaving the GC at different retention times were mixed with the fuel gas prior to burning in the FID combustor. The detector temperature was set on 260°C while the initial temperature was 250°C and a maximum temperature of 275°C was recorded. The test was aborted at 45 min.

3.12.7 Inductively coupled plasma (ICP) spectroscopic technique for inorganic elements measurement

The presence of metals and their concentrations in the sample solution is determined by measuring the specific light emitted by each metallic element in the sample. As the sample aerosol flows through the plasma torch, a spectrum of analyte-specific atomic-line emission is produced. A diffraction grating is used to disperse the spectrum so that the individual emission lines could be monitored by the photomultiplier tubes.

Preparations for the test

All the Teflon and glassware vessels should be thoroughly washed with tap water and detergent, 1:1 nitric acid and tap water then rinsed by deionised (DI) water.

Sample digestion

A 45 ml sample solution was prepared by carefully weighing (0.1~0.2) g of the UBF fuel and mix it with DI water. 5ml of concentrated nitric acid (HNO₃) was added to the sample solution. The digestion vessel, the pressure relief disc valve and the cap were weighed on a 0.01g accuracy balance. The name of the sample was recorded on the digestion vessel. A 50 ml of the prepared sample solution and nitric acid was poured into the digestion vessel. The digestion vessel was capped by the disc valve and the cap. The same

procedure was repeated for the rest of the samples. One blank digestion vessel is required for every 10 samples. In fact this sample dilution process is very important to reduce any physical interferences due to the change in sample viscosity and surface tension in the ICP apparatus.

The samples were finally placed in the microwave oven for 10 minutes at $160^{\circ}\text{C} \pm 4^{\circ}\text{C}$ then for another 10 minutes at $165\text{--}170^{\circ}\text{C}$. The samples were left in the microwave oven to cool down then transferred to cool down on the bench. The digestion vessels were weighed again and the weight was recorded. If the weight loss was more than 10% the sample was discarded. The digestion vessels were opened in a fume cupboard. The disc valve and the cap were washed a few times with DI water and the DI water was poured into the digestion vessel.

The name of each sample was written on a new disposable centrifuge tube. The tube was placed in a 50ml glass beaker which was placed on the balance pan. As the balance reading stabilises, the balance was tared-out.

1 ml of hydrochloric acid HCL, 7 ml of nitric acid HNO_3 and 2 ml of hydrogen peroxide H_2O_2 were poured gradually to the contents of the digestion vessel (digestate).

The digestate was poured into the disposable centrifuge tubes up to 48 ml line and the tube was placed again in the beaker on the balance pan. DI water was added to the tube to get 50 g on the balance reading. The tube was capped and the same procedure was applied to all the samples. All the tubes were kept in the fridge ready for the ICP test.

Sample delivery to ICP apparatus

Samples solutions were delivered to the apparatus by an auto-sampler. The sample is introduced to the ICP apparatus as an aerosol. The aerosol is produced by a nebuliser. These tiny sample droplets are prone to very high temperature to evaporate and be ionised by the plasma.

The torch

The plasma is produced in the plasma torch. The torch, in most of the designs, is simply consisted of three concentric quartz tubes. Attached to one end of

the tubes is an electromagnetic coil that apply interchangeable electromagnetic fields at a radio frequency of 27.12 MHz. Argon flows between the outer and middle tubes at a rate of 12~18 L/min. A spark plug is used to produce free electrons accelerated by the magnetic fields and change their flow direction as the magnetic field changes its direction. As the free electrons collide with argon atoms these in turn release one of their electrons. This process continues until an equilibrium state is reached between the released electrons and the ones fixed back on argon atoms which lost an electron. This argon ionisation process releases heat and ultraviolet rays and the temperatures could reach 10,000°K. Argon gas also flows at a rate of 1 L/min between the middle tube and the inner tube. This works as a sheath for the mixture of argon and sample aerosol that flows through the inner tube at a rate of 1 L/min. The high temperature evaporates the aerosol and the plasma ionises the sample elements.

The plasma torch was ignited and left to stabilise for 30~60 min. the apparatus was initially calibrated by standard solutions according to (EPA/SW-846 Methods 3015/3050B/6010B) [170].

3.13 Fuel spray characteristics

Using a different fuel could alter the injection process due to the unusual fuel characteristics. This became the motivation behind a thorough investigation of the fuel jet and spray formation to identify the major differences between PD and the BL fuel jet characteristics. Beyond dispute, these fuel blends have physical properties which are quite different from those of the pure PD. Data for the higher heat value (HHV) density and viscosity at the range of operational conditions were obtained from laboratory analysis. These data were merged with the physical and thermodynamic conditions of the diesel engine of interest to evaluate the dynamic behaviour of the fuel jet in 360° of crank rotation namely the compression stroke and the power stroke including the injection process. Engine operational conditions were calculated using a diesel dual thermodynamic cycle taking in account fuel injection adjustment at three different speeds namely, idle speed, maximum torque speed and rated power speed. Knowing the fuel jet properties could help to explain the major

combustion differences between the two fuels and the subsequent emissions. The fuel spray characteristics are explained in chapter 2 section 2.6.4.

3.14 Fuel injector inspection

Engine durability throughout the two year duration of the research was monitored. According to the United Biscuits Distribution Centre technical personnel, no extra repair and maintenance was performed for the test vehicle in comparison to the rest of the fleet. Nevertheless, sample fuel injectors were taken periodically from different cylinders for inspection and comparison with others being operated on PD. This practice was aiming to clarify the deposit formation and its intensity inside and around the injector holes. Deposit formation at these particular places could profoundly worsen the injection process and deteriorate the combustion process as well.

3.14.1 Fuel injector collection plan

Deposit accumulation in the combustion chamber was inspected periodically by taking a couple of fuel injectors at a time as shown in table 3.5. This process took two dimensions: The first is a visual comparison between the amount and composition of the deposits from the combustion of PD and UBF. The second dimension is watching the deposit growth and aging with time or the distance travelled by the vehicle using the same fuel.

Table 3.5 Fuel injectors deposit inspection plan.

No.	Vehicle REG.	Injector sequence	Fuel	Age	Mileage [km]	Distance travelled on UBF [km]
1	FE58 NSK	No.1	BL	Old	300,000	300,000
2	FE58 NSK	No.6	BL	Old	300,000	300,000
3	FE58 NSK	No.2	BL	Old	371,460	371,460
4	FE58 NSK	No.6	BL	6 months	371,460	71,460
5	FN11 SVC	No.1	PD	Old	360,000	0
6	FN11 SVC	No.6	PD	Old	360,000	0
7	FN11 SVC	No.1	BL	6 months	421,000	60,840
8	FN11 SVC	No.4	BL	Old	421,000	60,841
9	FN11 SVC	No.1	BL	6 months	482,400	61,200
10	FN11 SVC	No.6	BL	12 months	482,400	122,041

The effect of fuel type on the type and amount of deposit accumulation on the fuel injectors and their needles was achieved by comparing injector No.2 from the vehicle carrying Reg. No. plates FE58 NSK which was running on UBF for 371,460 km, and injector No.1 from the vehicle carrying Reg. No. plates FN11 SVC which was running on PD for 360,000 km. Each injector nozzle contains 7 holes of 0.2 mm dia. The amount and shape of the deposits vary from one hole to the other, therefore the comparison includes images of the cleanest and the worst cases from each injector.

To investigate the aging effects on the deposit accumulation, a visual comparison between two injectors installed on the same engine, operated by UBF but for different periods of time was performed. These two injectors are represented by items No.9 and No.10 in table 3.5. The first one was taken out after running on the engine for 61,200 km, while the latter operated for twice that distance.

3.14.2 Fuel injector inspection by the scanning electron microscope (SEM) and energy dispersive x-ray (EDX)

Fuel injectors were removed according to the plan demonstrated in table 3.5. Data about the removed injector was recorded, including HGV registration number, mileage and their sequential position on the engine. The injectors were carefully packed and labelled by the same aforementioned information. In order to disassemble the injectors, each one was dealt with individually to avoid mixing between the parts of different injectors. As a precautionary procedure to protect the SEM instrument, the injector nozzle and needle were submersed in a toluene bath in a labelled glass beaker for 24 hours. The nozzle and needle were washed thoroughly by acetone and placed in the oven to dry for an hour at 120°C.

Nozzles and needles were placed individually on small aluminium discs by a double sided sticker. All the samples are situated on a larger platform, which has multi degrees of motion freedom, in the SEM chamber. The machine was closed and air was replaced by nitrogen.

The SEM machine, shown in fig.3.24, works by producing a beam of electrons at the top of the Gemini column. The beam is accelerated as it flows down through a number of condenser lenses and objective apertures. The position of the electron beam on the sample surface was controlled by scan coils which were located above the objective lenses. The incident electron beam interacts

with the surface and the energy was dissipated and reflected in different ways as signals, secondary electrons and back scattered electrons, to be detected by a variety of signal detectors, Nanoscience Instruments [171].



Figure 3.24 Surface scanning electron microscopy.

LEO 1530: Gemini FEGSEM with Oxford Instruments Aztec Energy EDX system with 80 mm X-Max SDD detector - high resolution, low kV, secondary electron imaging plus EDX capabilities and KE STEM detector. (courtesy of LEMAS, University of Leeds).

The EDX was also performed in conjunction to SEM. As the electron beam hits the sample surface, electrons from the sample atoms will be released. Therefore, electrons from higher states will replace the released ones and the difference between the energy of the two electrons will be emitted as x-rays. Different components of the deposits emit different levels of x-rays which are detected as a charge pulse that is converted to a voltage proportional to the x-ray energy. This voltage is amplified and sent to a multichannel analyser. The elemental composition of the area under investigation is determined from the evaluation of spectrum of x-ray energy versus counts [172].

Chapter 4

The effects of C2G UBF on vehicle specific power and specific fuel consumption under real world driving conditions

High engine performance and low environmental pollution are the two inseparable objectives that engine manufacturers want to accomplish and optimise to get the most of the fuel energy at minimum emission levels. However, the increased concerns about the environmental deterioration caused by the transport sector paved the way to adopt new strategies for emission mitigation [1, 9]. Renewable fuels, bioethanol for spark ignition engines (SI) and biodiesel for compression ignition engines (CI), in conjunction with vehicle hybridisation, are considered as the best short term (transient) strategies to leapfrog to hydrogen fuel cell and vehicle electrification scenarios [2].

The direct use of non-esterified used cooking oil (UCO) as a fuel in a heavy goods vehicle (HGV) presented significant challenges. The differences in the physical and chemical properties of UCO and petroleum diesel (PD) at ambient temperatures are incredibly large [18]. Therefore fuel blends of low UCO proportions were expected to run the HGV.

On the other hand. In-vitro analysis revealed the high calorific value (CV) of UCO and its high response to temperature changes (see chapter 5 table 5.4). Increasing the UCO temperature brought its properties close to those of PD at the injection event. This amount of heat was already available on-board the HGV. Heat recovery from the HGV cooling system was quite sufficient for UCO preparation but it was only available after engine warm-up. Therefore dual fuel strategy was the remedy, as the vehicle was made to start with PD to warm-up and heat the UCO. The HGV was equipped with the Bioltec system that produces UCO and PD blends of 0%~100% UCO content depending on UCO's temperature and the preloaded engine performance maps.

The UCO used in this project is called Convert to Green Ultra-Biofuel (C2G UBF) after the provider company's name. It is merely UCO purified by powder filtration.

The current chapter investigates the HGV's engine performance as it runs on a blend of C2G UBF and petroleum diesel (PD) in comparison to pure PD. Of course, since the HGV was tested under real world driving conditions, it was

only possible to investigate the performance under road load variations. These road loads were gathered in a specially derived formula known as the vehicle specific power (VSP) (explained in chapter 2 section 2.5.2.1). Events like HGV acceleration, deceleration affect the performance. Wind resistance is also a kind of road load exerted on the engine. The power dissipated in wind resistance varies with the velocity cubed and could account for more than one third of engine power at high speeds. Road gradient in conjunction with HGV direction on the gradient and the extent and length of the gradient are also complex ways at which load is applied to the engine.

The HGV specific fuel consumption (SFC) was also investigated as a performance factor. In fact it is the measure of engines ability to convert a certain mass of fuel into power at different loads. In addition to the economic value of UBF, it was very important to assess the mileage the HGV could achieve on the BL fuel. Moreover most of the exhaust emissions are affected in one way or another by the amount of fuel consumed. This was another reason to measure and calculate the SFC.

Engine-out temperature (EoT) was under scrutiny throughout the tests because it gives an indication of the combustion temperature and it significantly affected the performance of the SCR and NO_x emissions to the receiving environment.

The driver-engine interaction is another factor to affect engine performance and emissions. Skilled drivers use their own senses to get the most of engine performance at the lowest levels of fuel consumption and minimum emissions. Unfortunately the driver's behaviour was not included as a variable in the analysis, since three drivers were involved and they were at the same level of training and driving skills.

Special attention was payed to different road segments or special emission peaks indicated throughout the trips. Among all is the high speed test on the M1 motorway as the vehicle is performing steadily at a high power output. This part of the journey is 12.3 km long and a 110 m downhill travel for the outbound direction. The HGV travels at a high speed of 83~96 km/h in this part of the journey. The lower boundary is the speed recommended by the fleet operator and the higher boundary is the regulated UK national speed limit. This is considered as a high speed/high output power section where the engine is running close to the speed of maximum power (1900 rpm).

The other instance is the vehicle operation under high torque on the ramp to merge on M1 in the outbound journey. This road segment is a straight and

inclined path. It is characterised by its 240 m length and 3% gradient. It immediately starts after a roundabout under the M1 overpass. The vehicle enters the ramp at a very low velocity and starts to accelerate to reach a steady speed of 83-96 km/h on an inclined road. It is considered as severe engine operation as a high torque is demanded therefore the engine was running at the speed of high torque (1100 rpm). The road profile is used as one of the major factors in the determination of vehicle specific power (VSP) which incorporates vehicle speed and acceleration.

Eventually, it was quite interesting to see how the calculated VSP is correlated with the engine control unit (ECU) load factor (LF) broadcast. The LF is a scale for engine response to the sum of external loads.

Multi-regression analyses were performed to determine the variables that significantly affect the HGV performance parameters. The best regression model to predict each performance parameter is calculated at different HGV operation modes.

4.1 Fuel type, blending ratio and delivery control effects on engine performance

The Bioltec system is simply a selective fuel mixing system, actuated by UBF temperature and the preloaded engine performance maps. Actually the UBF compartment of the fuel tank is heated by heat recovered from engine coolant. A heat exchanger is placed in the UBF compartment for coolant-UBF heat transfer. Usually the engine starts with PD especially in cold starts. It's the driver's choice whether to continue on PD or switch to UBF-PD blended (BL) fuel. Once the auto mode is selected the Bioltec system starts to mix the two fuels in different proportions according to the UBF temperature and the preloaded engine performance maps.

Fig 4.1 shows the correlation between UBF temperature and content in the fuel blend. This case is an arbitrarily chosen journey from the 32 test trips. The only difference that could be indicated is the engine start temperature. Cold starts delay UBF delivery to the engine as shown in fig.4.3. Apparently, at fuel temperatures lower than 45°C, no UBF is delivered to the fuel injection pump. Therefore, during the first 5 minutes of this particular journey, the HGV was running on pure PD. At temperatures between 45°C and 50°C, the UBF share in the blend is limited to 20%. For temperatures higher than 50°C up to 60°C the UBF content in the blend jumps to 80%. Over 60°C the engine is totally allowed to run on 100% UBF. The overall journey UBF/PD blending ratio

exceeded 93% at hot starts especially in warmer ambient conditions. As a journey average, for all the test runs throughout this research including all the cold and hot starts, 84.5% of the journey fuel was UBF. The fuel for the steady high speed HGV travel on the M1 is 100% pure UBF.

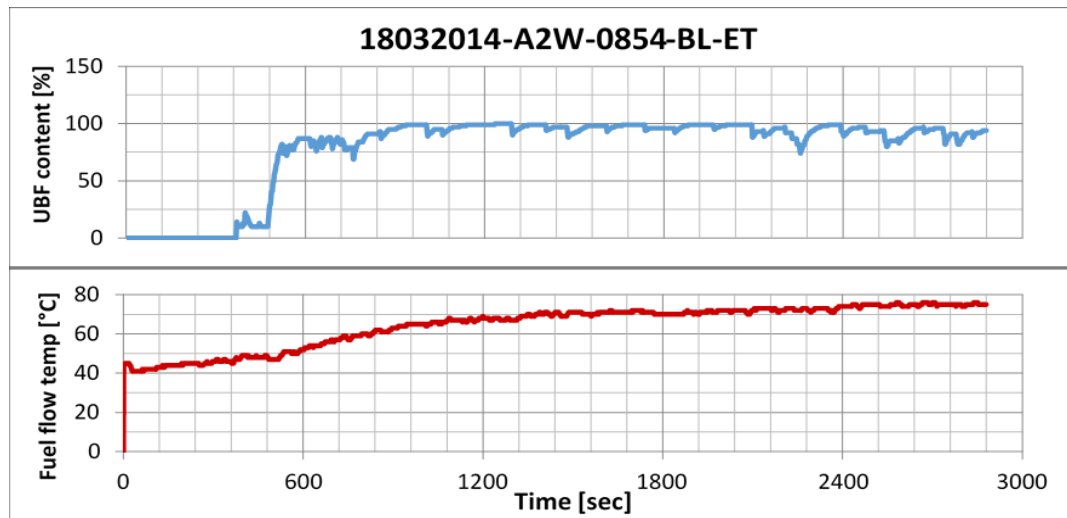


Figure 4.1 Bioltec system response to C2G UBF temperature. A cold start from Ashby towards Wigston.

Fig.4.2 illustrates the return journey in which the engine and flowing fuel were hot enough to let a fuel blend of 20% UBF to feed the engine immediately. UBF content increased to 75% at minute 3 to exceed 90% at minute 5. In this particular trip the HGV used more than 89% UBF as journey fuel.

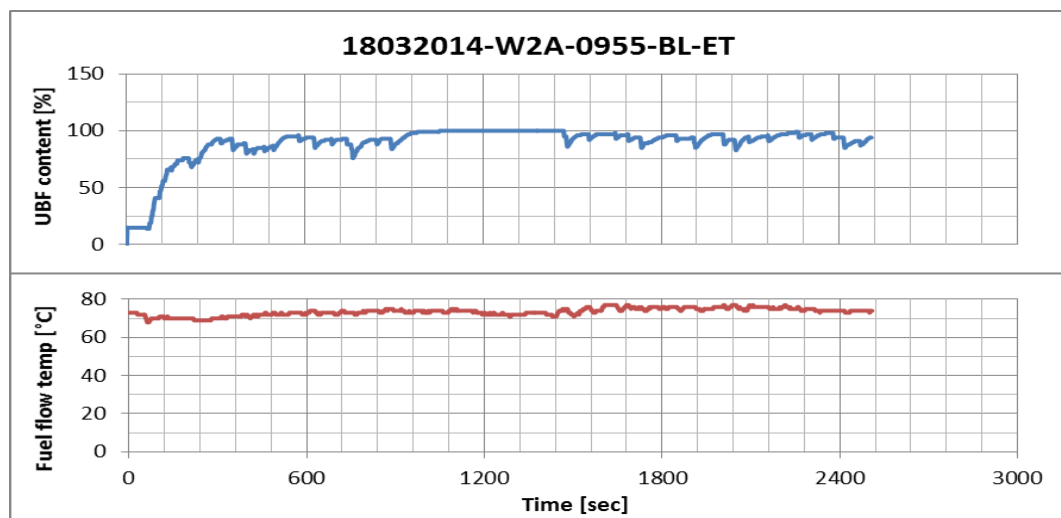


Figure 4.2 Bioltec system response to C2G UBF temperature. A hot start from Wigston towards Ashby.

The rate of fuel consumption for the two components of BL fuel is illustrated in fig.4.3. It is quite obvious that the vehicle was completely dependent on PD during the first 5 minutes of its journey because it was a cold start. At minute 9, the rate of PD consumption declined to almost 20% and it started to vanish especially in the steady state driving part of the journey, on the M1 for 12.3 km where the vehicle was travelling at 90 km/h. The tiny peaks in the rate of PD consumption graph are decided by the engine control unit (ECU) according to the preloaded engine performance maps. These are usually related to the changes encountered in road load and the driver's interaction.

The journey also included urban and suburban sections. The traffic was controlled by traffic lights and traffic calming and many roundabouts were encountered as shown in chapter three table 3.1.

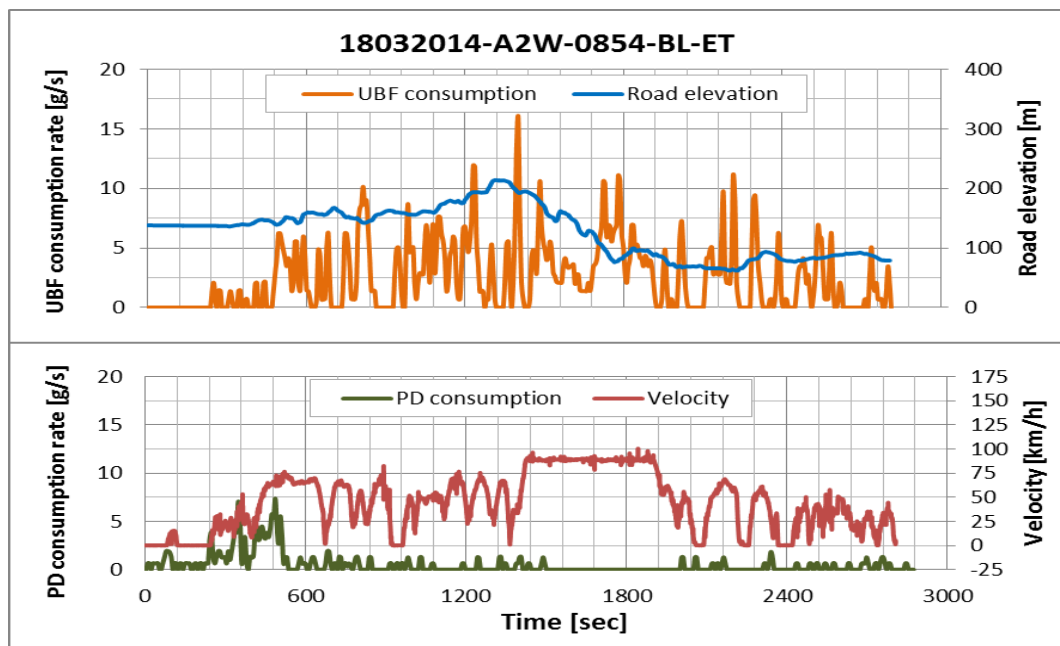


Figure 4.3 Rate of fuel consumption for C2G UBF and PD for the HGV journey in fig.4.1.

The rate of fuel consumption in the return journey is plotted in fig.4.4. The rate of UBF consumption is higher than the out bound journey with a very poor contribution of PD in the blend. The high rate of UBF consumption in the middle of the journey results from the high speed on the M1 motorway. A comparison between UBF consumption rate in the two directions at this particular section of the trip shows a higher consumption in the return direction due to HGV travel uphill and occasionally against the prevailing winds. This

is expected to affect the exhaust emissions which are discussed thoroughly in chapters six and seven.

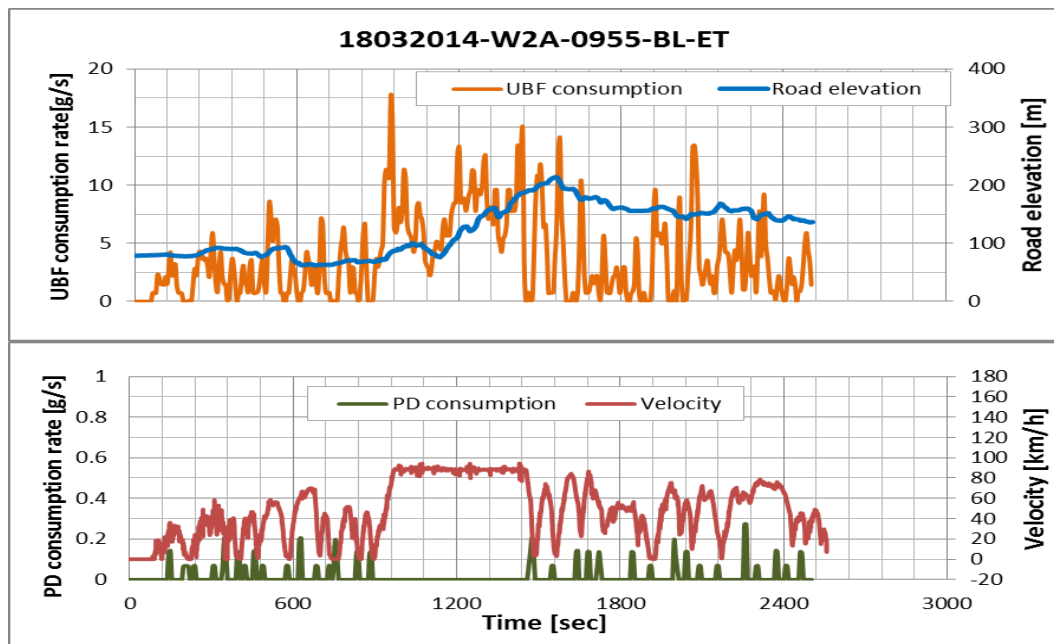


Figure 4.4 Rate of fuel consumption for C2G UBF and PD for the HGV journey in fig.4.2.

4.2 Vehicle specific power (VSP)

4.2.1 Vehicle specific power for the entire test series

The journey averaged vehicle specific power (VSP), which was explained in section 2.5.2.1 and section 3.9, is illustrated in fig.4.5. PD showed no difference in VSP as the payload doubled from 15.5 tonne to 31 tonne, nevertheless the BL fuel shows a 12%~18% increase in VSP as the payload doubled during the outbound journey and the inbound journey respectively. This could be indicated by comparing columns one and two or three and four. A comparison between the VSP at two different road directions (columns 1 & 3 or 2 & 4) shows a 65%~74% higher VSP during the return journey as the HGV was running on BL fuel at 15.5 tonne and 31 tonne respectively. The HGV increased its VSP by 62%~58% during the return journey while running on PD at the same load conditions. The higher VSP in inbound journey is due to the higher road load specifically road gradient as explained previously. Actually the HGV is gaining energy, especially when the HGV is loaded, as it

moves from Ashby De La Zouch to Wigston (A2W) due to the negative road gradient. In general a slightly lower VSP is indicated in the case of the BL fuel.

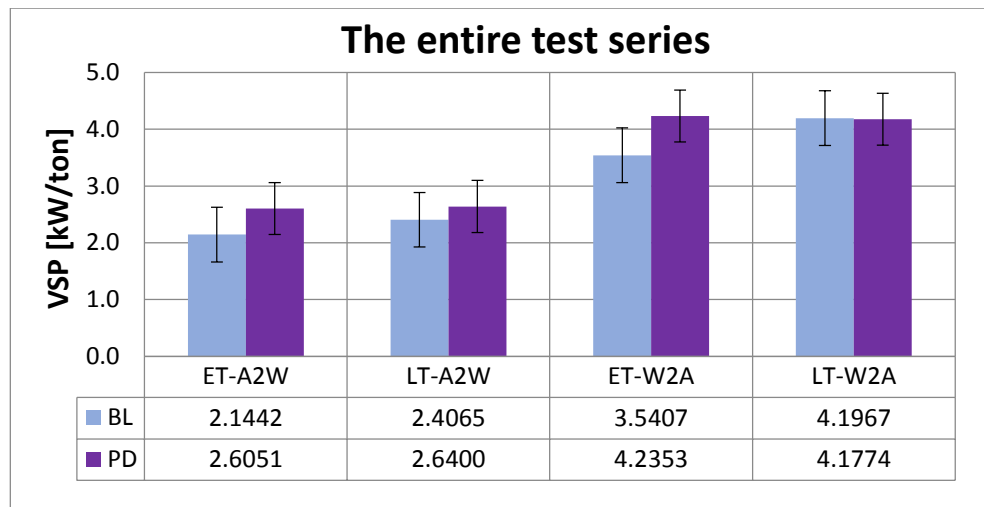


Figure 4.5 The effect of vehicle payload and road load on VSP during the entire journey. Data based on 32 trips. ET and LT are empty trailer and loaded trailer respectively. A2W and W2A are the HGV direction from Ashby to Wigston and Wigston to Ashby respectively.

4.2.2 The effect of fuel type on VSP in selected road sections throughout the HGV journey

4.2.2.1 Steady high speed HGV travel on M1 motorway

A comparison between fig.4.5 and fig.4.6 shows the same trend in the two graphs and the only difference is in the VSP scale which is higher in the case of the steady state operation. Actually the higher vehicle speed on the M1 (83-96 km/h) increases the rolling resistance, friction and air drag which varies with velocity cubed. Added to that the positive gradient resistance, as shown in the two columns to the right, as the HGV travels towards Ashby (W2A). Actually the plot doesn't indicate any significant effect of the fuel type on VSP. Apparently, this part of the journey is characterised by the steady HGV travel and therefore the occurrence of acceleration is very rare while the air resistance is very high due the high HGV speed. The difference between the road gradients of the outbound and inbound journeys increased the VSP by nearly 86% on average regardless of the fuel type and the amount of HGV payload.

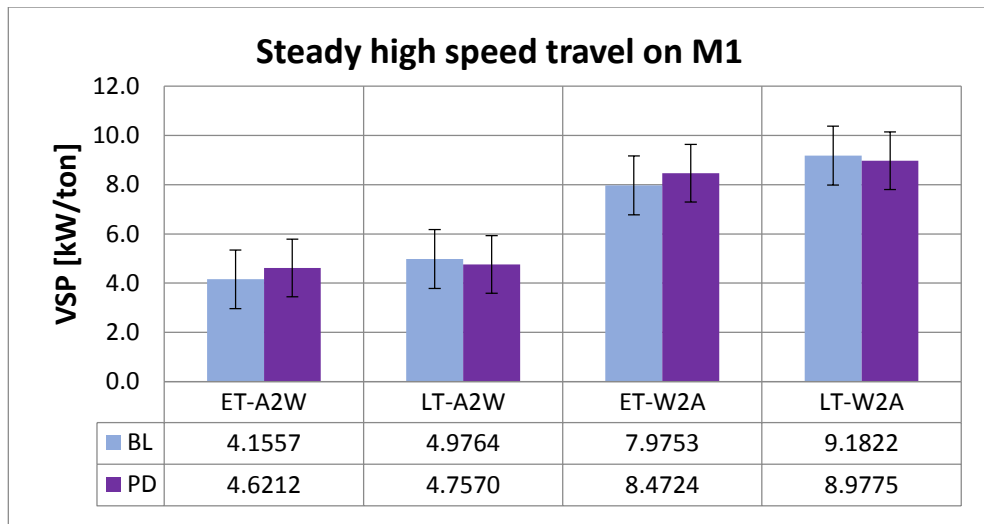


Figure 4.6 The effect of vehicle payload and road load on VSP. Steady high speed HGV travel on the M1. Data based on 32 trips. ET and LT are empty trailer and loaded trailer respectively. A2W and W2A are the HGV direction from Ashby to Wigston and Wigston to Ashby respectively.

4.2.2.2 High torque performance on the ramp to M1

The ramp to merge on to the M1 motorway was selected throughout the whole journey as a severe operational condition where the HGV requires a high torque to accelerate and overcome the gradient resistance. At this particular section, the road gradient was 3% for 240 m.

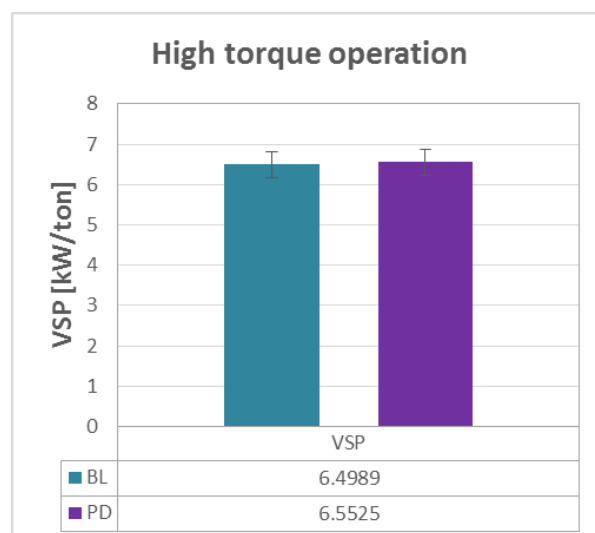


Figure 4.7 VSP for HGV performing under high torque conditions using BL fuel and pure PD. Data based on 16 test trips.

The HGV needed to speed-up from almost 0~10 km/h at the ramp foot to more than 83 km/h on the motorway. The bar chart in fig.4.7 indicates no difference in VSP for the two fuels in this particular test. Both of the fuels delivered the same power to overcome all the resistances (mainly acceleration and gradient resistances) under all load conditions. The VSP of the high torque operation is 55% higher than that of the entire journey average at the highest power demand.

4.3 Specific fuel consumption (SFC)

4.3.1 The effect of fuel type on specific fuel consumption for the entire journey

The specific fuel consumption for the vehicle operated by the BL fuel and pure PD is plotted in fig.4.8. The plot depicts a slightly higher SFC when the vehicle is operated by the BL fuel. This could be attributed to the lower mass based calorific value of the BL fuel which is counteracted by its higher density. Other physical properties also affected the fuel injection process and ultimately the combustion process. This will be discussed thoroughly in the next chapters.

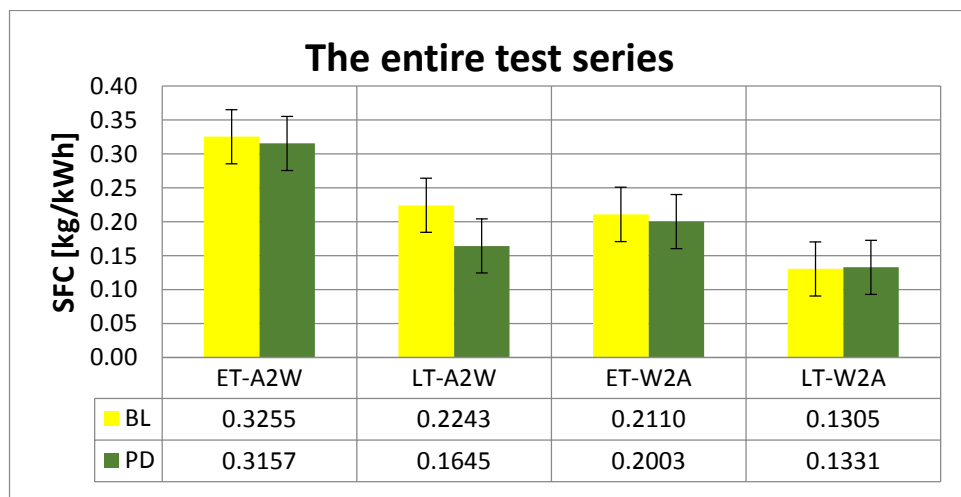


Figure 4.8 Specific fuel consumption for a HGV operated on different fuels, BL fuel and PD, under different payloads and road loads. The plots are based on 32 trips. ET and LT are empty trailer and loaded trailer respectively. A2W and W2A are the HGV direction from Ashby to Wigston and Wigston to Ashby respectively.

Doubling HGV payload (by comparing the first and second columns or the third and fourth columns) reduces the SFC, up to 38% for the BL fuel and up to 47% for the PD, depending on journey direction. The reduction of SFC is higher during the outbound journey because the HGV is dominantly traveling downhill. In other words, the HGV increases its dependence on gravity as the payload doubles.

The higher power demand is a result of increased vehicle load as payload or road load or both. Fig.4.9 shows lower SFC as the power demand increases which means a better fuel conversion to power at higher loads. The two fuels behaved the same way and completely coincided at moderate loads.

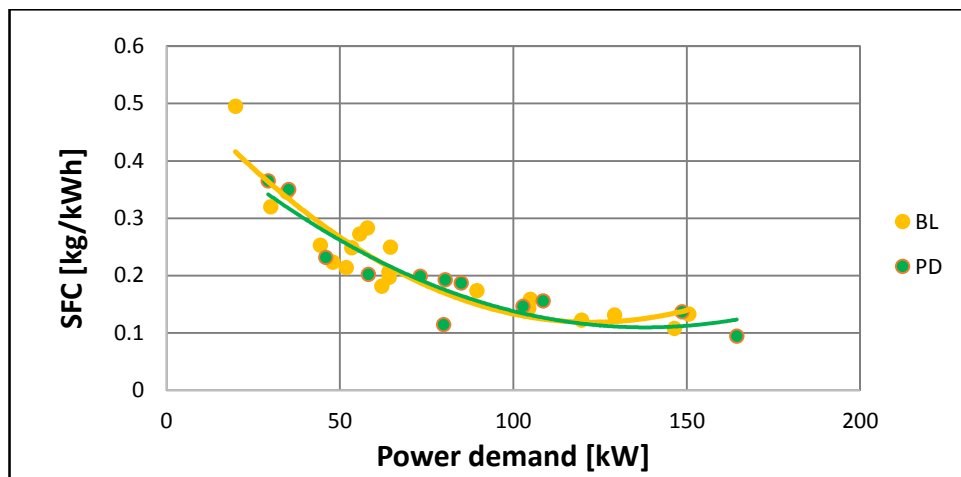


Figure 4.9 Vehicle SFC vs power demand for the HGV operated on different fuels, BL fuel and PD separately. Data based on 32 vehicle trips.

The data also exhibits a relatively high correlation between SFC and power demand with coefficients of regression higher than 0.85. The inversed correlation between SFC and power demand is attributed to the improved combustion process. Higher loads are associated with higher combustion temperatures due to the increased amount of fuel being injected, injection advancement and higher rate of heat release, higher injection pressure, more frequent occurrence of the combustion process at high speed operation, improved turbocharging action and better turbulence. All the aforementioned factors improved fuel atomisation, evaporation and mixing with air.

4.3.2 The effect of fuel type on specific fuel consumption for HGV travel under steady high speed conditions.

Vehicle travel at steady state speed between 83~96 km/h on the motorway for 12.3 km was also investigated. No tangible differences, in the SFC results, between the entire journey and the steady state condition could be seen by comparing figs.4.8 and 4.10. The plots exhibit the same trend and nearly the same SFC values at all loads.

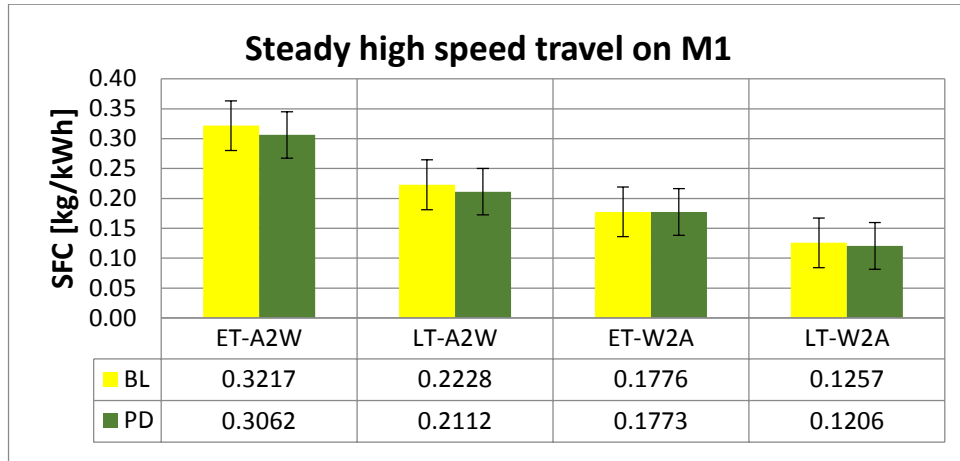


Figure 4.10 Specific fuel consumption for the HGV travelling at steady high speed on M1 motorway using BL fuel and PD separately. The plot is based on data analysis from 32 trips. ET and LT are empty trailer and loaded trailer respectively. A2W and W2A are the HGV direction from Ashby to Wigston and Wigston to Ashby respectively.

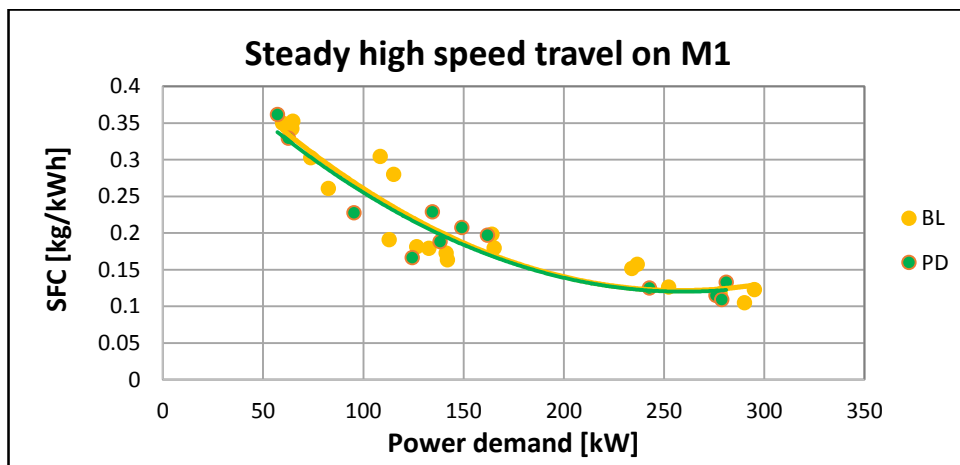


Figure 4.11 Specific fuel consumption vs vehicle power demand for the HGV traveling at steady high speed on M1 motorway. The plots are based on data from 32 trips.

The plot of SFC for the steady high speed condition is shown in fig.4.11. A strong similarity in the trend is indicated between fig.4.9 and fig.4.11. The only

exceptions are the higher coefficients of regression and the wider range of the power demand due to the higher HGV speeds.

4.3.3 The effect of fuel type on specific fuel consumption for a HGV travel under high torque conditions.

This part of the tests is characterised by the high torque required to overcome the acceleration resistance as the HGV is moving from a very low speed at the ramp foot (10~20 km/h) to (83~96 km/h) on the motorway. The other resistance to overcome is the 3% road gradient that persists for 240 m. Therefore, this action requires a very high gear ratio and engine operation close to the maximum torque speed (1100 rpm). The bar chart in fig.4.12 shows a considerable difference between the two fuels. Although the two fuels show a low SFC compared to the steady high speed condition, vehicle operation on BL fuel has a 12% higher SFC than the PD. Actually this could be attributed to the differences in the physical and chemical properties between the two fuels and the lower mass based calorific value of UBF (3.7~4.4% lower as presented in table 5.4) and their consequences on the combustion process.

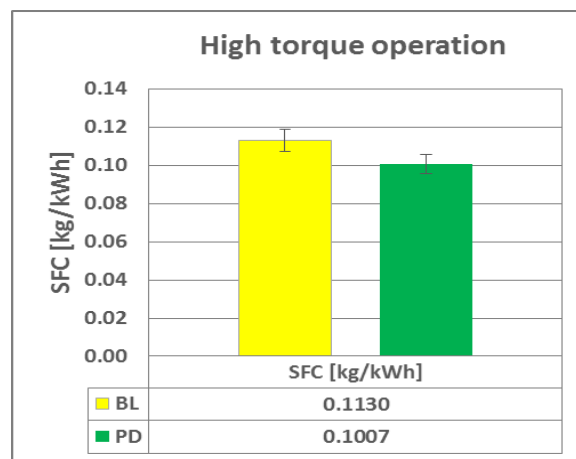


Figure 4.12 Specific fuel consumption for the HGV at high torque performance using BL fuel and PD separately. The plot is based on data analysis from 16 trips.

The relationship between SFC and power demand for the high torque condition is illustrated in fig.4.13. The BL fuel shows higher SFC at all power demands. It is also seen that the BL fuel graph is extended to higher power demands. This could be resulted from a human factor. The driver's behaviour

in the way they accelerate to the higher allowable speed could be one of the reasons.

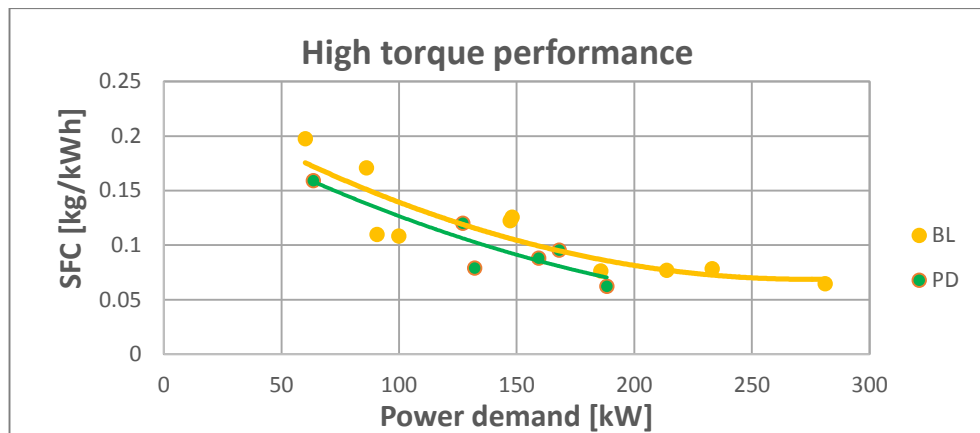


Figure 4.13 Specific fuel consumption vs vehicle power demand for the HGV under high torque travel using BL fuel and pure PD separately. The plots are based on data from 16 trips.

4.4 Engine-out temperature

Temperature is a measure of heat intensity. Engine-out temperature (EoT) is affected by the rate of fuel consumption, the calorific value of the fuel and the load exerted on the engine. EoT affects the quality and quantity of emissions, particularly NO_x and PM, and the efficiency of the exhaust after treatment facilities. The differences in properties between the BL fuel and pure PD was expected to have effects on the combustion temperature. Therefore, engine-out temperature was investigated throughout the real world tests.

Fig.4.14 shows the consistency and correlation between engine-out temperature and other factors like the rate of fuel consumption and engine load factor (LF) throughout an example outbound journey. All these engine responses are related to the road profile, traffic conditions and the driver's behaviour. Fig.4.15 is an example of an inbound journey. Generally the journey is an uphill travel especially the M1 motorway. A comparison with the outbound journey, reveals that the rate fuel consumption is 7.54% higher and the engine-out temperature is 7.7% higher due to an overall higher road load of 7.2%.

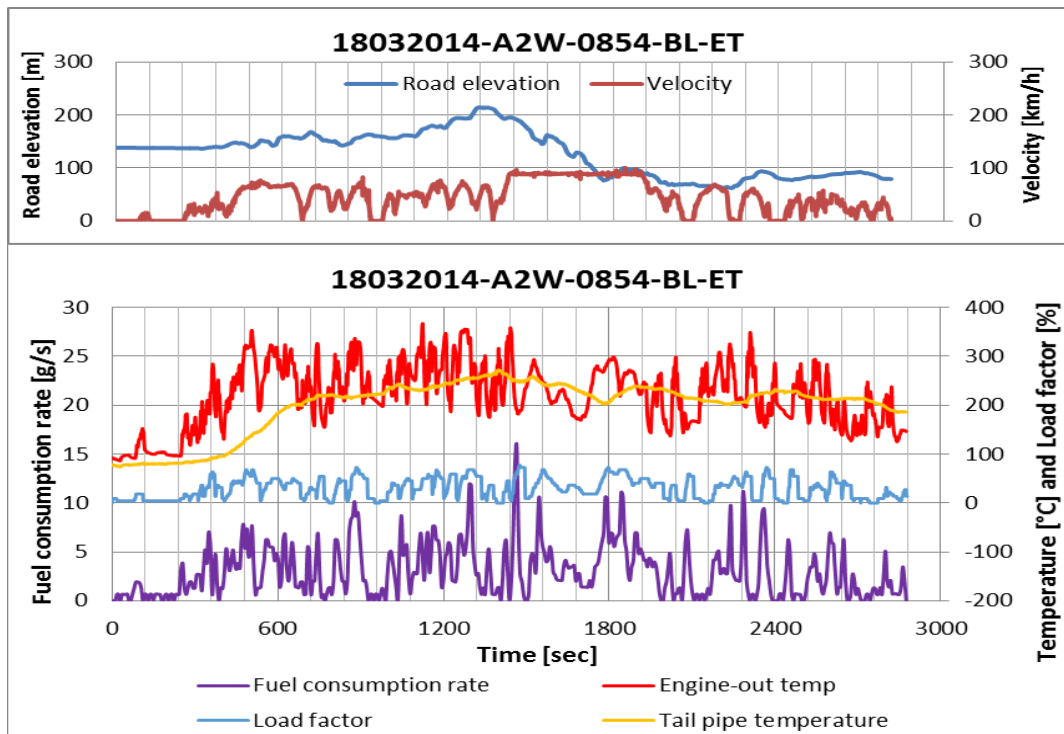


Figure 4.14 Engine-out temperature correlation with engine load factor, and the rate of fuel consumption during an example outbound journey of the HGV.

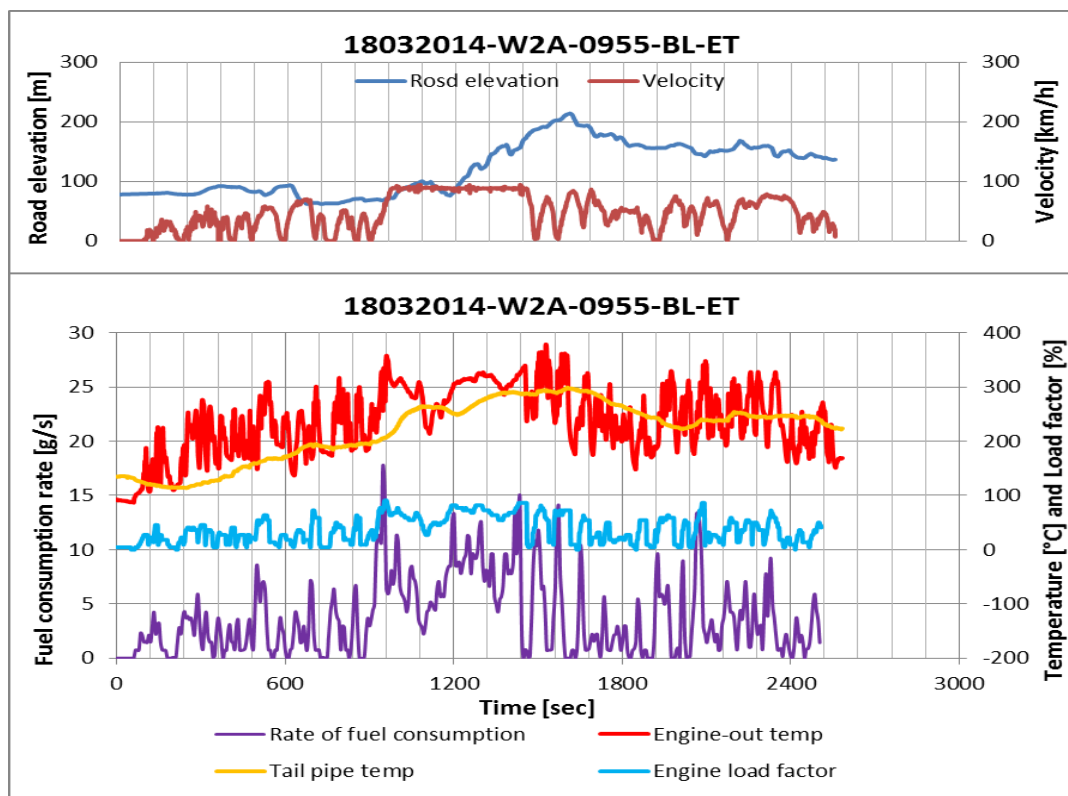


Figure 4.15 Engine-out temperature correlation with engine load factor, and the rate of fuel consumption during an example inbound journey of the HGV.

4.4.1 The effect of BL fuel on engine-out temperature during the entire test series

A small difference in engine-out temperature (EoT) is indicated between engine operation on BL fuel and PD as seen in fig.4.16.

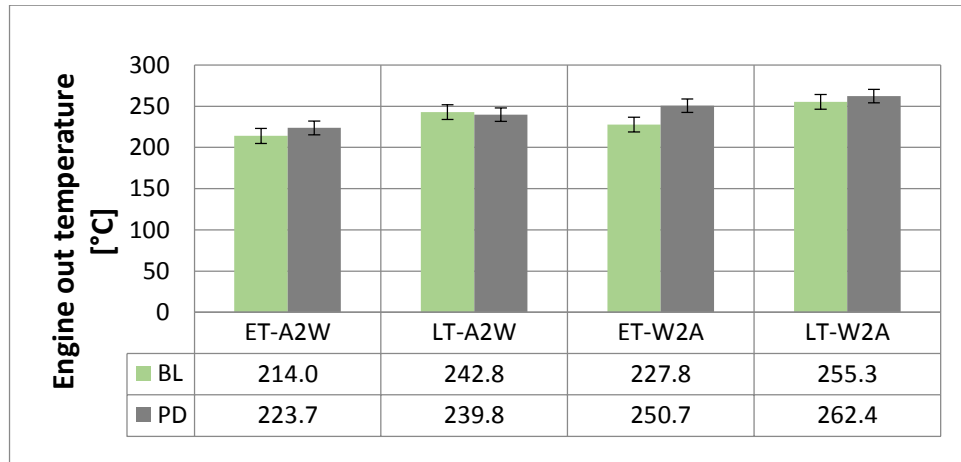


Figure 4.16 A comparison between engine-out temperatures for the vehicle operated on BL fuel and PD at different loads through the entire test series. Results are based on 32 trips. ET and LT are empty trailer and loaded trailer respectively. A2W and W2A are the HGV direction from Ashby to Wigston and Wigston to Ashby respectively.

Vehicle operated on BL fuel shows up to 9% lower engine-out temperature especially at low loads. However that difference vanishes at higher vehicle loads. The effect of increased road load, road gradient in particular, on EoT shows about 5% and 11% increase in EoT for BL fuel and PD respectively.

The lower engine-out temperature at low loads could arguably be related to the amount of fuel being consumed and the fuel conversion efficiency under these circumstances. Poorer fuel atomisation and mixing with air associated with a lower turbocharging efficiency and in-cylinder turbulence would certainly affect the fuel conversion efficiency.

4.4.2 The effect of using the BL fuel on engine-out temperature under steady high speed travel on the M1 motorway

During the steady high speed HGV travel on the M1 motorway, the vehicle used to travel at a high steady state velocity of (83~96km/h) regardless of the direction of movement and the amount of payload. The differences in engine-

out temperature between the two fuels is reduced as the load increases as explained in the previous section. However a huge difference between the temperatures of the outbound and inbound journeys is indicated in fig.4.17. A 50% increase in engine-out temperature is recorded in this section of the road in the return journey. This results from the higher road load (positive gradient and perhaps the prevailing winds opposing the vehicle travel). The steady state return journey recorded on average a 27% higher engine-out temperature compared to the entire journey average.

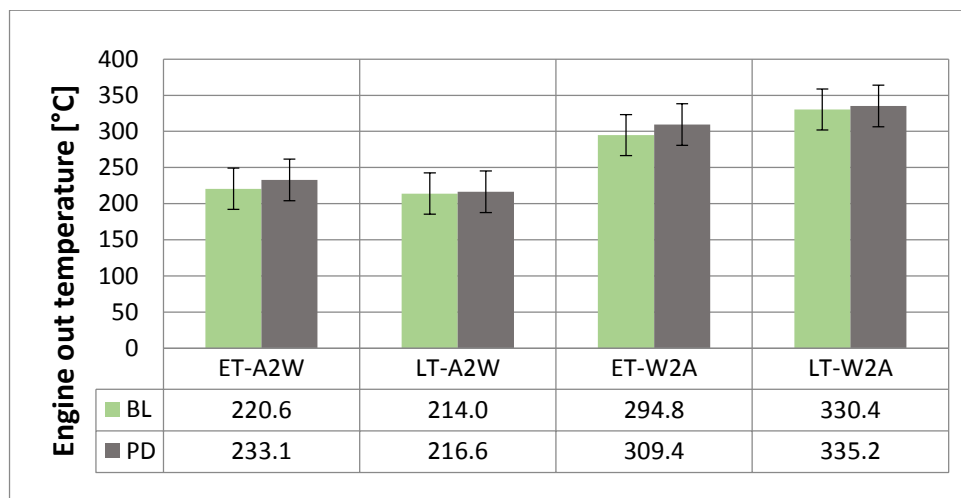


Figure 4.17 Engine-out temperature for the HGV operated on BL fuel in comparison to PD at different loads under steady high speed travel. Results are based on 32 trips. ET and LT are empty trailer and loaded trailer respectively. A2W and W2A are the HGV direction from Ashby to Wigston and Wigston to Ashby respectively.

4.4.3 The effect of using the BL fuel on the engine-out temperature under high torque performance

The 240 m ramp inclined at 3% on which the vehicle used to accelerate from almost stand still to 83 ~ 96 km/h to merge onto the M1, is a severe transient operation.

Although the vehicle operated on BL fuel showed higher SFC (see fig.4.12), the EoT of the two fuels shows no difference under these harsh conditions as illustrated in fig.4.18. However, the vehicle recorded a 6.5% higher engine-out temperature than the journey average engine-out temperature under the highest load conditions.

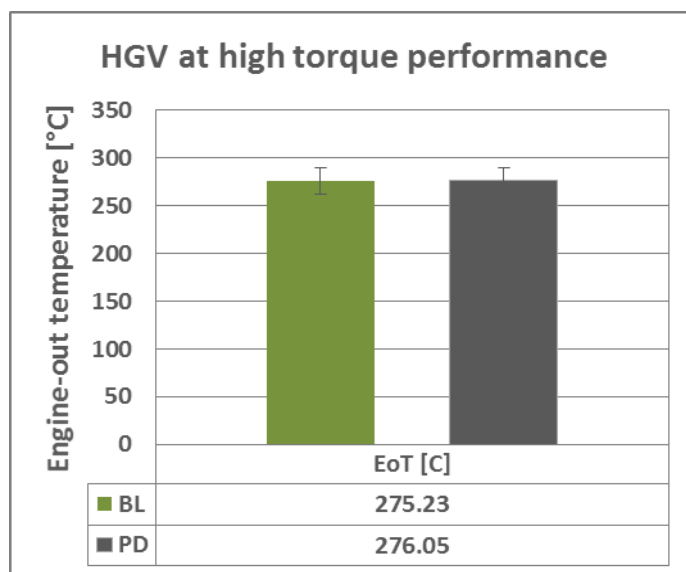


Figure 4.18 Engine-out temperature for the HGV under high torque performance. A comparison between BL fuel and PD. The plots are based on 16 tests with STERROR $\pm 11^{\circ}\text{C}$.

4.5 Statistical analysis

For better understanding of the effects of UBF utilisation in the BL fuel on the HGV performance, all the related factors were included as a group or individuals in the statistical analysis. Multi-regression analysis was performed for all the variables of the tests and this was followed by analysis of variance ANOVA. Levene's test for equality of variances and the t-test for the equality of means were performed for the steady high speed travel data.

4.5.1 Statistical analysis for the entire test series data

Multi-regression analysis was performed to predict VSP throughout the test series. HGV speed, acceleration, fuel type ,GVW, Journey direction, EoT, SFC, and the measured emissions were used in the analysis to predict VSP. The correlations and ANOVA are presented in table 4.1. The predicted model was obtained after 3 repetitions using the backward method. Only four variables were selected by the model to predict VSP with no signs of fuel type among the predictors. They are all significant, SFC possesses the strongest weight followed by trip direction. The adjusted R^2 is 0.861.

Table 4.1 Multi-regression analysis and ANOVA results to predict VSP throughout the entire test series.

Regression Vehicle Specific Power							
Coefficients							
Model		Unstandardized Coefficients	Sig.	Decision	Collinearity Statistics		
		B			VIF		
3	(Constant)	0.96812					
	Trip direction	0.64406	.003	HS	2.168		
	GVW [tonne]	-0.05	.001	VHS	2.668		
	EoT [°C]	0.01744	.001	VHS	1.960		
	SFC [kg/kWh]	-7.56106	.000	VHS	2.702		
Dependent Variable: Vehicle Specific Power [kW/tonne]							
Adjusted R ² = 0.861							
VSP = 0.96812 + 0.64406 DIR - 0.05 GVW + 0.01744 EoT - 7.56106 SFC							
Best model obtained after Three (3) repetitions, using backward method							
ANOVA							
Model		Sum of Squares	df	Mean Square	F	Sig.	Decision
3	Regression	28.457	4	7.114	49.146	.000	VHS
	Residual	3.908	27	0.145			
	Total	32.366	31				

Table 4.1 is in fact a combination of three tables. At the top is the table of predictors which incorporates the significant variables which are explicitly correlated to the dependent variable and others that are cross-correlated to each other to improve the value of the regression coefficient and the model significance.

B is the calculated coefficient for the interception of each one of the predictors. Sig. is the (p) value for each predictor, values $\leq .05$ are considered as significant at 95% level of confidence.

Collinearity Statistics is the indicator for the cross-correlation between the predictors. High collinearity means that variables are over-correlated against each other [173].

VIF is the variance inflation factor, high values mean predictor over-correlation. Satisfactory VIF values are between (1.065~1.218) [173].

The second sub-table incorporates the predictive model and the adjusted R² which is an indicator for the percentage that the model accounts for the variance of the dependent variable.

The third sub-table is the ANOVA table. ANOVA calculates how much variance comes from independent variables and how much is due to error [173].

F is the (F ratio) which the ratio of the variables variance to the error. Larger F ratios means that the result is less likely to be a matter of chance or alternative variables [173].

ANOVA shows that is very high significance (VHS), $F(4,27) = 49.146$ and $p = .000$. It is quite obvious that VSP is more likely affected by the road gradient as indicated in the direction term of the predicted model. Number 1 was assigned to Ashby De La Zouch to Wigston (A2W) which was mostly downhill HGV travel and number 2 assigned to W2A HGV travel. EoT increases with the VSP while the SFC is inversely proportional to VSP because of the improved combustion efficiency at higher power demand as explained earlier in the chapter.

Sum of Squares is the variance which is the mean of squared deviations from the mean

$$s^2 = \frac{\sum(x-\bar{x})^2}{N-1} \dots\dots\dots 4.1$$

$$\text{Mean Square} = \frac{\text{Sum of Squares}}{\text{df}} \dots\dots\dots 4.2$$

SFC was the dependent variable among the same aforementioned group of variables. The regression analysis and ANOVA results were demonstrated in table 4.2. After four repetitions using the backward method, the best model incorporated only three significant predictors. VSP has the strongest weight. ANOVA results show that the model is VHS, $F(3,28) = 49.313$ at 95% confidence and the adjusted $R^2 = 0.824$ which means that the model accounts for 82.4% of SFC variance. Type of fuel was insignificant and not selected by the model.

Table 4.3 depicts the multi-regression analysis and ANOVA results for EoT as a dependent variable to be predicted from the same aforementioned variables. After 2 repetitions using the backward method, the model selected five predictors. ToF is a significant predictor and possesses a strong weight. It is directly correlated to EoT. As number 1 was assigned to the BL fuel and 2 to PD, the correlation shows a higher combustion temperature from the PD. HGV velocity, GVW and VSP are significant predictors and probably have the

same weight. ANOVA results show that the model is VHS, $F(5,26) = 42.93$ at 95% confidence and the adjusted $R^2=0.871$.

Table4.2 Multi-regression analysis and ANOVA results to predict SFC throughout the whole journey.

Regression Specific Fuel Consumption							
Coefficients							
Model		Unstandardized Coefficients	Sig.	Decision	Collinearity Statistics		
		B			VIF		
4	(Constant)	0.25485					
	GVW [tonne]	-0.01	.000	VHS	1.566		
	EoT [°C]	0.00153	.004	HS	2.203		
	VSP [kW/tonne]	-0.07317	.000	VHS	1.521		
Dependent Variable: Specific Fuel Consumption [kg/kWh]							
Adjusted $R^2 = 0.824$							
SFC = 0.25485 - 0.01 GVW + 0.00153 EoT - 0.07317 VSP							
Best model obtained after Four (4) repetitions, using backward method							
ANOVA							
Model		Sum of Squares	df	Mean Square	F	Sig.	Decision
4	Regression	0.207	3	0.069	49.313	.000	VHS
	Residual	0.039	28	0.001			
	Total	0.246	31				

Table4.3 Multi-regression analysis and ANOVA results to predict EoT throughout the whole journey.

Regression Engine-out Temperature							
Coefficients							
Model		Unstandardized Coefficients	Sig.	Decision	Collinearity Statistics		
		B			VIF		
2	(Constant)	37.41434					
	Type of Fuel	6.82563	.020	S	1.030		
	Velocity [km/h]	2.42142	.000	VHS	1.607		
	GVW [tonne]	2.00000	.000	VHS	2.061		
	VSP [kW/tonne]	8.17685	.008	HS	4.738		
	SFC [kg/kWh]	70.12615	.060	NS	5.710		
Dependent Variable: Engine-out Temperature [°C]							
Adjusted $R^2 = 0.871$							
EoT = 37.41434 + 6.82563 ToF + 2.42142 V + 2.00 GVW + 8.17685 VSP - 70.12615 SFC							
Best model obtained after Two (2) repetitions, using backward method							
ANOVA							
Model		Sum of Squares	df	Mean Square	F	Sig.	Decision
2	Regression	11774.846	5	2354.969	42.930	.000	VHS
	Residual	1426.244	26	54.856			
	Total	13201.090	31				

4.5.2 Statistical analysis for the steady high speed HGV travel data

Table 4.4 is the group statistics for the effect of the fuel type on the performance factors listed in the table. The analysis shows no significant differences in the means and standard deviation of any of the performance factors as the vehicle operated on PD or the BL fuel.

Table 4.4 Statistical analysis showing the effect of fuel type on the group of engine performance factors under steady high speed conditions.

Group Statistics					
PERFORMANCE VARIABLES	TYPE OF FUEL	N	Mean	Std. Deviation	Std. Error Mean
Engine-out Temperature (EoT) [°C]	BL	20	264.95	51.7935	11.58137
	PD	12	275.70	55.5527	16.03667
VSP [kW/ton]	BL	20	6.57	2.3182	.51836
	PD	12	6.75	2.2603	.65249
SFC [kg/kWh]	BL	20	.21	.0826	.01847
	PD	12	.20	.0806	.02325

Table 4.4 shows the variances of the designated engine performance parameters as a result of fuel change.

where

N is the number of journeys.

Mean is the mean value for the journey averages in [g/kWh].

Std. Deviation (σ) is the square root of the variance, which is the average of the squared deviation of the score from the mean value of the group of scores [174].

$$\sigma = \sqrt{\frac{\sum(x-\bar{x})^2}{N}} \dots\dots\dots 4.3$$

Std. Error Mean is the standard deviation for the sampling distribution of the mean [174].

$$\text{Std. Error} = \frac{\sigma}{\sqrt{N}} \dots\dots\dots 4.4$$

Levene's test for equality of variances and t-test for equality of means show in table 4.5 no significant effect of using UBF in the BL fuel on any of the performance factors like SFC, VSP and EoT..

Table 4.5 Independent samples test. The effect of fuel type on vehicle performance factors under steady high speed HGV travel.

Independent Samples Test									
PERFORMANCE VARIABLES (Equal variances assumed)	Levene's Test for Equality of Variances		t-test for Equality of Means						
	F	Sig.	t	df	Sig. (2-tailed)	Mean Difference	Std. Error Difference	95% Confidence Interval of the Difference	
								Lower	Upper
Engine-out Temperature [°C]	.281	.600	-.553	30	.584	-10.7520	19.4269	-50.4270	28.9230
VSP [kW/ton]	.002	.967	-.211	30	.835	-.1766	.8388	-1.8897	1.5364
SFC [kg/kWh]	.478	.495	.429	30	.671	.0128	.0299	-.0482	.0739

t-test for equality of means was performed and demonstrated in table 4.5.

where

t is the calculated value of the test statistic

df is the degrees of freedom (No. of cases – 2)

Sig.(2-tailed) is the (p) value that holds the proportion of area the positive value of the test statistic cuts off in the upper tail in the t-distribution with the indicated df plus the proportion of area that the negative value of the test statistic cuts off in the lower tail [173].

Mean difference (g/kWh) is the difference in the mean value (from table 4.4) for the performance of each fuel.

Std. Error Difference is the difference between the standard error values of the two fuels.

Lower and Upper are the critical values that cut area equal to $\alpha/2$ from each side of the t-distribution[173].

4.5.3 Multi-regression analysis for the steady high speed HGV travel

HGV travel on the M1 motorway was observed to indicate the effects of the type of fuel on engine performance as the HGV is travelling steadily at a high speed. The engine is also running at high speed but with a low gear ratio. Therefore air resistance and road gradient are considered as the most effective variables affecting the VSP.

Multi-regression analysis was performed of the HGV velocity acceleration, fuel type ,GVW, Journey direction, EoT, SFC, and the measured emissions, NO_x upstream and downstream to SCR, CO, CO₂ and THC, were used in the analysis to predict VSP. Regression analysis and ANOVA were tabulated in table 4.6. After 9 repetitions using the backward method, the model selected three significant predictors. Among the predictors SFC has the strongest weight.

Table 4.6 Multi-regression analysis and ANOVA results for the prediction of VSP under steady high speed HGV travel.

Regression Vehicle Specific Power							
Coefficients							
Model		Unstandardized Coefficients	Sig.	Decision	Collinearity Statistics		
		B			VIF		
9	(Constant)	6.29158					
	GVW [tonne]	-0.06	.006	HS	1.647		
	EoT [°C]	0.02006	.000	VHS	2.581		
	SFC [kg/kWh]	-17.64502	.000	VHS	3.949		
a. Dependent Variable: Vehicle Specific Power [g/kWh]							
Adjusted R ² = 0.915							
VSP = 6.29158 - 0.06 GVW + 0.02006 EoT - 17.64502 SFC							
Best model obtained after Nine (9) repetitions, using backward method							
ANOVA							
Model		Sum of Squares	df	Mean Square	F	Sig.	Decision
9	Regression	28.457	3	48.773	111.756	.000	VHS
	Residual	3.908	28	0.436			
	Total	32.366	31				

ANOVA shows that the predicted model is VHS because $F(3,28) = 111.756$ and $p = .000$. The adjusted $R^2 = 0.915$. Again ToF was not included by the model as a predictor.

Table 4.7 Multi-regression analysis and ANOVA results for SFC as the dependent variable in a steady high speed HGV travel.

Regression Specific Fuel Consumption							
Coefficients							
Model		Unstandardized Coefficients	Sig.	Decision	Collinearity Statistics		
		B			VIF		
4	(Constant)	0.04435					
	Type Of Fuel	-0.02037	.000	VHS	1.823		
	NO _x -UP SCR [g/kWh]	0.09517	.011	HS	2.110		
	NO _x -DN SCR [g/kWh]	-1.34864	.032	S	2.070		
	CO ₂ [g/kWh]	0.26436	.000	VHS	5.369		
	THC [g/kWh]	0.46460	.000	VHS	6.099		
	GVW [tonne]	-0.001	.023	S	2.697		
	Velocity [km/h]	0.00139	.078	NS	1.313		
	VSP	-0.00851	.000	VHS	5.995		
Dependent Variable: Specific Fuel Consumption [kg/kWh]							
Adjusted R ² = 0.987							
SFC = 0.04435 - 0.02037 ToF + 0.09517 NO _x UPSCR - 1.34864 NO _x DN SCR + 0.26436 CO ₂ + 0.46460 THC - 0.001 GVW + 0.00139 V - 0.00851 VSP							
Best model obtained after Four (4) repetitions, using backward method							
ANOVA							
Model		Sum of Squares	df	Mean Square	F	Sig.	Decision
4	Regre	0.20039	8	0.02505	306.901	.000	VHS
	Resid	0.00188	23	0.00008			
	Total	0.20227	31				

Table 4.7 shows the multi-regression analysis and ANOVA results to predict SFC as a dependent variable. After 4 rounds using the backward method, 8 predictors were incorporated in the model. ToF is a VHS predictor for SFC and it is inversely correlated to SFC. Actually number 1 was assigned to BL fuel and 2 to PD, therefore the model indicates higher SFC for the BL fuel due to the lower calorific value and perhaps poorer fuel atomisation. The model also shows a very strong correlation between SFC and carbon dioxide CO₂ and total hydrocarbons THC. ANOVA results suggested that the model is VHS as $F(8,23) = 306.9$ and $p = .000$. The adjusted $R^2 = 0.987$. HGV velocity is also included in the model predictors but as a nonsignificant variable since the HGV travel is steady at high speed.

EoT was set as the dependent variable among the aforementioned list of variables. The regression analysis and ANOVA results were shown in table 4.8. After seven rounds using the backward method a model was built on five predictors. Trip direction and GVW are VHS predictors, VSP is also significant but, among these trip direction has the strongest weight. The inbound journey W2A has the higher impact as number 2 was assigned to it. A very strong

correlation is also indicated between CO₂, THC with EoT. The ToF does not show any significance that's why it hasn't been selected by the model. ANOVA shows that the model is VHS as $F(5,26) = 83.3$ and $p = .000$. The adjusted $R^2 = 0.93$.

Table 4.8 Multi-regression analysis and ANOVA results for EoT as the dependent variable in the steady high speed HGV travel on M1 motorway

Regression Engine-out Temperature							
Coefficients							
Model		Unstandardized Coefficients	Sig.	Decision	Collinearity Statistics		
		B			VIF		
7	(Constant)	-36.560					
	Trip Direction	100.235	.000	VHS	8.545		
	VSP [kW/tonne]	7.508	.030	S	8.736		
	CO ₂ [g/kWh]	92.614	.001	VHS	3.494		
	THC [g/kWh]	223.342	.006	HS	3.156		
	GVW [tonne]	2.000	.000	VHS	2.288		
Dependent Variable: Engine-out Temperature							
Adjusted $R^2 = 0.930$							
EoT = - 36.560 + 100.235 DIR + 7.508 VSP + 92.614 CO ₂ + 223.342 THC + 2.0 GVW							
Best model obtained after Seven (7) repetitions, using backward method							
ANOVA							
Model		Sum of Squares	df	Mean Square	F	Sig.	Decision
7	Regression	80742.382	5	16148.476	83.299	.000	VHS
	Residual	5040.423	26	193.862			
	Total	85782.805	31				

4.5.4 Statistical analysis for the vehicle performance under high torque performance

The effect of the fuel type on the vehicle performance was statistically analysed using multi-regression analysis. Table 4.9 reveals the best model For VSP prediction after two repetitions using the backward method. The model excluded the SFC, V, EoT, Tailpipe T, a, and φ and kept the load factor (LF), type of fuel (ToF) and gross vehicle weight (GVW). ANOVA analysis shows that the he model is very high significant $F(3,307)= 9331.19$ and $p = .000$. The adjusted R^2 is 0.989. In fact VSP is primarily affected by LF as a VHS parameter with a high coefficient. This means a good correlation between the calculated road load and the engine control unit (ECU) broadcast.

Type of fuel is the second significant parameter to predict VSP and It possesses a strong weight as well. As numbers 1 and 2 were assigned to BL fuel and PD respectively combined with the negative coefficient, it means that VSP is more affected by PD. Although GVW is included in the model, it shows a very weak contribution as a nonsignificant predictor.

Table 4.9 Multi-regression analysis and ANOVA results to predict the effect of fuel type and other performance variables on vehicle specific power. High torque condition.

Regression Vehicle Specific Power							
Coefficients							
Model		Unstandardized Coefficients	Sig.	Decision	Collinearity Statistics		
		B			VIF		
2	(Constant)	0.48755					
	Type of Fuel	0.84298	.053	S	1.012		
	GVW [tonne]	-0.03571	.070	NS	1.014		
	Load Factor	0.98173	.000	VHS	1.022		
a. Dependent Variable: Vehicle Specific Power [kW/tonne]							
Adjusted R² = 0.989							
VSP = 0.48755 - 0.84298 ToF - 0.03571 GVW + 0.98173 LF							
Best model obtained after Two (2) repetitions, using backward method							
ANOVA							
Model		Sum of Squares	df	Mean Square	F	Sig.	Decision
2	Regression	280612.668	3	93537.556	9331.191	.000	VHS
	Residual	3077.424	307	10.024			
	Total	283690.091	310				

The results of the multi-regression analysis to predict the effect of ToF, GVW, EoT, VSP, V, a, and φ on vehicle load factor LF are shown in table 4.10. ANOVA analysis shows that the model is VHS as $F(4,306) = 8055.389$ and $p = .000$. The adjusted R^2 is 0.989. VSP very significantly correlated to LF and processes the highest coefficient. GVW is also a significant predictor with moderate effect. Although ToF is a non-significant individual predictor, it has a considerable strength in the model.

Table 4.10 Multi-regression analysis results to predict the effect of fuel type and other performance variables on HGV LF. High torque condition.

Regression Load Factor							
Coefficients							
Model		Unstandardize	Sig.	Decision	Collinearity		
		d Coefficients			Statistics		
		B			VIF		
4	(Constant)	0.68357					
	Type of Fuel	-0.77801	.077	NS	1.014		
	GVW [tonne]	0.05677	.010	HS	1.225		
	EoT [°C]	-0.00559	.065	NS	1.295		
	VSP [kW/ton]	1.01002	.000	VHS	1.081		
a. Dependent Variable: Load Factor							
Adjusted R ² = 0.989							
LF = 0.68357 - 0.77801 ToF + 0.05677 GVW - 0.00559 EoT + 1.01002 VSP							
Best model obtained after Four (4) repetitions, using backward method							
ANOVA							
Model		Sum of Squares	df	Mean Square	F	Sig.	Decision
4	Regression	287989.	4	71997.300	8055.389	.000	VHS
	Residual	3122.60	306	10.205			
	Total	291111.	310				

4.6 Conclusions

The temperature of the UBF is a crucial factor that determines the timing and amount of UBF in the BL fuel. Therefore cold starts delay UBF delivery to the engine. Once the UBF temperature exceeded 60°C, the HGV might run on 100% pure UBF. The overall journey UBF/PD blending ratio exceeded 93% at hot starts especially in warmer ambient conditions and a journey average of 84.5% is considered. As the UBF content in the blend increases, PD content decreases. That's why the fuel of the steady high speed HGV travel on M1 is 100% pure UBF and perhaps this part of the journey is the best to study the differences between the performance and emissions of the two fuels at high speed HGV travel. Due to the inclined nature of this road segment, HGV direction very much affected the VSP, SFC, EoT and the emissions.

The entire test series

The VSP increased by 12% during the outbound journey and 18% during the inbound journey as the payload doubled from 15.5 tonne to 31 tonne for the HGV operated on BL fuel.

Doubling HGV payload reduces the SFC, up to 38% for the BL fuel and up to 47% for the PD, depending on journey direction. The two fuels behaved the same way and completely coincided at moderate loads. The data also exhibits a relatively high correlation between SFC and power demand with coefficient of regression higher than 0.85.

Vehicle operated on BL fuel showed up to 9% lower engine-out temperature especially at low payloads. However, that difference vanished at higher vehicle loads. EoT during the return journey was 5% and 11% higher than that of the outbound journey for the BL fuel and PD respectively.

Statistical analysis revealed a strong correlation between EoT and ToF and EoT is higher for PD.

Steady high speed HGV operation

On the M1 motorway, the VSP is 86% higher during the inbound journey compared to the outbound journey on average regardless of the fuel type and the amount of HGV payload. This figure is higher than that obtained from the entire journey data.

No tangible differences in the SFC results were indicated between the entire journey and the steady high speed condition.

The differences in engine-out temperature between the two fuels was reduced as the load increased. However a 50% increase in EoT was recorded in this section of the road in the return journey. This resulted from the higher road load (positive gradient and perhaps the prevailing winds opposing the vehicle travel). The steady state return journey recorded on average 27% higher EoT compared to the entire journey average.

Statistical analysis indicated that ToF is a very high significant predictor for SFC, and PD possesses a lower SFC compared to the BL fuel. Actually the model indicates higher SFC for UBF due to its lower calorific value and perhaps poorer fuel atomisation.

High torque HGV operation

No difference in VSP between the two fuels was indicated in this particular test. Both of the fuels delivered the same power to overcome all the resistances, mainly acceleration and gradient resistances under all payloads.

The VSP of the high torque operation was 55% higher than that of the entire test series average at the highest power demand.

Although the two fuels showed low SFC compared to the steady high speed condition, the HGV operated on BL fuel had a 12% higher SFC than PD.

The two fuels showed no difference in EoT under these harsh conditions. However, the HGV recorded 6.5% higher EoT than that of the entire journey average under highest load conditions.

Chapter 5

Evaluation of fuel physical and chemical properties and their effect on fuel injection characteristics, fuel consumption and engine deposits

The major concern in this chapter is the relationship between fuel properties, injection characteristics and combustion chamber deposits. Knowing the fuel density could explain the injection timing advancement and duration which is a challenging objective. Fuel viscosity and surface tension are also interesting parameters for the elucidation of the injection process and ultimately, the fuel-air mixing process. On the other hand, analysis of the fuel molecular structure provided relevant answers for the differences between the physical and thermal properties of the base fuel and the surrogate. Therefore, twelve fuel samples from four seasons were collected, analysed and grouped into four seasonal batches. Both neat and blends of the UBF with PD were investigated

5.1 Analysis of fuel properties affecting its precombustion behaviour

5.1.1 General

Within the HGV under investigation, Fuel properties vary as it flows, beyond the Biotec fuel system, to the combustion chamber. The fuel journey passes through the fuel injection pump, the high pressure line to the injector, the nozzle sac and nozzle tip. The fuel pressure and temperature, after the fuel injection pump, could reach 180 MPa and around 70°C respectively. At this particular section, the density of PD is 910 kg/m³, the speed of sound wave is 1925 m/s and the bulk modulus of elasticity is 3270 MPa [175]. At the same aforementioned conditions the density of rapeseed oil is 980 kg/m³, the speed of sound wave is 1960 m/s and the bulk modulus of elasticity is 3670 MPa [176]. Rapeseed oil density is quite close to C2G UBF density at the range of test temperatures (see fig.5.2). In fact, fuel issuing from the injector holes experiences the same pressure as that of the combustion chamber which is around 9~23.5 MPa from the start of injection (SOI) to the point of maximum heat release as calculated for this particular HGV engine. The fuel temperature also increases from 90°C in the nozzle tip [14] to 450°C at SOI then to temperatures as high as 2900°C during the combustion process in this particular engine. It is quite difficult to reach these conditions in the lab and

due to the lack of data on UCO in the literature, the analysis in this research will depend on fuel tests at temperatures ranging from 15~110°C. Mathematical models and comparisons to other oils of known properties at the same conditions were used for fuel property prediction at higher temperatures and pressures.

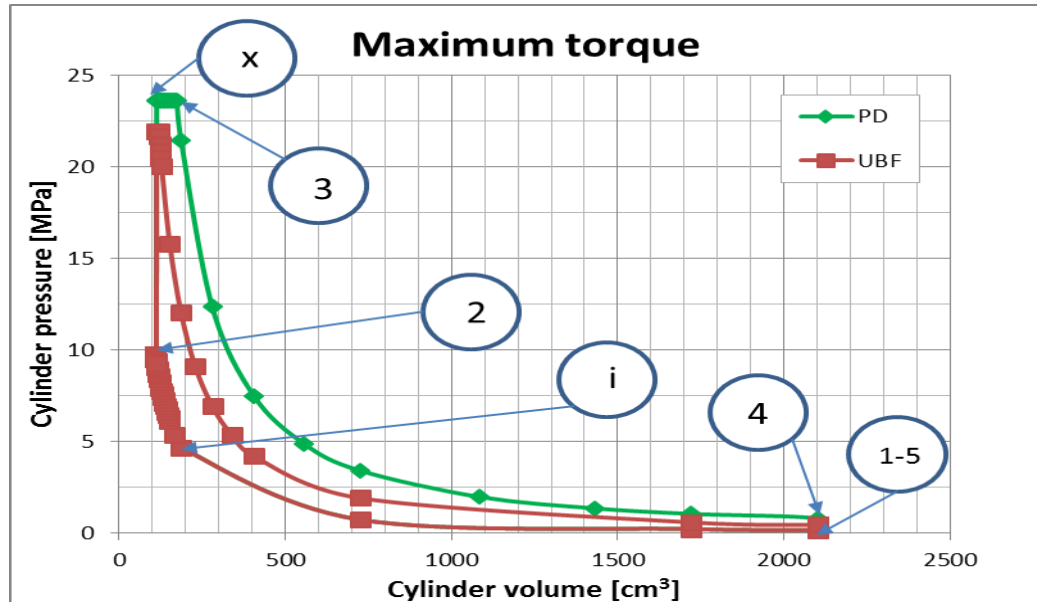


Figure 5.1 P-V diagram for the test HGV DICI engine at maximum torque; A comparison between UBF and PD combustion. (1) start of compression stroke, (i) start of injection, (2) end of compression stroke, (x) end of constant volume combustion and start of constant pressure combustion, (3) end of constant pressure combustion, (4) end of power stroke and (5) start of suction stroke. The properties of the events are explained in table 5.1 below.

Table 5.1 Calculated gas pressure, temperature and density through 360° crankshaft rotation of the HGV engine under maximum torque speed using diesel dual cycle. Data for UBF combustion.

Piston travel extremes	CA	point	V_g cm ³	P_g kPa	T_g K	ρ_g kg/m ³
	Deg.					
BDC	-180	1	2101.35	0.18	308.34	2.00
	-15	i	152.12	6.13	772.95	27.65
	-5	2	112.79	9.19	858.25	37.29
TDC	0	TDC	107.83	9.76	871.87	39.01
	5	x	112.79	21.91	2051.36	37.22
	7.638	3	119.39	21.91	2935.84	26.01
BDC	180	4	2101.35	0.46	1075.97	1.48
	180	5	2101.35	0.18	308.34	1.48

The P-V diagram shown in fig.5.1 is based on a simulation for the diesel dual cycle using HGV engine specifications demonstrated in table 3.1 and fuel specifications in table 5.2 as inputs. A summary of the gas volume (V_g), gas pressure (P_g), temperature (T_g) and density (ρ_g) from UBF at the main points of the cycle are presented in table 5.1. Theoretically calculated, the peak pressure obtained from UBF is 7.1 % lower than its counterpart from PD. The temperature is also lower by 9.3 %. Therefore the exhaust gas pressure is about 44% lower than that of PD. In the same way, the exhaust temperature is 10.4% lower for the UBF. These exhaust figures will affect the turbocharging performance and the overall engine output power. The low exhaust pressure will also increase the residual gas in the cylinder.

The exhaust gas residual in the cylinder are 1.76% and 1.15% for UBF and PD respectively. Obviously, a higher charge dilution is expected for the succeeding cycle in case of UBF.

As demonstrated in fig.5.1 and table 5.1, the engine pressure ratio, which is the ratio of (P_x/P_2) as the piston enters and leaves its upper dwell, are 2.57 and 2.39 for PD and UBF respectively. Therefore a higher pressure peak can be observed for the PD. This could increase the rate of pressure rise of PD higher than that of UBF. Similarly, the cut-off ratio, which represents the range of cylinder volume at which the pressure is kept constant after the start of combustion (V_3/V_x), are 1.53 and 1.05 for PD and UBF respectively. This means that the combustion of PD is more likely to extend longer though the expansion stroke. It is the reason why the PD exhaust gas remains at higher temperature and pressure throughout the expansion stroke.

5.1.2 Fuel density

In vitro analysis of C2G UBF density showed a slight difference in C2G UBF densities throughout the year which was either related to the manufacturer's seasonal fuel specifications and/or perhaps different feedstocks. The C2G UBF winter batches were 0.735% less dense than the summer batches at 15°C. Fig.5.2 is a comparison between C2G UBF density and PD density. It is quite obvious that C2G UBF is denser than PD by 6.73% at 15°C. Although C2G UBF behaves similarly as PD, their density varies inversely to temperature, the difference between C2G UBF and PD densities continue to increase to 7.6% at 100°C which is the fuel temperature at the injector tip prior to injection into the combustion chamber [13, 14]. In general the density of UBF is higher than that of PD, which could be attributed to its molecular weight

and the number of double bonds. According to Ramirez-Verduzco et al.[131], the density increases with the number of the double bonds in the fuel chemical structure and it varies inversely with the molecular weight of the fuel (see table 5.2).

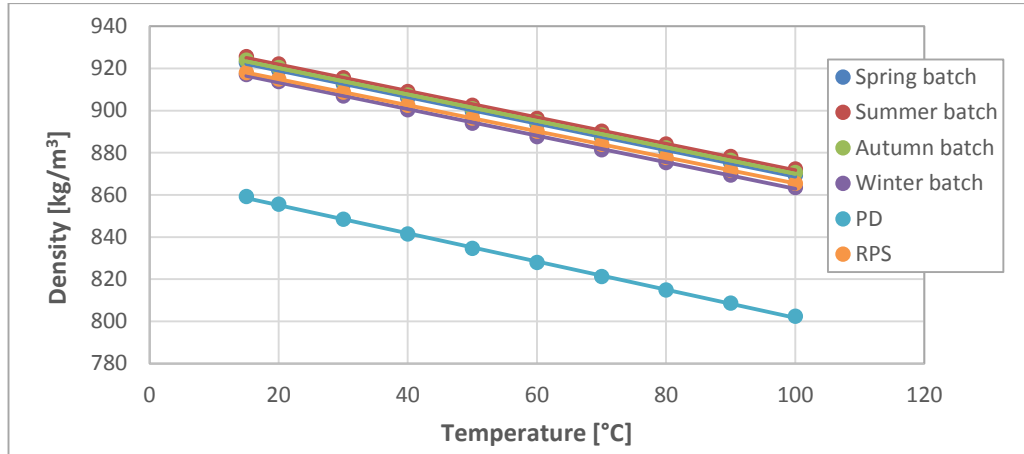


Figure 5.2 Fuel density variation with temperature, C2G UBF from different seasonal batches in comparison to PD and rape seed oil.

Fig.5.3 shows UBF density variation with temperature and the effect of dilution by PD on its density. It is obvious that the C2G UBF density decreases as its percentage in the blend decreases.

In contrast to the temperature effect, high fuel injection pressures increase fuel density [175]. Fuel metering in diesel engines is volumetrically controlled, therefore higher fuel densities mean more fuel mass is introduced to the combustion chamber per each injection process [167]. Although higher densities of C2G UBF could result in a relatively richer combustion, it could also compensate for its lower heating value compared to PD.

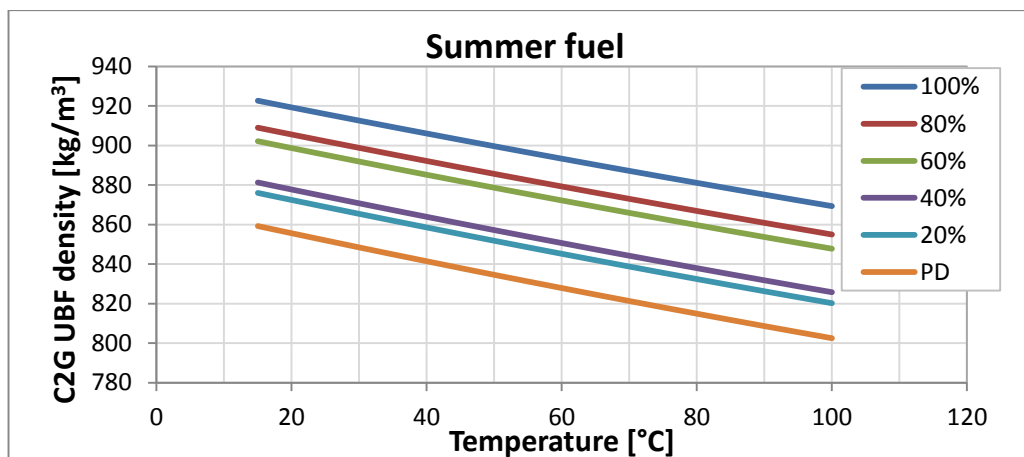


Figure 5.3 Fuel density variation with temperature. Comparison among C2G UBF and its blends to PD. Data are based on three samples and five dilutions for each sample.

5.1.3 Fuel viscosity

According to the Reference Diesel Fuel standard properties 99/96/EC (Euro III), the kinematic viscosity ranges between 2.5~3.5 mm²/s at 40°C. Lab analysis for C2G UBF showed values of kinematic viscosity up to 15 fold higher at the same temperature. High fluid viscosity could increase the friction coefficient thereby reducing the flowrate in certain circumstances. High fuel viscosity has been proven to decrease the spray cone angle and increase the penetration length [6]. C2G UBF batches were taken at different seasons and there was a huge difference among their kinematic viscosities at low temperatures as shown in fig.5.4. However, the difference decays to negligible values at temperatures higher than 90°C. These seasonal differences could be attributed to the differences of C2G UBF feedstock and the manufacturer assessment for the cost and demanded fuel specifications. The gap between the kinematic viscosity of C2G UBF and PD also shrinks to nearly 8 fold higher than that of PD 90°C.

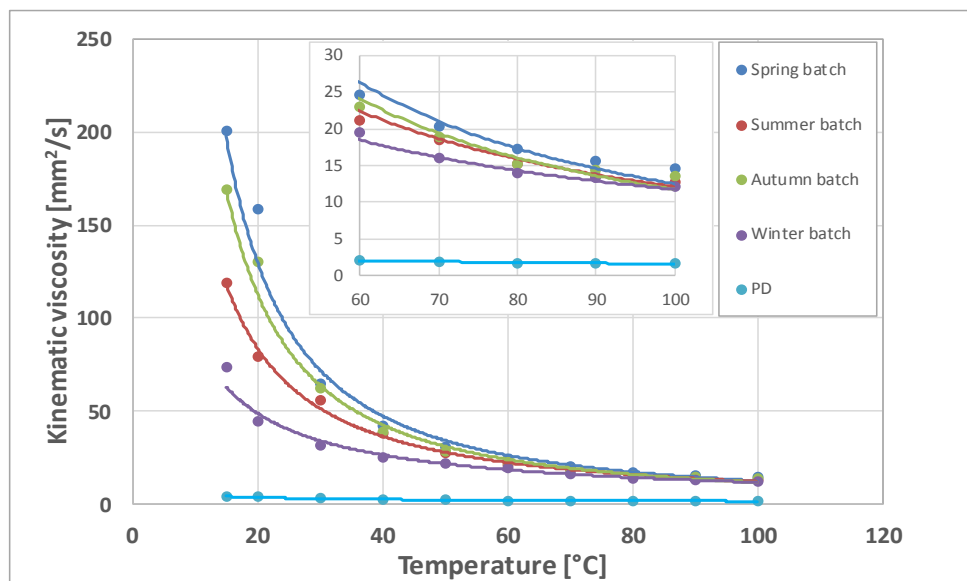


Figure 5.4 Variation C2G UBF kinematic viscosity with temperature. A comparison between C2G UBF collected at different seasons to PD.

Fig.5.5 illustrates the effect of C2G UBF blending ratio with PD at different temperatures. At 40°C the kinematic viscosity of 100% UBF is 15 fold higher than that of PD. This difference decays to 7.25 fold as the temperature increases to 100°C. Increasing the temperature from 40°C to 100°C, reduces the kinematic viscosity of UBF and PD to 35% and 70% of their initial values respectively. The huge variation in UBF properties with temperature

encouraged the fleet operators to use it as a surrogate fuel after being preheated.

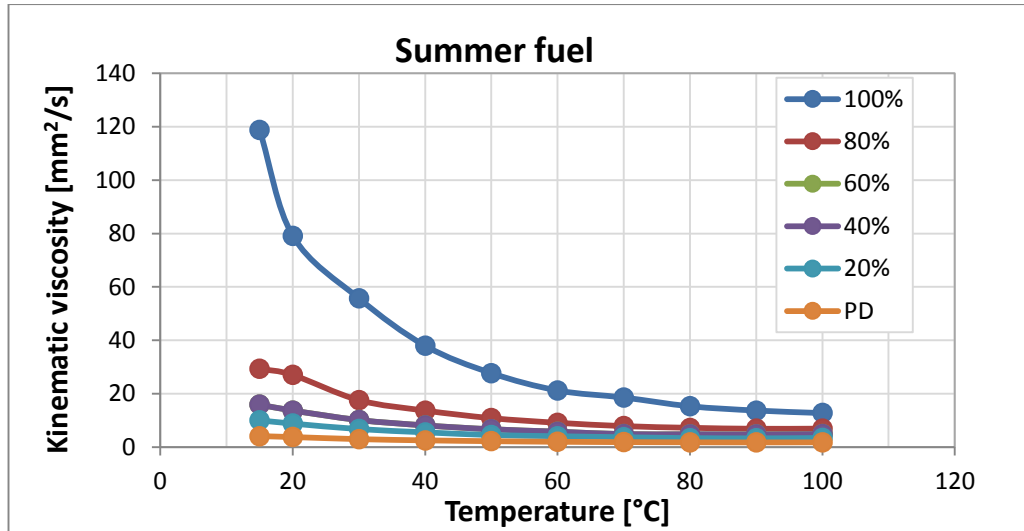


Figure 5.5 Variation of C2G UBF kinematic viscosity with temperature and UBF content in the blend compared to PD.

Two ranges of blending ratios are envisaged in the graph. The first from 0%~80% UBF content in the blend, in which the kinematic viscosity increases by 0.64 mm²/s per 10% UBF increase in the blend at 100°C. The second range covers UBF content in the blend from 80% to 100%. The rate of increase of UBF kinematic viscosity is 2.9 mm²/s per 10% increase in UBF content at 100°C. The kinematic viscosity of the 80% UBF content is about 4 fold higher than that of PD.

The higher kinematic viscosity of UBF could be related to its chemical structure. Table 5.2 shows the decrease in the kinematic viscosity with the increase of degree of unsaturation of the free fatty acid (FFA) of the same carbon number.

Table 5.2 GC-FID analysis of C2G UBF

Component	Chain length	NO. of carbon dual bonds	MW _i	CN _i	v _i @40°C	ρ _i @20°C	HHV _i
Name (i)			g/mol		mm ² /s	g/cm ³	MJ/kg
Palmitate	C16	0	270.45	73.88	4.33	0.86	39.56
Palmitoleate	C16	1	268.43	53.27	3.56	0.88	39.30
Stearate	C18	0	298.50	82.35	5.53	0.86	40.18
Oleic	C18	1	296.49	61.74	4.55	0.87	39.93
Linoleic	C18	2	294.47	41.13	3.75	0.89	39.68
	C20	0	326.56	90.82	6.90	0.86	40.70
	C20	1	324.54	70.21	5.70	0.87	40.45

5.1.4 Fuel surface tension

Fuel surface tension is defined as the ability of the fluid to hold a certain configuration against pressure differences inside and outside the fuel body. It is measured in force per unit length [mN/m] units. Although the surface tension of the fuels under investigation is inversely proportional to temperature, C2G UBF has a higher rate of change than PD. The rate of change for pure UBF is 0.074 mN/m per °C while the rate of change for PD is 0.05 mN/m per °C. Increasing the fuel temperature from 20°C to 100°C reduces the surface tension of PD and UBF by 9.6% and 17.5% respectively as shown in fig.5.6. The surface tension for C2G UBF at 100°C is 37.5% higher than that of PD. This means that UBF is more resistant to changing its configuration under external stimuli. Increasing the ambient pressure also reduces the surface tension but to a lower extent than that of the temperature [177].

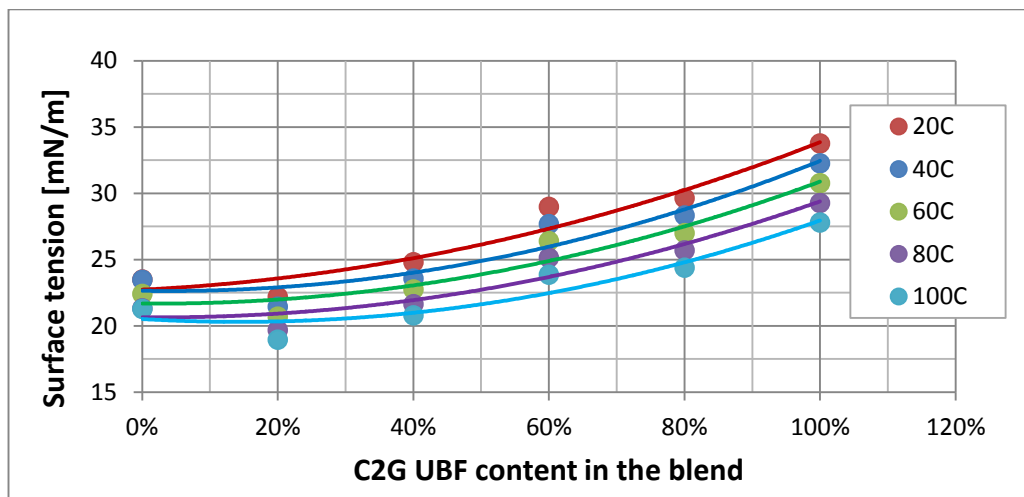


Figure 5.6 Variation of surface tension with blending ratio and temperature. A comparison between C2G UBF and PD. Data averaged for three fuel samples.

Under low injection pressures (around 20 MPa), the fuel surface tension and density are the key factors affecting the fuel spray characteristics [20]. However, modern high injection pressure systems are designed to deliver the fuel at pressures as high as 200 MPa. Therefore surface tension effects vanishes while viscosity effects prevail [6, 12, 54].

5.1.5 UBF chemical structure

Gas chromatography-flame ionisation detector (GC-FID) analysis of C2G UBF revealed the types of fatty acid content and their percentage presence in C2G UBF fuel as shown in table 5.3. The dominant carbon chain in C2G UBF is

C18 which is classified as 52% Oleic FFA (C18:1) and 28% as Linoleic FFA. Therefore C18 was used in the derivation of the Chemical formula of C2G UBF as $C_{18}H_{34}O_2$ in conjunction with CHNS-O analysis results.

Table 5.3 GC-FID analysis for C2G UBF data averaged for two samples.

Component	Chain length	NO. of carbon dual bonds	Peak Time	Area	Adjusted	MW _i	HHV _i
Name			[min]	[%]	Amount	g/mol	MJ/kg
Palmitate	C16	0	24.95	6.66	0.52	270.45	39.56
Palmitoleate	C16	1	26.203	0.17	0.01	268.43	39.30
Stearate	C18	0	28.871	2.01	0.16	298.50	40.18
Oleic	C18	1	30.096	51.95	4.05	296.49	39.93
Linoleic	C18	2	31.664	28.13	2.19	294.47	39.68
	C20	0	32.237	0.59	0.05	326.56	40.70
	C20	1	33.483	8.74	0.68	324.54	40.45
C2G UBF	$C_{18}H_{34}O_2$			98.25	7.66	291.62	39.19

5.2 Analysis of fuel properties affecting the combustion process and emissions

5.2.1 Fuel heating value

The heating value of the fuel is simply the amount of energy stored per unit mass or volume of the fuel. Engines are built to extract and convert this energy to heat and mechanical power. Properly designed and built engines extract more from the same amount of fuel.

Table 5.4 is a comparison between the heating values of C2G UBF and those of PD. The table shows a shortage of 3.7% and 4.45% in the higher heating value (HHV) and the lower heating value (LHV) of UBF respectively. Due to the higher density of the UBF, the volumetric HHV and LHV are higher than those of the PD by 3.67% and 2.9% respectively.

Table 5.4 Comparison between HHV and LHV for PD and UBF on mass and volumetric bases. Data obtained from four fuel samples.

Fuel type	HHV (MJ / kg)	LHV (MJ / kg)	ρ (kg/m ³)	HHV (MJ / L)	LHV (MJ / L)
Av. UBF	41.393	38.649	906.200	37.510	35.024
PD	43.000	40.450	841.440	36.182	34.036
$\Delta\%$	-3.737	-4.452	7.696	3.672	2.902

The relatively high mass based heating value of UBF is affiliated to the high carbon content especially C18 which represents almost 80% of the total carbon components of C2G UBF. The higher the molecular weight of the fuel, the higher it's heating value [131] concluded.

5.2.2 CHNS-O analysis

The CHNS-O analyses were taken into consideration to have a better understanding of the major elements of the C2G UBF and their differences with respect to those of PD. The outcome is quite helpful in the characterisation of the fuel for a better understanding of the combustion process and the subsequent pollution.

The ratio of carbon to hydrogen in the fuel was determined by CHNS-O analysis. Results are demonstrated in table 5.5. It is quite obvious that C2G UBF and PD have the same C/H atom ratio, nevertheless, C2G UBF contains 12.44%wt less carbon than PD. Similarly, C2G UBF contains 10.7% less hydrogen and 12% oxygen that doesn't exist in PD. There is also 0.3%wt nitrogen presence in the surrogate fuel.

Table 5.5 CHNS-O analysis for the C2G UBF and PD as a base fuel.

Fuel type	C/H	C	H	N	S	O
		% wt	% wt	% wt	% wt	% wt
C2G UBF	0.529	75.727	12.035	0.299	0	11.939
PD	0.522	86.49	13.48	0	0.0267	0

5.2.3 Determination of metals in the fuel

Determination of the inorganic elements in the fuel is another objective of the study. Combustion chamber deposits and the emissions could be qualified through these comparative analyses. A comparison between the inductively coupled plasma (ICP) analysis for the fuel and the ones obtained from the scanning electron microscope SEM EDX for the fuel injectors could provide evidence about the deposits, their quantity and components and perhaps the involvement of lube oil in the emissions. ICP analysis for the C2G UBF is presented in table 5.6. The major inorganic elements from the largest quantity are silicone, phosphorus, bromine, calcium and potassium respectively. There is a very tiny presence of zinc in the UBF. The cavitation phenomena at the

entrance of the injector hole results in fuel evaporation and the accumulation of zinc deposits in the injector hole.

Table 5.6 ICP test results for C2G UBF

Sample batch	Na	Mg	Al	Si	P	S	K	Ca	Cr	Fe	Zn	Se	Br	I
	ppm	ppm	ppm	ppm	ppm	ppm	ppm	ppm	ppm	ppm	ppm	ppm	ppm	ppm
Spring	0.000	0.904	11.806	645.231	161.395	0.000	7.341	27.723	0.934	2.858	-0.038	-0.181	112.826	8.153
	3.539	2.053	15.386	772.046	245.499	8.941	12.952	46.722	0.794	5.947	8.316	-0.195	121.617	1.962
	0.000	1.072	10.574	640.169	172.018	4.816	5.331	17.239	0.000	2.898	-0.063	0.618	108.020	5.044
Spring Av.	1.180	1.343	12.589	685.816	192.971	4.586	8.541	30.561	0.576	3.901	2.738	0.080	114.154	5.053
Summer	3.385	1.181	13.079	642.985	159.836	19.552	9.067	30.062	0.000	2.588	4.091	0.220	68.553	0.022
	5.239	1.649	23.532	544.970	186.445	0.000	9.203	62.585	0.732	1.341	6.049	0.204	80.806	1.811
	6.018	3.770	19.381	901.579	201.784	0.000	5.197	32.394	0.432	3.053	27.189	0.548	39.105	0.000
	3.635	2.324	29.215	545.059	0.000	0.000	9.434	59.094	0.000	5.629	-0.303	0.000	0.000	0.574
	0.000	5.978	5.366	435.754	95.664	0.000	32.481	16.925	0.000	-0.016	-0.087	0.242	0.000	0.067
Summer Av.	3.655	2.980	18.115	614.069	128.746	3.910	13.076	40.212	0.233	2.519	7.388	0.243	37.693	0.495
Autumn	7.671	3.310	67.924	678.859	137.775	0.000	4.672	158.312	0.795	1.622	-0.189	-0.029	17.917	0.000
	2.218	0.509	6.272	455.110	38.884	0.000	0.549	22.048	0.483	-0.020	3.592	0.095	0.000	1.094
Autumn Av.	4.944	1.909	37.098	566.984	88.329	0.000	2.611	90.180	0.639	0.801	1.701	0.033	8.959	0.547

5.2.4 Thermo-gravimetric analysis for the fuel

Thermo-gravimetric analysis for C2G UBF revealed that 98.8% of the fuel evaporated when it was heated to 600°C. The results show that 98.7% of the fuel is VOF while the elemental carbon (EC) represent only 0.09%. The first derivative of mass with respect to time shows the point of inflection in the mass-time diagram shown in fig.5.7. The inflection occurs at 424°C. These results would be compared to the data obtained from the exhaust analysis after the combustion process.

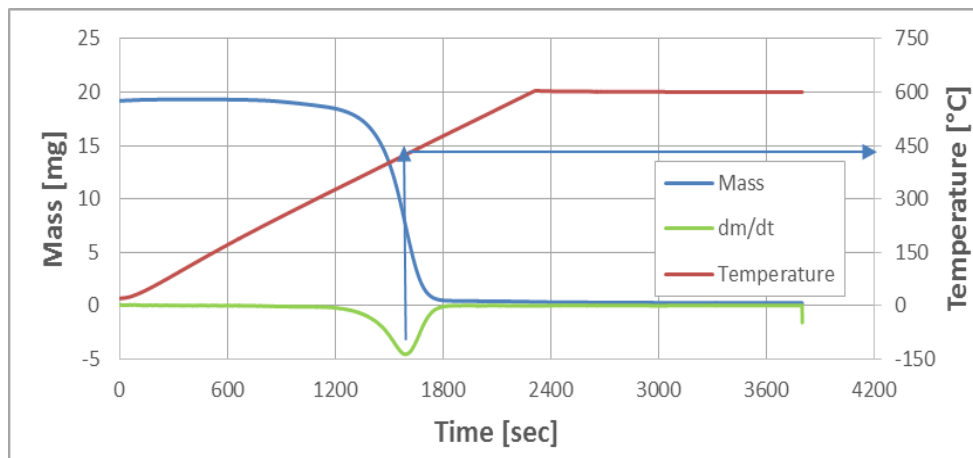


Figure 5.7 TGA analysis for C2G UBF. Data are averaged for four samples.

5.3 Fuel injection characteristics

5.3.1 Fuel jet length

The fuel jet penetration length is calculated by eq.2.7. The maximum allowable distance for the fuel jet to stretch axially from the start of injection (SOI) decreases slightly as the piston approaches its upper dwell at TDC. At the TDC the fuel jet could stretch for only 4.8 cm before collision to the piston bowl wall (see fig.3.2). Fig.5.8 illustrates the fuel jet length from the SOI at different engine speeds namely, idle speed (560 rpm), speed of maximum torque (1100 rpm) and the speed of maximum power (1900 rpm). A thorough investigation of the plots reveals that there are two rates of fuel jet growth. A high rate of jet growth at the beginnings followed by a lower rate of growth towards the end.

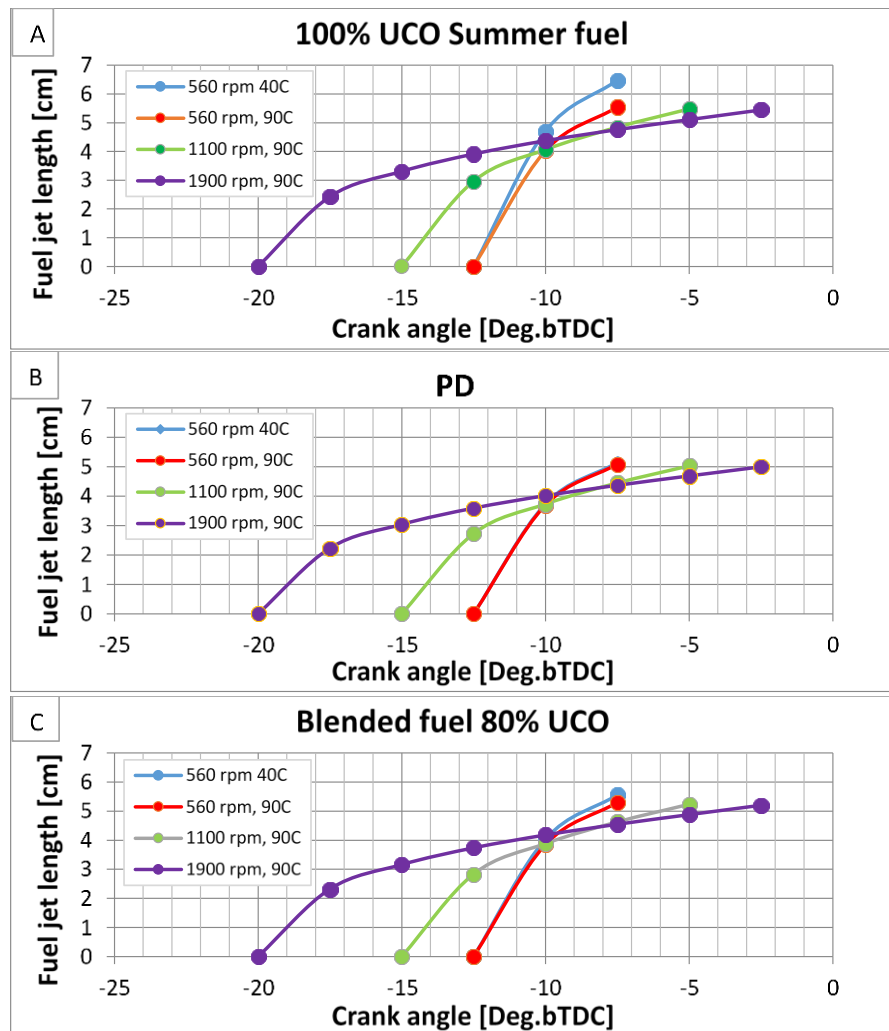


Figure 5.8 Fuel jet length as a function of crank angle. A comparison among (A) UBF and its (B) 80% blend with PD to (C) pure PD. Fuel temperature and engine speed the controlling factors.

The sluggishness in the second part could be attributed to increasing gas pressure and density [155] as the piston moves towards its upper dwell. The fuel jet also faces a counter flow of air being force from the cylinder walls towards the centre as the piston approaches the TDC. This air is squeezed between the piston crown flat rim and the cylinder head and forced to flow towards the centre. The plots also show that, in spite of the injection advancement at higher speeds, the rate of jet growth is lower. It is a logical consequence for the higher rate of change of the combustion chamber environment such as pressure and temperature at higher engine speeds. Moreover, the plots exhibit the effect of temperature decrease on the rate of fuel jet growth. Pure UBF at 40°C experiences a higher rate of growth than at 90°C particularly as the piston get closer to the TDC. This phenomena is affiliated to the prevalence of viscosity effects (larger droplets) over inertia effects (lower jet velocity) (see fig.5.9) [18]. Therefore the Bioltec system delivers minimum quantities of UBF at temperatures around 45°C and allows the engine to run on 100% UBF at fuel temperatures over 70°C.

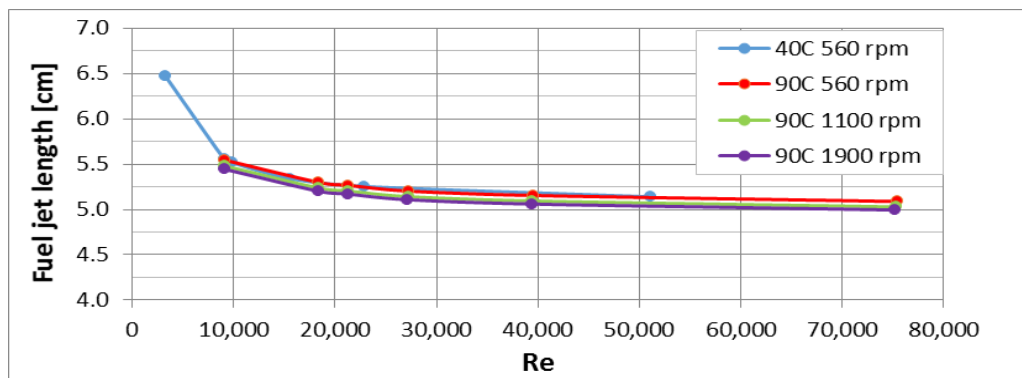


Figure 5.9 Fuel jet penetration as a function of jet Reynolds number for UBF at different engine speeds.

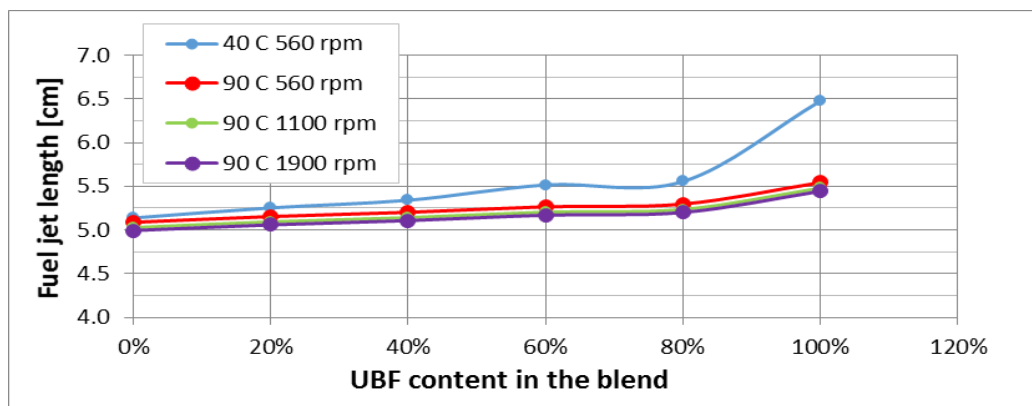


Figure 5.10 Variation of fuel jet penetration with UBF content in the blend at different engine speeds and temperatures.

The fuel jet penetration length increases as the UBF content in the blend increases as shown in fig.5.10. Higher rates of change are observed at UBF content exceeding 80% in the blends. This is entirely related to the kinematic viscosity and surface tension effects of UBF as discussed earlier in this chapter.

5.3.2 Fuel mean droplet size

The mean droplet size is calculated by Sauter mean diameter (SMD) equation demonstrated in chapter 2 eq.2.11. The mean droplet size for the droplets injected earlier are smaller than those which are injected later during the compression stroke because of the exponential increase in air/gas pressure. Ideally, making a perfect air-fuel mixture could be accomplished when both of the components are of the same phase. During the injection process, part of the fuel could be mechanically evaporated and the rest of the fuel should be thermally evaporated.

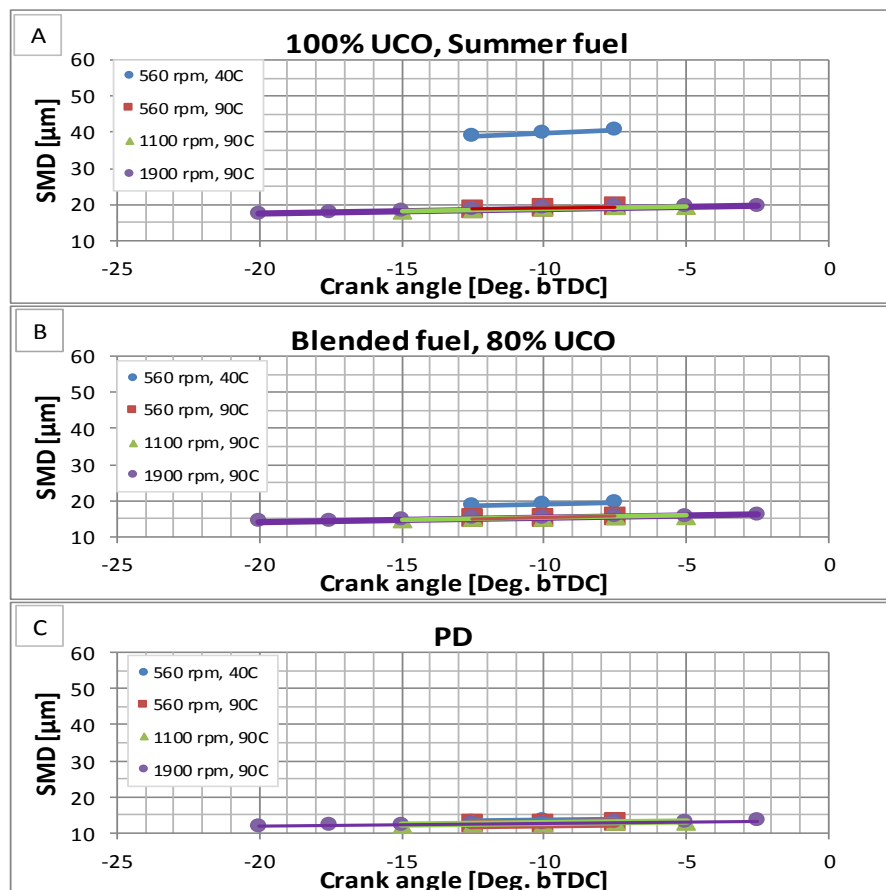


Figure 5.11 Variation of fuel SMD with injection timing and duration at different fuel temperatures and engine speeds for (A) 100% UBF, (B) 80% UBF blend with PD and (C) pure PD.

Among the residence time, boiling point of the fuel, the SMD plays a key role in the evaporation of the fuel. A larger temperature gradient from the droplet centre to its surface is expected for droplets of larger SMDs. Therefore they continue to contain the heat then evaporate suddenly. Droplets of small SMD keep undergoing cycles of surface evaporation and cooling, as their temperature decreases due to the evaporation process, until they vanish [133].

Fig.5.11 shows the slight increase in mean droplet size throughout the injection process which is an inevitable result of the continuous decrease in the pressure difference (ΔP) between the injection pressure and the combustion chamber pressure.

The pressure in the cylinder continues to increase as the piston get closer to the TDC which will adversely affect the atomisation process and larger fuel droplets are found in the spray. Larger fuel mean droplet sizes are recognised as the UBF content in the blend increases particularly at lower temperatures. At 90°C the pure UBF SMD is 48% larger than that of PD, this difference increases to 213% at 40°C.

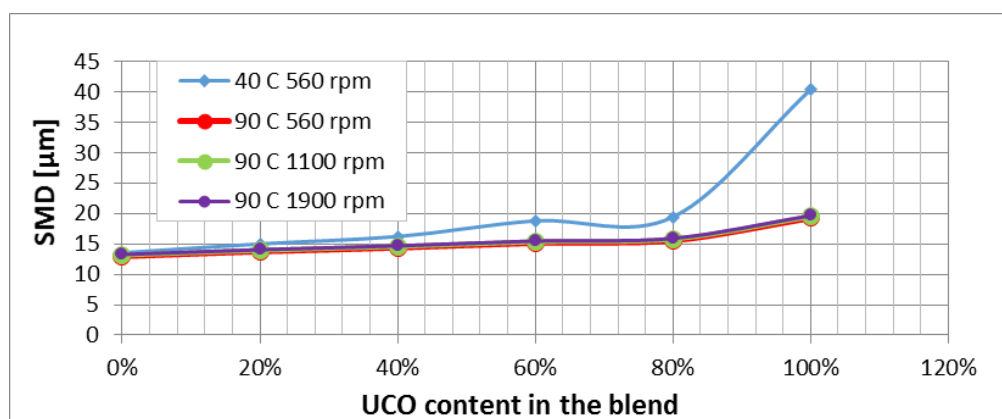


Figure 5.12 Fuel SMD as a function of UBF content in the blend at various fuel temperatures and engine speed.

Fig.5.12 exhibits larger fuel droplets observation as the UBF content in the blend increases at a given engine speed especially at lower temperatures. This is definitely attributed to the higher surface tension of UBF which is 44% higher than that of PD at the same temperature as discussed previously in the chapter.

The SMD for pure UBF at 90°C is nearly half the SMD for the same fuel at 40°C. This is also related to the surface tension property of the fuel which is inversely proportional to temperature.

The above analysis shows that UBF droplets are larger than those of PD under all circumstances. This will make the droplets to absorb more heat for longer periods of time then they evaporate suddenly to form a leaner mixture packet with air. This is perhaps the cause of the longer physical ID period. Once the mixture in the leaner packet suddenly burns the rate of heat release will be very high to reach high temperature peaks during the diffusion flames. This could arguably be one of the reasons behind the high NO_x emissions from BL fuel combustion.

5.3.3 Fuel Spray Cone Angle

The spray cone angle is calculated by eq.2.12. Figure 5.13 depicts the variations of fuel jet cone angle from the start of injection (SOI) to the end of injection (EOI) at different engine speeds and for different fuels. All the graphs follow the same trend in which the cone angle increases throughout the injection process. This could be affiliated to the lower fuel flowrate at the SOI (effect of injector needle), followed by the growing shear and drag of the combustion chamber environment as the injection process extends to the start of combustion (SOC). Moreover, the fuel spray faces an air stream moving towards the centre of the combustion chamber as the gap between the piston crown rim and cylinder head decreases, which applies a dynamic pressure on the fuel spray. Fuel flow through the injector holes (0.2 mm dia.) at a very high injection pressure (180 MPa) could result in fuel cavitation (a flow induced boiling) which atomises and evaporates part of the fuel while it is still in the nozzles. The sudden enlargement in the fuel jet as it emerges from the nozzle holes into a relatively low pressure environment will further enhance the atomisation and evaporation of the fuel. However, there might be a part of the fuel issuing in a cylindrical configuration.

The shear slows down the fuel jet and peels off the fuel from the cylindrical jet, while the drag opposes the flow leading to a lower velocity and a larger cross-section for a given flowrate. This will break down the fuel configuration from the cylindrical shape to small droplets. On the other hand a better air entrainment and mixing with fuel is expected.

A thorough investigation of fig.5.13 A shows that increasing the UBF temperature from 40°C to 90°C increases the spray cone angle by 33%. Fig.5.13 C shows only a 2% increase in PD spray cone angle for the same temperature increase. A comparison between fig.5.13 A and C, shows that the spray cone angle at 90°C is smaller in the case of UBF by nearly 15% due

to its higher density, viscosity and surface tension, and hence a longer jet length and larger SMD.

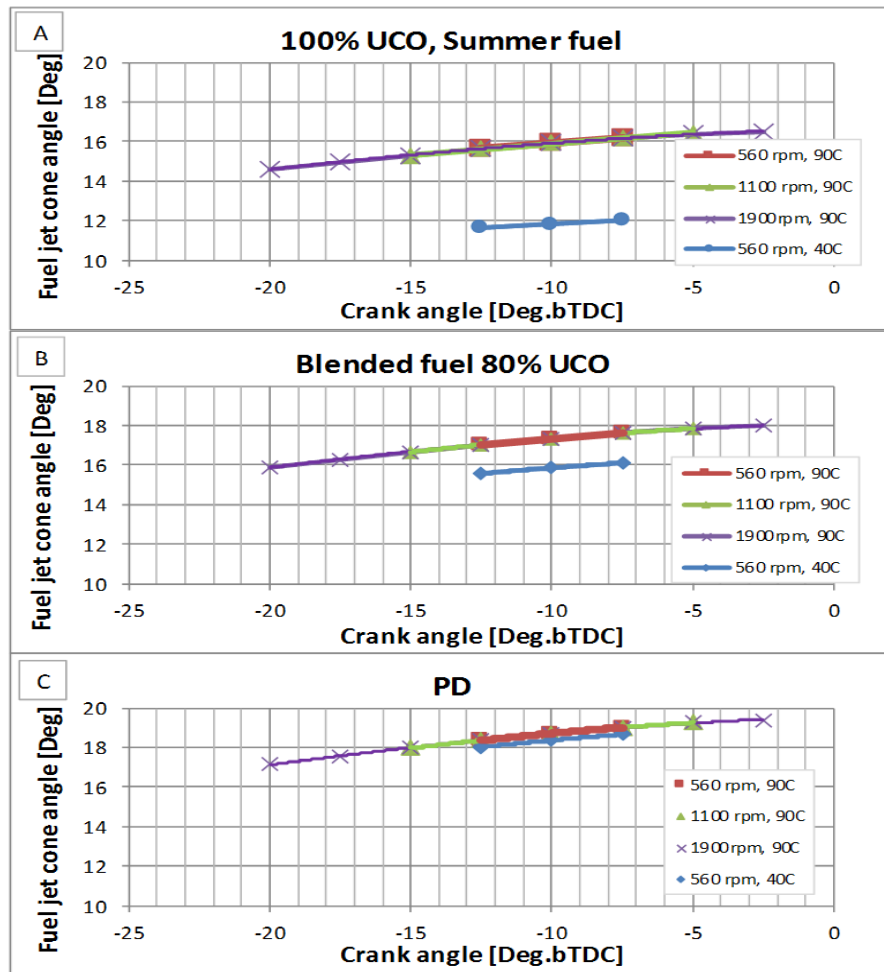


Figure 5.13 Fuel spray cone angle variation with crank angle at different engine speeds, fuel temperature and mixing ratios for UBF and PD. (A) 100% UBF, (B) 80% UBF blend with PD and (C) pure PD.

Fig.5.13 B shows that half of the reduction in spray cone angle occurs as UBF content in the blend exceeds 80%. This conclusion is more apparent in fig.5.14. Apparently the fuel spray cone angle is inversely proportional with the UBF content in the blend. The lower the fuel temperature the steeper the correlation is.

Reducing the viscosity effects could be achieved by increasing the fuel speed through the nozzle holes. Fig.5.15 shows how higher Reynolds numbers increase the spray cone angle. This can only be achieved by higher injection pressures, smaller nozzle holes or low viscosity fuels. In the current research,

the injection process will be affected by the presence of UBF in the fuel blend especially when the HGV is travelling at high steady speed on the M1 motorways.

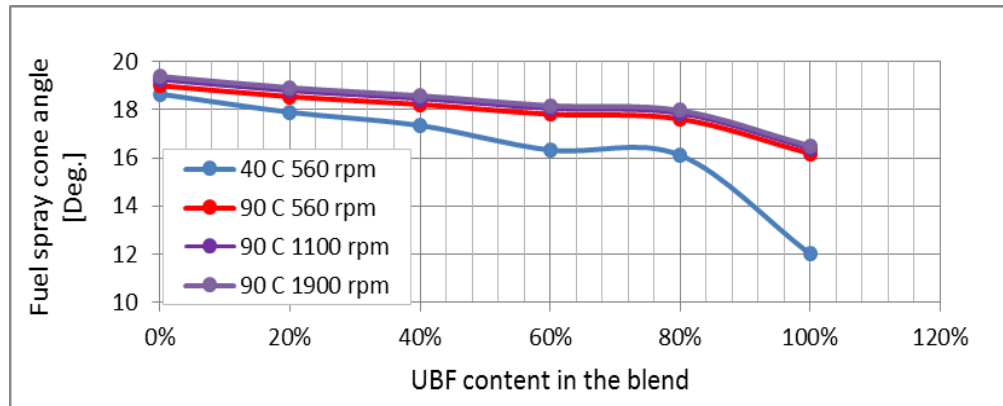


Figure 5.14 fuel spray cone angle variation with UBF content in the blend at various temperatures and engine speeds.

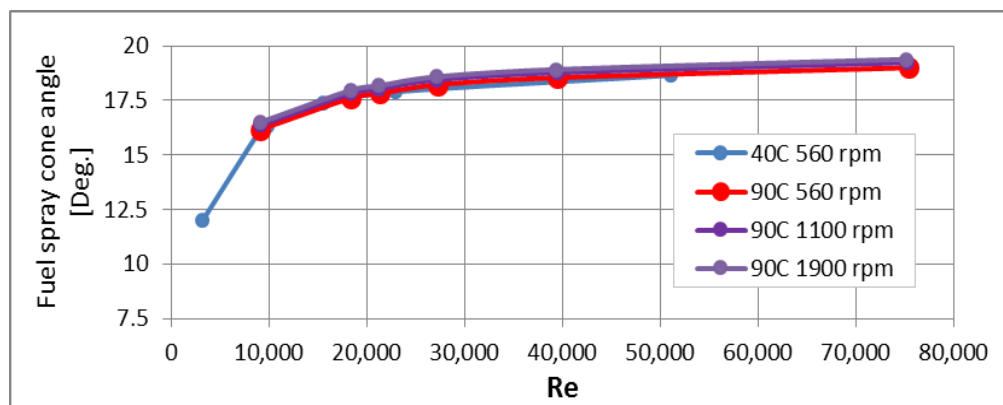


Figure 5.15 variation of fuel spray cone angle with Reynolds number for various fuel temperatures and engine speeds.

5.3.4 Fuel jet velocity

The fuel jet velocity across the nozzle holes is affected by the injection timing. Advanced injection timing allows for a higher jet velocity. In a particular injection, the amount of fuel being injected at the SOI is faster than the amount being injected at the EOI. This could happen not only because of the nozzle closure, it is actually affected by the growing pressure in the combustion chamber followed by the aforementioned consequences and as demonstrated in fig.5.16 and air counter flow against the fuel spray.

In figure 5.16 the rate of fuel jet speed reduction is 1.6% for PD and UBF, However UBF exhibits a 4.1% lower speed along the injection process. The

fuel jet speed is also affected by the fuel temperature. Increasing the fuel temperature from 40°C to 90°C increases the fuel jet speed by 1.65% due to the reduction in fuel viscosity and friction effects. Putting the fuel spray under scrutiny, reveal that droplets have different sizes and speeds. Therefore a droplet size distribution could be expected from the velocity differences. Droplets travelling at higher speeds might be peeled off and collapse and they lose momentum and slow down. Slower droplets could remain large and overtake the small ones, the higher the combustion chamber gas density the more obvious the phenomena would be [133].

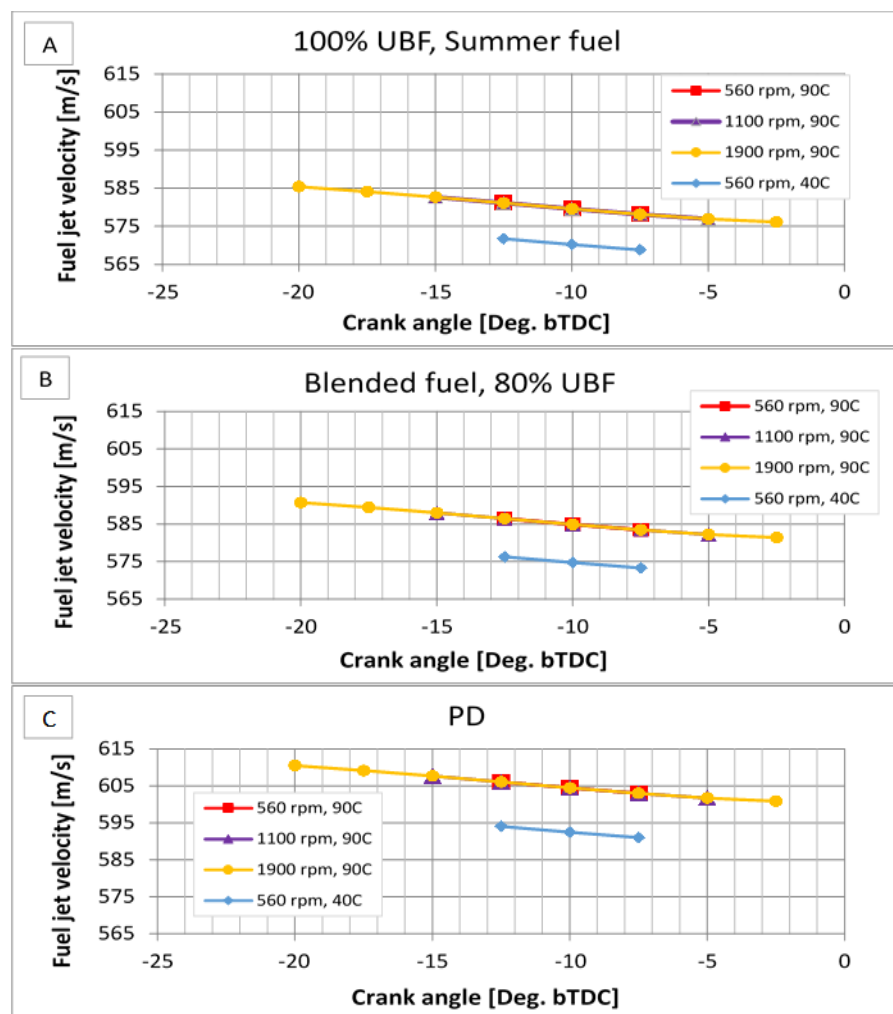


Figure 5.16 variation of fuel jet velocity with crank angle for different fuel temperatures and at different engine speeds. (A) 100% UBF, (B) 80% UBF blend with PD and (C) pure PD.

5.4 Effect of the fuel properties on combustion chamber deposits

5.4.1 Visual comparison between fuel injectors operated on PD and UBF

Images from the scanning electron microscope (SEM) are presented in fig.5.17. It is quite obvious that deposit accumulation on the holes is uneven. Most of the deposit accumulation and build-up is on the outer surface and shoulder of the injector. It seems that once the deposits started to form around the injector holes, they are built-up to a certain thicknesses and then cracked down and removed by mechanical and thermal stimuli. Although most of the deposit build-up is around the nozzle holes, the build-up process could move backwards inside the holes as shown in fig.5.17D. It is also seen that the deposits on the injector operated on PD are thicker and grow faster.

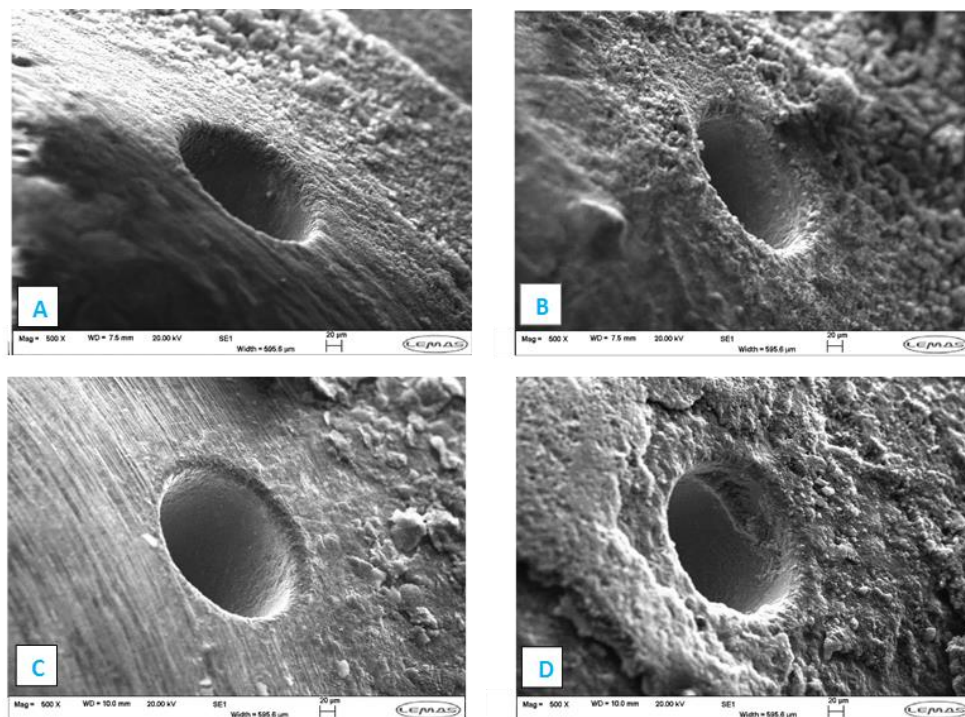


Figure 5.17 SEM electron images for fuel injectors being operated on different fuels.

- A. Injector No.2 from vehicle FN58 NSK operated on UBF for 371,460 km. The cleanest hole
- B. Injector No.2 from vehicle FN58 NSK operated on UBF for 371,460 km. The worst hole
- C. Injector No.6 from vehicle FN11 SVC operated on PD for 360,000 km. The cleanest hole.
- D. Injector No.6 from vehicle FN11 SVC operated on PD for 360,000 km. The worst hole

It could arguably attributed to the carbonaceous nature of the deposits as PD carbon content is 12.5% higher than UBF as shown earlier in this chapter.

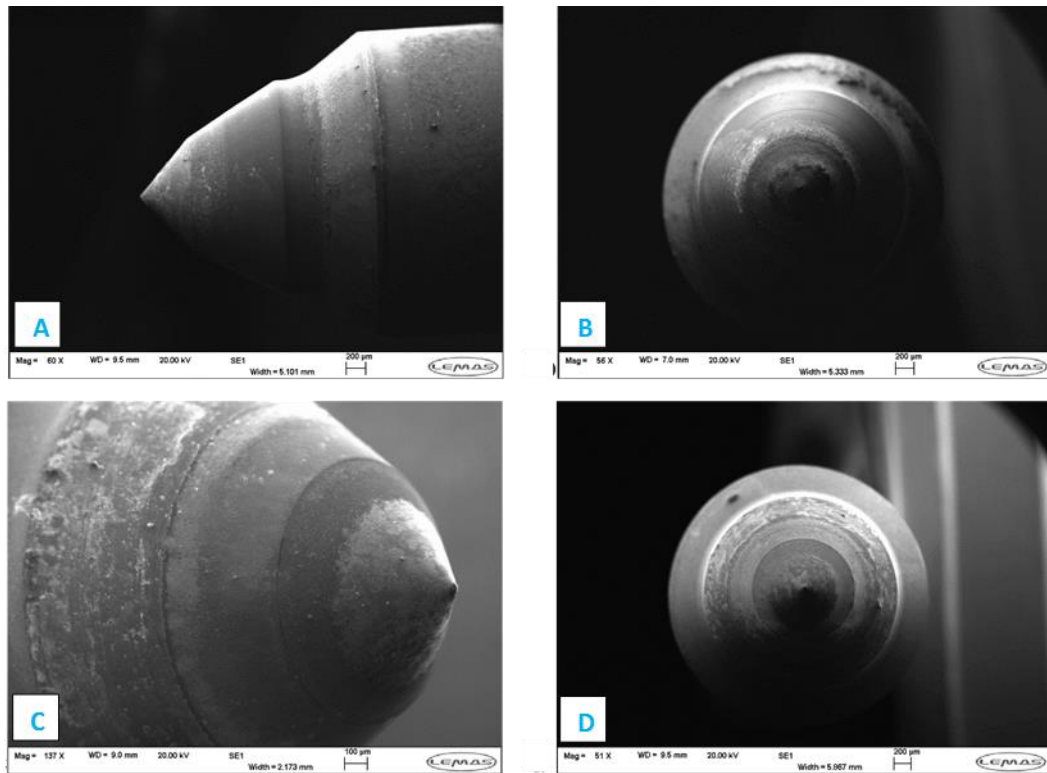


Figure 5.18 SEM images for the needles of the fuel injectors operated on different fuel.

- A. Needle for injector No.2 taken from vehicle FN58 NSK operated on UBF for 371,460 km (Side view).
- B. Needle for injector No.2 taken from vehicle FN58 NSK operated on UBF for 371,460 km (Front view).
- C. Needle for injector No.6 taken from vehicle FN11 SVC operated on PD for 360,000 km (Side view).
- D. Needle for injector No.6 taken from vehicle FN11 SVC operated on PD for 360,000 km (Front view).

Deposit accumulation on the injector needle, shown in fig.5.18, usually appears on the conical surfaces from the needle tip to its cylindrical surface except the middle part which is rubbed-out as the needle rests on its seat. These deposits are most likely formed from the combustion flames back-flow into the nozzle sacs. Although the higher surface tension of the UBF leads to more injector surface wetting, which is expected to burn and form more deposits, no clear evidence of any difference between the deposits of the two fuels was discernible.

5.4.2 Visual comparison for the effect of engine operation duration on deposit accumulation from different fuels

A visual comparison between two injectors installed on the same engine, operated by UBF but for different periods of time is shown in fig.5.19. The purpose is to investigate the aging effects on the deposit accumulation. Images (A and B) in fig.5.18 belong to the injector which was taken out after running on the engine for 61,200 km, while the latter two images were for the injector operated for twice that distance.

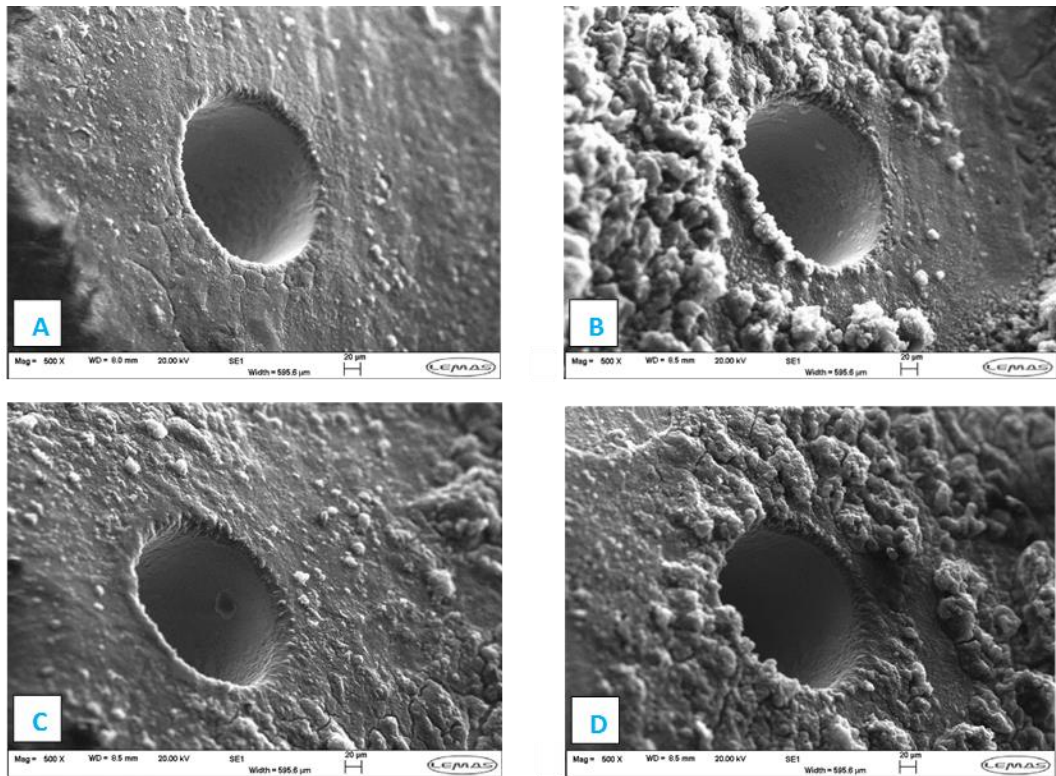


Figure 5.19 SEM images for injector holes operated on UBF on the same engine for different durations.

- A. Injector No.1 from vehicle FN11 SVC operated on UBF for 61,200 km. The cleanest hole
- B. Injector No.1 from vehicle FN11 SVC operated on UBF for 61,200 km. The worst hole
- C. Injector No.6 from vehicle FN11 SVC operated on UBF for 122,041 km. The cleanest hole.
- D. Injector No.6 from vehicle FN11 SVC operated on UBF for 122,041 km. The worst hole

The major difference between the two cases presented in fig.5.19 is the deformation in the circular geometry of the injector holes due to the uneven deposit accumulation with injector aging. Actually this deformation might affect

the symmetry of the fuel cone issuing from the injector. The second concern is the type of deposit formation.

The ones that take the cluster shape are more susceptible to burning and removal due to the heat accumulation in their protruding tips. Perhaps the layer type formation is more detrimental and difficult to remove. Apparently a thicker layer could be observed around and inside the older injectors in fig. 5.19 C & D. Fig.5.20 A & B is an example of a huge cluster type accumulation. The observer could easily see the large groove between the injector shoulder and the deposit cluster getting ready for separation.

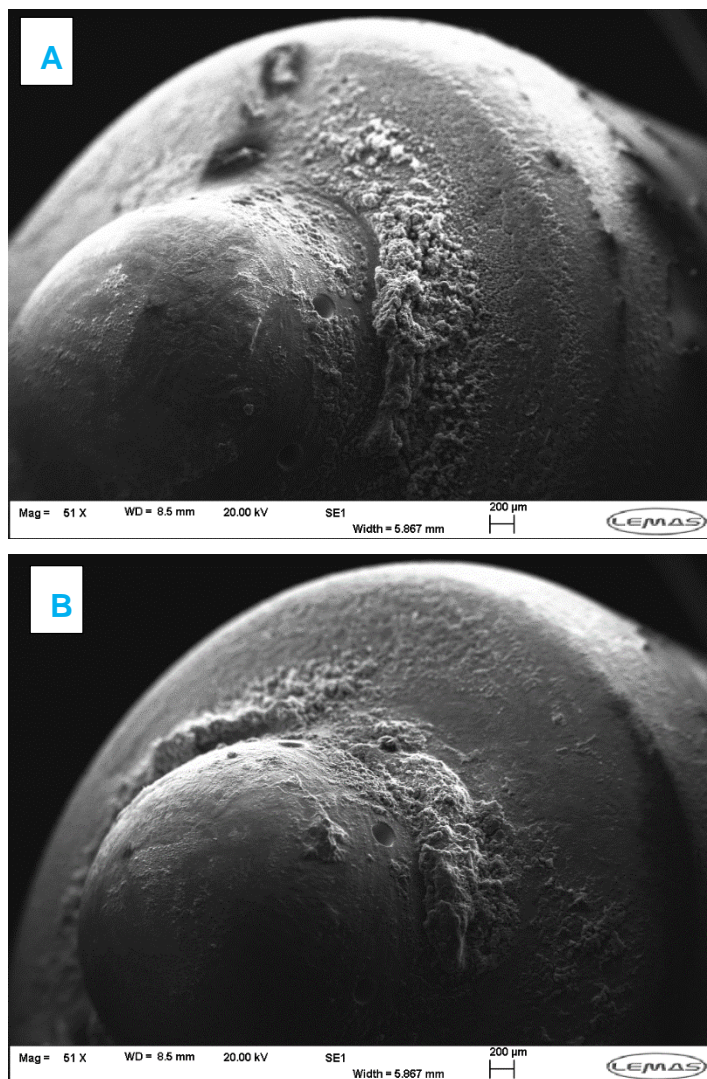


Figure 5.20 A & B SEM images for a fuel injector shoulder

5.4.3 Visual comparison for the combustion chamber deposits in two identical engines

Injectors collected from two identical engines operated on UBF for the same period of time was also investigated. The idea is to detect the drivability effects on the deposit formation. The two injectors showed nearly the same layer type deposit thickness with the exception of fig.5.21B in which a cluster accumulation on one side of this particular hole could be seen.

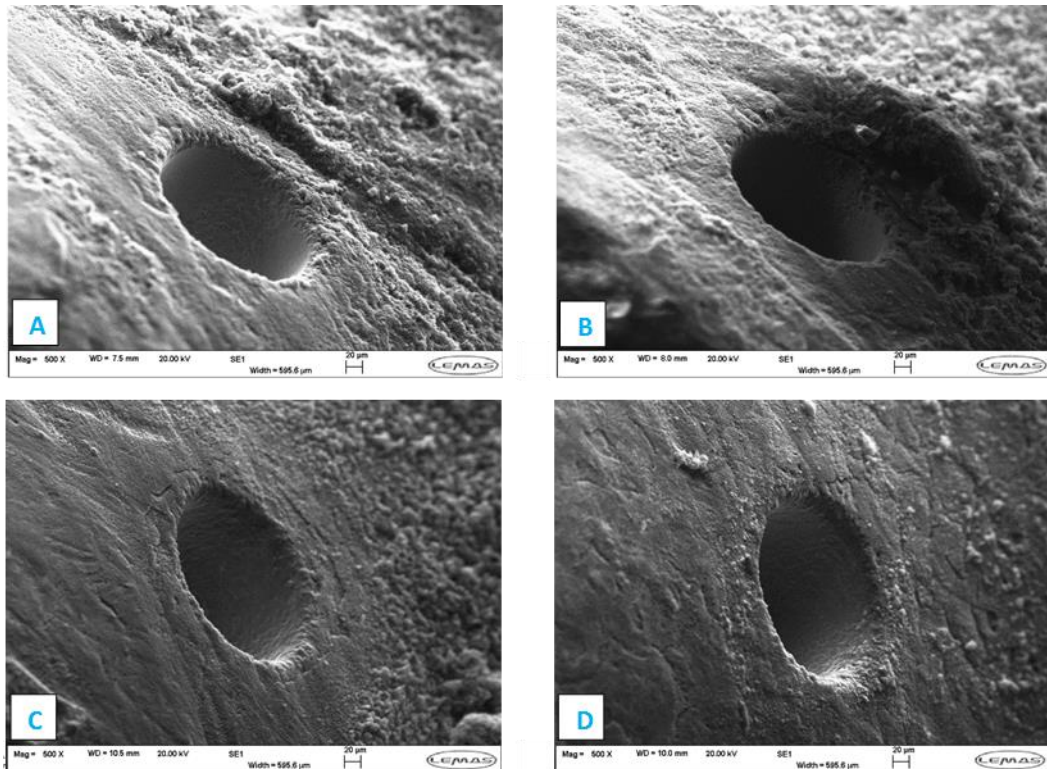


Figure 5.21 SEM images for two injectors operated on UBF, running for nearly the same distance on two identical engines

- A. Injector No.6 from vehicle FN58 NSK operated on UBF for 71,460 km. The cleanest hole
- B. Injector No.6 from vehicle FN58 NSK operated on UBF for 71,460 km. The worst hole
- C. Injector No.1 from vehicle FN11 SVC operated on UBF for 60,841 km. The cleanest hole.
- D. Injector No.1 from vehicle FN11 SVC operated on UBF for 60,841 km. The worst hole

5.4.4 Chemical analysis by energy dispersive x-ray (EDX)

Elemental analysis for arbitrarily chosen deposit areas were performed on the fuel injectors. Fig.5.22 is an example for the comparison between two fuel injectors operated on two different fuels. Fig.5.22A shows the EDX analysis

for the injector operated on the BL fuel, while fig.5.22B exhibits the same analysis for the injector operated on PD.

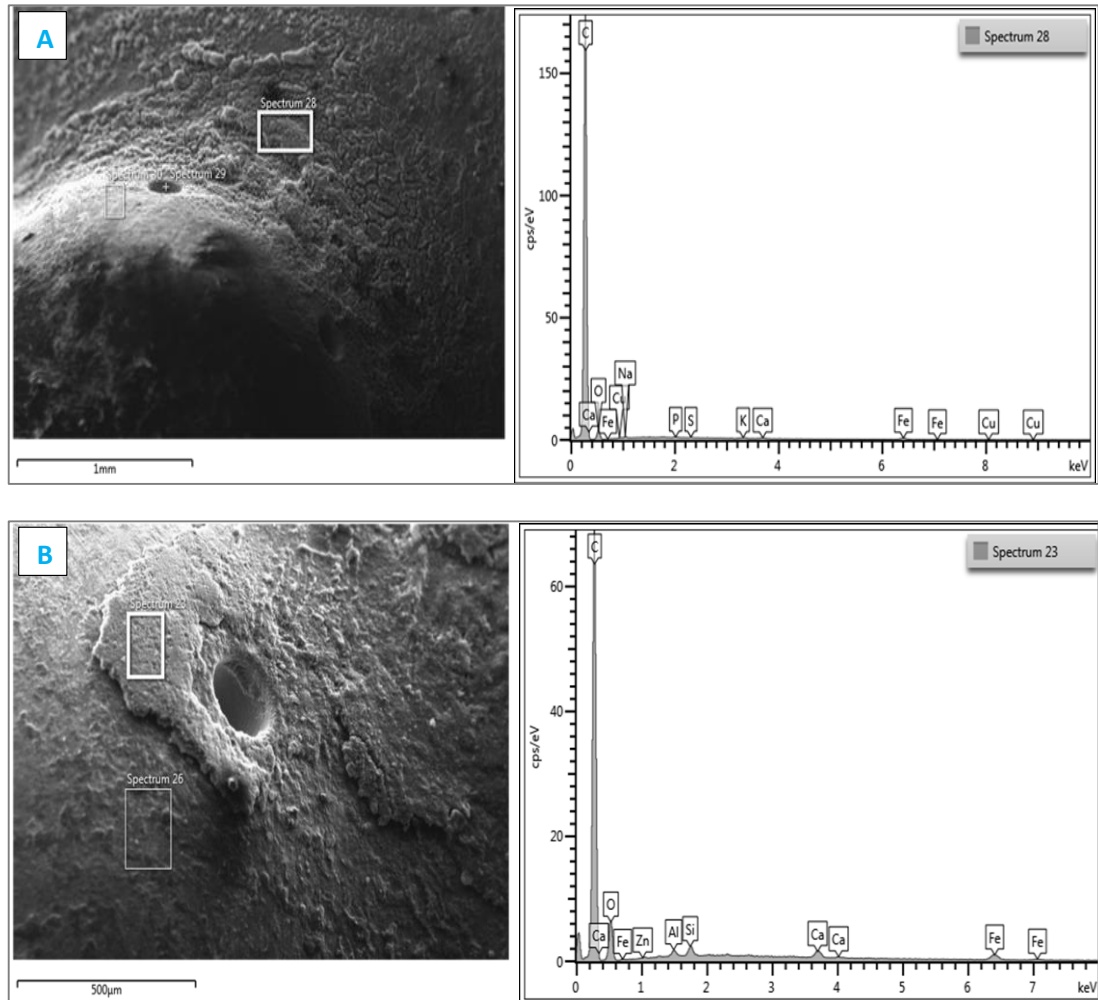


Figure 5.22 EDX analysis for the deposits on the injector shoulder.

- A. Injector No.2 from vehicle FN58 NSK operated on UBF for 371,460 km.
- B. Injector No.6 from vehicle FN11 SVC operated on PD for 360,000 km.

The results show that the predominant component is carbon. Although carbon content in UBF fuel is about 12.4% lower than that of PD, the EDX analysis showed higher carbon in the BL fuel deposit. In fact carbon presence in the deposits from the BL fuel combustion in this particular position is more than twice that of the PD. Other common elements found at considerable amounts are oxygen and calcium, however their amounts are doubled in the case of the BL fuel deposits. UBF deposits are unique by the presence of sodium, phosphorous and traces of potassium while no traces of zinc is observed.

There is a good agreement between EDX results and those obtained from the ICP test for UBF in terms of same major components found in the fuel and the deposits, however, no correlation between their quantities is perceptible.

5.5 Conclusions

The main purpose of this chapter is to find the suitability of C2G UBF as a surrogate for PD in terms of its bilateral effects on the injection process and the deposits in the combustion chamber. In this context, UBF has actually proven to be a surrogate to PD in HGV for the following reasons:

1. At room conditions, the physical properties of C2G UBF are very much different from the European standard properties of PD. However, the very high sensitivity of UBF to temperature reduces the differences to acceptable limits for engine operation.
2. The combustion chamber deposits were found to be similar or even less than those produced from the PD combustion.
3. The mass based heating value of UBF is lower than that of PD, however the volumetric heating value is higher due to its higher density.
4. Fuel analysis revealed that optimum operational results could be expected from fuel blends at temperatures higher than 60°C and blending ratio less than 80% UBF.
5. PD combustion extends longer throughout the expansion stroke.
6. More exhaust gas residual in the cylinder is expected from UBF.
7. The fuel jet penetration length increases as the UBF content in the blend increases. The rate of fuel jet growth is directly proportional to the UBF content in the BL fuel. However, higher rates of change are observed at UBF content exceeding 80% in the blends.
8. In spite of the injection advancement at higher speeds, the rate of jet growth is lower.
9. The mean droplet size for the droplets injected earlier are smaller than those which are injected later during the compression stroke because of the exponential increase in air/gas pressure.
10. At 90°C the pure UBF SMD is 48% larger than that of PD.
11. Increasing the pure UBF temperature from 40°C to 90°C reduces the SMD by 50%.
12. The larger UBF droplets than those of PD could resist more in the combustion chamber and absorb more heat until they evaporate

suddenly. This results in leaner mixture packets that burn with a very high rate of heat release.

13. The cone angle increases throughout the injection process.
14. Increasing the temperature from 40°C to 90°C increases the spray cone angle by 25% and 2% for pure UBF and PD respectively.
15. The spray cone angle at 90°C is smaller in the case of UBF by nearly 15% compared to PD, half of the reduction in spray cone angle occurs as UBF content in the blend exceeds 80%.
16. Reducing the viscosity effects could be achieved by increasing fuel speed through the nozzle holes. Higher Reynolds numbers increase the spray cone angle. This can only be achieved by higher injection pressures, smaller nozzle holes or low viscosity fuels.
17. UBF exhibits a 4.1% lower speed along the injection process. Increasing the fuel temperature from 40°C to 90°C increases the fuel jet speed by 1.65%.

Using UBF and its blends with the PD showed considerable variations in the fuel jet characteristics especially at high UBF content blends and at low temperatures. The variations in fuel jet characteristics for this particular engine under the specified operational conditions are demonstrated in table 5.7. The table indicates the change of fuel jet characteristics in percentage for each 10% increase in UBF content in the blend delivered to the engine at 40°C and 90°C respectively for a fully extended jet to its maximum allowable length.

Table 5.7 Variation of fuel jet characteristics per 10% increase in UBF content in the BL fuel

Temperature [°C]	UBF content [%]	SMD [%]	Fuel jet cone angle [%]	Fuel jet length [%]
40	0-80	5.42	-1.70	1.01
	80-100	77.35	-11.00	8.96
90	0-80	2.50	-0.91	0.52
	80-100	14.15	-3.80	2.42

The data shows that the variation of the fuel jet characteristics with UBF content could be classified into two ranges. The first one is the percent change

in spray characteristics for UBF content variation in the blend from 0-80%, which follows a nearly constant rate of change of jet characteristics, and the change in jet characteristics at 40°C is about twice those at 90°C.

The second range is the variation of UBF content in the blend from 80% to 100% (pure UBF) which shows a great difference in jet characteristics. Comparing the fuel jet characteristics for this range at 90°C with 0-80% shows that: the rate of increase of SMD is 5.5 times higher, the rate of cone angle decrease is about 4 times lower and the rate of jet length increase is 4.7 times higher. Performing the same comparison at 40°C gives the SMD increase, α decrease and S increase in the following sequence: 14.25, 6.45 and 8.84 times respectively.

It could be concluded that engine speed has a negligible effect on the SMD and jet velocity, while the fuel temperature plays a key role in spray characteristics. Therefore it is more convenient to operate the engine on blends with UBF content up to 80% to avoid higher fuel consumption and higher pollution load on the exhaust after treatment system compared to using 100% UBF. Although the higher fuel viscosity deteriorates the combustion process and engine output, the higher fuel density could compensate for the lower heating value of UBF and to lower the expected increase in fuel consumption to obtain the same power output.

Chapter 6

Quantitative and qualitative comparison for HGV PM emissions produced from C2G UBF and its blends with PD to PD obtained under real world driving conditions

The trade-off between particulate matter (PM) and nitrogen oxides (NO_x) is the chronic conundrum of diesel combustion [16, 178]. Therefore, it is the engine manufacturers choice which one to suppress within the combustion chamber and to mitigate the other by an efficient aftertreatment facility (see chapter 2). The heavy goods vehicle (HGV) under investigation is designed to fight PM throughout the combustion process. Using a sophisticated high pressure fuel injection system to deliver the fuel at pressures up to 180 MPa from seven 0.2 mm diameter nozzle-orifices is one of the efficient facilities. It delivers the fuel as tiny spherules with a smaller mean diameter than the low pressure ones. Combustion chamber configuration to allow direct fuel injection from a centrally positioned fuel injector is another feature. Fuel spray is directed to the centre of the inverted mushroom-shaped combustion chamber carved in the piston crown. This insures a better fuel mixing with air and minimizes fuel reaching cylinder walls and piston ring crevices. Fuel spherules trajectories are directed to slide on the inverted mushroom-shaped piston crown rather than impingement. The fate of the spherules is either evaporation due to the high piston surface temperature or re-entrainment to the main air stream. Swirls and tumbles of the charged air due the turbocharging efficiency and properly designed inlet and outlet ports have their own effect to approach the premixed charge compression ignition (PCCI) concept. In fact all the above features were based on the petroleum diesel PD properties. Now, the question is, will it work with the Convert to Green Ultra Biofuel (C2G UBF)?

UBF C2G is a purified used cooking oil used as fuel in a HGV in this research. The HGV is fitted with a dual fuel tank and fuel heating and mixing facilities. The fuel mixer is called the bioltec system (described in chapter 3) which produces petroleum diesel (PD) and UBF mixtures according the UBF temperature and the preloaded engine performance maps.

The two fuels, petroleum diesel (PD) and the blended (BL) fuel, were examined in a HGV under real world driving conditions. PM measurements were accomplished, as stated in chapter three, with filter preparation before the on-board PM sampling process. Two PM sampling systems were installed on-board to collect PM emissions simultaneously. Samples for cumulative PM_{2.5}

mass and PM₁₀ size distribution were collected and preserved for laboratory analysis. In-vitro analysis consisted of gravimetric and thermo-gravimetric analysis (TGA). The results were adjusted to [g/kWh] units for comparison purposes between the two fuels and with EURO 5 emission standards. Therefore PM sampling and analyses covered the mass, component speciation and size distribution of PM emitted from the combustion of each one of the test fuels under real world driving conditions.

The laboratory work also included the precombustion fuel analysis. Fuel TGA, gas chromatography-flame ionisation detection (GC-FID) and inductively coupled plasma (ICP) were performed to assist answering the aforementioned question. Added to that the conclusions obtained from Chapters 4 and 5 about the effect of the BL fuel on the combustion process and HGV performance and the fuel injection properties are quite helpful to provide reasonable answers.

As a matter of fact, the main objective of the chapter is to detect any differences in PM emissions between PD and the BL fuel under real world tests. However, it is quite important to mention that, a scan for the fuel consumption and the contribution of C2G UBF in the average fuel consumption of the trips varies from 76% to 93%. The lower limit came from the cold start journeys where the UBF was deliberately not delivered to the combustion chamber as explained in chapter four. Therefore the abbreviation BL fuel means 84.5% UBF contribution, on average, in the journey fuel consumption.

6.1 Quantitative analysis for PM collected cumulatively by filtration

A visual inspection for the PM loaded filters give an impression of the nature of the material collected on the filters. It is quite obvious that the upper two filters in fig.6.1 were more likely collecting PM dominated by soot (EC). In fact these two filters were collecting PM from the exhaust of a heavy goods vehicle (HGV) which was operated on petroleum diesel (PD). The major difference between these two filters is found in the weight of PM collected. Obviously the loaded vehicle (top right) collected more and its emission factor is higher. The lower filters were collecting PM from the exhaust of a vehicle being operated on the blended fuel (BL). The filters were coated by a grey-light brown colour, which could be an indication of a lower soot content in the PM. In the same

manner, gravitational analysis showed that loaded HGV (bottom right) collected more PM than the empty one. The amount of PM collected from the vehicles operated on PD is higher than those obtained from the vehicles operated on BL fuel.

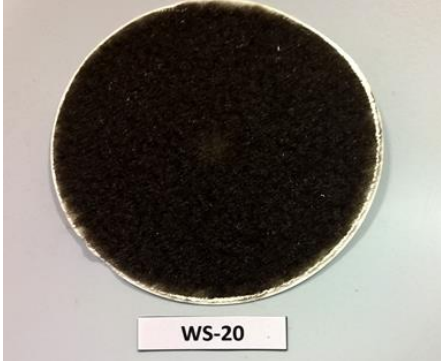

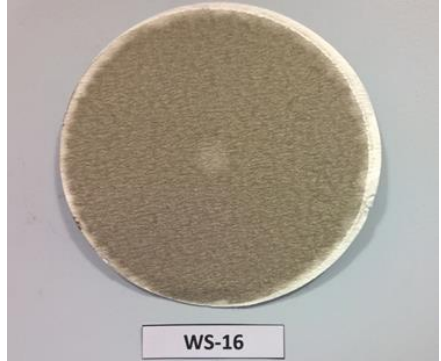
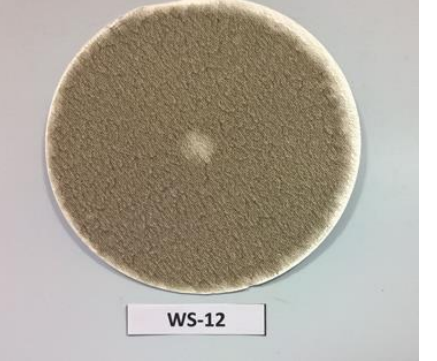
	
Filter No. 20-PD-ET-W2A Fuel: PD Load: 15.5 tonnes PM mass: 0.8018 mg PM EF: 0.00656 g/kWh	Filter No. 8-PD-LT-W2A Fuel: PD Load: 28.82 tonnes PM mass: 0.9837 mg PM EF: 0.0082 g/kWh
	
Filter No. 16-BL-ET-W2A Fuel: BL Load: 15.5 tonnes PM mass: 0.3454 mg PM EF: 0.0024 g/kWh	Filter No. 12-BL-LT-W2A Fuel: BL Load: 28.82 tonnes PM mass: 0.4296 mg PM EF: 0.001623 g/kWh

Figure 6.1 Visual inspection of GF/F filters showing PM collected from HGV exhaust in real world driving under different loads. The upper two were taken from HGV operated on PD while the lower two from HGV operated on BL fuel.

PM data obtained from the gravitational analysis for the GF/F filters were subjected to further processing by combining PM concentration data to the HGV performance parameters and dynamics. The idea is to obtain PM

emissions in units of g/kWh which makes the results more comparable at different operational conditions and with the EURO 5 emission standards.

Fig.6.2 is a comparison between PM emission factor (EF) data obtained from HGV fuelled with the BL fuel and PD respectively. Each column in fig.6.2 is a comparison between PM EF from the vehicle operated by the BL fuel or PD. Comparing columns one and two shows the variation in PM emissions with HGV payload on the same road direction when the vehicle is mostly moving down-hill from Ashby De La Zouch towards Wigston (A2W). The same analysis is true for columns three and four where the only difference is the vehicle is mostly moving up-hill in the inbound journey (W2A). In order to investigate the road load effect, a comparison between columns one and three also between columns two and four is inevitable.

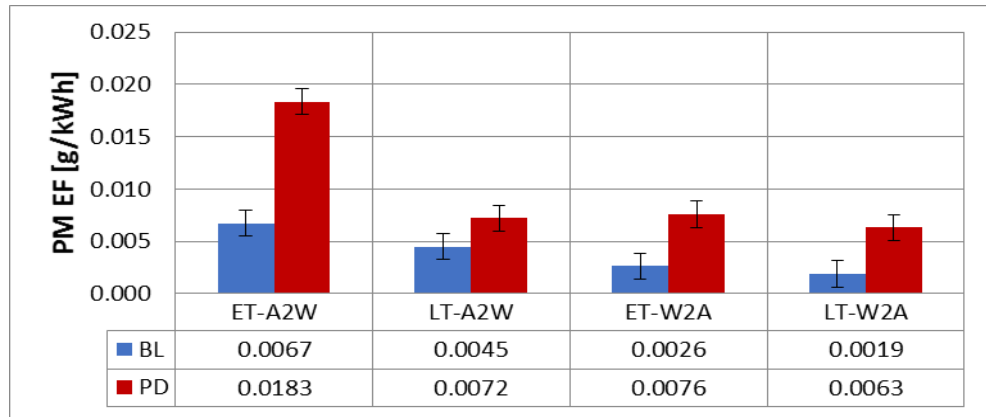


Figure 6.2 PM emission factor for the combustion of BL fuel and PD under different operational conditions. ET and LT are empty trailer and loaded trailer respectively. A2W and W2A are the HGV direction from Ashby to Wigston and Wigston to Ashby respectively. The data are the average of 20 trips for the BL fuel, 5 per trip category, and 14 trips for PD, 2~5 trips per category. SE ± 0.001253 .

It is obvious that PM emissions from the HGV fuelled with BL is far below EURO-V emissions standard (0.02 g/kWh). PM reduction due to renewable fuel usage may vary between (37-70%) depending on the type and amount of load. The bar chart shows that PM emissions are inversely proportional to the power demand. Road-load seems to be more effective on PM reduction than the pay-load. A comparison between columns 2 and 3 is a good evidence since the loaded vehicle moving from A2W is moving downhill especially for the 12.3 km road segment on M1 where the elevation drops for 110m. This means that the vehicle is gaining kinetic energy from the change in height

potentials. A higher power demand is required as the vehicle is moving in the opposite direction from W2A.

Fig.6.3 illustrates PM emission factor variation against vehicle specific power (VSP), which is the amount of power required to overcome all the road resistances per tonne of the vehicle load (explained in chapter 2 & 3). Although the two fuels exhibit the same trend, in which PM EF is inversely proportional to VSP, the PM emissions from the BL fuel are less than half their counterparts from PD. The graph also shows an excellent correlation between BL fuel PM emissions with VSP. In fact VSP is implicitly affected by the HGV pay load through its effects on vehicle speed, acceleration, air resistance and road gradient which are considered as road loads.

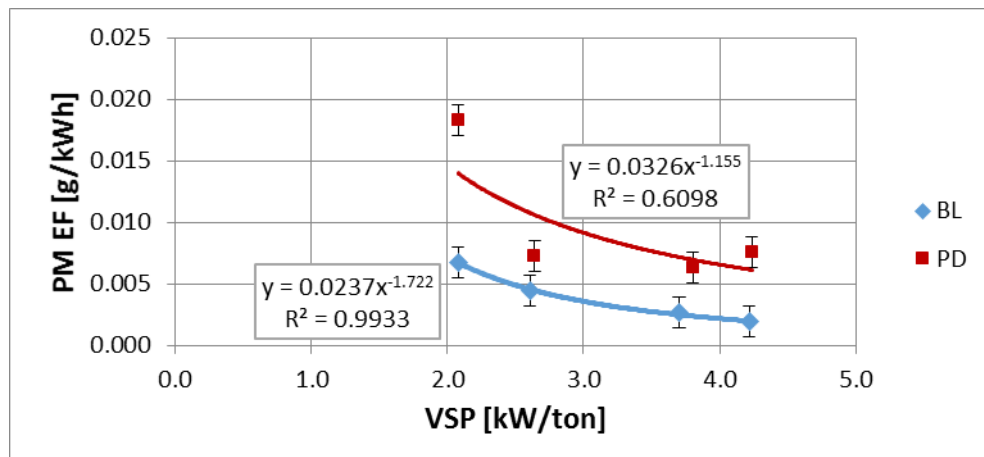


Figure 6.3 Vehicle PM EF versus VSP. A comparison between PM emissions from PD and BL fuel at different HGV performance conditions. The data are averages for 14 and 20 trips for the PD and BL fuels respectively. SE \pm 0.001253.

Therefore higher VSP values mean severe engine operation, higher temperature, lower speeds to approach maximum torque speed and richer combustion. The lower PM EF figures at higher VSP could be related to the improved combustion efficiency due to the higher combustion temperatures to burn out the soot and keep the volatiles in the gaseous phase. The VSP could be related to high torque low velocity operation and vice versa. Each one of these conditions has its own characteristics on PM emissions. Therefore it is hard to decide which is which in the journey average analysis. However, engine performance analysis (Chapter 4) showed the HGV is mostly

working at low equivalence ratio ($\varphi < 1$). The theoretically calculated engine peak temperatures was 2900°C and 2650°C for PD and UBF respectively.

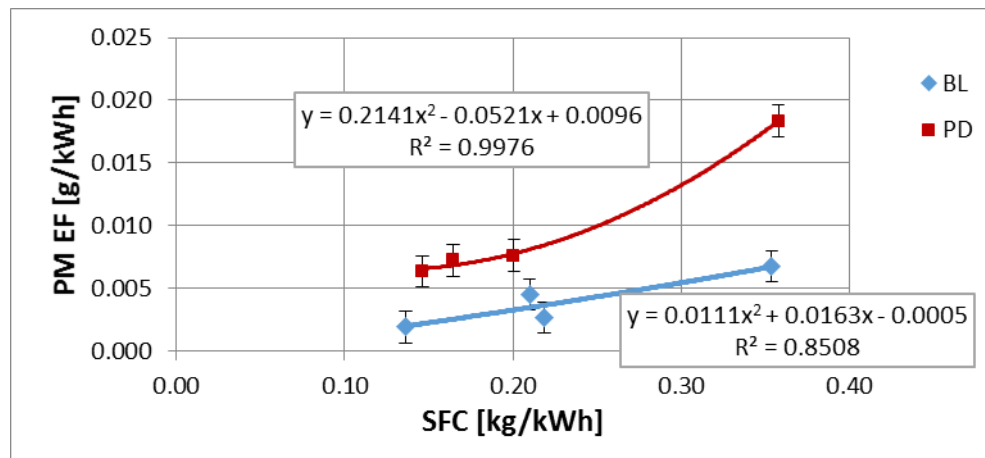


Figure 6.4 PM EF versus SFC. A comparison between conventional PD emissions and C2G UBF. The data are averages for 14 and 20 trips for the PD and UBF respectively. SE \pm 0.001253.

Fig.6.4 exhibits the relation between PM EF and HGV specific fuel consumption SFC. The SFC indicates, how well the engine is converting fuel mass into mechanical work, in this context, lower SFC means better combustion efficiency. PM EF for the BL fuel and PD are directly proportional to SFC. Both of the fuels show higher PM EF as the SFC increases, however PD is more likely to produce higher PM at elevated SFC. The utilisation of C2G UBF in the BL fuel reduces the PM by 65% at every SFC level. It is important to mention that fig.6.4 does not contradict fig.6.3 as the SFC decreases with VSP increase which means that the engine is more fuel efficient at higher VSP. The two fuels show a very high correlation between PM EF and SFC.

6.2 Qualitative analysis for PM_{2.5} emissions from the combustion of PD and BL fuel in HGV (Thermo-gravimetric analysis)

A comparison between TGA analysis for PM_{2.5} collected from HGV operated on PD and BL fuel is illustrated in fig.6.5. The data presented are for empty trailer condition. The plots show that PM_{2.5} from PD is nearly twice that of the BL fuel. That difference in PM is mostly related to the elemental carbon (EC) component of the PD which was discussed earlier in fig.6.1. Increasing the

HGV payload reduces the PM emissions as shown in fig.6.6 and the domination of EC component in the PD PM emissions is very clear. In other words the two fuels nearly produce the same amount of volatile organic fraction (VOF) while the EC component is about 70% higher in the case of PD.

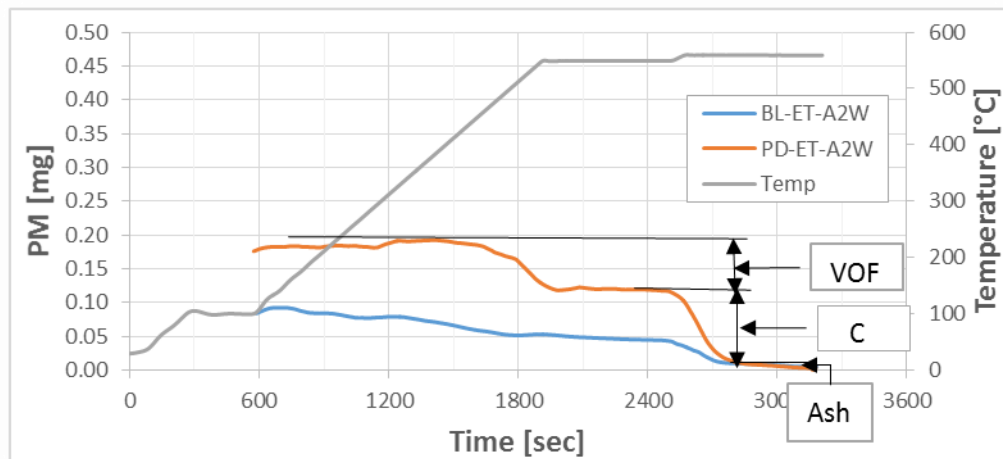


Figure 6.5 Thermo-gravimetric analysis (TGA) for PM_{2.5} collected on GF/F filters. A comparison between BL fuel and PD PM components for an empty trailer HGV trip.

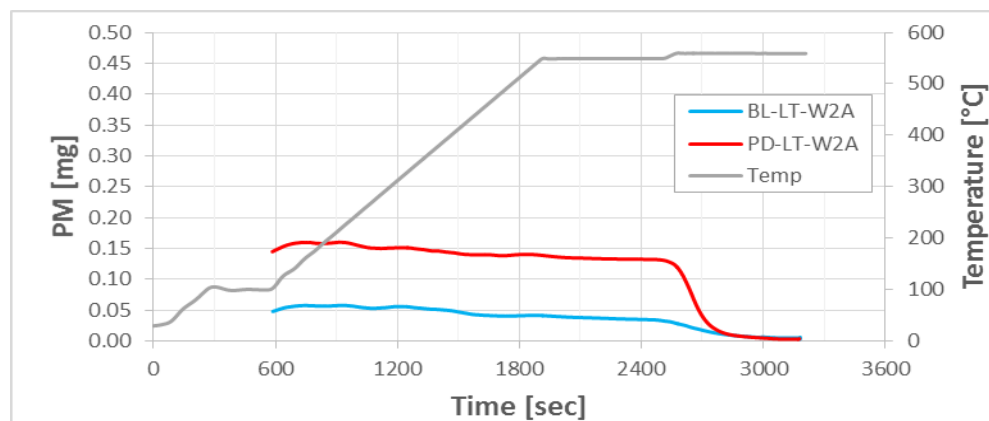


Figure 6.6 Thermo-gravimetric analysis (TGA) for PM_{2.5} collected on GF/F filters. A comparison between BL fuel and PD PM components for a loaded trailer HGV trip.

TGA analyses for PM components speciation are summarised in fig.6.7, fig.6.11 and fig.6.14 at different HGV load conditions. The graphs generally show higher PM emissions from the vehicles operated on PD. Elemental carbon (EC) comprises the majority of PD PM emissions whether the vehicle is traveling with a loaded trailer or an empty trailer. Organic carbon (VOF) is the dominant component in the BL fuel especially at low load HGV operation.

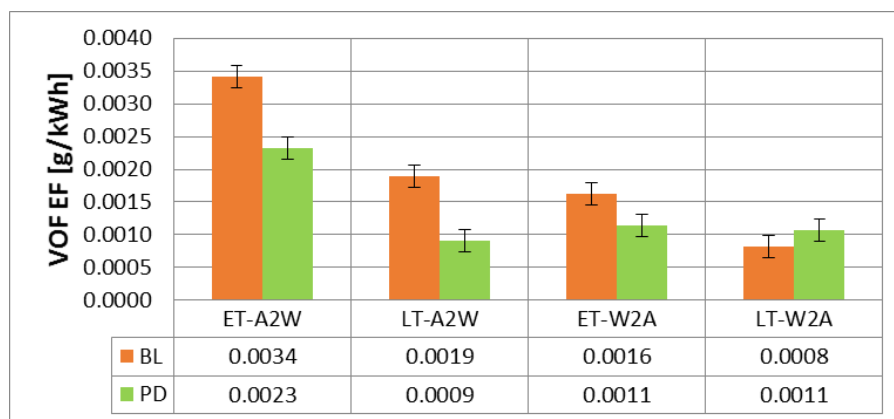


Figure 6.7 VOF EF obtained from a HGV operated on PD and BL fuel under different operational conditions. ET and LT are empty trailer and loaded trailer respectively. A2W and W2A are the HGV direction from Ashby to Wigston and Wigston to Ashby respectively. The data are the average of 20 trips for the BL fuel, 5 trips per category, and 14 trips for PD, 2-5 trips per category. SE $\pm 1.69E-04$.

Fig.6.7 illustrates the emission factor for the volatile organic fraction (VOF) of $PM_{2.5}$. VOF is the dominant component in the BL fuel PM emissions. It represents 42%~62% of the total PM mass depending on vehicle load conditions. The VOF figure is lower for the PD, it only represents 12.6%~17% of the total PM mass as demonstrated in table 6.1. The higher the load the lower the VOF emissions for both of the fuels. Increasing the load reduces VOF EF emissions by 76 % for the BL fuel and 53.5 % for PD.

Table 6.1 Percentage of PM components from the BL fuel and PD at different payloads and road loads. Data based on TGA for samples obtained from 30 real world trips.

Fuel type	PM & its components		Trip characteristics			
			ET-A2W	LT-A2W	ET-W2A	LT-W2A
BL	VOF	%	50.85	41.97	61.62	43.05
	C	%	40.39	50.47	18.75	46.30
	Ash	%	8.76	7.56	19.63	10.64
	PM	%	100	100	100	100
PD	VOF	%	12.62	12.69	14.92	17.00
	C	%	83.09	83.19	78.26	78.89
	Ash	%	4.30	4.12	6.82	4.11
	PM	%	100	100	100	100

Table 6.1 is a demonstration of the percentage contribution of each PM component in the total PM_{2.5} formation at different HGV pay loads and road loads. BL fuel have the propensity to produce more VOF than EC at all HGV operational conditions except for the loaded HGV during the outbound journey. In this particular case the EC components is higher due to the insufficient combustion temperatures, explained in the next paragraph, to burnout the soot.

The effect of BL fuel substitution for PD is summarised in table 6.2. In which the increase in the VOF component is very apparent except for the loaded HGV during the inbound journey. This could be attributed to the very high combustion temperatures under this high load condition that kept the VOF in the gaseous phase rather than a condensate accumulated on other particles or forming new particulates. In fact the higher load reduces the PM emissions, therefore the exemption lies in the loaded HGV during the outbound journey. In this particular case which is dominantly a downhill travel, the HGV used its doubled GVW as a potential for its movement or less dependence on engine power and fuel. A cooler combustion is expected especially in the M1 section of the journey as the HGV is travelling at speeds higher than 83 km/h depending, to higher extents, on its GVW. This is reflected on the reduced PM_{2.5} reduction as the BL fuel substitutes PD at this particular HGV operation.

Table 6.2 Variation of PM_{2.5} emissions and its components from the combustion of the BL fuel in comparison to those of PD in HGV at different Payloads and road loads.

PM & its components		Trip characteristics			
		ET-A2W	LT-A2W	ET-W2A	LT-W2A
VOF	[%]	47.64	106.15	43.95	-23.86
EC	[%]	-82.19	-62.17	-91.65	-82.35
Ash	[%]	-25.28	14.58	0.35	-22.14
PM	[%]	-63.36	-37.64	-65.14	-69.93

Fig.6.8 is an illustration for the variation of VOF EF with VSP. The vehicle emits higher levels of VOF at low VSP especially from the BL fuel. PD produces about 48% less VOF than UBF at low VSP. This might be affiliated to the lower injection pressure to produce larger droplets and lower combustion temperature especially for the BL fuel which encourages the VOF to remain in the liquid phase and faster condensation. However, this

difference decays to zero as the VSP increases. This could be attributed to the higher combustion temperatures which keep the volatiles in the gaseous phase and higher fuel efficient combustion at high VSP.

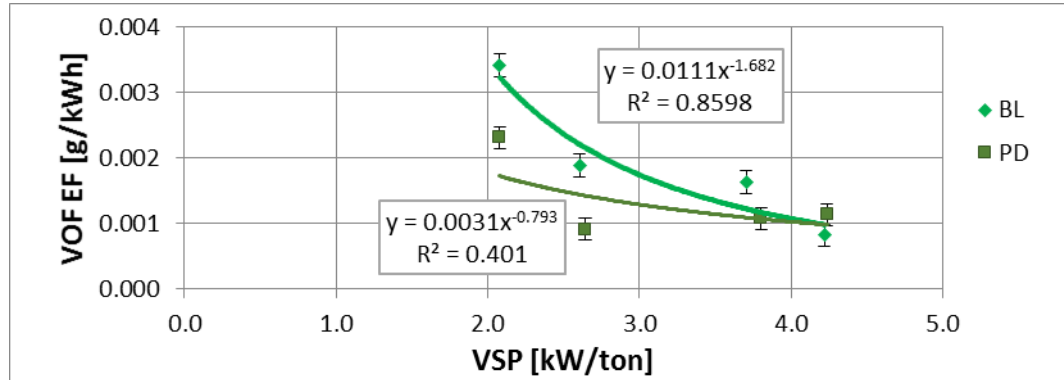


Figure 6.8 VOF EF as a function of VSP for PD and BL fuel. The data are averages for 14 and 20 trips for the PD and BL fuel respectively. SE \pm 1.69E-04.

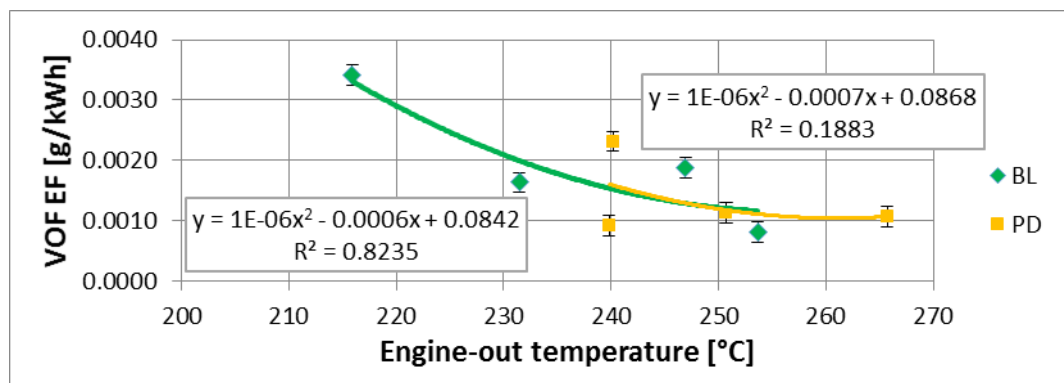


Figure 6.9 VOF as a function of engine-out temperature. The data are averages for 14 and 20 trips for the PD and BL fuel respectively. SE \pm 1.69E-04.

Fig.6.9 exhibits engine-out temperature (EoT) for the BL fuel in comparison to that of the PD. It is quite obvious that VOF produced from the combustion of BL fuel is produced and travel at a temperature range which is pretty wider but lower than that of the PD VOF. Lower temperatures enhance heavy VOF condensation, coagulation and growth [94]. The maximum theoretical in-cylinder temperature was calculated by applying Diesel Dual Cycle to the HGV engine dimensions and the calorific values of PD and UBF. The results revealed 2650°C for UBF against 2900°C for PD.

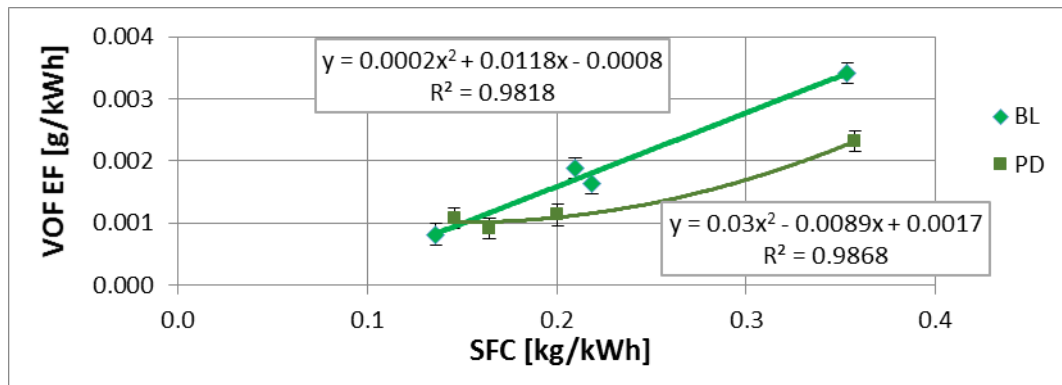


Figure 6.10 VOF EF as a function of SFC for PD and BL fuel. The data are averages for 14 and 20 trips for the PD and BL fuel respectively. SE \pm 1.69E-04.

The variation of VOF EF with vehicle specific fuel consumption (SFC) are demonstrated in Fig.6.10. The plots exhibit a direct proportionality between VOF EF and SFC and a very significant coefficient of regression is recorded for the two fuels. The BL fuel produces higher levels of VOF especially at higher SFC. This could be attributed to the lower combustion efficiency at high SFC, lower combustion temperatures and a lower overall global temperature. Since the BL fuel droplets are larger they might need more heat and time to evaporate and since the UBF density is higher its heat capacity might be higher as well. It is also good to mention that the amount of exhaust gas residual in the cylinder is higher in the case of BL fuel. All these factors work together to reduce the global temperature for a higher VOF production.

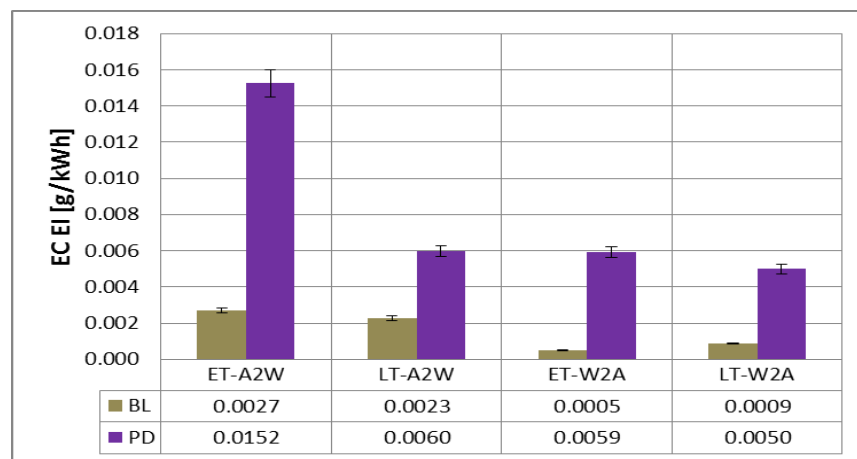


Figure 6.11 Elemental carbon (EC) emission factor, a comparison between BL fuel and PD under different vehicle operational conditions. ET and LT are empty trailer and loaded trailer respectively. A2W and W2A are the HGV direction from Ashby to Wigston and Wigston to Ashby respectively. The data are the averages for 20 trips for the BL fuel, 5 per trip category, and 14 trips for PD, 2-5 trips per category.

Fig.6.11 depicts the amount of elemental carbon contribution in PM emissions from the BL fuel and PD. In contrast to the BL fuel, the graph shows that PD has more propensity to produce EC than VOF. EC contribution in PD particulate emissions varies between (78.26~83.19%), while the figure is (18.75~50 %) for the BL fuel both depending on the vehicle pay-load and road-load. The higher the load the lower the EC emissions. The higher soot emissions from the combustion of PD could arguably be related to the slightly higher equivalence ratio and higher carbon content in the fuel. Therefore higher soot precursors are produce which are not completely burned even at higher PD combustion temperatures.

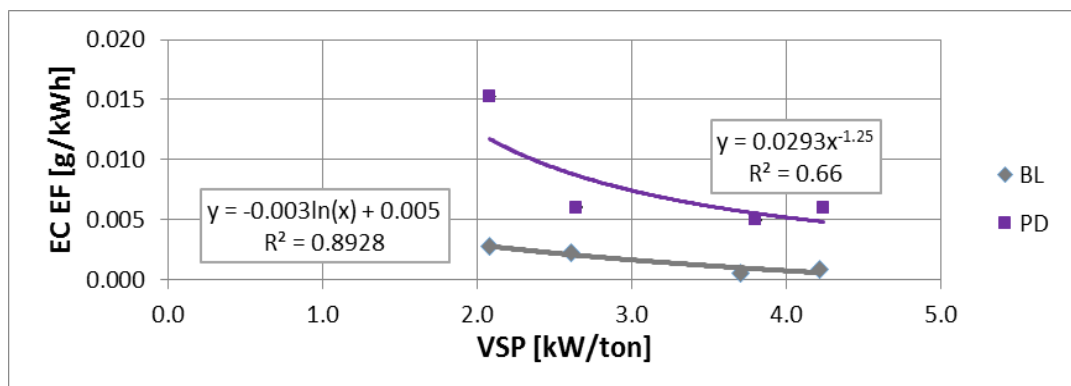


Figure 6.12 EC EF versus VSP from PD and BL fuel PM emissions. The data are averages for 14 and 20 trips for the PD and UBF respectively. SE \pm 2.84E-05.

Fig.6.12 depicts the reduction in EC EF as the vehicle power demand increases. The graph shows that BL fuel produces 80% less EC emissions than PD at all power demands. A very high regression coefficient is recorded between C EF and VSP especially for the BL fuel.

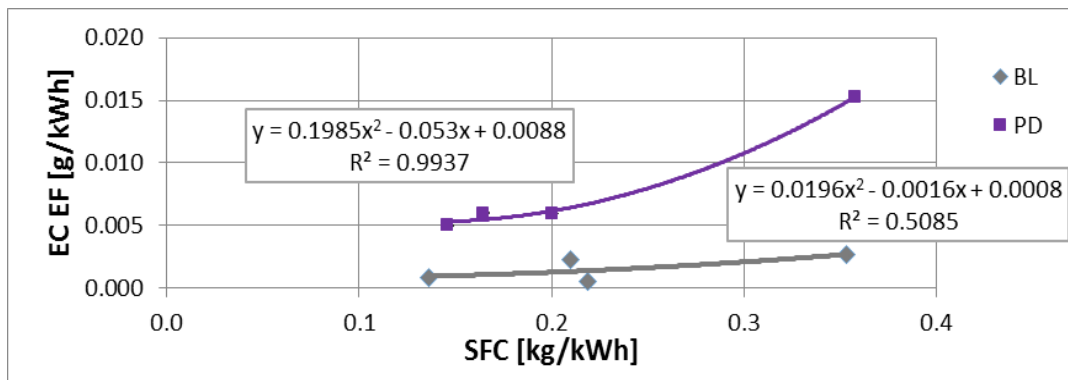


Figure 6.13 EC EF as a function of SFC for a HGV operated on PD and UBF. The data are averages for 14 and 20 trips for the PD and UBF respectively. SE \pm 2.84E-05.

Fig.6.13 shows the propensity of PD to produce higher levels of EC than VOF. The utilisation of BL fuel reduces the EC by more than 80%. The graphs also show that EC increases as the SFC increase especially for the PD combustion. It is quite obvious that the slope of the curve is steeper as the SFC increases. The higher the SFC the poorer is the fuel conversion efficiency. Therefore for a given SFC the BL fuel produces less EC. This could be affiliated to the lower soot precursor formation in the premixed flame zone of the BL fuel due to its higher O₂ content and the formation of the radicals which react with the PAH.

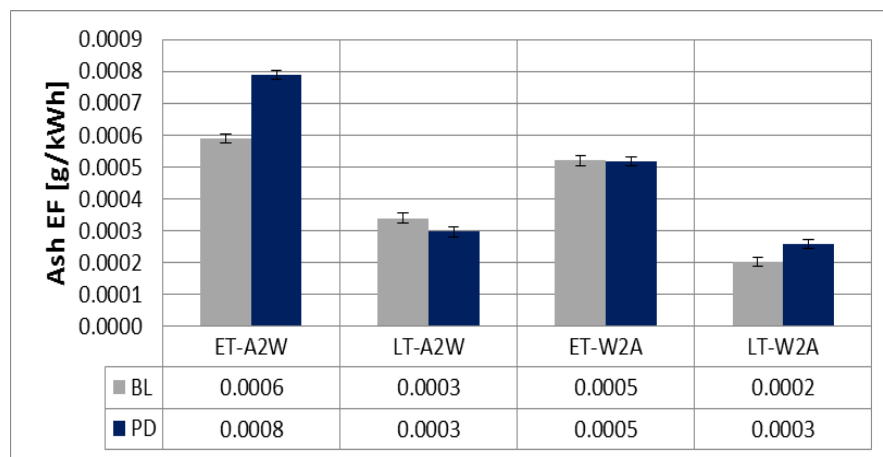


Figure 6.14 Ash emission factor, a comparison between BL fuel and PD under different vehicle operational conditions. ET and LT are empty trailer and loaded trailer respectively. A2W and W2A are the HGV direction from Ashby to Wigston and Wigston to Ashby respectively. The data are the average of 20 trips for the BL fuel, 5 per trip category, and 14 trips for PD, 2-5 trips per category. SE $\pm 1.46E-05$

Fig.6.14 is the plot for ash content in PM emissions from a HGV operated on BL fuel and PD under the same operational conditions. The general trend is an inverse correlation between the amount of ash emitted and the load. The higher the load the lower the amount of ash emitted. The percentage of ash contained in the PM emitted from the BL fuel varies between (7.56%~19.63%), while the percentage from PD varies between (4.1%~6.82%).

Table 6.3 shows that the BL fuel increases the VOF EF by 46.4%~36% depending on the HGV payload. This could be attributed to the lower combustion temperatures of the BL fuel and perhaps high temperature distillates in the BL fuel. EC EF is very much reduced as the BL fuel was used. The reduction in EC EF varies between 85%~71% depending on the HGV payload since the EC in the PD is very high as presented earlier in Fig.6.11.

Table 6.3 The effect of using C2G UBF in the BL fuel on PM_{2.5} emission components from HGV under different loads.

PM component EF	Units	Empty trailer		Variation %	Loaded trailer		Variation %
		BL	PD		BL	PD	
VOF	g/kWh	0.00252	0.00172	46.42	0.00135	0.00099	35.94
C	g/kWh	0.00161	0.01059	-84.84	0.00157	0.00549	-71.33
Ash	g/kWh	0.00055	0.00065	-15.12	0.00027	0.00028	-2.56
PM	g/kWh	0.00468	0.01297	-63.88	0.00320	0.00676	-52.73

Ash is also reduced and the total PM EF reduces by 64%~53% at low payload and high payload respectively. In other words doubling the HGV payload reduces the PM EF by 11% .

6.3 Statistical analysis

6.3.1 Analysis of variances

Performing statistical analysis for PM EF data for the two fuels reveal that the major difference in the mean values is quite apparent in the elemental carbon component. PD scores nearly 5 fold higher EC values as shown in table 6.4. However the BL fuel produces 50% more VOF. To superimpose, PD produces more than twice the PM produced by the BL fuel.

Table 6.4 Analysis of variance for PM EF obtained from HGV operation on PD and BL fuel. The units are in (g/kWh).

Group Statistics					
	TYPE OF FUEL	N	Mean	Std. Deviation	Std. Error Mean
PM	Blended Fuel	16	.003941	.002502	.000626
	Petroleum Diesel	10	.009247	.005980	.001891
ASH	Blended Fuel	16	.000413	.000330	.000083
	Petroleum Diesel	10	.000368	.000297	.000094
EC	Blended Fuel	16	.001590	.001525	.000381
	Petroleum Diesel	10	.007532	.005164	.001633
VOF	Blended Fuel	16	.001938	.001106	.000277
	Petroleum Diesel	10	.001287	.001122	.000355

Table 6.5 shows the Levene's test for equality of variances and t-test for equality of means for the PM EF data used in table 6.4. The t-test indicated a

very significant difference between the two fuels in their EC component. This difference is also significantly reflected in the total PM value.

Table 6.5 Levene's test for equality of variances and t-test for the equality of means for PM EF and its components. The units are in (g/kWh).

		Independent Samples Test								
		Levene's Test for Equality of Variances		t-test for Equality of Means						
		F	Sig.	t	df	Sig. (2-tailed)	Mean Difference	Std. Error Difference	95% Confidence Interval of the Difference	
									Lower	Upper
PM	Equal variances assumed	1.895	.181	-3.162	24	.004	-.005305	.001678	-.008768	-.001843
ASH	Equal variances assumed	.149	.703	.348	24	.731	.000045	.000128	-.000220	.000309
EC	Equal variances assumed	3.761	.064	-4.356	24	.000	-.005942	.001364	-.008758	-.003126
VOF	Equal variances assumed	.047	.830	1.454	24	.159	.000652	.000448	-.000273	.001577

6.3.2 Multi-regression analysis

Multi-regression analysis reveals that SFC and EoT are significantly affecting the amount of VOF in the HGV exhaust as shown in table 6.6. VOF varies directly with SFC, the higher the SFC the greater the amount of VOF as a component of the total PM. EoT adversely affects VOF emissions since a higher EoT is the outcome of a higher combustion temperature which evaporates and burn the heavy end distillates of the fuel. The EoT also keeps the VOF in the vapour phase rather than particulates or condensate on soot particles.

After 7 backward attempts the model possesses an adjusted R² of 0.586. ANOVA analysis shows F(2,23) = 18.686 for p = .000. This reflects the high significance of the model in which SFC is the strongest variable.

Table 6.6 Multi-regression analysis for PM_{2.5}. VOF is the dependent variable.

Regression VOF							
Coefficients							
Model		Unstandardized Coefficients	Sig.	Decision	Collinearity Statistics		
		B			VIF		
7	(Constant)	0.00536					
	Engine-Out Temperature [°C]	-0.00002	.022	S	1.636		
	Specific Fuel Consumption [kg/kWh]	0.00653	.002	HS	1.363		
a. Dependent Variable: Volatile Organic Compounds [g/kWh]							
Adjusted R Square = .586							
VOF = 0.00536 - 0.00002 EoT + 0.00653 SFC							
Best model obtained after seven (7) repetitions, using backward method							
ANOVA							
Model		Sum of Squares	df	Mean Square	F	Sig.	Decision
7	Regression	0.00002	2	0.00001	18.686	.000	VHS
	Residual	0.00001	23	0			
	Total	0.00003	25				

Table 6.7 PM regression analysis. EC as the dependent variable.

Regression Elemental Carbon							
Coefficients							
Model		Unstandardized Coefficients	Sig.	Decision	Collinearity Statistics		
		B			VIF		
6	(Constant)	-0.01848					
	Type Of Fuel (1 for BL & 2 for PD)	0.00833	.000	VHS	1.641		
	HGV Load (1 for ET, 2 for LT)	0.00331	.031	S	1.832		
	Specific Fuel Consumption [kg/kWh]	0.02954	.000	VHS	1.347		
a. Dependent Variable: Elemental Carbon-C [g/kWh]							
Adjusted R Square = .684							
EC = - 0.01848 + 0.00833 ToF + 0.00331 L + 0.02945 SFC							
Best model obtained after six (6) repetitions, using backward method							
ANOVA							
Model		Sum of Squares	df	Mean Square	F	Sig.	Decision
6	Regression	0.00036	3	0.00012	19.055	.000	VHS
	Residual	0.00014	22	0.00001			
	Total	0.00049	25				

Table 6.7 shows the results of the regression analysis when EC was held as the dependent variable. After six backward rounds, the analysis revealed that type of fuel (ToF) has a very high significant effect (VHS) on EC emissions

and PD is the most effective fuel. Similarly SFC has the a VHS effect on EC emissions and possesses the strongest weight in the model. The higher the SFC the higher the amount EC produced. HGV load also significantly affected the EC emissions. The model possesses an adjusted R^2 of 0.684. ANOVA shows that the model is statistically significant $F(3,22) = 19.055$ and $p = .000$. Ash is significantly affected by SFC with a direct correlation as shown in table 6.8. The obtained model, after 8 repetitions, accounts only 37% of the ash variance. The low R^2 might be resulted from other variables which are not accounted for in the experiments.

Table 6.8 PM regression analysis. Ash as a dependent variable.

Regression Ash							
Coefficients							
Model	Unstandardized Coefficients		Sig.	Decision	Collinearity Statistics		
	B				VIF		
8	(Constant)	-7.19E-05					
	Specific Fuel Consumption [kg/kWh]	2.13E-03	.001	VHS	1		
a. Dependent Variable: Ash [g/kWh]							
Adjusted R Square = .369							
ASH = - 7.1897E-05 + 2.1252E-03 SFC							
Best model obtained after eight (8) repetitions, using backward method							
ANOVA							
Model	Sum of Squares	df	Mean Square	F	Sig.	Decision	
8	Regression	0.000001	1	0.000001	15.63	.001	VHS
	Residual	0.000001	24	0			
	Total	0.000002	25				

Table 6.9 exhibits the results for $PM_{2.5}$ regression analysis. The analysis show that SFC has a VHS effect on PM variation and has the strongest weight in the model. ToF has a VHS effect on PM variation. PM is directly proportional to ToF therefore PD is considered to be more effective on PM emissions. The obtained model, after 6 backward repetitions, has an adjusted $R^2 = 0.691$. This means that there might be other variables, which has not been included in the analysis, which might increase the value of R^2 . ANOVA shows that the model is significant and $F(3,22) = 19.66$ and $p = .000$.

Table 6.9 PM regression analysis, total PM as a dependent variable.

Regression Particulate Matter							
Coefficients							
Model		Unstandardized Coefficients	Sig.	Decision	Collinearity Statistics		
		B			VIF		
6	(Constant)	-0.01736					
	Type Of Fuel (1 for BL, 2 for PD)	0.00777	.000	VHS	1.641		
	HGV Load (1 for ET, 2 for LT)	0.00298	.068	NS	1.832		
	Specific Fuel Consumption [kg/kWh]	0.0395	.000	VHS	1.347		
a. Dependent Variable: Particulate Matter [g/kWh]							
Adjusted R Square = .691							
PM = - 0.01736 + 0.00777 ToF + 0.00298 L + 0.03950 SFC							
Best model obtained after six (6) repetitions, using backward method							
ANOVA							
Model		Sum of Squares	df	Mean Square	F	Sig.	Decision
6	Regression	0.00043	3	0.00014	19.659	.000	VHS
	Residual	0.00016	22	0.00001			
	Total	0.00059	25				

6.4 Particle size distribution by inertial impaction

PM₁₀ is ultimately classified into nine smaller size ranges using Andersen's impactor. The principle is to collect progressively smaller D50% of the specified size range as the exhaust sample moves downward to the end of the impactor. Photos for PM collected in two different journeys for the HGV operated by PD and BL fuel are shown in fig's.6.15 and 6.16 respectively. The dark spots represent the PM collected by impaction on GF/A filter papers. The size of the collected particulates decreases as they flow downwards through the first eight impactor stages. To provide higher inertia to the smaller or less dense particulates for impaction, they should be flowing through progressively smaller jets. That's why the diameter of the dark spots on the filter paper is getting smaller and their numbers are progressively increasing. The last photo is the impactor back-up filter where particulates smaller than 0.4 microns are captured on the GF/F filter.

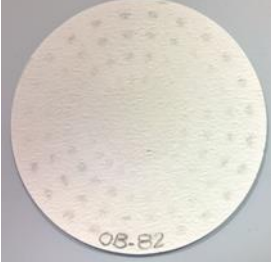
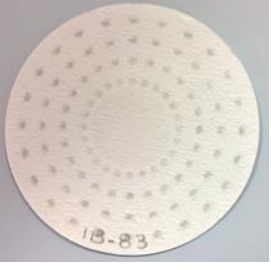
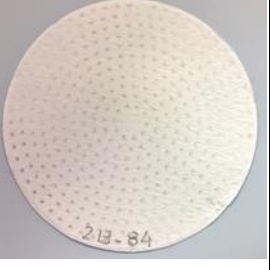






			
PM size $\geq 9\mu\text{m}$ PM = 0.014 mg/m^3 PM EF= 0.0001 g/kWh	PM size = $9\sim 5.8\mu\text{m}$ PM = 0.03 mg/m^3 PM EF= 0.0003g/kWh	PM size = $5.8\sim 4.7\mu\text{m}$ PM = 0.014 mg/m^3 PM EF= 0.0001g/kWh	PM size = $4.7\sim 3.3\mu\text{m}$ PM = 0.026 mg/m^3 PM EF= 0.0003g/kWh
			
PM size = $3.3\sim 2.1 \mu\text{m}$ PM = 0.018 mg/m^3 PM EF= 0.0002g/kWh	PM size = $2.1\sim 1.1 \mu\text{m}$ PM = 0.057 mg/m^3 PM EF= 0.0006g/kWh	PM size = $1.1\sim 0.7 \mu\text{m}$ PM = 0.049 mg/m^3 PM EF= 0.0005g/kWh	PM size = $0.7\sim 0.4 \mu\text{m}$ PM = 0.077 mg/m^3 PM EF= 0.0008g/kWh
	Filters No. 82 ~90 Fuel: PD Load: 15.5 tonne PM mass: 1.023 mg/m^3 PM EF: 0.0103 g/kWh		
PM size = $0.4\sim 0.0\mu\text{m}$ PM = 0.738 mg/m^3 PM EF= 0.0074g/kWh			

Figure 6.15 Visual comparison for PM collected at different stages of Andersen's impactor. The HGV was operated on PD and travelling with empty trailer.

The photos in fig.6.15 represent PM₁₀ obtained from the exhaust of a HGV running on PD with empty trailer. It could be inferred from the photos that the majority of PM mass obtained from PD combustion lies in fine particle range below 2.1 microns. This raises real health concerns as smaller particulates might penetrate more deeply in the respiratory system. Therefore they have a great chance to reach the circulation system through the alveolar membrane. This might lead to premature death of old and sick people due to respiratory and cardiovascular systems disease [179, 180].

Figure 6.16 exhibits PM size distribution for a HGV running on C2G UBF. It is very hard to visualise the dark spots on the first row of the photos, but that doesn't mean nothing had been collected on them. In fact more PM mass of this size range is collected than their counterparts from the PD. This could be arguably related to the type of particulate being collected which are substantially different from those of the PD. Differences in size distribution and in the ingredients are related to PM formation in the combustion chamber and the mechanisms of growth.

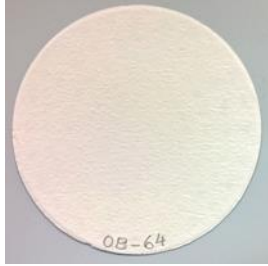
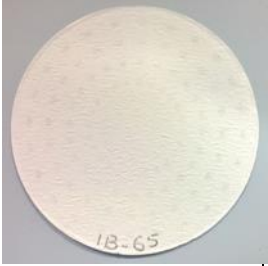
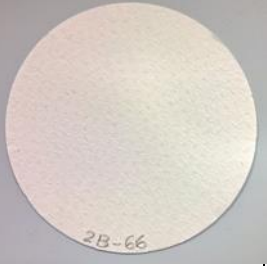
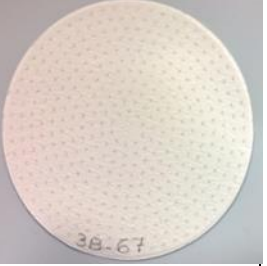
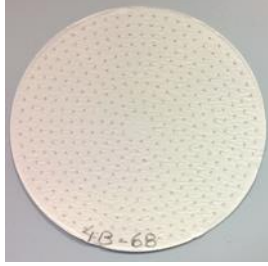

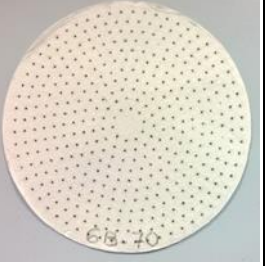
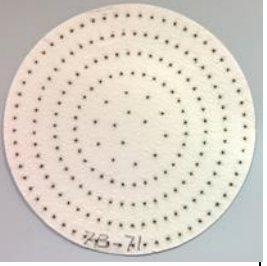

			
PM size = >9 μm PM= 0.043 mg/m ³ PM EF=0.0004g/kWh	PM size = 9~5.8μm PM= 0.036 mg/m ³ PM EF=0.0003g/kWh	PM size= 5.8~4.7μm PM =0.029 mg/m ³ PM EF=0.0003g/kWh	PM size = 4.7~3.3μm PM = 0.026 mg/m ³ PM EF=0.0002g/kWh
			
PM size = 3.3~2.1μm PM= 0.026 mg/m ³ PM EF=0.0002g/kWh	PM size= 2.1~1.1μm PM= 0.046 mg/m ³ PM EF=0.0004g/kWh	PM size= 1.1~0.7μm PM= 0.043 mg/m ³ PM EF=0.0004g/kWh	PM size= 0.7~0.4μm PM= 0.046 mg/m ³ PM EF=0.0004g/kWh
	Filters No. 64 ~72 Fuel: BL Load: 15.5 tonne PM mass: 0.594 mg/m ³ PM EF: 0.0053 g/kWh		
PM size = 0.4-0.0μm PM= 0.297 mg/m ³ PM EF=0.0026g/kWh			

Figure 6.16 Visual comparison for PM collected at different stages of Andersen's impactor. The HGV was running on BL fuel and travelling with empty trailer.

Andersen's impactor results for the vehicle travelling with empty trailer is shown in fig.6.17. Most of the PM lie in the particulate size range smaller than $2.1\mu\text{m}$ for PD and the BL fuel. Although the BL fuel produces slightly higher PM for the size range above $9\mu\text{m}$, PD show its superiority in the size range below $2.1\mu\text{m}$. The ratio of $\text{PM}_{2.1}$ to PM_{10} is 87.6% and 74% for PD and BL fuel respectively. The graph indicates that the BL fuel is capable of reducing $\text{PM}_{2.1}$ by 65.5%.

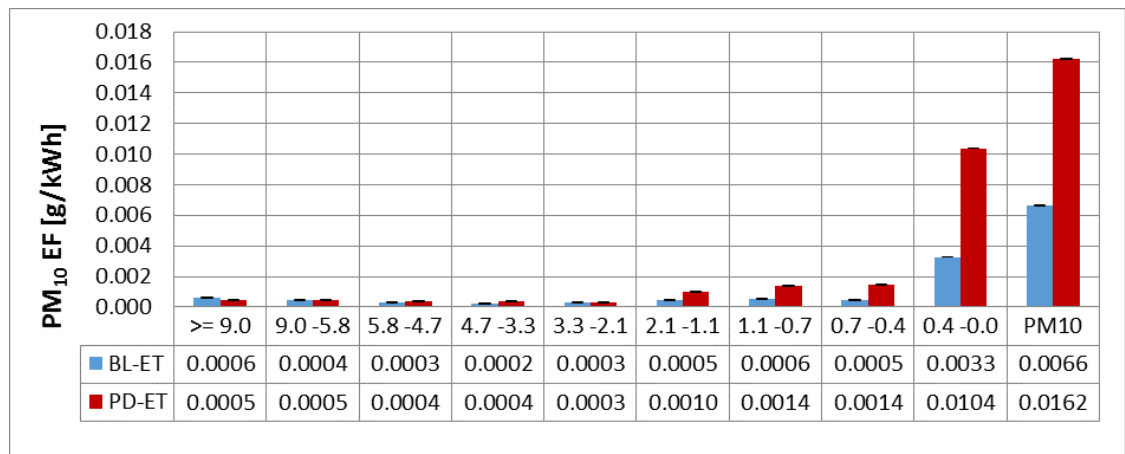


Figure 6.17 Size distribution for PM_{10} EF for PD and BL fuel obtained from a HGV traveling with an empty trailer. The data are averaged for (6) round trip journeys. $\text{SE} \pm 3.366\text{E-}5$.

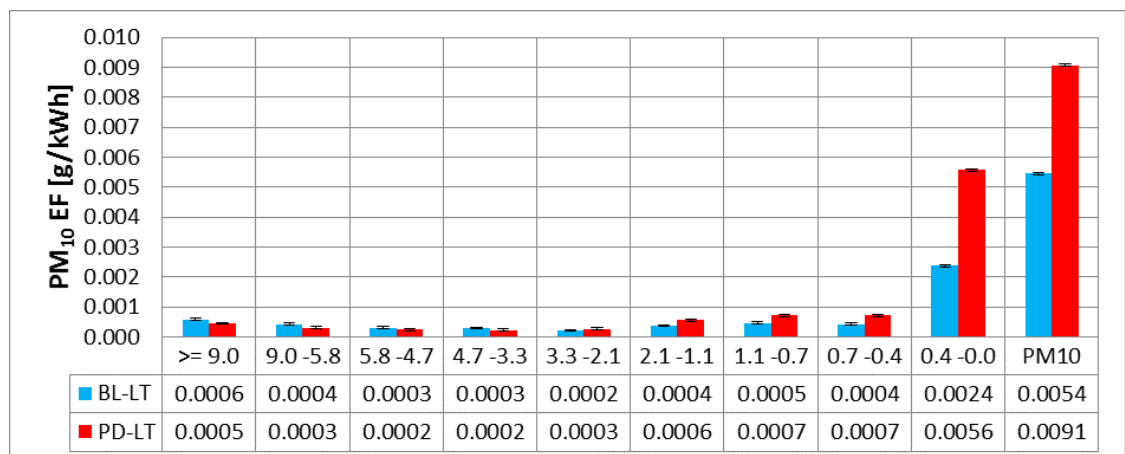


Figure 6.18 Size distribution for PM_{10} EF from PD and BL fuel obtained from a HGV traveling with loaded trailer. The data are averaged for (7) round trip journeys. $\text{SE} \pm 3.366\text{E-}5$.

A comparison between fig.6.17 and fig.6.18 reveal that, HGV's travelling with a loaded trailer produces lower PM_{10} emissions especially in the smaller size range below $2.1\mu\text{m}$. In spite of the tiny magnitude, BL fuel produces 33%

higher PM in the size range above 3.3 μ m and 51.3% lower PM in the size range below 2.1 μ m. The contribution of PM_{2.1} in the total amount of PM₁₀ collected from PD and BL fuel combustion are 77% and 68.5% respectively. At high loads, BL fuel reduces PM_{2.1} by 52%.

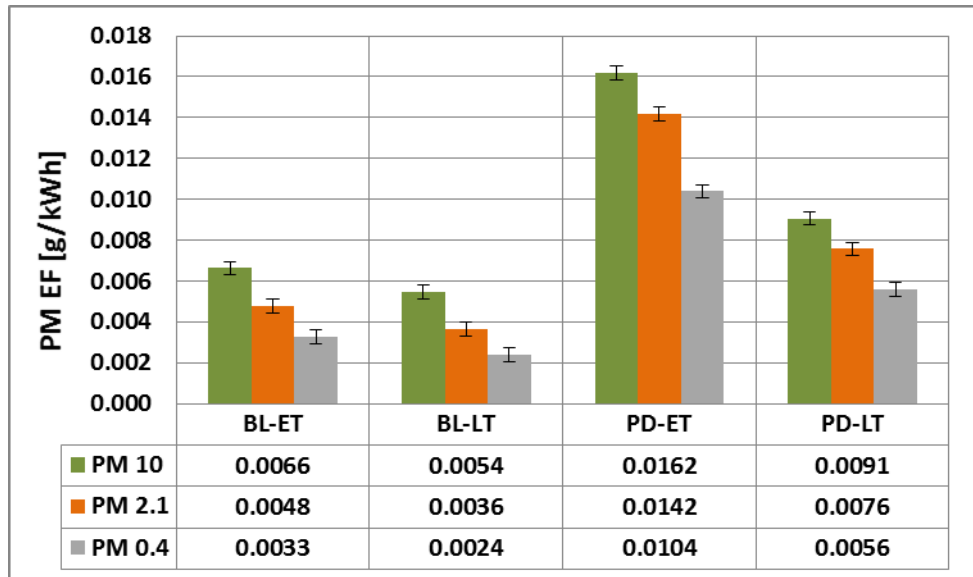


Figure 6.19 PM EF for three PM size ranges obtained from HGV operated on PD and C2G UBF at different operational conditions. ET and LT are empty trailer and loaded trailer respectively. The data are averaged from 13 round trip journeys. $SE \pm 3.366E-4$.

Fig.6.19 illustrates PM size distribution in terms of PM EF. Three size ranges are identified, specifically PM₁₀, PM_{2.1} and PM_{0.4} collected from HGV running on PD and on BL fuel at different operational conditions. The analysis revealed that HGV operated on PD produces more fine particulates than the BL fuel. HGV operation on the BL fuel produces about 60% and 40% less PM₁₀ compared to the same category from PD while running empty and loaded respectively. The BL fuel reduces PM_{2.1} by 66.5% in the empty trailer test and 52% for loaded trailer test. A reduction of 68.5% and 57.5% is discernible in PM_{0.4} at the same aforementioned conditions as shown in table 6.10.

Increasing the HGV payload from 15.5~31 tonne reduces PM size distribution. Accordingly, a reduction in PM₁₀ of 17% and 44% is indicated for the BL fuel and PD respectively.

Table 6.10 PM₁₀ size segregation for BL fuel and PD emissions and the % variation PM EF at each impactor stage as the BL fuel substitutes PD.

PM EF [g/kWh]	Impactor stage	PM size range [μm]	Empty trailer		Variation %	Loaded trailer		Variation %
			BL	PD		BL	PD	
			0	>= 9.0	0.00060	0.00048	26.96	0.00058
1	9.0-5.8	0.00043	0.00046	-6.52	0.00042	0.00031	37.26	
2	5.8-4.7	0.00032	0.00036	-12.23	0.00031	0.00024	29.00	
3	4.7-3.3	0.00024	0.00039	-39.81	0.00029	0.00024	23.17	
4	3.3-2.1	0.00028	0.00033	-16.76	0.00022	0.00027	-19.47	
5	2.1-1.1	0.00047	0.00097	-52.05	0.00038	0.00057	-33.71	
6	1.1-0.7	0.00056	0.00137	-58.91	0.00047	0.00071	-34.24	
7	0.7-0.4	0.00045	0.00144	-68.70	0.00042	0.00071	-41.04	
F	0.4-0.0	0.00328	0.01039	-68.44	0.00237	0.00557	-57.50	
	PM _{2.1}	0.00476	0.01417	-66.42	0.00363	0.00756	-51.98	
	PM ₁₀	0.00662	0.01620	-59.10	0.00545	0.00907	-39.90	

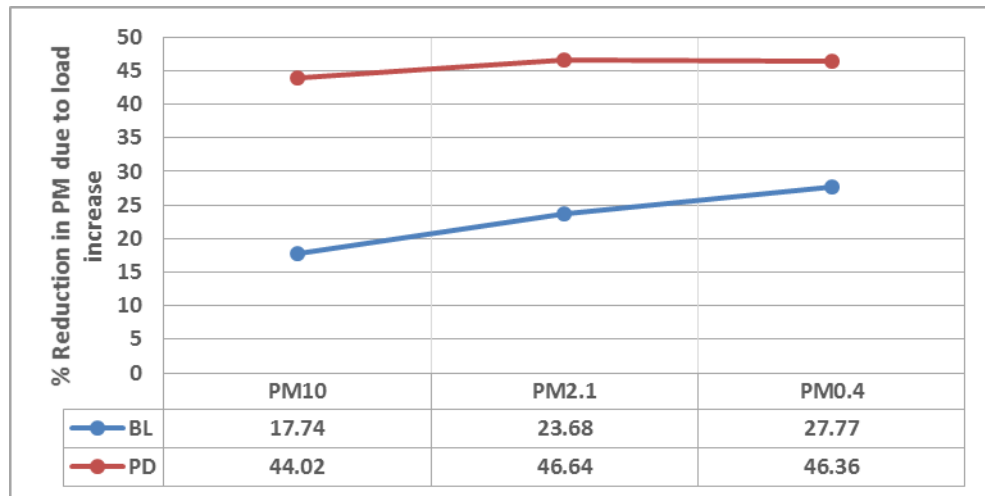


Figure 6.20 Effect of load increase on selected PM sizes from PD and BL fuel combustion. Data averaged for 13 round trip journeys.

Comparing the increasing PM component from table 6.2 and the increasing size range from table 6.10 reveals that VOF for size range above 9 μm at the low load operation are both increasing, similarly VOF and PM size range above 3.3 μm for the high load. This means that more VOF is produced from the BL fuel that condenses and agglomerates due to the lower combustion temperatures.

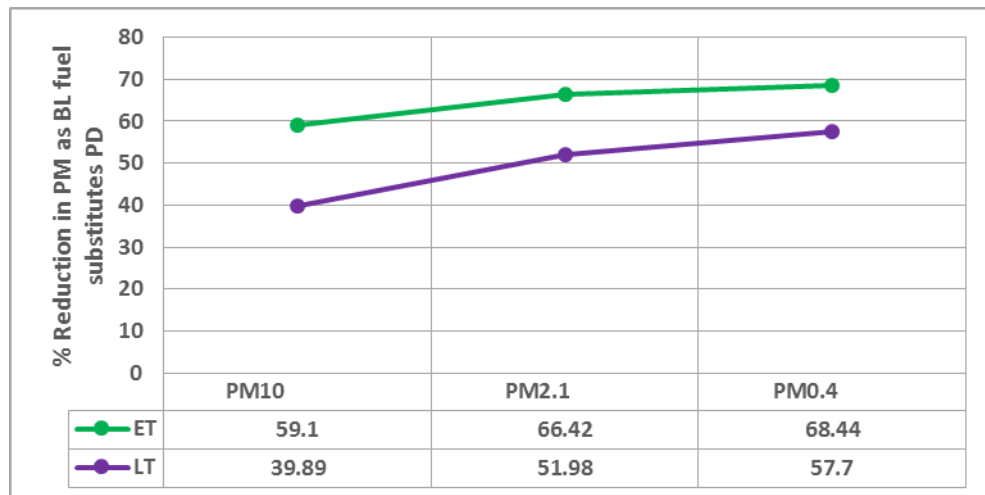


Figure 6.21 Reduction in selected PM sizes as BL fuel substitutes PD. Data are the averages of 13 round trip journeys.

The plots in fig 6.21 show that PD PM emissions are more affected by load increase. This could be attributed to the higher combustion temperatures of PD compared to that of the BL fuel.

The smaller particulates produced from PD combustion could arguably be related to the nature of the PD PM emissions, which are dominantly soot, that eventually convert to CO under PD high temperature combustion. Provided that, the high combustion temperature that delays particulate growth by condensation, coagulation and agglomeration as they travel along the exhaust pipe.

The plots in fig.2.20 and fig.2.21 depict that smaller particles are more susceptible to the reduction as load increases. In other words PM reduction efficiency is higher in the smaller particle size ranges especially for the BL fuel.

The injection pressure of the test HGV varies directly with power output to a maximum of 180 MPa. Therefore, increasing the load improves fuel atomisation and increases the spray cone angle. No droplet collision is expected as the ratio of the mean distance between the droplets to the mean droplet diameter increases. Therefore a better mixing with hot air facilitates faster evaporation and SOC. Under these high speed operations, the premixed flame is considered as adiabatic due to the limited heat radiation. Therefore lower soot precursors are produced, more radicals and a higher temperature diffusion flame is expected to burnout the soot.

6.5 Thermo-gravimetric analysis for PM_{0.4}

The potential health effects of the fine particulates necessitated further analysis to include component segregation for PM size regime below 0.4 µm. Andersen's impactor back-up filters were analysed by TGA. These are GF/F filters carrying PM in the size range below 0.4µm.

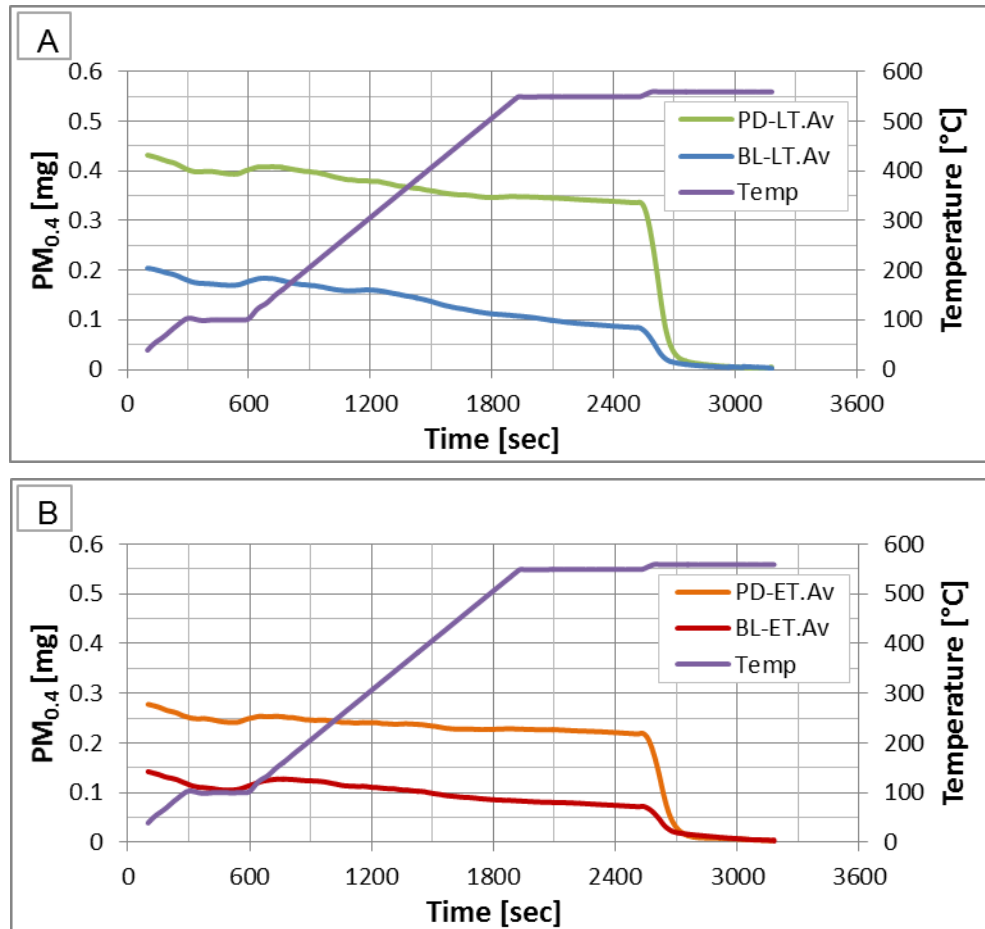


Figure 6.22 TGA test results for PM_{0.4} collected on Andersen's back-up filter. The plots show the effect of fuel type on PM emissions under different HGCV load conditions. The data are averages of 3 round trip journeys per category. SE±0.0364.

Fig.6.22 depicts the PM_{0.4} components for PD and BL fuel under high load (A) and low load (B). The BL fuel seems to contain less EC component of PM_{0.4} especially when the HGCV is operated at high loads. This could be attributed to the higher oxygen and hydrogen content of C2G UBF to produce the radicals which react with soot precursors.

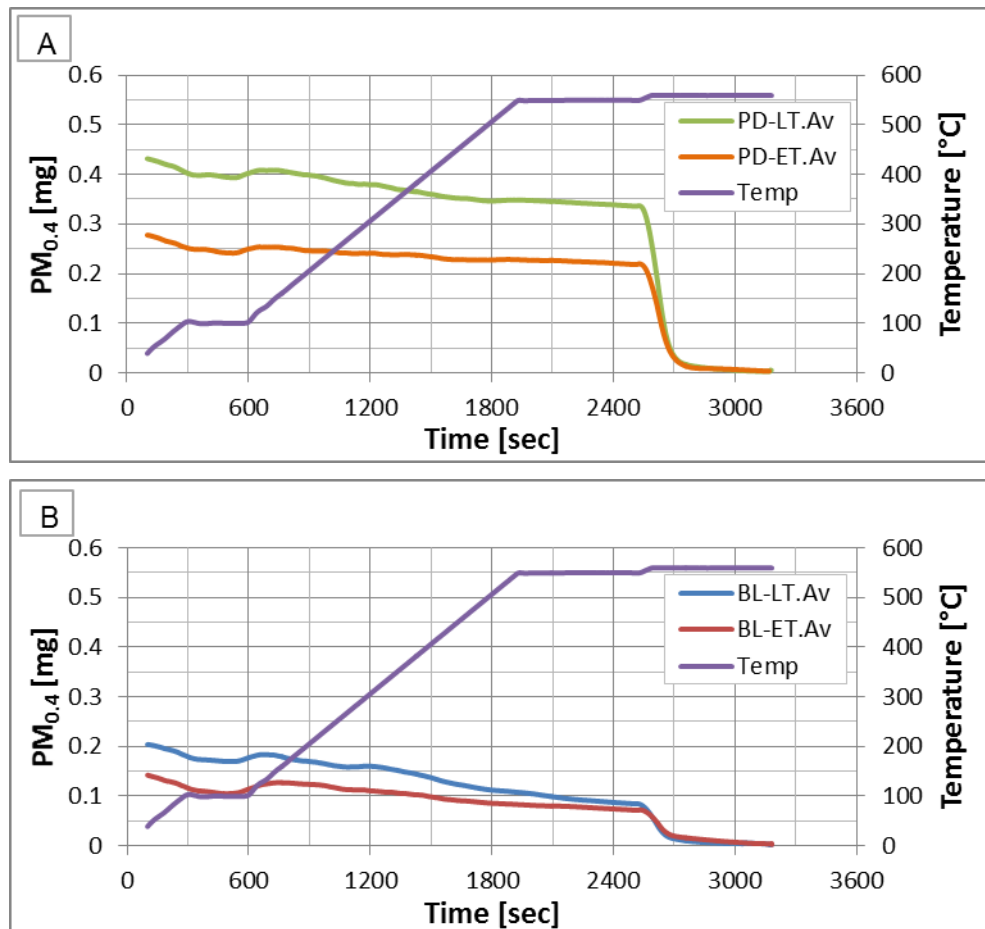


Figure 6.23 TGA test results for PM_{0.4} collected on Andersen's back-up filter. The plots show the effect of load on PM emissions from HGV operation on PD and BL fuel. The data are averages of 3 round trip journeys per category. SE±0.0364.

The TGA analysis for the PM_{0.4} collected by the Andersen's back-up filters are plotted in fig.6.23 (A) and (B) to show the effect of HGV payload on PM_{0.4} components. The plots show the characteristics of PM_{0.4} emitted from vehicle operation on PD and the BL fuel separately. It is quite obvious that PD produces more PM_{0.4} of EC nature. It is also indicated that vehicle load increase is increasing the mass of the EC component. Fig.6.23 (B) shows that PM_{0.4} from the BL fuel combustion is about evenly divided between EC and VOF. In this particular case the load increase is increasing the mass of VOF component of PM_{0.4}. This is probably related to the effect of the outbound journey of the loaded HGV in which less fuel energy is used as the HGV is moving mostly downhill. A cooler combustion and exhaust gases lead to the higher VOF mass collected.

The major components of PM_{0.4} are VOF and EC. The contribution of EC and VOF is about the same for the BL fuel which is around 40-50% per component,

while EC is the dominant component in PD $PM_{0.4}$ emissions, its contribution is more than 75% as shown in fig.6.24.

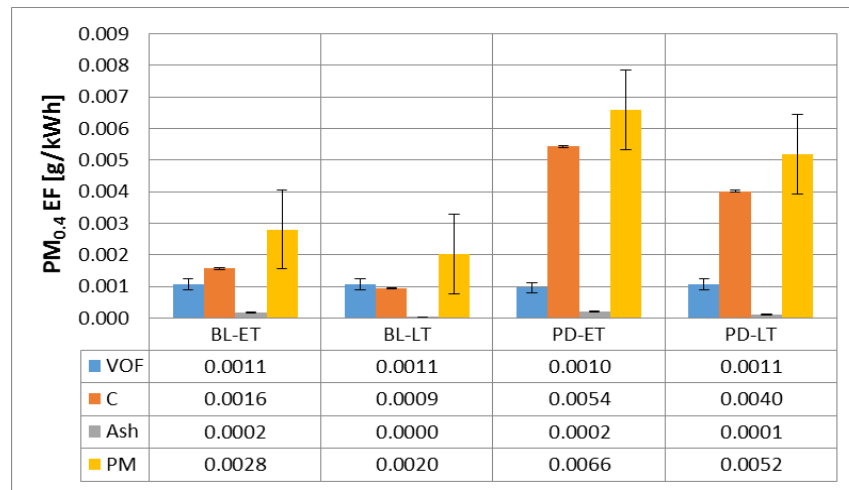


Figure 6.24 a comparison for $PM_{0.4}$ and its components emitted from the combustion of the BL fuel and PD in a HGV under different loads. ET and LT are the empty and loaded trailer respectively. The data are the average of 9 round trip journeys.

Elemental carbon plays a major role in $PM_{0.4}$ reduction since PD $PM_{0.4}$ is predominantly (75%) EC and substituting PD by the BL fuel, which is less EC producer, could reduce $PM_{0.4}$ by 57.5%~61% in empty trailer and loaded trailer tests respectively as demonstrated in table 6.11.

Table 6.11 Variation of $PM_{0.4}$ components as BL fuel substitutes PD at different HGV loads

$PM_{0.4}$ μm	Units	Empty trailer		Variation %	Loaded trailer		Variation %
		BL	PD		BL	PD	
VOF	g/kWh	0.00107	0.00095	12.05	0.00107	0.00106	0.16
C	g/kWh	0.00157	0.00542	-71.04	0.00094	0.00401	-76.65
Ash	g/kWh	0.00016	0.00021	-24.99	0.00002	0.00010	-77.72
PM	g/kWh	0.00280	0.00659	-57.53	0.00203	0.00518	-60.90

6.6 Conclusions

The previous analyses show that the presence of C2G UBF in the blended fuel is very effective in PM emission reduction. The combustion of C2G UBF produces lower but coarser PM emissions [181]. In general it could be inferred from the previous analysis that:

1. Unlike the BL fuel, PD $PM_{2.5}$ emission contains around 75% EC and less than 20% VOF.
2. The use of C2G in the BL fuel reduces the $PM_{2.5}$ EF by 65% at 15.5 tonne gross vehicle weight (GVW) and 54% as the payload is doubled to 31 tonnes. These results are consistent to those obtained from the PM size segregation system as shown in 3 below.
3. PM size segregation analysis shows that BL fuel produces 65.5% less $PM_{2.1}$ than PD at 15.5 tonne GVW and 52% less $PM_{2.1}$ at 31 tonne GVW.
4. EC EF for $PM_{2.5}$ is reduced by 85% at 15.5 tonne GVW and it decreases to 71% as the payload is doubled to 31 tonne.
5. VOF EF as a component of the $PM_{2.5}$ increases as the HGV was operated on the BL fuel by 46% and 36% depending on the HGV payload the higher the load the lower the VOF emission.
6. The most $PM_{2.5}$ component affected by the presence of C2G UBF in the BL fuel is the EC which is reduce by more than 70%.
7. Statistical analysis showed that SFC is the strongest variable that affect $PM_{2.5}$ emissions. The analysis also revealed that PD has higher propensity to $PM_{2.5}$ emission especially the EC component.
8. The ratio of $PM_{2.1}/PM_{10}$ is 87.6% and 74% for PD and the BL fuel respectively at 15.5 tonne GVW.
9. The ratio of $PM_{2.1}/PM_{10}$ is 77% and 68.5% for PD and BL fuel respectively at 31 tonne GVW.
10. Most of the PD PM mass lies in the smaller size ranges, or PD produces more PM of the size range below 2.1 μm .
11. TGA for $PM_{0.4}$ indicated that BL fuel produces less EC component than PD especially at high HGV payloads.
12. A loaded HGV moving downhill produces more PM emissions.

In order to explain the above conclusions, it is quite useful to demonstrate some of in-vitro analysis related to the differences of fuel properties as listed in table 6.12 and explained below

1. Fuel GC-FID analysis revealed that carbon to hydrogen ratio is almost the same for PD and C2G UBF which is 52%.
2. Although CHNS analysis for the fuels showed 12.44%wt lower carbon content in C2G UBF than PD, the hydrogen content is also lower by 10.7%wt. The analysis also indicated 11.94%wt oxygen content in C2G UBF which doesn't exist in PD.
3. The absence of sulphur in C2G UBF while it represent about 0.3%wt of the ULSF.
4. The stoichiometric A/F ratio is 12.2 for C2G UBF compared to 14.7 for the PD. This makes the UBF combustion always 2.5 A/F ratio units leaner.

Table 6.12 In-vitro analysis for C2G UBF and PD chemical structure and thermal properties.

Fuel type	GC-FID		CHNS analysis					CN
	Formula	C/H	HHV kg/kJ	LHV kg/kJ	C % wt	H % wt	O % wt	
C2G UBF	$C_{18}H_{34}O_2$	0.529	39.348	36.802	75.727	12.035	11.939	53 ⁽¹⁾
PD	$C_{12}H_{23}$	0.522	43	40.454	86.49	13.48	0	52 ⁽²⁾
Variation	%	1.341	-8.493	-9.028	-12.44	-10.7	11.939	1.923

(1) Anand et al. [51]

(2) UK market PD specifications

High soot formation is expected from C2G UBF at the early stages of the combustion process during fuel pyrolysis due to the high carbon content [95]. In fact the higher oxygen content enhances soot oxidation at higher temperatures [97]. This higher oxygen content affects the AF ratio in a way that C2G UBF possesses a stoichiometric AF ratio of 12.2 which makes it, intrinsically, 2.5 units leaner than PD. This will drive to a lean premixed combustion process. On the other hand, the relatively high hydrogen content could produce the hydroxyl radicals OH. OH radicals react with the aromatics to hinder the growth of polycyclic aromatic hydrocarbons (PAH) the precursors of soot. The OH radicals also react for further soot oxidation and conversion to CO at the higher temperature diffusion flames at the flame periphery [98].

The reason why C2G UBF is producing relatively higher VOF than C, especially for PM larger than 3.3 μm , could be affiliated to the lower heating value of C2G UBF which is 8.5% lower than its counterpart from PD which results in a lower combustion temperature. The higher cetane number (CN) of C2G UBF, 2% higher than PD CN, increases the rate of heat release to peak close to the TDC. This early and low temperature combustion would end at the beginning of power stroke leading to a cooler global in-cylinder environment along the power stroke. Bearing in mind that the rate of particle growth is inversely proportional to the global temperature [25] [90] [91], therefore there is more chance for the VOF particles to form, condense and to coagulate in the case of the BL fuel.

The effect of C2G UBF on PM reduction is more apparent at higher loads. The engine temperature is higher as the HGV is operated at high loads. This would lead to a higher combustion efficiency (lower SFC). Therefore, lower unburnt hydrocarbon (HC) from fuel and lube oil is expected [101]. At the same time the injection pressure is higher leading to a finer fuel atomisation with a larger injection cone angle [18]. This accelerates the premixed combustion phase which is considered as an adiabatic process by limiting the amount of heat dissipation in radiation. Therefore the higher temperature diffusion flame mitigates the soot [99].

Chapter 7

Quantitative and qualitative comparison for engine gaseous emissions produced from the utilisation of C2G UBF as a surrogate to PD

Gaseous emissions from compression ignition (CI) engines were considered as a threat to the environment and human health [180, 182]. Their mitigation within the engine became a design requirement. Failure to achieve that goal should be compensated by heavy and expensive exhaust aftertreatment facilities [22]. Since the related environmental legislations are progressively becoming more and more stringent over the years, therefore meeting these standards is a real challenge especially when the general trend is directed towards the renewable fuels. In fact using the existing diesel technologies, which were profoundly designed to operate on petroleum diesel (PD), to operate on a fuel-like oil of unsecured source is a dilemma from the engineering point of view.

In this context, and as the environmental performance of used cooking oil in HGV is the aim of this project, the study entirely focused on carbon dioxide (CO₂) as a greenhouse gas as a part of the UK's efforts to decrease the carbon foot print [183]. Other gaseous emissions considered in the project are the emissions regulated under EURO V standards as the HGV under investigation is categorised under these standards.

A special attention was paid to nitrogen oxides due to the trade-off between NO_x and the particulate matter (PM) which lead engine manufacturers to adopt various strategies to compromise between these two emissions as demonstrated in chapter two. The test heavy goods vehicle (HGV), Mercedes-Benz Axor-C 2543, selected to suppress PM within the combustion process and attached the selective catalytic reduction (SCR) as the exhaust gas aftertreatment system to tackle NO_x emissions. However, using the SCR as NO_x aftertreatment facility has its own effects on NO_x emissions. In fact there is a mutual interaction between SCR and the exhaust gases. The catalyst in the SCR is heated by the exhaust gases to become fully active at temperatures around 300°C. This increases the SCR efficiency in NO_x removal. Therefore, any reduction in the exhaust gas temperature will be reflected on SCR performance associated by a time lag to recover its previous high performance status.

Using purified used cooking oil, known as C2G UBF, in the blends with petroleum diesel (PD) deeply concerned the fuel manufacturer and the fleet

operator evenly. To be accepted as a surrogate to PD in HGV, in addition to its high economic value, UBF should provide the evidence of being environmental friendly and not to deteriorate engine performance and durability which was discussed in Chapters 4 and 5.

The vast majority of researchers in the literature believed that engine-out NO_x complies to Zeldovich theorem that is NO_x is directly proportional to the combustion temperature. Mixture strength is another factor that contribute to NO_x formation. Others believe that rich mixture packets in a lean global environment at a given temperature, is another active factor leading to higher NO_x formation [1].

Gaseous pollutants were measured mainly by the Fourier-Transform Infra-Red apparatus (FT-IR). The exhaust gas sampling probe was installed in the tailpipe at the SCR outlet. The sample probe was fixed at the centre of the pipe cross-section. The gaseous sample was pumped through a heated line to the FT-IR for speciation and the data were logged in a laptop computer. As the SCR is particularly designed to mitigate NO_x emissions, another NO_x detection probe was installed upstream to the SCR. This probe is called the zirconia solid electrolyte (ZSE). It generates electrical signals in proportion to the NO_x concentration in the exhaust gas. The signal is amplified and read by Horriba OBD 1000. Data for vehicle speed, position, direction and elevation from sea level were logged into a second laptop computer. The rate of fuel consumption, fuel temperature and mixing ratio and engine load factor were measured by the Bioltec system and logged in to a third laptop computer.

HGV performance and emission characteristics were calculated for the entire journey as the vehicle was selectively running on PD or the BL fuel. For better understanding of the effects of the BL fuel, special HGV performance conditions were carefully selected. The steady-high speed performance on the M1 motorway was considered since it was characterised by the engine operation at speeds close to the maximum power speed of 1900 rpm and the fuel used was 100% pure UBF when the auto mode was selected. The other feature of this particular road segment is the continuous gradient which was negative for the outbound journey from Ashby De La Zouch to Wigston (A2W) and positive in the other way around. The second interesting road segment was the 240 m long ramp to merge on M1 motorway. This segment is characterised by the 3% positive gradient on which the HGV accelerates from a very low speed to reach 83~96 km/h. The lower boundary is the one recommended by the fleet operator while the upper boundary is the maximum

allowable UK national speed limit for HGV's. The HGV is expected to operate around the speed of maximum torque (1100 rpm) throughout this section.

The average UBF/PD ratio in the fuel blends varies from 76% to 93% depending on the engine start temperature, the ambient temperature and the HGV payload. An average of 84.5% is considered for the entire journey.

Data from the aforementioned operational conditions were statistically analysed to understand the type and strength of the correlation between the variables and how they are affected by the type of fuel, precisely the gaseous emissions.

7.1 Gaseous emissions from the HGV during the whole journey

7.1.1 Physical analysis for the observed variations in HGV emissions and performance caused by switching from PD to the BL fuel

According to the previous demonstration in chapter four, a good harmony and correlation exists between engine-out temperature (EoT), engine load factor (LF) and the rate of fuel consumption. Fig.7.1 depicts the history of downstream SCR NO_x emissions from the HGV engine as the vehicle payload was 31 tonne. This was for a typical outbound journey from the United Biscuits Midlands Distribution Centre in Ashby De La Zouch heading towards Wigston. High combustion temperature is a major enhancement factor for NO_x formation according to Zeldovich [56]. It is true that the measured engine-out temperature follows that of the combustion, but it doesn't reflect exactly the detailed temperature effects during each combustion process. Therefore the amount of NO_x emitted is not necessarily always related to high EoT as shown in fig.7.1. The role of the exhaust gas temperature is more likely to affect the performance of the SCR system. It is quite clear that NO_x emissions for the first eight minutes of the journey are relatively high compared to the rest of the journey. This is attributed to the cold SCR system because SCR works efficiently at temperatures around 270°C. Any fluctuation in tailpipe NO_x emissions is primarily related to the variations in the road load and the amount of fuel delivered to the engine due to the drivers assessment and the traffic regulations. It was observed that the SCR performed very poorly for the first 6~7 minutes of each cold start journey even though the engine was warm to its specified design temperature.

Fig.7.1 is an arbitrarily chosen journey identified in the chart title as (17032014-A2W-1802-BL-LT) actually this could be decoded to (Date of journey-Journey direction-time-type of fuel-type of load). The general trend in fig.7.1 is, the higher the temperature the higher the SCR NO_x dissociation efficiency and the lower the amount of NO_x emitted from the tailpipe. In fact some deviations from this general criteria could be indicated especially when low amounts of fuel were originally delivered to the engine as the HGV travelled on a declining road segment (moving downhill). The higher the payload the greater the potential energy possessed by the vehicle at the hill top. Therefore during the downhill travel, the vehicle converts its potential energy to kinetic energy and there is less dependence on fuel energy.

This will reduce the amount of fuel consumed, the combustion temperature and the amount of NO_x generated. However, it also reduces the gas temperature and ultimately the SCR temperature. The net effect is reduced SCR NO_x dissociation efficiency and a sudden increase in NO_x from the tailpipe is indicated.

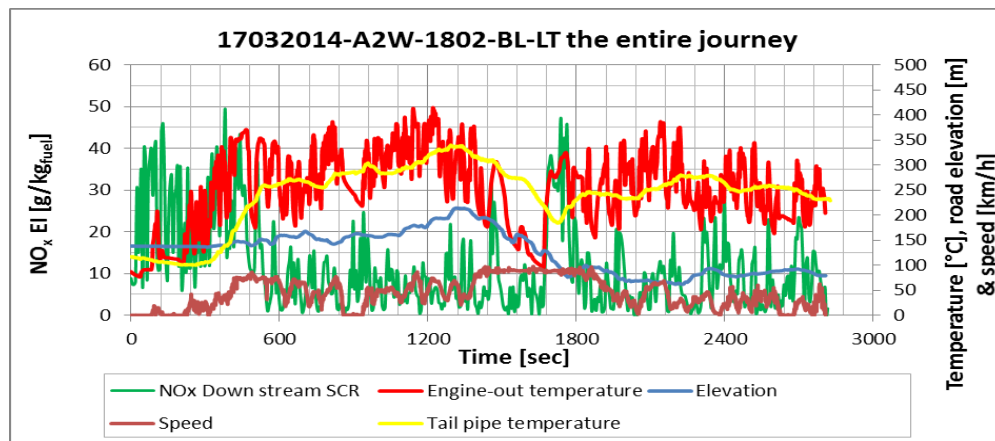


Figure 7.1 NO_x downstream SCR emissions, engine-out temperature, road elevation and HGV speed during a real world journey from Ashby de la Zouch towards Wigston. The vehicle payload is 31 tonnes. 86.5% of the journey's fuel is C2G UBF.

A thorough investigation of fig.7.2 shows that NO_x emissions downstream to SCR is very much related to the rate of fuel consumption, however some areas of low fuel consumption rate and high NO_x emissions could be spotted on the graph. These are mainly due to the lower SCR temperatures due to a cold start or vehicle downhill travel followed by a sudden power demand.

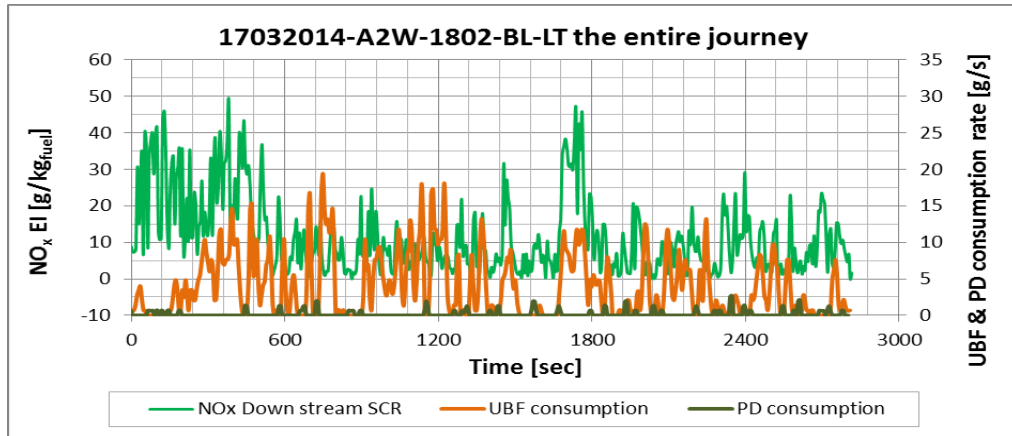


Figure 7.2 NO_x downstream to SCR emissions vs the amount of fuel consumed during a real world journey from Ashby De La Zouch to Wigston. The vehicle payload is 31 tonnes and 86.5% of the journeys fuel is C2G UBF.

7.1.2 Statistical analysis for the observed variations in HGV emissions and performance caused by the BL fuel in comparison to PD

Data obtained from the various measurement instruments were time aligned for event consistency as explained in section 3.11. This was followed by data analysis and representation. The statistical analysis helped to find the variables that significantly affected the targeted emissions. Analysis of variance was performed to indicate any significance differences between the BL fuel and PD on the emissions.

Table 7.1 Analysis of variance for BL fuel and PD and their effects on gaseous emissions.(The whole journey is considered). [g/kWh]

Emissions	TYPE OF FUEL	N	Mean	Std. Deviation	Std. Error Mean
NO _x Up stream SCR	BL	20	23.1245	26.2114	5.8611
	PD	12	18.7102	16.7907	4.8470
NO _x Down stream SCR	BL	20	2.0526	1.2379	0.2768
	PD	12	0.9996	0.8494	0.2452
CO	BL	20	0.5217	0.2709	0.0606
	PD	12	1.7843	2.1749	0.6278
CO ₂	BL	20	343.4487	147.6106	33.0067
	PD	12	282.9342	111.8131	32.2777
THC	BL	20	4.6148	4.0808	0.9125
	PD	12	3.3887	2.9441	0.8499

The variables included in the statistical analysis are, type of fuel (ToF), type of load (ToL), engine-out temperature (EoT), vehicle specific power (VSP), vehicle velocity (V), gross vehicle weight (GVW), trip direction (DIR), NO_x downstream SCR, NO_x upstream SCR, CO, CO₂ and THC.

A comparison between the mean values reveals higher NO_x upstream to SCR emissions from the BL fuel, with a reasonable difference in standard deviation. The difference in mean value is much higher in the NO_x downstream to SCR. A considerable reduction in CO is indicated for the favour of BL fuel but the difference in STDEV is also high which reduces its reliability. Higher CO₂ from BL fuel is indicated from the difference in the mean values. THC is also higher for the BL fuel.

Table 7.2 t-test for equality of means for the effect of fuel type, BL fuel compared to PD, on gaseous emissions (g/kWh) through the entire test series.

Independent Samples Test					
Emissions (Equal variances assumed)	t-test for Equality of Means				
	t	df	Sig. (2- tailed)	Mean Difference	Std. Error Difference
NO _x Up stream SCR	.340	30	.736	4.4143	1.0140
NO _x Down stream SCR	1.922	30	.064	1.0530	0.0316
CO	-2.400	30	.023	-1.2626	-0.5673
CO ₂	.757	30	.045	60.5145	0.7291
THC	-1.522	30	.138	1.2261	0.0626

The table shows a significant difference in the CO emissions between the two fuels but the difference is regarded as meaningless due to data scatter. Multi-regression analysis for the combined effects of fuel and vehicle performance parameters on the emissions are shown in tables 7.3 to 7.7.

Table 3.7 exhibits the most influential factors on engine-out NO_x. After six repetitions using the backward method, the best model was predicted by the type of vehicle load (ToL), GVW and SFC. The three variables were very highly significant (VHS) predictors, nevertheless ToL and GVW are over

correlated as they possess high VIF, while SFC possesses the strongest weight.

Analysis of variance (ANOVA) shows that the model is VHS as $F(3,28) = 25.4$ and $p = .000$. The adjusted $R^2 = 0.702$ for the predicted model which means that the model accounted for 70% of NO_x Upstream SCR variances.

Table 7.3 Multi-regression analysis and ANOVA for the effect of fuel type and other performance parameters on engine-out NO_x . across the entire test series. Data based on 32 trips.

Regression NO_x upstream SCR							
Coefficients							
Model		Unstandardized Coefficients	Sig.	Decision	Collinearity Statistics		
		B			VIF		
6	(Constant)	-0.07964					
	Type of Load (1 for ET and 2 for LT)	0.149621	.000	VHS	10.93		
	Gross Vehicle Weight [tonne]	-0.0087	.001	VHS	10.848		
	Specific Fuel Consumption [kg/kWh]	0.52232	.000	VHS	1.555		
a. Dependent Variable: NO_x upstream [g/kWh]							
Adjusted R Square = 0.702							
NO_x upstream SCR = - 0.07964 + 0.149621 ToL - 0.0087 GVW + 0.52232 SFC							
Best model obtained after six (6) repetitions, using backward method							
ANOVA							
Model		Sum of Squares	df	Mean Square	F	Sig.	Decision
6	Regression	0.07142	3	0.02381	25.398	.000	VHS
	Residual	0.02624	28	0.00094			
	Total	0.09766	31				

Table 7.4 is specified to the NO_x emissions from the tailpipe or downstream to the SCR. After 5 repetitions using the backward method, type of fuel (ToF), vehicle velocity (V), vehicle specific power (VSP), and specific fuel consumption (SFC) are the most influential factors on vehicle NO_x emissions. Among the predictors, SFC has the strongest weight in the model. The adjusted $R^2 = 0.856$ which means that the model accounts for 85.6% of NO_x variance. ANOVA indicated that the model is VHS. $F(4,27) = 47$ and $p = .000$. As number (1) was assigned to BL fuel and (2) for PD, with the presence of the negative sign, this means more NO_x is produced from the BL fuel.

Table 7.4 Multi-regression analysis and ANOVA for the effect of fuel type and HGV performance parameters on NO_x downstream to SCR through the entire test series. Data based on 32 trips.

Regression NO _x downstream							
Coefficients							
Model		Unstandardized Coefficients	Sig.	Decision	Collinearity Statistics		
		B			VIF		
5	(Constant)	-4.95E-05					
	Type of Fuel (1 for BL fuel and 2 for PD)	-0.00126	.007	HS	1.029		
	Vehicle Speed [km/h]	-1.70E-04	.006	HS	1.589		
	Vehicle Specific Power [kW/ton]	0.00129	.003	HS	3.71		
	Specific Fuel Consumption [kg/kWh]	0.04052	.000	VHS	3.124		
a. Dependent Variable: NO _x downstream [g/kWh]							
Adjusted R Square = 0.856							
NO_x downstream SCR = - 4.953E-05 - 0.00126 ToF - 0.00017 S + 0.00129 VSP + 0.04052 SFC							
Best model obtained after five (5) repetitions, using backward method							
ANOVA							
Model		Sum of Squares	df	Mean Square	F	Sig.	Decision
5	Regression	0.00026	4	6.40E-05	46.9937	.000	VHS
	Residual	0.00004	27	1.00E-06			
	Total	0.00029	31				

Table 7.5 Multi-regression analysis and ANOVA for the effect of fuel type and HGV performance variables on CO emissions throughout the entire test series. Data based on 32 trips.

Regression CO Emission							
Coefficients							
Model		Unstandardized Coefficients	Sig.	Decision	Collinearity Statistics		
		B			VIF		
8	(Constant)	-0.0013					
	Type of Fuel (1 for BL fuel and 2 for PD)	0.00188	0.023	S	1		
a. Dependent Variable: CO Emission [g/kWh]							
Adjusted R Square = 0.133							
CO = - 0.00130 + 0.00188 ToF							
Best model obtained after eight (8) repetitions, using backward method							
ANOVA							
Model		Sum of Squares	df	Mean Square	F	Sig.	Decision
8	Regression	0.00003	1	0.00003	5.762	0.023	S
	Residual	0.00014	30	0			
	Total	0.00016	31				

Table 7.5 shows that the type of fuel is the only variable that significantly affected CO emissions. After 8 repetitions using the backward method the obtained model has $R^2 = 0.133$ or the model accounts for 13.3% of CO variances unless other variables are affecting CO emissions which are substantially not included in the analysis. ANOVA reveals that the model is significant as $F(1,30) = 5.762$ at $p = .023$. The model suggested that PD produces higher levels of CO compared to the BL fuel.

Table 7.6 Multi-regression analysis and ANOVA for the effect of fuel type and HGV performance parameters on CO₂ emissions throughout the entire test series. Data based on 32 trips.

Regression CO ₂ Emission							
Coefficients							
Model	Unstandardized Coefficients	Sig.	Decision	Collinearity Statistics			
				B	VIF		
8	(Constant)	-0.05248					
	Specific Fuel Consumption [kg/kWh]	1.92862	.000	VHS	1		
a. Dependent Variable: CO ₂ Emission [g/kWh]							
Adjusted R Square = 0.871							
CO₂ = - 0.05248 + 1.92862 SFC							
Best model obtained after eight (8) repetitions, using backward method							
ANOVA							
Model	Sum of Squares	df	Mean Square	F	Sig.	Decision	
8	Regression	0.91439	1	0.91439	210.895	.000	VHS
	Residual	0.13007	30	0.00434			
	Total	1.04446	31				

Table 7.6 shows the multi-regression analysis for CO₂ as the dependent variable. All the aforementioned variables were included in the analysis. After 8 repetitions using the backward method, SFC was selected as the only predictor for CO₂ model. SFC is a VHS predictor and has a strong weight. The model has an adjusted $R^2 = 0.871$ which means that the model accounts for more than 87% of the CO₂ variances. ANOVA suggested that the model is VHS, $F(1,30) = 210.895$ at $p = .000$.

Setting total hydrocarbons (THC) as the dependent variable, the multi-regression analysis and ANOVA for the aforementioned variables of the whole journey is presented in table 7.7. After 7 repetitions using the backward

method, the THC model was built on two predictors. ToF and SFC were selected by the model in which SFC shows VHS and possesses the strongest weight. The adjusted $R^2 = 0.556$ which means that the model accounts for 55.6% of THC variance. ANOVA shows that the model is VHS and $F(2,29) = 20.412$ at $p = .000$. ToF and SFC are directly proportional to THC.

Table 7.7 Multi-regression analysis and ANOVA for the effect of fuel type and HGV performance parameters on THC emissions during the entire test series. Data are based on 32 trips.

Regression Total Hydrocarbon							
Coefficients							
Model		Unstandardized Coefficients	Sig.	Decision	Collinearity Statistics		
		B			VIF		
7	(Constant)	-0.06427					
	Type of Fuel (1 for BL fuel and 2 for PD)	0.04956	0.005	HS	1.0195		
	Specific Fuel Consumption [kg/kWh]	0.53822	.000	VHS	1.0195		
a. Dependent Variable: Total Hydrocarbon [g/kWh]							
Adjusted R Square = 0.556							
THC = - 0.06427 + 0.04956 ToF + 0.53822 SFC							
Best model obtained after seven (7) repetitions, using backward method							
ANOVA							
Model		Sum of Squares	df	Mean Square	F	Sig.	Decision
7	Regression	0.07961	2	0.0398	20.412	.000	VHS
	Residual	0.05655	29	0.00195			
	Total	0.13616	31				

7.1.3 Analysis for the correlations suggested by the multi-regression models and their effect on HGV emissions

In general, the real world tests showed that tests performed by BL fuel (84.5% UBF content on average) produced higher levels of NO_x . Fig.7.3 shows a clear difference between the NO_x emission factor (EF) for the two fuels at all vehicle payloads and road loads. The net difference varies depending on the type of load (ToL) and a maximum of 123% is observed in the empty trailer on the inbound journey from Wigston (ET-W2A).

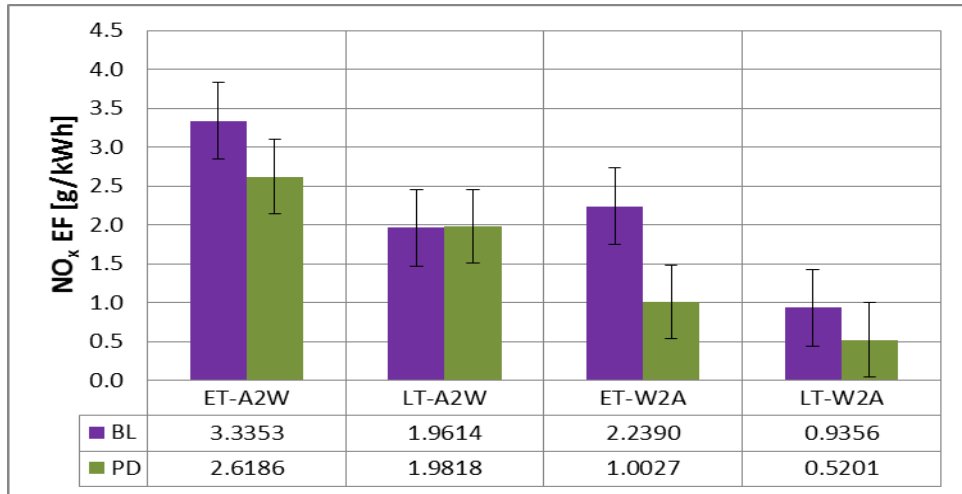


Figure 7.3 NO_x EF at the tailpipe of a HGV fuelled with BL fuel and PD. Data based on 32 real world trips. ET and LT are the HGV empty trailer and loaded trailer respectively. A2W is the outbound journey from Ashby to Wigston while W2A is the inbound journey.

Increasing the payload reduces the NO_x EF for BL fuel and PD by 58% and 48% respectively. The road load also reduces the NO_x EF by more than 50% for the BL fuel and more than 70% for the PD.

The NO_x EF is high at low HGV power demands as shown in fig.7.4. The higher the power demand the lower the tailpipe NO_x EF.

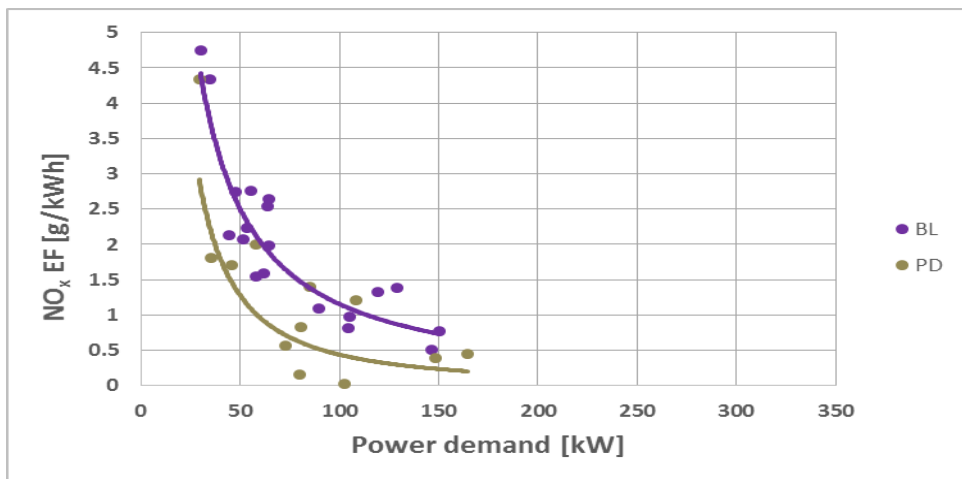


Figure 7.4 Tailpipe NO_x emission factor vs vehicle power demand obtained from real world HGV tests. The graphs compare between NO_x EF from BL fuel and PD. Data based on 32 real world trips.

NO_x EF is also directly proportional to the specific fuel consumption SFC as plotted in fig.7.5.

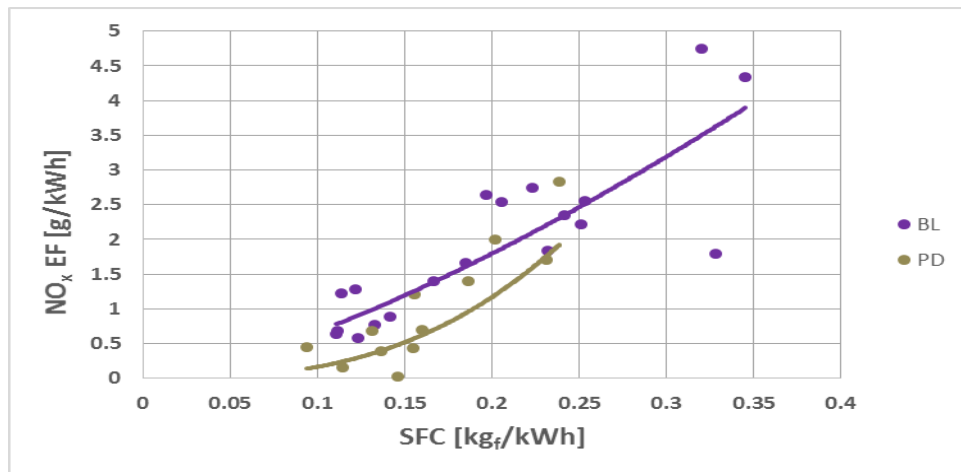


Figure 7.5 NO_x emission factor vs vehicle specific fuel consumption obtained from real world HGV tests. The graphs compare between NO_x EF from BL fuel and PD.

Actually SFC is the indicator of the efficiency of fuel conversion to energy. The higher the power demand the lower the SFC (as explained in chapter 4 Fig.4.9).

There is a possible confusion between the amount of NO_x emitted and the NO_x emission factor (NO_x EF). High NO_x emissions are most likely related to higher combustion temperatures. In diesel engines, higher combustion temperatures occur at high power demand. In this case more fuel is injected at higher pressures (in pump-line-injector system) and better fuel atomisation is obtained. This reduces the physical delay period which will result in an adiabatic low radiation premixed combustion followed by a high temperature diffusion flame to produce more NO_x [16].

The other scenario is that NO_x emissions maximise at equivalence ratio close to unity ($\varphi = 1$). Diesel combustion is generally lean, however, due to the late in-cylinder fuel injection, rich mixture packets form. When these rich packets burn they produce lower levels of NO_x. The sooner the packets burn the richer they are and lower NO_x is produced [1]. Therefore by increasing the load the injection pressure increases in the pump-line-injector system. This will break down the packets to smaller and leaner packets (perhaps individual spherules) to be closer to the stoichiometric condition where high NO_x is produced.

NO_x EF is the mass of NO_x produced per unit energy produced. Bearing in mind, that SFC is also the mass of fuel per unit energy produced. Therefore at higher loads when the SFC is lower because of the improved efficiency of combustion, the NO_x EF should also be lower.

The above analysis is true for the tailpipe NO_x emissions except that the higher exhaust gas temperature increases the SCR NO_x removal efficiency. Therefore tailpipe NO_x is lower at higher loads or power demands.

The higher NO_x emissions from the BL fuel could arguably be related to the nitrogen embedded in the fuel itself (see table 5.5). The BL fuel has a longer physical ID period due to its high viscosity and poorer atomisation characteristics compared to PD [126]. This gives the BL fuel more time to transfer deeper in the combustion chamber and form leaner mixtures with the surrounding air. On the other hand, the distillation temperature of the BL fuel components is very close to each other (see fig.2.1) which makes the whole fuel components evaporate nearly at the same time. This significantly shortens the premixed flame duration as it is taking place under adiabatic conditions. Therefore no heat is dissipated by radiation and most of the combustion heat is released throughout the diffusion flame to produce very high temperatures and higher levels of NO_x compared to PD [16]. The CHNS-O analysis revealed (see table 5.5) that there is 11.9% O₂ imbedded in the UBF which doesn't exist in PD. This results in a substantially leaner combustion of the BL fuel (about 2.5 units of A/F ratio). As a result, the combustion of the BL fuel is closer to equivalence ratio of unity ($\varphi = 1$) where NO_x reaches its maximum (see fig.2.10) [1, 57].

A comparison between CO₂ emissions from the two fuels at different loads is illustrated in fig.7.6. The BL fuel produces 11% higher levels of CO₂ than PD for ET, this difference increases to 56% at LT in the outbound journey. This is an inevitable result of better oxidation of CO and combustion of the elemental carbon due to the higher O₂ content in the UBF and the injection characteristics of UBF. Increasing the payload reduces CO₂ EF due to the decrease in SFC at higher loads which is an indicator of the improved efficiency of combustion as seen in fig.7.7.

During the inbound journey (columns 3 and 4) a slightly tangible difference is indicated between the two fuels and the combination of the payload and road load furtherly supresses CO₂ emissions (column 4 in fig.7.6). The total reduction in CO₂ EF between the outbound ET and the inbound LT is 65% and 57% for the BL fuel and PD respectively.

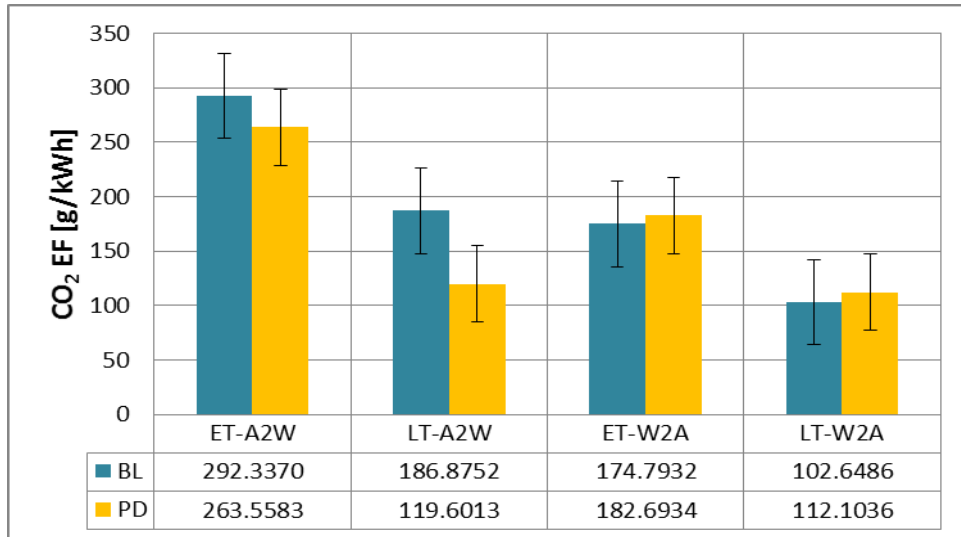


Figure 7.6 CO₂ EF from real world tests of a HGV fuelled by BL fuel and the PD. Data based on 32 real world trips. ET and LT are the HGV empty trailer and loaded trailer respectively. A2W is the outbound journey from Ashby to Wigston while W2A is the inbound journey.

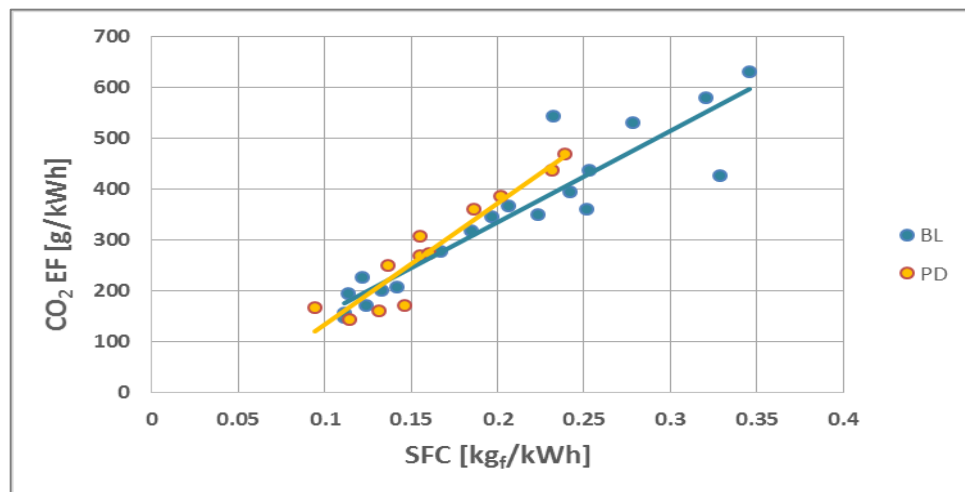


Figure 7.7 CO₂ EF vs vehicle SFC obtained from real world HGV tests. The graphs compare between CO₂ EF from BL fuel and PD.

Total hydrocarbon (THC) emissions from the BL fuel is higher than that of PD especially at low loads. Fig.7.8 shows that THC EF from the BL fuel is about 63% higher than that produced from PD. This difference shrinks to 9% at higher loads (column 4 fig.7.8). In fact increasing the load reduces the THC EF by 69% and 55% for BL fuel and PD respectively. According to the regression analysis for THC, it reveals a significant relation between THC and SFC. A plot of the correlation is illustrated in Fig.7.9.

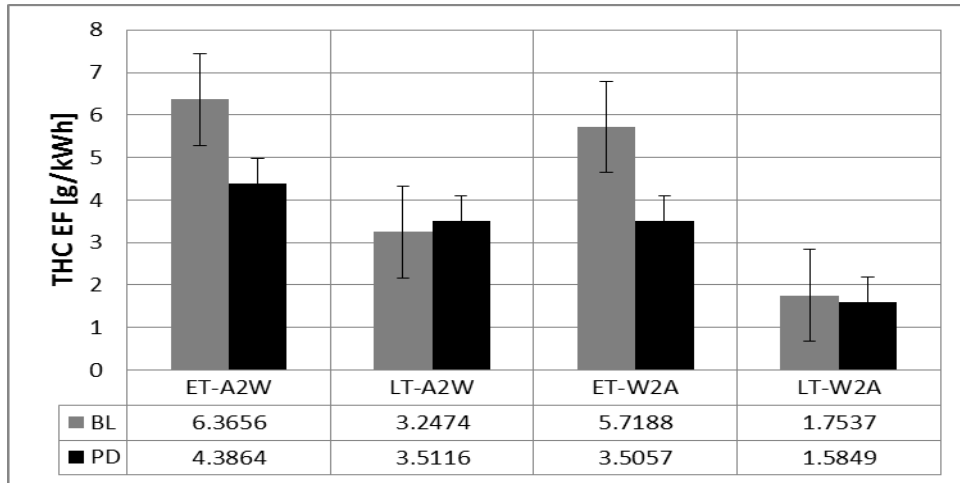


Figure 7.8 THC EF from real world tests of a HGV fuelled by BL fuel and the PD. Data are based on 32 trips. ET and LT are the HGV empty trailer and loaded trailer respectively. A2W is the outbound journey from Ashby to Wigston while W2A is the inbound journey.

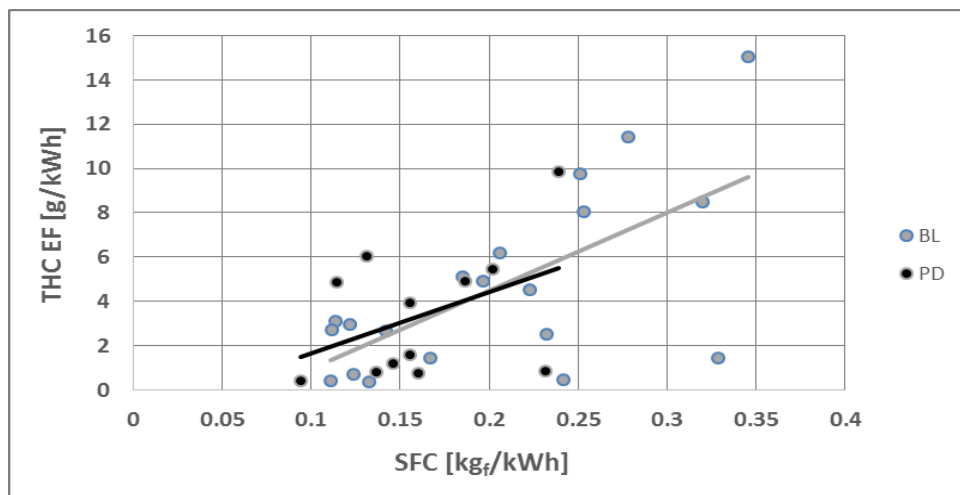


Figure 7.9 THC EF vs SFC obtained from real world HGV tests. The graphs compare between THC EF from BL fuel and PD. Data are based on 32 real world trips.

A direct proportionality between THC EF and SFC is indicated, the lower the SFC the lower the THC EF for both of the fuels. This could be attributed to the improved combustion characteristics indicated by lower SFC.

The difference in THC at low loads could arguably be related to the differences in the fuel properties which affects the injection and combustion characteristics. There is a trade-off between the THC and the VOF, especially the heavy end distillates, emitted as PM for both of the fuels.

7.2 Gaseous emissions from the HGV travelling at steady-high speed on M1 motorway

7.2.1 Physical analysis of the observed variations in HGV emissions caused by switching from PD to the BL fuel during steady-high speed HGV travel

Modern HGV engine designs included many sophisticated environmental technologies worked to reduce in-cylinder and engine-out emissions. To this context, it is quite interesting to analyse the HGV behaviour under specific operational conditions while using different fuels. In this section, steady-high speed HGV travel is taken under scrutiny. This road segment is characterised by its 12.3 km length and continuous gradient. The difference in road elevation between the two ends is 110 m, therefore the outbound journey, from Ashby De La Zouch to Wigston (A2W) on M1 is a downhill HGV travel. The HGV partially depends on its gravity to travel in this direction. The higher the payload the greater is the potential energy at the top of the hill. The situation is reversed in the return journey because the HGV uses more fuel to climb the hill. In both travel directions, the HGV travels at a constant speed of 83–96 km/h. The engine is running close to the maximum power speed (1900 rpm) at a low gear ratio. The journey fuel is not the BL fuel it is 100% pure UBF as explained in chapter four.

NO_x emissions under steady-high speed conditions is illustrated in fig.7.10. The HGV travelled on M1 motorway at a constant speed around 90 km/h. During this road segment the 31 tonne HGV is moving downhill.

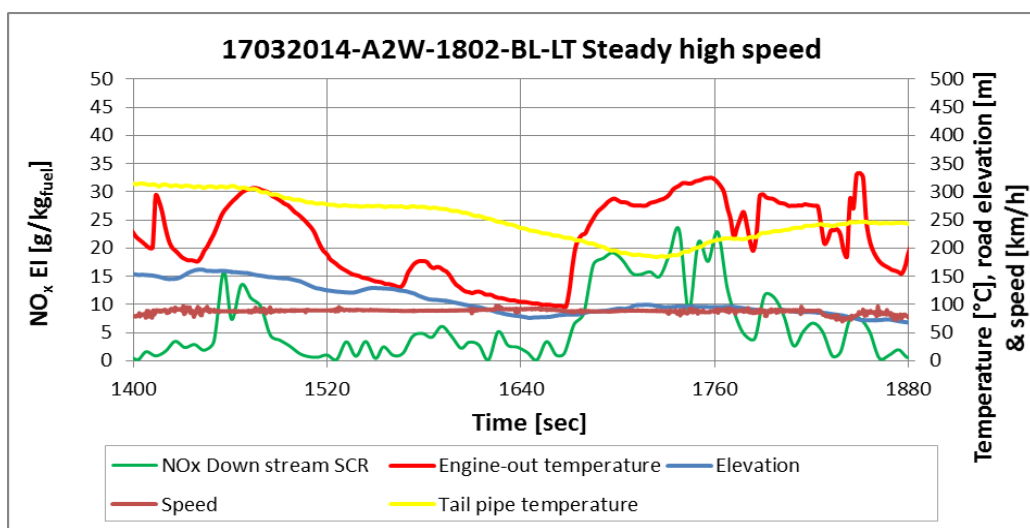


Figure 7.10 NO_x downstream to SCR variation with temperature, vehicle speed and road gradient. Steady-high speed HGV travel on M1 motorway.

The NO_x peaks twice during this interval, both are related to the higher rate of fuel consumption due to minor local road inclinations (see fig 7.4). The second peak looks higher and wider because it is assisted by the lower SCR temperature. This could be indicated from the differences between the EoT and the tailpipe temperature. That difference is utilized in heating the relatively cool SCR.

In other words, moving downhill with lower rates of fuel consumption made the engine to pump cooler exhaust to the SCR. This will obviously cool down the SCR and deteriorate its performance as the power demand increases under any circumstances.

Fig.7.11 shows the tight correlation between NO_x emitted from the tailpipe and the rate of fuel consumption specifically for UBF.

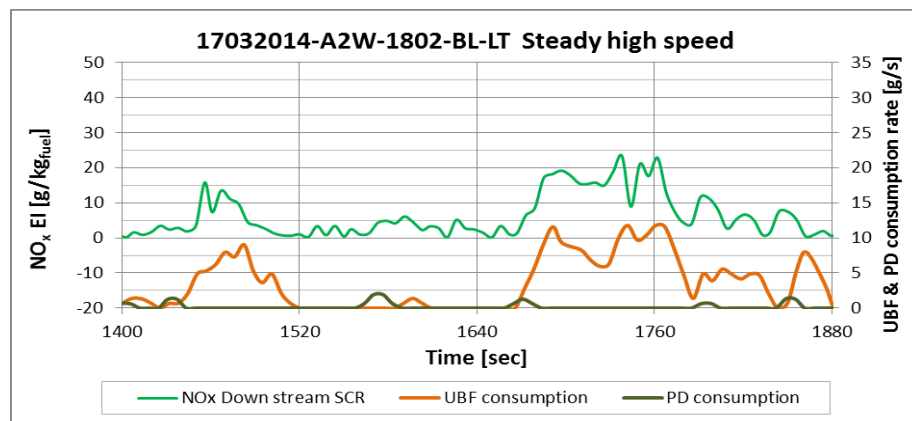


Figure 7.11 NO_x EI downstream to SCR in correlation to the rate of UBF and PD consumption. A HGV moving on M1 motorway at steady-high speed.

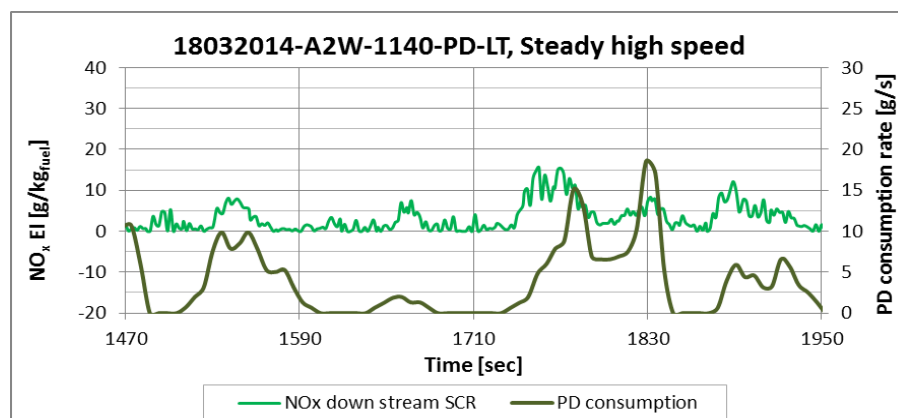


Figure 7.12 NO_x EI downstream to SCR in correlation to the rate of PD consumption. A HGV moving on M1 motorway at steady-high-speed.

Fig.7.12 exhibits the correlation between the tailpipe NO_x EI and the rate of PD consumption for a HGV traveling at steady high-speed on M1 motorway. A comparison with fig.7.11 shows the same correlation between tailpipe NO_x EI and the rate of fuel consumption, the comparison shows lower NO_x EI emitted from PD compared to the UBF.

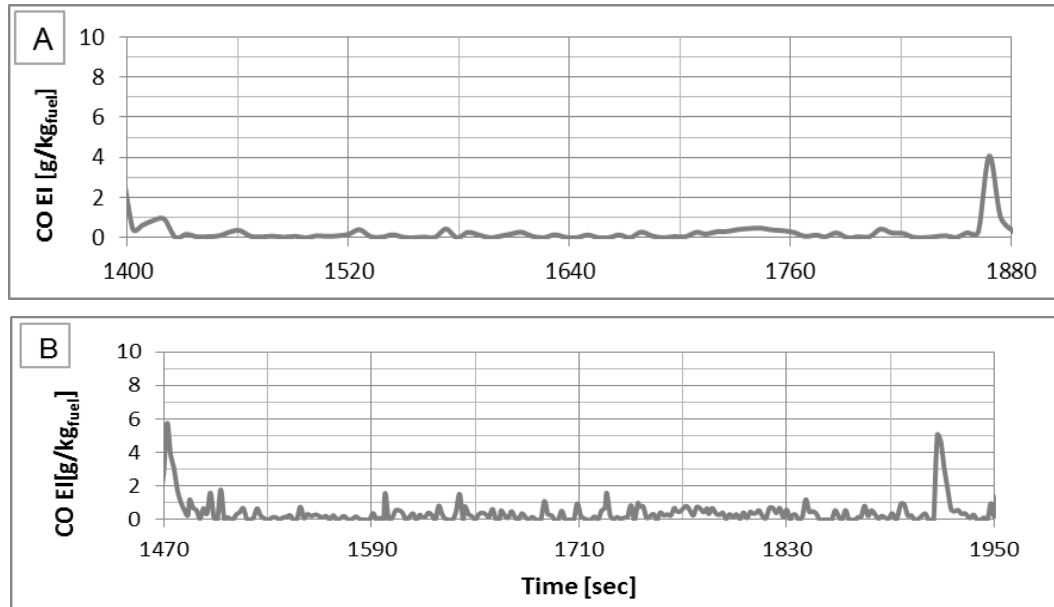
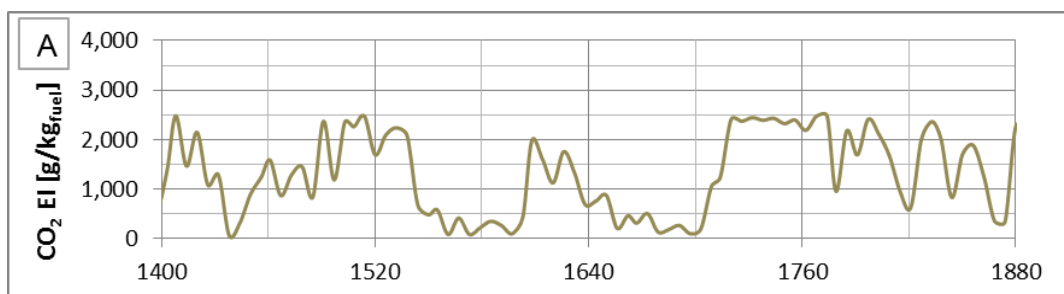


Figure 7.13 Comparison between real world CO EI from (A) UBF and (B) PD from a HGV traveling at steady-high speed on M1 motorway.

A comparison between real world CO emissions from a HGV traveling at a steady high-speed using pure UBF in one trip and PD in the other is demonstrated in fig.7.13. The two instances are in the same direction from A2W. Both of the plots show very low levels of CO EI however plot (A), which represents the UBF case, exhibits lower CO emissions compared to PD. Although the combustion temperature of UBF is lower, by 6% on average on M1, which is expected to lead to higher CO emissions [1], the higher oxygen content in UBF seem to be more effective to change CO into CO_2 .



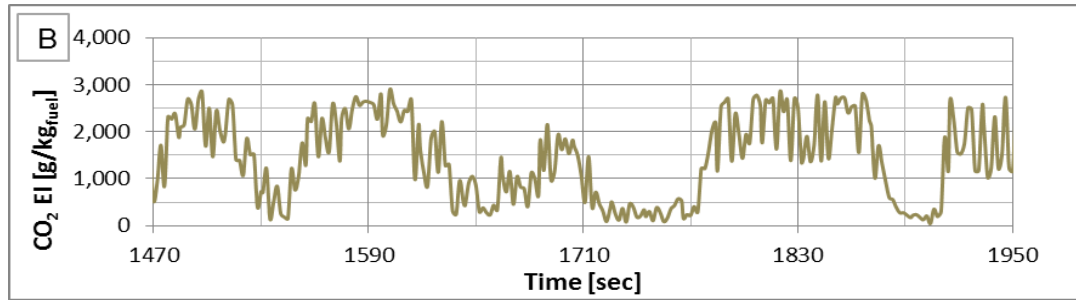


Figure 7.14 Comparison between real world CO₂ EI from (A) UBF and (B) PD from a HGV traveling at steady-high speed on M1 motorway.

Fig.7.14A. is the real world CO₂ EI from the HGV travelling on M1 and fuelled by UBF. The Plot shows lower CO₂ EI from UBF when compared to that of PD in fig.7.14B. Although the engine behaviour was the same, since the two plots are consistent along M1, UBF produces lower CO₂ along this particular part of the journey. This could be attributed to 12.44%wt higher carbon content in PD compared to the UBF.

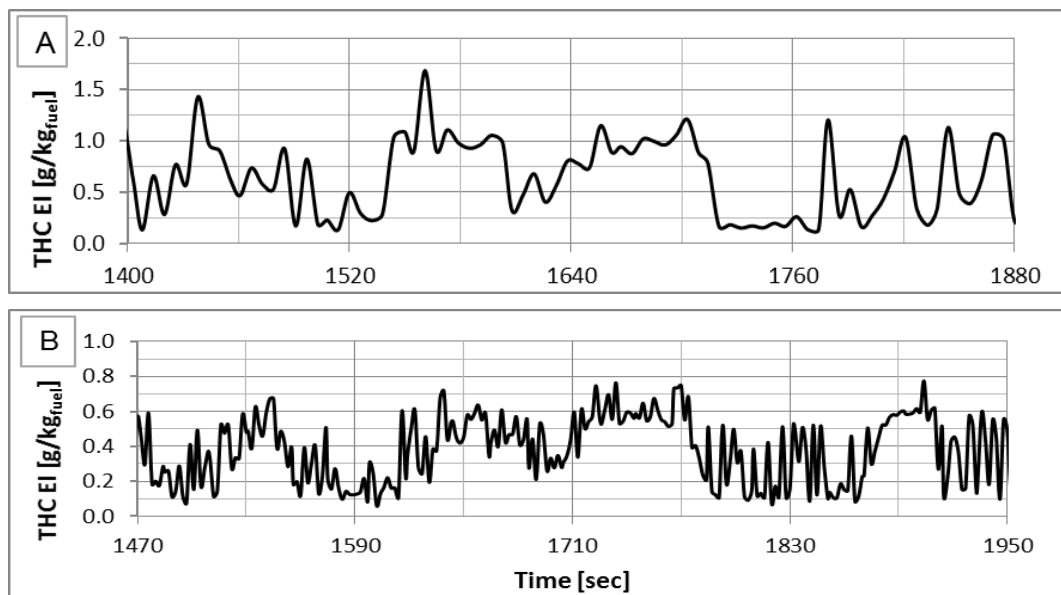


Figure 7.15 Comparison between real world THC EI from (A) UBF and (B) PD from a HGV traveling at steady-high speed on M1 motorway.

Fig.7.15 compares between THC EI for UBF and PD in plots (A & B) respectively. The UBF shows higher peaks but on average PD produces higher THC EI along M1 motorway. The higher peaks in the UBF case could be affiliated to the improper UBF atomisation during the small local transitions that require more fuel injection while the lower average THC EI in the UBF case could be attributed to the leaner combustion of UBF due to the higher oxygen content.

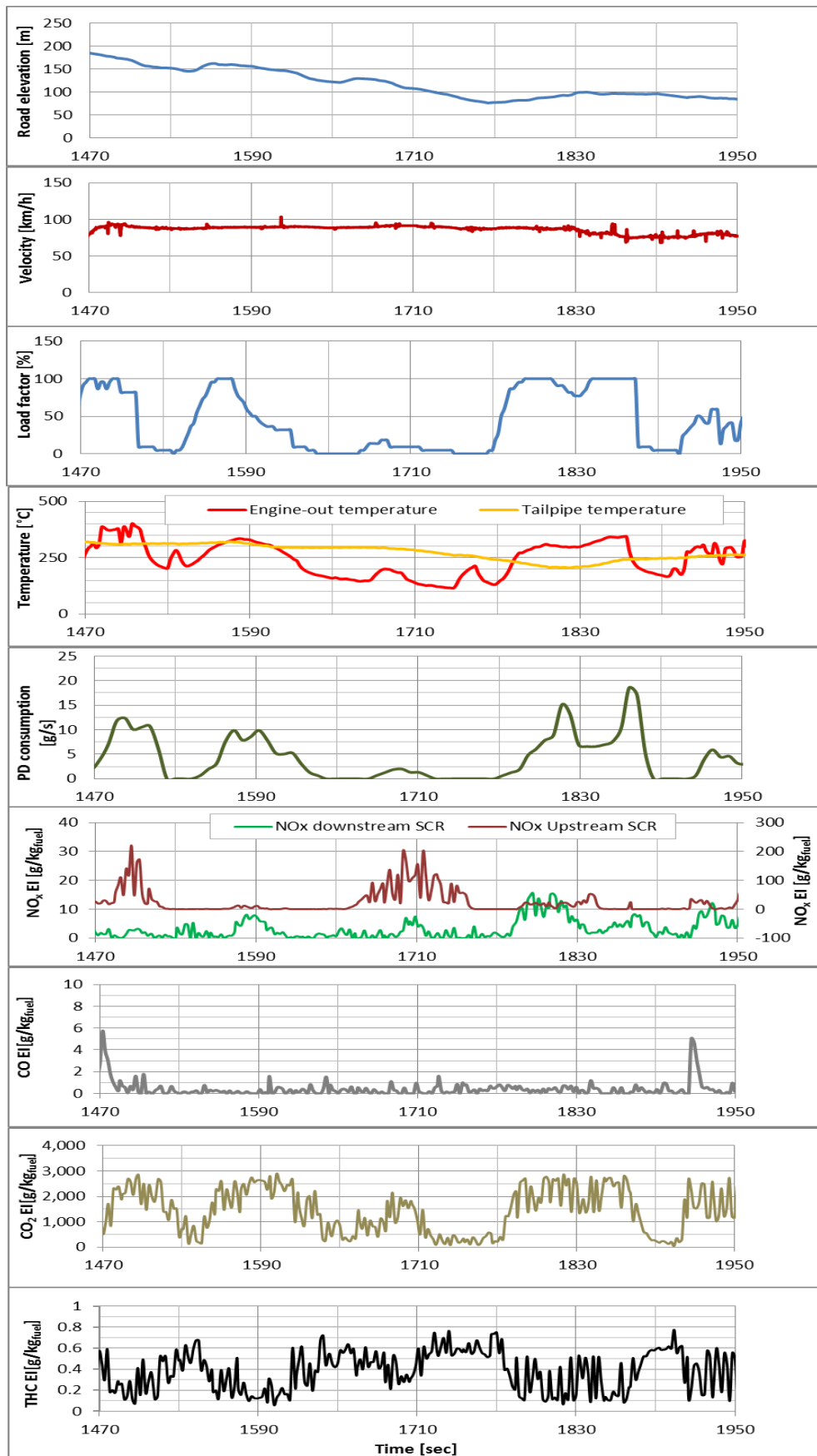


Figure 7.16 HGV gaseous emissions related to engine performance and road load. A sample journey (18032014-A2W-1140-PD-LT)

Fig.7.16 shows a sample for the history of gaseous emissions for a HGV during a steady high speed travel on M1 motorway. The figure shows how the road gradient and minor fluctuations and driver compliance to the UK national speed limits is reflected to engine performance and the emissions through the combustion process. All the events are time aligned as stated in chapter 3 and the emissions are presented in terms of emission index EI in [g/kgf]. The plots show the precise engine response through its load factor (LF) to the fluctuations in road gradient. Before that, is the driver's interference by controlling the rate of fuel consumption. This in return directly affected the combustion temperature as indicated in the EoT.

A thorough investigation for the emissions show that they are correlated to the rate of fuel consumption and combustion temperature. As the HGV is fitted with a selective catalytic reduction (SCR) to tackle NO_x, the NO_x downstream to SCR is also affected by the SCR status.

The higher the rate of fuel consumption, the higher the engine-out temperature (EoT). This is associated by a higher levels of NO_x upstream to SCR and CO₂, while CO and THC are lower.

7.2.2 Statistical analysis for the observed exhaust emissions caused by UBF and PD combustion during steady-high speed HGV travel on the M1 motorway

Statistical analysis for the data obtained from 32 trips on M1 motorway are presented in table 7.8. The table shows considerable differences in emissions mean values due to switching the fuel from PD to UBF. Comparing the means show that UBF EF is 15% higher in engine-out NO_x. The BL fuel doubles the tailpipe NO_x EF of PD. CO EF is about 99% lower for the BL fuel compared to PD. THC EF for the UBF is about 73% higher than that of PD. the increase THC EF is definitely related to the lower overall combustion temperature of UBF. The BL fuel produces about 8% less CO₂ than PD.

Table 7.8 Analysis of variance for UBF and PD and their effects on gaseous emissions.(Steady-high speed HGV travel on M1 Motorway). Analysis base on 32 vehicle trips. Data units are in [g/kWh].

Group Statistics					
EMISSIONS	TYPE OF FUEL	N	Mean	Std. Deviation	Std. Error Mean
NO _x Up stream SCR	UBF	20	27.68092	38.57918	8.62657
	PD	12	23.98262	26.76193	7.72550
NO _x Down stream SCR	UBF	20	1.89237	1.28679	0.28774
	PD	12	0.98677	1.04064	0.30041
CO	UBF	20	0.20061	0.23789	0.05319
	PD	12	1.25379	2.41882	0.69825
CO ₂	UBF	20	387.73575	170.95433	38.22655
	PD	12	422.36781	204.53728	59.04483
THC	UBF	20	8.88946	11.89936	2.66078
	PD	12	5.10901	4.91225	1.41805

Testing the data by 2-tail t-test at 95% confidence, as shown in table 7.9, indicates that UBF is more likely to affect the THC emissions.

Table 7.9 t-test for equality of means for the effect of fuel type on gaseous emissions (Steady-high speed HGV travel on M1). Data units are in [g/kWh].

Emissions (Equal variance assumed)	t-test for Equality of Means				
	t	df	Sig. (2-tailed)	Mean Difference	Std. Error Difference
NO _x Up stream SCR	.292	30	.773	3.6983	.9011
NO _x Down stream SCR	.194	30	.085	.9056	-.0127
CO	.482	30	.063	-1.0532	-.6451
CO ₂	.602	30	.552	-34.6321	-20.8183
THC	-2.148	30	.040	3.7805	1.2427

Multi-regression analyses for all the variables mentioned in section 7.2.2 were performed and the results were tabulated in tables 7.10~7.13. All the table parameters are defined in section 7.2.2.

Table 7.10 shows engine-out NO_x EF as the dependent variable. After four repetitions using the backwards method, the best model is produced by five predictors. Type of load (ToL) and SFC are VHS predictors with SFC having the strongest weight. GVW is also a significant predictor. The adjusted R² =

0.7 which means that the model accounts for 70% of engine-out NO_x variance. ANOVA analysis shows that the model is VHS and $F(5,26) = 15.45$ at $p = .000$.

The GVW is inversely proportional to NO_x EF upstream to SCR, while a direct proportionality is indicated SFC and the NO_x upstream to SCR. Vehicle velocity and VSP are included as predictors to improve the model but they are nonsignificant variables.

Table 7.10 Regression analysis for the effect of fuel type and other performance parameters on engine-out NO_x. (Data exclusively represent the steady high speed HGV travel).

Regression NO _x Upstream SCR							
Coefficients							
Model		Unstandardized Coefficients	Sig.	Decision	Collinearity Statistics		
		B			VIF		
4	(Constant)	0.12491					
	Type of Load (1 for ET and 2 for LT)	0.17959	.000	VHS	11.158		
	Gross Vehicle Weight [tonne]	-0.01	.019	S	12.233		
	Vehicle Speed [km/h]	-0.00591	.063	NS	1.232		
	Vehicle Specific Power [kW/ton]	0.015	.057	NS	6.428		
	Specific Fuel Consumption [kg/kWh]	1.14375	.000	VHS	8.504		
Dependent Variable: NO _x upstream [g/kWh]							
Adjusted R Square = 0.700							
$NO_{x\text{Upstream SCR}} = 0.12491 + 0.17959 \text{ ToL} - 0.01 \text{ GVW} - 0.00591 \text{ S} + 0.01500 \text{ VSP} + 1.14375 \text{ SFC}$							
Best model obtained after four (4) repetitions, using backward method							
ANOVA							
Model		Sum of Squares	df	Mean Square	F	Sig.	Decision
4	Regression	0.10851	5	0.0217	15.448	.000	VHS
	Residual	0.03653	26	0.0014			
	Total	0.14504	31				

Table 7.11 exhibits NO_x downstream to SCR (at the tailpipe) as the dependent variable. The same aforementioned variables were included in the analysis. The best suggested model has two predictors and was obtained after 7 repetitions using the backward method. Trip direction (DIR) is a VHS with the strongest weight followed by GVW. The adjusted $R^2 = 0.43$ which means that the model accounts for 43% of tailpipe NO_x EF variance. ANOVA indicates the model is VHS and $F(2,29) = 12.673$ at $p = .000$. The analysis reveal that the road load is more significant than the payload and they are inversely proportional to tailpipe NO_x EF.

Table 7.11 Regression analysis for the effect of fuel type and other performance parameters on NO_x downstream to SCR. (Data exclusively represent the steady state vehicle travel).

Regression NO _x downstream							
Coefficients							
Model		Unstandardized Coefficients	Sig.	Decision	Collinearity Statistics		
		B			VIF		
7	(Constant)	0.01492					
	Direction (1 for A2W and 2 for W2A)	-0.00371	.001	VHS	1.002		
	Gross Vehicle Weight [tonne]	-2.35E-04	.002	HS	1.002		
a. Dependent Variable: NO _x downstream [g/kWh]							
Adjusted R Square = 0.430							
NO_x Downstream SCR = 0.01492 - 0.00371 DIR - 2.3451E-04 GVW							
Best model obtained after seven (7) repetitions, using backward method							
ANOVA							
Model		Sum of Squares	df	Mean Square	F	Sig.	Decision
7	Regression	0.00023	2	0.00011	12.673	.000	VHS
	Residual	0.00026	29	0.00001			
	Total	0.00048	31				

Table 7.12 Multi-regression analysis for the effect of fuel type and other variables on CO₂ emissions. (Data exclusively represent the steady-high speed HGV travel).

Regression CO ₂ Emission							
Coefficients							
Model		Unstandardized Coefficients	Sig.	Decision	Collinearity Statistics		
		B			VIF		
7	(Constant)	-0.44782					
	Direction (1 for A2W and 2 for W2A)	0.16827	.000	VHS	2.329		
	Specific Fuel Consumption [kg/kWh]	2.74315	.000	VHS	2.329		
a. Dependent Variable: CO ₂ Emission [g/kWh]							
Adjusted R Square = 0.850							
CO₂ = - 0.44782 + 0.16827 DIR + 2.74315 SFC							
Best model obtained after seven (7) repetitions, using backward method							
ANOVA							
Model		Sum of Squares	df	Mean Square	F	Sig.	Decision
7	Regression	0.8615	2	0.43075	88.778	.000	VHS
	Residual	0.14071	29	0.00485			
	Total	1.00221	31				

Carbon dioxide emitted from the HGV at steady high-speed operation is very much affected by the vehicle direction or road load and the SFC as demonstrated in table 7.12. The two variables show very high significance difference in CO₂ emissions, they are directly proportional to CO₂, however, SFC has got the strongest weight. No signs for the type of fuel is indicated which means that ToF makes no significant differences to CO₂ EF during steady high-speed operation. After 7 repetitions using the backward method the suggested model was selected with adjusted R² = 0.85. It means that the model accounts for 85% of CO₂ variance. ANOVA shows that the model is VHS as F(2,29) = 88.778 at p = .000.

CO EF regression analysis from the HGV in steady-high speed conditions doesn't show any correlation with any of the variables. Therefore no model was obtained.

Table 7.13 Regression analysis for the effect of fuel type and other performance parameters on THC. (Data exclusively represent the steady high speed performance).

Regression THC Emissions							
Coefficients							
Model	Unstandardized Coefficients	Sig.	Decision	Collinearity Statistics			
	B			VIF			
6	(Constant)	0.20865					
	Direction (1 for A2W and 2 for W2A)	-0.0853	.000	VHS	1.002		
	Type Of Fuel (1 for BL fuel and 2 for PD)	0.04645	.001	VHS	1.007		
	Gross Vehicle Weight [tonne]	-1.53E-03	.058	NS	1.009		
a. Dependent Variable: THC [g/kWh]							
Adjusted R Square = 0.680							
THC = 0.20865 - 0.08530DIR + 0.04645 ToF - 1.5313E-03 GVW							
Best model obtained after six (6) repetitions, using backward method							
ANOVA							
Model	Sum of Squares	df	Mean Square	F	Sig.	Decision	
6	Regression	0.07891	3	0.0263	22.982	.000	VHS
	Residual	0.03205	28	0.00114			
	Total	0.11096	31				

THC EF is affected by the type of fuel. The type of fuel (ToF) has the strongest weight and causes a VHS difference on THC EF as shown in the multi-regression analysis demonstrated in table 7.13. Road load (DIR) has the same

effect (VHS), while GVW is non-significant. After six repetitions using the backward method, the final model based on the three aforementioned predictors was established with $R^2 = 0.68$. This means that the model accounts for 68% of THC variance.

The model shows that THC EF is inversely proportional to road load. The higher the road load the lower THC or the return journey produces lower THC emissions per unit energy produced. However, the type of fuel ToF is directly proportional to THC and PD produces higher levels of THC.

7.2.3 Analysis for the correlations suggested by the multi-regression models and their effect on HGV emissions throughout the steady-high speed HGV test

The two variables suggested by the tailpipe NO_x EF statistical model for the steady high-speed HGV travel are the GVW (payload) and the journey direction (road load).

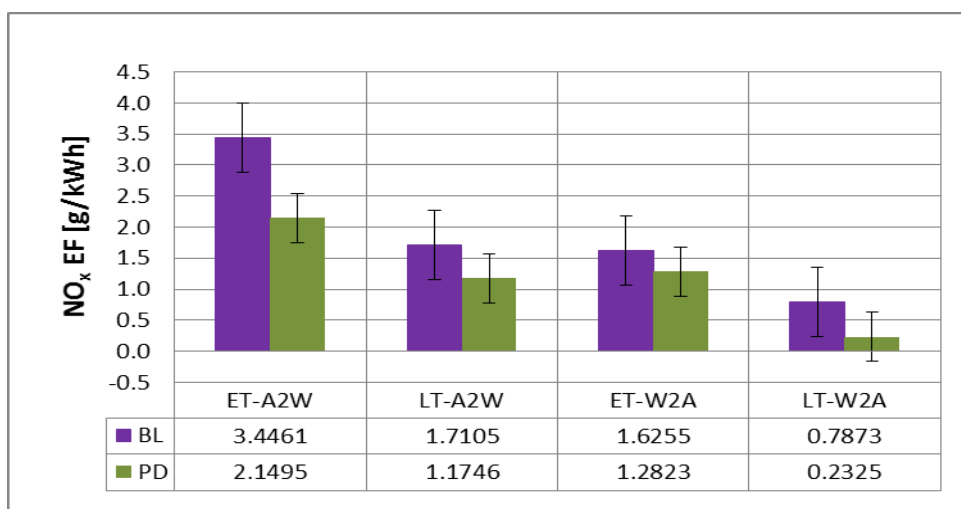


Figure 7.17 Tailpipe NO_x EF from real world tests of a HGV fuelled with UBF and the PD travelling at steady high speed. ET and LT are the HGV empty trailer and loaded trailer respectively. A2W is the outbound journey from Ashby to Wigston while W2A is the inbound journey. Data based on 32 real world trips.

As seen in fig.7.17 UBF always produces higher tailpipe NO_x emissions per unit energy produced. Increasing the payload reduces NO_x EF by 50% and 46% for UBF and PD respectively while, increasing the road load reduces the NO_x EF for UBF by 52% at ET and LT respectively. The road load seems to affect PD more apparently, it reduces NO_x EF by 40% and 80% for ET and LT respectively.

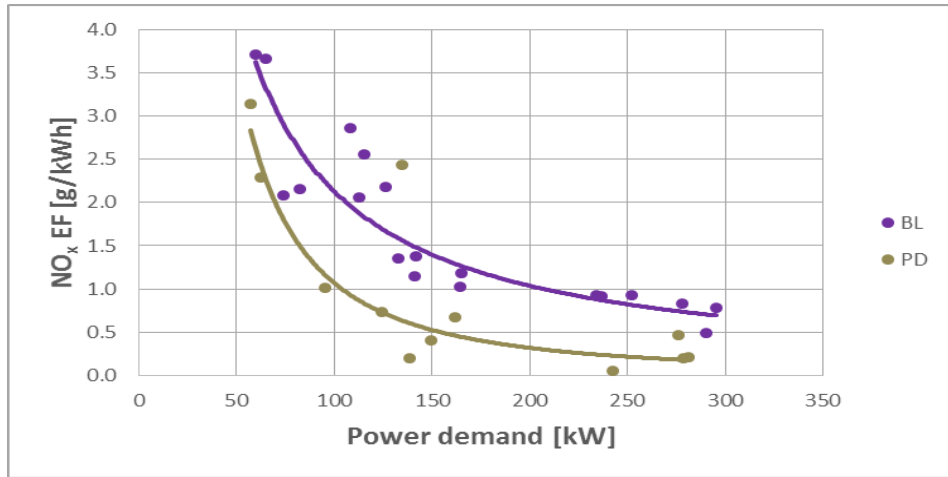


Figure 7.18 Tailpipe NO_x EF vs vehicle power demand obtained from steady high speed HGV travel in real world test. The graphs compare between NO_x EF from UBF and PD. Data based on 32 trips.

The increased power demand shown in fig.7.18 is actually resulted from the payload and the road load increase. The graph shows that UBF is producing higher levels of NO_x at all power demands. It also shows that the higher the power demand the lower the NO_x EF. Actually SFC is implicitly related to HGV power demand in an inverse manner as seen in fig.7.19. In other words higher SFC occurs at lower loads as explained in chapter 4 section 4.3.

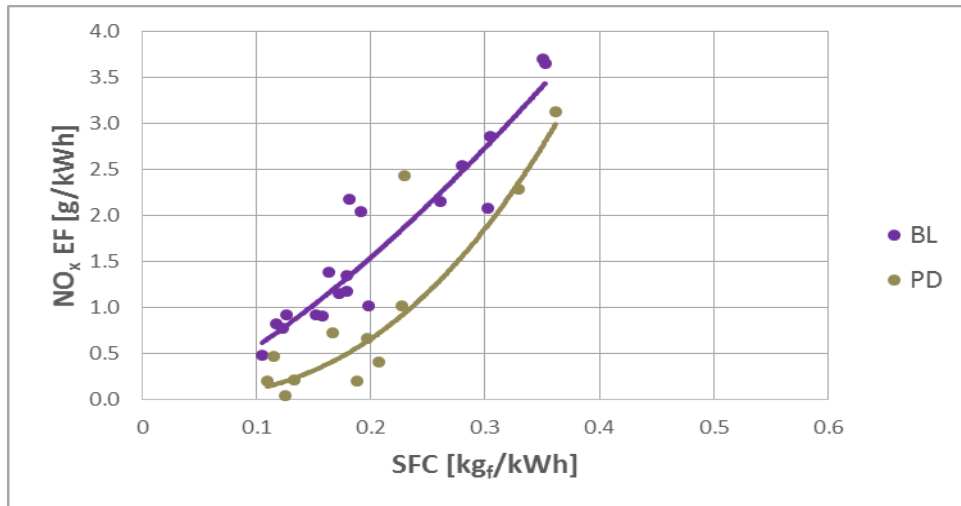


Figure 7.19 Tailpipe NO_x EF as a function of SFC for a HGV travelling at high steady speed. Data base on 32 real world trips.

The graph covers a smaller range of tailpipe NO_x EF and SFC than that of the entire journey. Its only because of the operational conditions are limited to the high speed operation. The high engine speed increases the frequency of combustion occurrence to lead to a higher engine temperature. This action is counteracted by improved performance of the engine cooling system due to the larger amount of air passing through the radiator and the continuous air

changes in the engine compartment added to that the higher speed of coolant circulation.

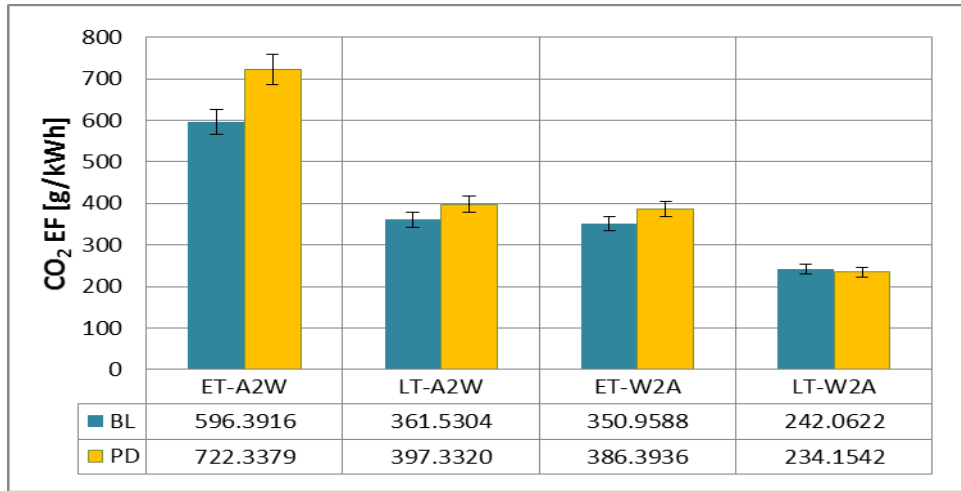


Figure 7.20 CO₂ EF from real world tests of a HGV fuelled with UBF and the PD travelling at steady high speed. ET and LT are the HGV empty trailer and loaded trailer respectively. A2W is the outbound journey from Ashby to Wigston while W2A is the inbound journey. Data based on 32 real world trips.

Carbon dioxide CO₂ depends mainly on the amount of fuel consumed and the completeness of the combustion process. This could be affiliated to the opposite influences of higher amounts of fuel consumed at higher loads which is counteracted by the higher efficiency of combustion as explained earlier. Fig.7.20 shows that PD produces higher levels of CO₂ emissions than UBF especially at low loads. Increasing the combined load reduces CO₂ EF by 59% and 67% for UBF and PD respectively.

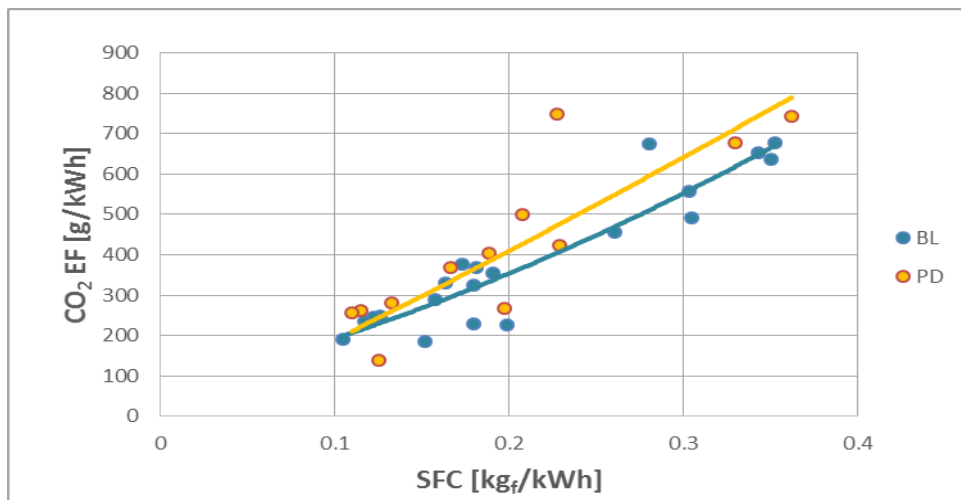


Figure 7.21 CO₂ EF as a function of SFC for a HGV travelling at high steady speed. Data base on 32 real world trips.

This phenomenon is more apparent in fig.7.21, which indicates a lower mass of CO₂ per kWh is produced at lower mass of fuel consumed per kWh.

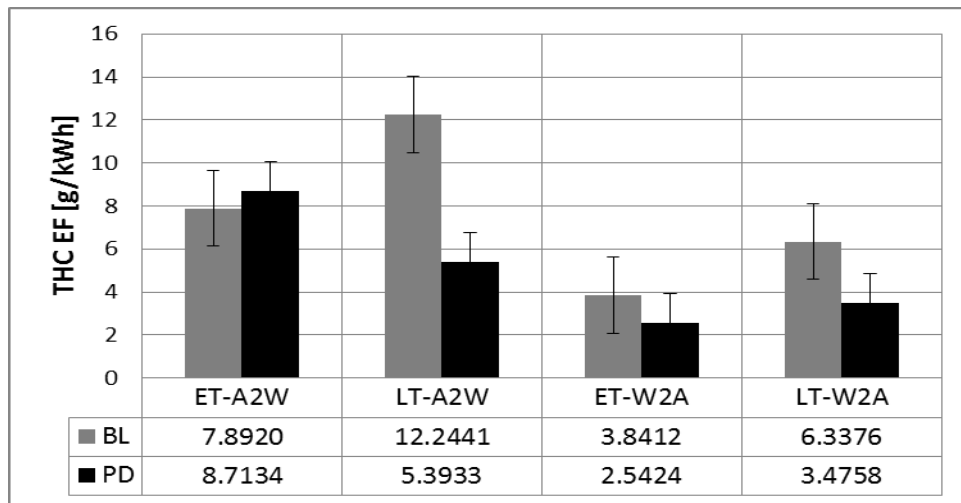


Figure 7.22 THC EF from real world tests of a HGV fuelled with UBF and the PD travelling at steady high-speed. ET and LT are the HGV empty trailer and loaded trailer respectively. A2W is the outbound journey from Ashby to Wigston while W2A is the inbound journey. Data based on 32 real world trips.

According to the aforementioned multi-regression model (table 7.13), THC is significantly affected by the ToF. This trend is verified in fig.7.22 in which higher THC EF is produced from the BL fuel especially at low road loads. UBF produces 9% lower THC EF at low loads, however this difference increases to 126% at high loads. As the vehicle is set to run on UBF, the return uphill journey reduces THC emissions by 51% while empty and 48% while loaded. The reduction figure is 70% for ET and 35% for LT respectively while running on PD. In general, UBF produces higher levels of THC EF which might be related to its physical characteristics which detrimentally affects its performance under high speed operation.

7.3 Gaseous emissions from the HGV under high torque performance

Transitions during HGV travel are crucial conditions at which many changes take place in engine performance and emissions. Unfortunately transients are usually short and prompt, especially the pulse wise ones, therefore only limited amount of data could be obtained.

In order to mimic the transient properties in a well-defined segment throughout the journey, the ramp to merge into M1 motorway was selected in which the HGV is accelerating from a very low velocity, perhaps from standstill at the

ramp foot to 83~96 km/h on the motorway. The lower limit is the HGV velocity recommended by the fleet operator and the upper limit is the UK's regulated national speed limit. The gradient is 3% and the road length is 240 m. For a HGV to accelerate, the engine should run close to the maximum torque speed (1900 rpm for the HGV under investigation) at high gear ratios which reduces progressively as the HGV gradually pickup speed. Gear ratio change take place automatically for the HGV under investigation. Different fuel consumption, engine-out temperature and engine emissions are expected to occur in this road segment.

7.3.1 Physical analysis for the observed variations in HGV emissions caused by high torque performance; A comparison between PD and the BL fuel

This segment of the journey is illustrated in fig.7.23. The high peak in NO_x is actually an outcome from the higher fuel consumption particularly UBF as seen in fig.7.24. Although a high EoT associated the high BL fuel consumption, the tailpipe temperature is decreasing due to the previous road section. This means a very high dose of engine-out NO_x entered the SCR and treated to the levels shown in fig.7.24.

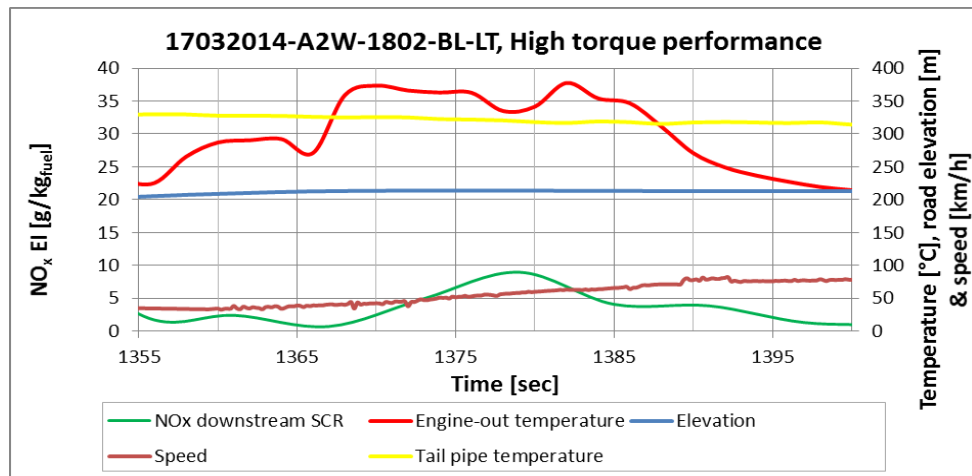


Figure 7.23 NO_x EI downstream to SCR in correlation to temperature, road gradient and speed. The engine is operated under high torque conditions. The loaded HGV is accelerating on a 240m long ramp.

Fig.7.24 illustrates how the tailpipe NO_x EI is mainly affected by the fuel consumption especially UBF which is the active fuel in this transition.

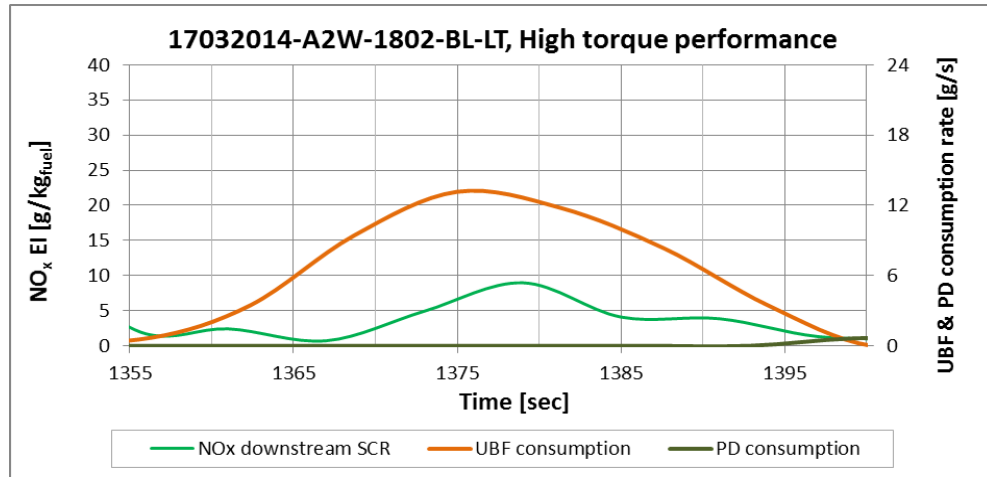


Figure 7.24 NO_x EI downstream to SCR correlated to the amount of UBF consumption under high torque performance. The GVW is 31 tonnes and the HGV is accelerating on an inclined ramp to merge on M1 motorway.

7.3.2 Statistical analysis for the observed variations in HGV emissions caused by the BL fuel under high torque engine performance

The analysis of variance for the effect of fuel type on the emissions are demonstrated in table 7.14. Very high differences in engine-out NO_x and CO are indicated due the fuel change.

Table 7.14 Analysis of variance for BL fuel and PD and their effects on gaseous emissions from a HGV under high torque conditions. Data in [g/kWh].

Group Statistics					
Emissions [g/kWh]	TYPE OF FUEL	N	Mean	Std. Deviation	Std. Error Mean
NOx-up stream SCR	BL	69	8.83198	11.66199	3.36653
	PD	242	21.98091	22.42359	9.15439
NOx-down stream SCR	BL	69	0.87918	0.91263	0.26345
	PD	242	0.37503	0.30974	0.12645
CO	BL	69	0.23876	0.22819	0.06587
	PD	242	0.97312	0.90505	0.36949
CO ₂	BL	69	195.84897	96.55410	27.87277
	PD	242	164.37513	87.59125	35.75898
THC	BL	69	2.12900	1.52200	0.68109
	PD	242	2.12649	1.48500	0.66419

To decide whether these differences are significant, the data were tested by t-test for the equality of means which is a two tailed test as exhibited in table 7.15. The t-test confirms the latter (CO) significance. Other emissions do not show any significant differences due to fuel change during the high torque vehicle performance.

Table 7.15 Levene’s test for equality of variance and t-test for equality of means for the effect of fuel type on gaseous emissions from HGV under high torque operation. Data units in [g/kWh].

Emissions	t-test for Equality of Means				
	t	df	Sig. (2-tailed)	Mean Difference	Std. Error Difference
NO _x Up stream SCR	-1.560	14	.141	-13.148927	-5.787866
NO _x Down stream SCR	1.272	14	.224	.504153	.137003
CO	-2.439	14	.029	-.734363	-.303613
CO ₂	.652	14	.525	31.473842	-7.886212
THC	-1.100	14	.290	.002509	.016900

The t-test shows a reduction in engine-out NO_x and CO as the BL fuel substitutes PD throughout the high torque test. Tailpipe NO_x is higher and CO₂ and THC as well.

The data were furtherly processed by regression analysis and the results are shown in tables 7.16 through 7.20.

Table 7.16 shows the multi-regression analysis for the HGV travel under high torque conditions. The variable incorporated are GVW, EoT, ToF, V, load factor (LF), SFC, VSP, equivalence ratio (φ), engine-out NO_x, tailpipe NO_x, CO, CO₂, NO₂/NO_x and THC. All the table parameters are as explained in section 7.1.2.

The dependent variable is engine-out NO_x. After seven repetitions nine predictors were selected by the model. GVW is a VHS predictor with a very good variable inflation factor but the coefficient is low, it is inversely proportional to engine-out NO_x. Vehicle velocity is nonsignificant variable. LF is VHS with a very good VIF but the coefficient is low, it is directly proportional to engine-out NO_x.

SFC is perhaps the strongest predictor because it is VHS with a relatively good VIF and reasonable coefficient. The ratio of NO₂/NO_x is another significant, good VIF and appropriate coefficient. Other variable possess high

VIF. The adjusted $R^2 = 0.932$ which means that the model accounts for 93.2% of the engine-out NO_x variance. ANOVA shows that the model is VHS as $F(9,301) = 475.895$ at $p = .000$.

Table 7.16 Multi-regression analysis for the effect of fuel type and other performance variables on engine-out NO_x . (Data exclusively represent high torque engine performance).

Regression NO_x -up stream SCR							
Coefficients							
Model		Unstandardized Coefficients	Sig.	Decision	Collinearity Statistics		
		B			VIF		
7	(Constant)	0.00792					
	GVW [tonne]	-0.00054	.000	VHS	1.092		
	Velocity [km/h]	0.00007	.072	NS	1.146		
	Load Factor	0.00013	.000	VHS	1.205		
	SFC [kg/kWh]	0.01932	.000	VHS	1.801		
	CO [g/kWh]	-0.30843	.002	HS	29.179		
	CO ₂ [g/kWh]	-0.00922	.000	VHS	110.311		
	Ratio of NO ₂ to NO _x	-0.01193	.043	S	1.042		
	THC [g/kWh]	-0.00396	.072	NS	1.706		
	NO _x -DN SCR [g/kWh]	0.44413	.000	VHS	86.094		
Dependent Variable: NO_x -up stream SCR [g/kWh]							
Adjusted $R^2 = 0.932$							
$\text{NO}_x\text{UPSCR} = 0.00792 - 0.00054 \text{ GVW} + 0.00007 \text{ V} + 0.00013 \text{ LF} + 0.01932 \text{ SFC} - 0.30843 \text{ CO} - 0.00922 \text{ CO}_2 - 0.01193 \text{ NO}_2/\text{NO}_x - 0.00396 \text{ THC} + 0.44413 \text{ NO}_x\text{DN SCR}$							
Best model obtained after seven (7) repetitions, using backward method							
ANOVA							
Model		Sum of Squares	df	Mean Square	F	Sig.	Decision
7	Regressi	1.348	9	0.150	475.895	.000	VHS
	Residual	0.095	301	0.000			
	Total	1.442	310				

Setting NO_x downstream to SCR as the dependent variable, a model was developed based on 9 predictors. Engine-out NO_x is VHS predictor with the strongest weight and the VIF is relatively good. THC, NO_2/NO_x have nearly the same effect. GVW, V and LF are high significant variable but their coefficient is small. SFC is another VHS predictor for the dependent variable. After 7 repetitions using the backward method, the best model had an adjusted $R^2 = 0.997$, which means that the model accounts for 99.7% of tailpipe NO_x variance. ANOVA suggested that the model is VHS as $F(9,301) = 11966.47$ and $p = .000$.

Table 7.18 exhibits the multi-regression analysis for CO as the dependent variable. After 9 repetitions using the backward method, the best is based on 7 predictors. GVW is inversely proportional to CO EF, it is considered as a

significant predictor with good VIF value but the coefficient is too small. Load factor (LF) has the same properties as GVW except it is directly proportional to CO EF. CO₂ is a VHS predictor but the VIF is very high which means it is over correlated same as NO_x EF. THC and φ are probably working as the most reliable predictors and having the strongest weight. The predictive model has adjusted R² = 0.967 that means it accounts for 96.7% of CO variance. ANOVA indicates that the model is VHS as F(7,303) = 1281.868 and p = .000.

Table 7.17 Multi-regression analysis for the effect of fuel type and other performance variables on NO_x downstream to SCR. (Data exclusively represent high torque engine performance).

Regression NO _x -Downstream SCR							
Coefficients							
Model		Unstandardized Coefficients	Sig.	Decision	Collinearity Statistics		
		B			VIF		
7	(Constant)	-0.01131					
	GVW [tonne]	0.00114	.000	VHS	1.077		
	Velocity [km/h]	-0.00022	.005	HS	1.129		
	Load Factor	-0.00033	.000	VHS	1.174		
	SFC [kg/kWh]	-0.04797	.000	VHS	1.625		
	CO [g/kWh]	0.60886	.001	HS	29.168		
	CO ₂ [g/kWh]	0.02230	.000	VHS	32.778		
	Ratio of NO ₂ to NO _x	0.02741	.018	S	1.037		
	THC [g/kWh]	0.01371	.001	HS	1.667		
	NO _x -UP SCR	1.71132	.000	VHS	3.663		
Dependent Variable: NO _x -Downstream SCR [g/kWh]							
Adjusted R ² = 0.997							
NO _x DN SCR = - 0.01131 – 0.00114 GVW - 0.00022 V - 0.00033 LF - 0.04797 SFC + 0.60886 CO + 0.02230 CO ₂ + 0.02741 NO ₂ /NO _x – 0.01371 THC + 1.71132 NO _x UP SCR							
Best model obtained after seven (7) repetitions, using backward method							
ANOVA							
Model		Sum of Squares	df	Mean Square	F	Sig.	Decision
7	Regression	130.599	9	14.511	11966.470	.000	VHS
	Residual	0.365	301	0.001			
	Total	130.964	310				

Table 7.18 Multi-regression analysis for the effect of fuel type and other performance variables on CO. (Data exclusively represent high torque engine performance).

Regression CO							
Coefficients							
Model		Unstandardized Coefficients	Sig.	Decision	Collinearity Statistics		
		B			VIF		
9	(Constant)	0.00224					
	GVW [tonne]	-0.00017	.014	S	1.127		
	Load Factor	0.00005	.019	S	1.189		
	CO ₂ [g/kWh]	0.00132	.000	VHS	190.393		
	THC [g/kWh]	-0.00313	.007	HS	1.387		
	NO _x -UPSCR [g/kWh]	-0.09002	.003	HS	12.624		
	NO _x -DNSCR [g/kWh]	0.04676	.002	HS	264.235		
	Equivalence ratio (φ)	0.00338	.020	S	1.292		
Dependent Variable: CO [g/kWh]							
Adjusted R ² = 0.967							
$CO = 0.00224 - 0.00017 GVW + 0.00005 LF + 0.00132 CO_2 - 0.00313 THC - 0.09002 NO_{x\ UPSCR} - 0.04676 NO_{x\ DNSCR} + 0.00338 \varphi$							
Best model obtained after Nine (9) repetitions, using backward method							
ANOVA							
Model		Sum of Squares	df	Mean Square	F	Sig.	Decision
9	Regression	0.95361	7	.13623	1281.868	.000	VHS
	Residual	0.03220	303	.00011			
	Total	0.98582	310				

The regression analysis for the effect of ToF and HGV performance variables on CO₂ emissions are presented in table 7.19. The analysis revealed that the only factor, in transient HGV operation, that significantly affected CO₂ emissions is SFC.

In table 7.19 CO₂ is the dependent variable. After 7 repetitions using the backward method the best model obtained has 9 predictors. All the predictors are significant at different levels. CO and the NO_x are over correlated as indicated by their high VIF. SFC has the strongest weight followed by THC, GVW and LF respectively. The model has R² = 0.996 which indicates that it accounts for 99.6% of CO₂ variance. ANOVA shows that the model is VHS as F(9,301) = 8664.891 and p = .000.

Table 7.19 Multi-regression analysis for the effect of fuel type and other performance variables on CO₂. (Data for HGV at high torque performance).

Regression CO ₂							
Coefficients							
Model	Unstandardized Coefficients		Sig.	Decision	Collinearity Statistics		
	B				VIF		
7	(Constant)	0.252					
	GVW [tonne]	-0.038	.000	VHS	1.111		
	Velocity [km/h]	0.009	.005	HS	1.129		
	Load Factor	0.011	.000	VHS	1.202		
	SFC	1.984	.000	VHS	1.637		
	Ratio of NO ₂ to NO _x	-1.115	.022	S	1.038		
	CO	22.244	.006	HS	29.409		
	THC	-0.457	.011	S	1.688		
	NO _x -UP _{SCR}	-62.448	.000	VHS	6.458		
	NO _x -DN _{SCR}	39.192	.000	VHS	45.219		
Dependent Variable: CO₂ [g/kWh]							
Adjusted R² = 0.996							
$\text{CO}_2 = - 0.252 - 0.038 \text{ GVW} + 0.009 \text{ V} + 0.011 \text{ LF} + 1.984 \text{ SFC} - 1.115 \text{ NO}_2/\text{NO}_x + 22.244 \text{ CO} - 0.457 \text{ THC} - 62.448 \text{ NO}_x \text{ UP}_{\text{SCR}} + 39.192 \text{ NO}_x \text{ DN}_{\text{SCR}}$							
Best model obtained after Seven (7) repetitions, using backward method							
ANOVA							
Model		Sum of Squares	df	Mean Square	F	Sig.	Decision
7	Regress	166204.	9	18467.159	8664.891	.000	VHS
	Residua	641.510	301	2.131			
	Total	166845.	310				

THC is the dependent variable in table 7.20. Amongst all the 15 incorporated variables and after 9 repetitions using the backward method, the best predictive model is obtained based on 7 predictors. They are all significant at different levels. CO and NO_x downstream to SCR are over correlated. SFC and the equivalence ratio (φ) are the predictor of the strongest weight followed by HGV acceleration, velocity and EoT respectively. The adjusted R² = 0.531 which indicates that the model accounts for 53.1% of THC variance. ANOVA indicates that the model is VHS as F(7,303) = 51.127 and p = .000.

Table 7.20 Multi-regression analysis for the effect of fuel type and other performance variables on THC. (Data for HGV under high torque operation).

Regression Total Hydrocarbons							
Coefficients							
Model	Unstandardized Coefficients		Sig.	Decision	Collinearity Statistics		
	B				VIF		
9	(Constant)		0.367				
	EoT	[°C]	-0.001	.001	VHS	1.097	
	Velocity	[km/h]	-0.004	.000	VHS	1.079	
	Acceleration	[m/s ²]	-0.052	.027	S	1.032	
	SFC		0.549	.000	VHS	1.190	
	CO	[g/kWh]	-7.222	.000	VHS	21.968	
	NO _x -DNSCR	[g/kWh]	0.725	.000	VHS	21.800	
	Equivalence ratio (φ)		0.536	.000	VHS	1.157	
Dependent Variable: Total Hydrocarbons [g/kWh]							
Adjusted R ² = 0.531							
THC = 0.367 - 0.001 EoT- 0.004 V – 0.052 a + 0.549 SFC – 7.22 CO + 0.725 NO _x DNSCR + 0.536 φ							
Best model obtained after nine (9) repetitions, using backward method							
ANOVA							
Model	Sum of Squares	df	Mean Square	F	Sig.	Decision	
9	Regression	60.508	7	8.644	51.127	.000	VHS
	Residual	51.228	303	0.169			
	Total	111.736	310				

7.3.3 Analysis for the factors suggested by the predictive models and their effect on HGV emissions under high torque performance.

In the real world, transition usually take place in accelerations by pushing the accelerator and in gear shifts also in decelerations and braking action. These actions usually affect the flow of fuel and air. Definitely, these stimuli are associated by a time lag between the amount of fuel and air for a precise mixing ratio even in turbo-charged engines. Therefore a very different mixture is introduced to the combustion process to change its characteristics and the emissions as well.

The selected road segment to demonstrate the transitional mode of a HGV in real world is a ramp inclined at 3% and about 240m long. The HGV enters the

ramp after leaving a roundabout. Therefore the vehicle starts to accelerate from 10-20 km/h at the beginning to 83~96 km/h, the allowable speed range on M1 motorway for HGVs. The automatic gearbox makes many gear changes to keep the engine at its maximum torque and the vehicle to pick up speed. Maximum acceleration occurs at higher gear ratios, to decrease gradually to the top gear. The HGV continues to accelerate even beyond the ramp to reach the required speed.

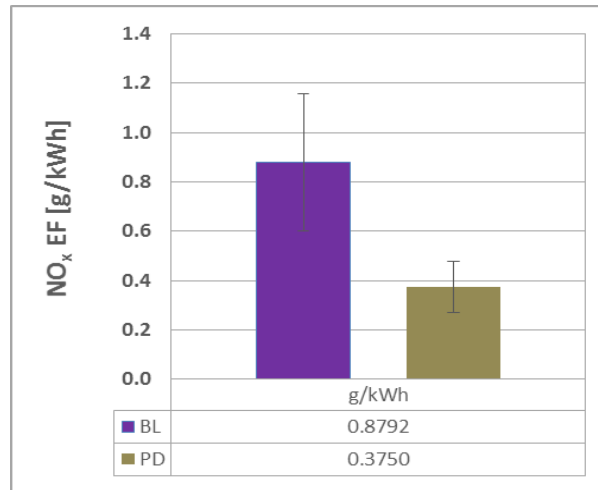


Figure 7.25 Tailpipe NO_x EF obtained from a HGV under high torque performance using two different fuels; BL fuel (84.6 % UBF on average) and PD. Data based on 16 real world trips.

Fig.7.25 shows that NO_x EF obtained at the tailpipe of a HGV under high torque performance. It is quite obvious that BL fuel doubles the amount of NO_x emissions per kWh compared to PD. However it is still far below the EURO V standard of 2 g/kWh. Fig.7.26 shows that NO_x at the tailpipe is directly proportional to the SFC. The higher the power demand the lower the SFC and NO_x from the tailpipe for the two fuels. However, a difference in NO_x is quite wide at high SFC then the BL fuel reduces the gap to almost zero at the lower SFC achieved by the two fuels.

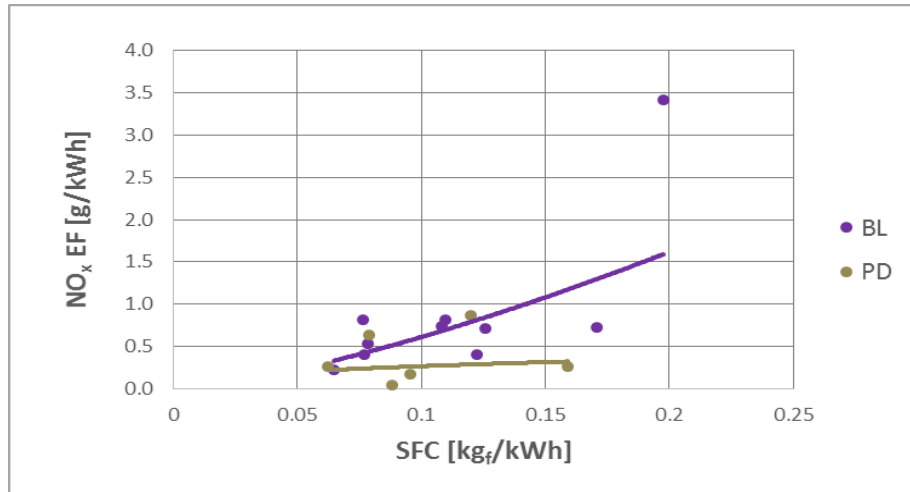


Figure 7.26 NO_x EF as a function of SFC for a HGV under high torque conditions using two different fuels; BL fuel and PD. Data based on 16 trips.

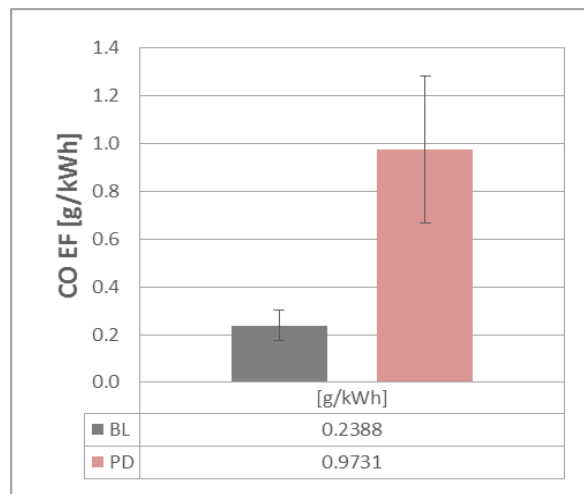


Figure 7.27 CO EF obtained from a HGV under high torque performance using two different fuels; BL fuel and PD. Data based on 16 trips

Fig.7.27 supports that fact and shows that the BL fuel produces 75% less CO EF which is most likely being converted to CO₂ due to the improved oxidation.

CO₂ during the HGV under high torque performance seems to be higher from the BL fuel as shown in fig.7.28. In fact CO₂ follows the amount of fuel consumed, as stated by the predictive model in table 7.19, and better oxidation of CO to CO₂.

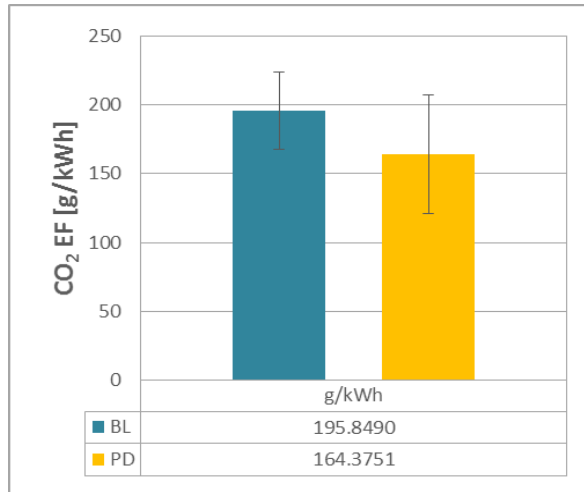


Figure 7.28 CO₂ EF obtained from a HGV under high torque performance using two different fuels; BL fuel and PD. Data based on 16 trips.

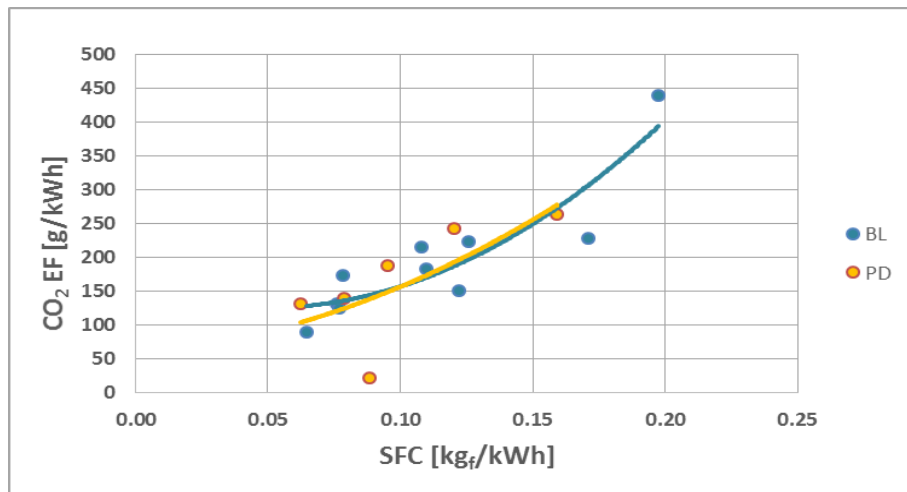


Figure 7.29 CO₂ EF as a function of SFC obtained from a HGV in a high torque performance using two different fuels; BL fuel and PD. Data based on 16 trips.

The general trend in CO₂ behaviour is identical for PD and its surrogate. SFC shown in fig 7.29 indicates a very high significant effect on CO₂. The higher the power demand the lower the SFC and the lower the CO₂ emissions. This could be attributed to the improved combustion efficiency at higher power demands. The higher fuel injection pressure at higher power demand, reduces the physical delay period by the improved fuel atomisation and it accelerates the adiabatic premixed flame to result in a higher diffusion flame temperature for better CO oxidation.

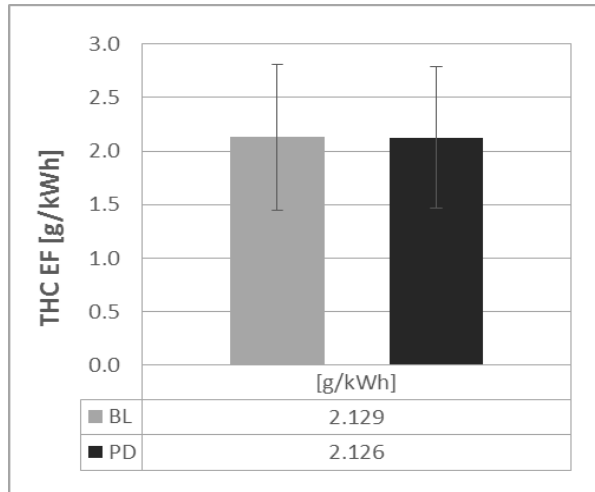


Figure 7.30 THC EF obtained from a HGV in a high torque performance using two different fuels; BL fuel and PD. Data based on 16 trips.

THC EF levels is nearly the same for the two fuels as the HGV was teste on the high torque performance. As shown in fig.7.30 BL fuel produces nearly the same amount of THC as PD under high torque performance.

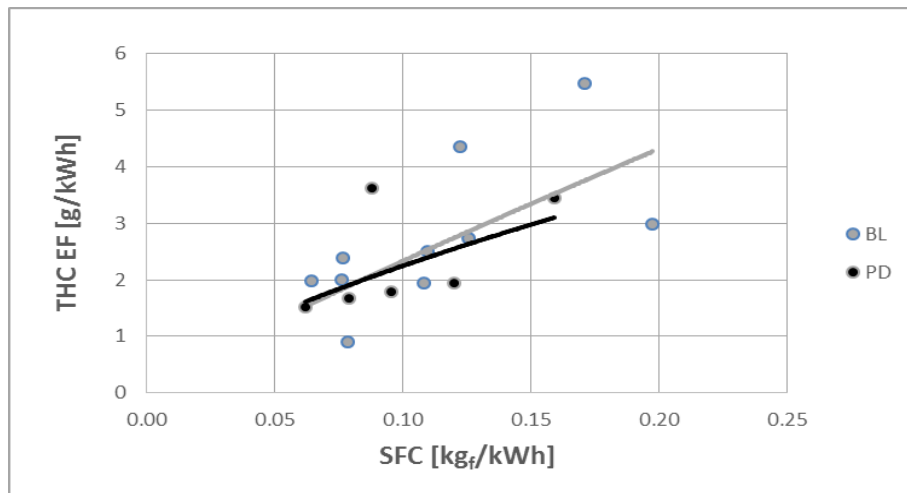


Figure 7.31 THC EF obtained from a HGV in a transition and fuelled with two different fuels; BL fuel(84.6% UBF on average) and PD. Data based on 16 trips.

Fig.7.31 indicates that THC increases with the SFC, the lower the SFC the lower the THC EF. This is related to the improved combustion efficiency. Although BL fuel combustion is at lower temperature than PD, it produces slightly higher THC per unit energy produced. Probably it is the THC

conversion to particulates at lower exhaust temperatures by condensation and adsorption is the reason behind the THC control from the BL fuel.

7.4 Conclusions

The physical and statistical analysis demonstrated earlier throughout the chapter revealed that emissions from this particular HGV tested in the real world could depend on one independently working variable or more. The mode of vehicle operation, whether it is steady-high speed, high torque performance or mixed is very decisive on the influential variables and their degree of effectiveness. One variable could appear in one operational condition with a certain strength and may vanish as the type of operation changes.

7.4.1 Engine-out NO_x emission status

1. The ToF explicitly effected engine-out NO_x EF. HGV travel at steady high speed produces 23.5% higher NO_x EF while running on BL fuel. In contrary, during the high torque performance it produces 59.8% less NO_x EF.
2. GVW is inversely proportional to NO_x EF and it makes VHS differences in engine-out NO_x EF at all operational conditions. Increasing the payload increases the rate of fuel consumption while the SFC is lower due to the improved engine performance. A higher combustion temperature is expected and higher engine-out NO_x is produced.
3. SFC is a VHS predictor for engine-out NO_x EF in all modes of engine operation with a positive proportionality. This means the lower the SFC the lower the engine-out NO_x EF. Logically, SFC is an indicator for the efficiency of fuel conversion to energy, lower SFC is achieved at high engine performance as the combustion efficiency improves due to the higher injection pressure and combustion temperature. Since SFC and NO_x EF both represent mass of substance per unit energy produced by the engine, the lower SFC at high loads will produce lower NO_x EF.
4. During the steady-high speed HGV performance both vehicle velocity (V) and vehicle specific power (VSP) are insignificant variables. In fact the adverse effect of V and VSP, while V is an effective term in VSP, means that the road gradient term of VSP is playing a very effective role. This argument supports the previous explanations in GVW and SFC.

5. During the high torque performance, LF is a VHS predictor of engine-out NO_x. In fact the engine performance is not that much changing. It is changing from the high torque to high power. Therefore the weight of the LF as a predictor is not strong as seen in table 7.16.

7.4.2 NO_x downstream to SCR emissions status

It is important to bear in mind that NO_x downstream to SCR is very much affected by the SCR performance whereas SCR performance is affected by the exhaust gas temperature and NO_x upstream SCR. This might give a completely different NO_x EF figure from the engine-out NO_x EF.

NO_x issued from the tailpipe is affected by the following variables at different levels

1. The type of fuel ToF causes a HS differences in NO_x emissions. Its effect is clearer through the whole journey data. PD has a lower tailpipe NO_x EF.
2. SFC has a VHS effect on tailpipe NO_x EF which is represented by a direct proportionality for the same aforementioned reasons in the engine-out NO_x EF. Due to the high variance inflation factor (VIF) SFC is cross correlated to VSP. SFC in the high torque performance is inversely proportional to tailpipe NO_x EI. This could be attributed to the deterioration in SCR performance as its temperature drops from the previous downhill road section and low HGV speed at the roundabout under the M1 overpass.
3. GVW causes a HS difference in the tailpipe NO_x EF. GVW is inversely proportional to tailpipe NO_x.

7.4.3 Carbon monoxide emissions status.

Incomplete combustion is expected to produce more CO. Although the regression models explained very low percentage of CO behaviour, The BL fuel causes a significant decrease in CO emissions in the entire test series. This could be attributed to the improved oxidation of CO, and its conversion to CO₂, due to the 11.9% extra O₂ presence in the UBF.

7.4.4 Carbon dioxide emissions status

CO₂ is an inevitable outcome of the combustion process. CO₂ is directly proportional to the amount of fuel burned and it depends on the completeness

of the combustion process to the final products. Complete combustion produces more CO₂ than intermediate products.

1. The most influential variable that affect CO₂ emissions is SFC through the three operational modes. The higher the SFC the higher the CO₂ EF.
2. Journey direction (DIR) represents the effect of road gradient which is quite apparent in the steady high speed HGV performance. It is inversely proportional to CO₂ EF. The greater the positive gradient of the road the lower the SFC which means lower CO₂ EF.
3. The increase in engine load factor (LF) in the high torque performance is caused by the higher rate of fuel consumption which increases the rate of CO₂ emissions.
4. CO₂ emissions from the BL fuel seems to be higher under high torque performance while it is lower under steady high speed performance. This is arguably related to the amount of fuel consumed per kWh produced under each operational condition (SFC).

7.4.5 Total hydrocarbon emissions status

THC and specifically methane is a greenhouse gas that is more stringent to the environment than CO₂.

1. Type of fuel (ToF) significantly affects THC emissions especially in the whole journey and the steady high speed vehicle performance.
2. The presence of high HC in the exhaust gases is a clear indicator of incomplete combustion which is usually associated by higher CO emissions.
3. The SFC is another variable to contribute significantly in THC EF especially during the mixed mode and high torque HGV performance. It seems that transitions alters the AF ratio to sudden enrichment and perhaps a slight turbo-lag may assist to furtherly deteriorate the combustion efficiency. The steady high speed operation doesn't show any contribution of SFC in THC emissions. In fact the HGV during its steady high speed travel has no fluctuation in the amount of fuel injected and it achieves a relatively low SFC enhanced by higher turbocharging performance for a more complete combustion. Nevertheless, higher THC EF is indicated during the steady high speed performance followed by mixed operation and the high torque performance.

4. The effect of journey direction is clearer in the steady high speed operation. Consider no acceleration and traffic obstacles, the only variable that might affect the HGV performance is the road load and specifically road gradient. THC emissions in steady high speed HGV travel is inversely proportional to the road gradient. However negative gradient could produce higher THC levels. It is quite understandable that HGV travel downhill especially the loaded one is partially using its gravity to move. A lower power demand and associated by a cooler combustion process which will certainly lead to higher HC and CO emissions [1]. Added to that this mode of engine operation with lower in-cylinder pressure enables more lubrication oil to move in between piston crevices to the combustion chamber which is another source of unburnt HCs.

7.4.6 The overall variations in gaseous emissions from fuelling the HGV with BL fuel in comparison to PD.

The aforementioned analysis show differences in the gaseous emissions from the two fuels. Although the magnitude of difference is not too high but as a percentage, some of them are really high as shown in table 7.21 and fig.7.25. These differences are related in one way or another to the physical, chemical and thermodynamic properties of the fuel in one hand and the operational conditions on the other hand.

Table 7.21 The overall variations in gaseous emissions from the utilization of BL fuel in a HGV (84.5% UBF) compared to PD.

EMISSIONS	Difference in BL fuel emissions compared to PD					
	Entire test series		Steady high speed		High torque	
	g/kWh	%	g/kWh	%	g/kWh	%
NO _x Up stream SCR	4.414	23.593	3.698	15.421	-13.149	-59.820
NO _x Down stream SCR	1.053	105.341	0.906	91.774	0.504	134.431
CO	-1.263	-70.761	-1.053	-84.000	-0.734	-75.465
CO ₂	60.515	21.388	-34.632	-8.200	31.474	19.148
THC	1.226	36.182	3.780	73.996	0.003	2.544

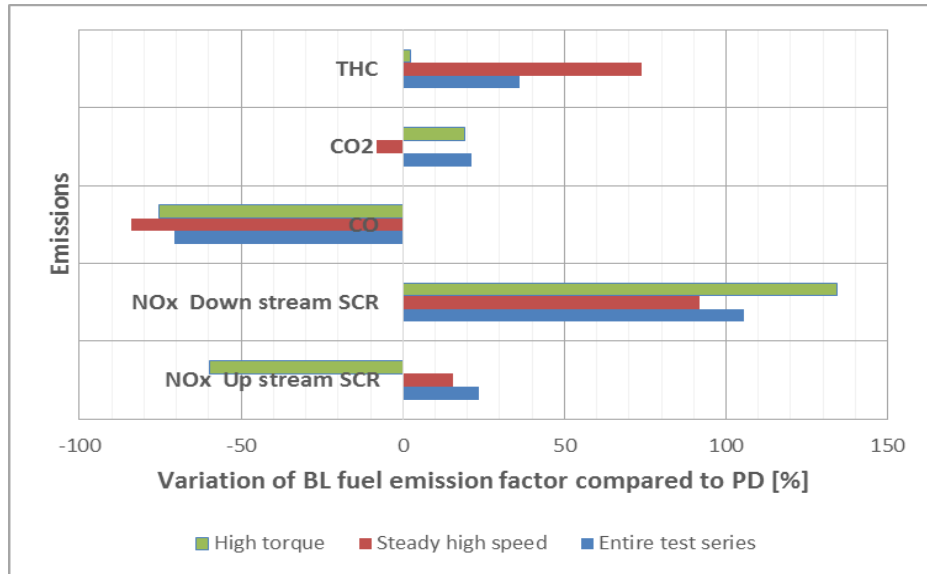


Figure 7.32 variation in HGV emissions tested under real world conditions due to the utilisation of different fuels under specified operational conditions. The values are percentages of pollutant EF

Chapter 8

Final conclusions and recommendations for future work

8.1 The conclusions

The in-vitro analysis revealed that UBF/PD blending ratios up to 80% possess kinematic viscosities closer to that of PD especially at high temperatures above 70°C. The difference become more obvious at temperatures around 45°C as fuel blending starts in the Biotec system. However, a UBF/PD blending ratio of 100% was recorded all the way on the M1 motorway and the journey average was 84.5% for the entire test series. This achievement already exceeded the target set by RED to substitute 10% of PD in the transport sector by renewable fuels by 2020.

The fuel temperature plays a key role in spray characteristics. Therefore it is more convenient to operate the engine on blends with UBF content up to 80% to avoid higher fuel consumption and higher pollution load on the exhaust after treatment system compared to using 100% UBF. At 90°C when the UBF content in the blend is confined between 0~80% the variations in fuel jet characteristics, per 10% UBF content increase in the blend, is limited. The mean droplet diameter increases linearly by 2.5%. Similarly, the spray cone angle decreases by 0.91% and the penetration length increases by 0.52%. These differences are much larger as the engine is fed by BL fuel of 80~100% UBF at 90°C. The droplet mean diameter increases by 14.15% per 10% UBF increase in the blend while the fuel jet cone angle decreases by 3.8% per 10% increase in UBF content in the blend. The jet penetration length increases by 2.42% per 10% increase in UBF content in the blend. These variations in fuel jet characteristics are expected to change the combustion scenario. The start of combustion could be detained followed by a sudden high rate of heat release. These combustion conditions are usually leading to higher NO_x emissions and lower PM emissions. The THC also increases as part of the unburnt large droplets might survive the combustion process.

Although the higher fuel viscosity deteriorates the combustion process and the engine output, the higher fuel density could compensate for the lower heating value of the UBF and to lower the expected increase in fuel consumption to obtain the same power output.

The HGV power output and vehicle driveability was the same for the two fuels when tested under steady high speed and high torque performance.

UBF show 4.2~5% higher SFC than PD when the HGV was travelling at steady high speed on the M1 motorway. The higher figure is recorded for the higher GVW and road resistances. The HGV on BL fuel under high torque performance showed 12% higher SFC than PD, nevertheless the two fuel showed a lower SFC compared to that of the steady high speed HGV travel.

The difference in the engine-out temperature EoT for the two fuels was small. However, the magnitude of EoT for the two fuels was critically low in the case of HGV travel downhill on M1 motorway under high GVW. It adversely affected the SCR performance especially on cold weathers. Therefore there were some tailpipe NO_x emission peaks on the M1 motorway during the outbound journey as the driver tried to accelerate.

Particulate matter emission analysis revealed that, the use of UBF in the BL fuel reduced PM_{2.5} EF by 65% at 15.5 tonne GVW and 54% as the payload is doubled to 31 tonnes. The most PM_{2.5} component affected by the presence of C2G UBF in the BL fuel is the EC which was reduced by more than 70%. The ratio of PM_{2.1}/PM₁₀ for PD was 13% and 9% higher than that of the BL fuel at low and high GVWs respectively. On the other hand, HGV operated on the BL fuel produced 46% and 36% lower PM_{2.5} than PD at low and high GVWs respectively.

Gaseous emissions analysis showed that C2G UBF produces higher emissions than PD depending on the operation mode with an exception for CO which is always lower. The tailpipe NO_x is higher by 90~134% at steady high speed and high torque performances respectively. In fact the higher tailpipe NO_x emissions for the BL fuel is related to the high diffusion flame temperature, the combustion peak temperatures, and the amount of oxygen contained in the fuel. However, the variation in SCR performance due to its temperature variation seriously affect the tailpipe NO_x emissions. CO is lower for the BL fuel. CO reduction varies between 75~84% during the high torque and steady high speed performance respectively. THC is higher for the BL fuel. THC increase varies between 2.5%~74% during high torque and steady high speed operation. CO₂ depends on the amount of fuel consumption and the completeness of the combustion process. THC is also dependent on the SFC and the engine operational mode.

Although the injection pressure increases at higher engine power, the fuel injection analysis showed fuel jet deterioration at engine operation on 100% UBF which was the case as the HGV travelled on M1 motorway at steady high speed.

The UCO used as a fuel in this particular HGV showed a significant reduction in PM compared to PD and a huge carbon footprint reduction potential since there is no CO₂ additions to the carbon life cycle.

8.2 Recommendations for future work

In the light of current research there are still some gaps in knowledge related to the injection characteristics and UBF properties other than those covered by the current study. These include:

1. The determination of UBF bulk modulus of elasticity (BME) under high pressures similar to the fuel injection pressure of the designated engine. It'll be quite useful to determine the speed of pressure propagation in the fuel pipes and how they affect the injection timing and duration. Liquids of higher BME could result in advanced start of injection (SOI) and keep the injector needle open for a longer period of time. This action if not contained by the engine control unit (ECU) could alter the injection process and the combustion scenario.
2. Determination of UBF ignition delay (ID) using the ignition quality tester. It offers a better understanding of the combustion process. This might draw a road map for a better combustion control through ECU algorithm upgrade to adjust the injection process or use a different injection strategy for each fuel.
3. To develop new mathematical models for the fuel injection characteristics under high injection pressures. These models are quite useful to simulate the real injection process at pressures as high as 200 MPa.
4. Although heating the UBF reduces its viscosity to satisfactory levels, the high injection pressure counteracts that. Therefore, it is quite important to perform viscosity measurements at conditions similar to those undergone in the high fuel pressure line.
5. Perform the real world tests for UBF on EURO 6 compliant HGVs. This needs a thorough investigation for the engine specifications and combustion chamber configuration followed by a deep understanding

for the high pressure common rail fuel injection system and its injection strategy.

In general the increasing demand and usage of UCO in HGVs is primarily related to its low cost, carbon footprint reduction and PM mitigation.

8.3 Proposed strategies for further HGVs emissions mitigation using non-esterified UCO.

1. The highest HGV emissions per unit work done (g/kWh) occurs when the HGV travels unloaded. In order to minimise the unloaded travels, the fleet operators should adapt a HGV sharing strategy through a robust communication system.
2. HGV (tractor only) hybridisation for urban travels between loaded trailer dispatch station to the next loaded trailer pickup station. This needs batteries in proportion to the tractor weight and the short duration of travel (probably 30 minutes).
3. Develop ECU algorithms to improve the communication between the ECU and the Bioltec system to:
 - Rate the Bioltec system for 80% maximum UBF content in the BL fuel.
 - Control the injection timing, as the auto mode is selected, to improve the fuel injection characteristics and minimise the emissions.
4. Use of the plug-in SCR heating system prior to the cold start journey. This will mitigate NO_x emissions during the first 9 minutes of the journey.

List of References

1. Kalghatgi, G., *Fuel / Engine Interactions*. 2014, USA: SAE International. 255.
2. Morey, B., *Future Automotive Fuels and Energy*. 1st ed. 2013, USA: SAE International. 93.
3. European Commission, *Strategy for Reducing Heavy-Duty Vehicles' Fuel Consumption and CO₂ Emissions*, 2014: Brussels.
4. Yim, S. and S. Barrett, *Public Health Impacts of Combustion Emissions in the United Kingdom*. Environmental Science and Technology, 2012. **46**.
5. European Commission. *European Commission Directorate-General for Climate Action*. Available from: http://ec.europa.eu/clima/policies/transport/vehicles/index_en.htm.
6. Dernotte, J., et al., *Experimental Study of the Influence of Fuel Physical Properties on the Diesel Injection Process in Non-vaporizing Conditions*. 24th European conference on liquid atomization and spray systems, Estoril, Portugal., 2011.
7. Cipolat, D. and D. Valentim, *Comparison of Theoretical and Experimental Diesel and DME Injection Spray Characteristics*. Fuel Processing Technology, 2013. **107**: p. 36-43.
8. Delacourt, E., B. Desmet, and B. Besson, *Characterisation of Very High Pressure Diesel Sprays Using Digital Imaging Techniques*. Fuel, 2005. **84**: p. 859-867.
9. Richards, P., *Automotive Fuels Reference Book*. 3rd ed. 2014, USA: SAE International. 840.
10. Oki, M., S. Matsumoto, Y. Toyoshima, K. Ishisaka, N. Tsuzuki *180 MPa Piezo Common Rail System*. SAE Technical paper, 2006(2006-01-0274).
11. Pulkrabek, W.W., *Engineering Fundamentals of the Internal Combustion Engine*. 1997, USA: Prentice Hall. 411.
12. Dernotte, J., et al., *Influence of Physical Fuel Properties on the Injection Rate in a Diesel Injector*. Fuel, 2012. **96**(2012): p. 153-160.
13. Pickett, L.M., et al., *Comparison of Diesel Spray Combustion in Different High-Temperature, High-Pressure Facilities*. SAE Int. J. Engines 2010-01-2106, 2010. **3**(2): p. 156-181.

14. Pickett, L.M., J. J. López, *Jet-Wall Interaction Effects on Diesel Combustion and Soot Formation*, 2005, SAE International.
15. Rosseel, E. and R. Sierens, *The Physical and the Chemical Part of the Ignition Delay in Diesel Engines*. SAE Technical Paper, 1996(961123).
16. Mueller, C.J., A.L. Boehman, and G.C. Martin, *An Experimental Investigation of the Origin of Increased NO_x Emissions when Fueling a Heavy-Duty Compression-Ignition Engine with Soy Biodiesel*. SAE Int. J. Fuels Lubr. 2009-01-1792, 2009. **2**(1): p. 789-816.
17. Siebers, D.L., B. Higgins, and L. Pickett, *Flame Lift-Off on Direct-Injection Diesel Fuel Jets: Oxygen Concentration Effects*, 2002, SAE International.
18. Dizayi, B., et al., *Evaluation of the Effect of Fuel Properties on the Fuel Spray and Jet Characteristics in a HGV DI Diesel Engine Operated by Used Cooking Oils*. Applied Mechanics and Materials, 2014. **694**: p. 3-12.
19. Hemmerlein, N., et al., *Performance, Exhaust Emissions and Durability of Modern Diesel Engines Running on Rapeseed Oil*, 1991, SAE International.
20. Ejim, C.E., B. Fleck, and A. Amirfazli, *Analytical Study for Atomisation of Biodiesels and Their Blends in a Typical Injector: Surface Tension and Viscosity Effects*. Fuel, 2007. **86**: p. 11.
21. Queimada, A.J., et al., *Prediction of Viscosities and Surface Tensions of Fuels Using a New Corresponding States Model*. Fuel, 2006. **85**: p. 4.
22. Eastwood, P., *Critical Topics in Exhaust Gas Aftertreatment*. 2000, Hertfordshire, England: Research Studies Press Ltd. 405.
23. Kook, S., et al., *The Influence of Charge Dilution and Injection Timing on Low-Temperature Diesel Combustion and Emissions*, 2005, SAE International.
24. Palash, S.M., et al., *Impacts of Biodiesel Combustion on NO_x Emissions and their Reduction Approaches*. Renewable and Sustainable Energy Reviews, 2013. **23**(0): p. 473-490.
25. Tree, D.R. and K.I. Svensson, *Soot Processes in Compression Ignition Engines*. Progress in Energy and Combustion Sciesce, 2007. **33**: p. 36.
26. Sheehan, J., et al., *Life Cycle Inventory of Biodiesel and Petroleum Diesel for Use in an Urban Bus*, 1998, National Renewable Energy Laboratory

USA.

27. Liu, Z., et al., *Real-World Operation Conditions and On-Road Emissions of Beijing Diesel Buses Measured by Using Portable Emission Measurement System and Electric Low-Pressure Impactor*. Science of the Total Environment, 2011. **409**: p. 5.
28. United Kingdom, M.o.T., *Renewable Transport Fuel Obligation statistics: period 7, 2014/15 report 6*, 2016: UK.
29. Crawford, M.H., *Feasibility and Emissions of Compression Ignition Engines Fuelled with Waste Vegetable Oil*, 2003, University of South Florida, Department of Environmental Science and Policy: USA.
30. Lapuerta, M., J. Rodríguez-Fernández, and J.R. Agudelo, *Diesel Particulate Emissions from Used Cooking Oil Biodiesel*. Bioresource Technology, 2008. **99**(4): p. 731-740.
31. Zhang, H., Q. Wang, and S.R. Mortimer, *Waste Cooking Oil as an Energy Resource: Review of Chinese Policies*. Renewable and Sustainable Energy Reviews, 2012. **16**(7): p. 5225-5231.
32. Metayer, C., et al., *Cooking Oil Fumes and Risk of Lung Cancer in Women in Rural Gansu, China*. Lung Cancer, 2002. **35**(2): p. 111-117.
33. Hribernik, A. and B. Kegl. *Performance and Exhaust Emissions of an Indirect-Injection (IDI) Diesel Engine when Using Waste Cooking Oil as Fuel*. 2009. Columbus, OH, United States: American Chemical Society.
34. Delzer, G.C. and S.W. McKenzie, *Five-day Biochemical Oxygen Demand: U.S. Geological Survey Techniques of Water-Resources Investigations*. 2003: USA.
35. Cho, H.M., S. Maji, and B.D. Pathak, *Waste Cooking Oil as Fuel in Diesel Engines*, 2008, The Automotive Research Association of India.
36. Vojtisek-Lom, M., M. Pechout, and A. Barbolla, *Experimental Investigation of the Behavior of Non-Esterified Rapeseed Oil in a Diesel Engine Mechanical Fuel Injection System*. Fuel, 2012. **97**: p. 157-165.
37. Pugazhivadivu, M. and K. Jeyachandran, *Investigations on the Performance and Exhaust Emissions of a Diesel Engine Using Preheated Waste Frying Oil as Fuel*. Renewable Energy, 2005. **30**(2005): p. 2189-2202.
38. Dorn, B. and R. Zahoransky, *Non-Esterified Plant Oils as Fuel -Engine Characteristics, Emissions and Mutagenic effects of PM*, 2009, Consiglio Nazionale delle Ricerche.

39. Lonza, L., et al., *EU Renewable Energy Targets in 2020: Analysis of Scenarios for Transport*, in *JRC Scientific and Technical Reports* 2011, Joint Research Centre: EU. p. 70.
40. United Kingdom, M.o.T., *Renewable Transport Fuel Obligation statistics: period 1, 2008/09 report 6*, 2010: UK.
41. United Kingdom, M.o.T., *Renewable Transport Fuel Obligation statistics: period 2, 2009/10 report 6*, 2011: UK.
42. United Kingdom, M.o.T., *Renewable Transport Fuel Obligation statistics: period 3, 2010/11 report 6*, 2012: UK.
43. United Kingdom, M.o.T., *Renewable Transport Fuel Obligation statistics: period 4, 2011/12 report 6* 2013: UK.
44. United Kingdom, M.o.T., *Renewable Transport Fuel Obligation statistics: period 5, 2012/13 report 6* . , 2014: UK.
45. United Kingdom, M.o.T., *Renewable Transport Fuel Obligation statistics: period 6, 2013/14*, 2015: UK.
46. Li, Y., et al., *Simulation of N₂O Emissions from Rain-Fed Wheat and the Impact of Climate Variation in Southeastern Australia*. *Plant Soil*, 2008. **309**: p. 12.
47. Grau, B., et al., *Environmental Life Cycle Assessment of Rapeseed Straight Vegetable Oil as Self-Supply Agricultural Biofuel*. *Renewable Energy*, 2013. **50**(0): p. 142-149.
48. Talens Peiró, L., et al., *Life Cycle Assessment (LCA) and Exergetic Life Cycle Assessment (ELCA) of the Production of Biodiesel from Used Cooking Oil (UCO)*. *Energy*, 2010. **35**(2): p. 889-893.
49. Fontaras, G., et al., *Integrated Environmental Assessment of Energy Crops for Biofuel and Energy Production in Greece*. *Renewable Energy*, 2012. **43**: p. 201-209.
50. Li, H., Jim Ebner, Peipei Ren, Laura Campbell, Buland Dizayi, Seyed Hadavi., *Determination of Carbon Footprint using LCA Method for Straight Used Cooking Oil as a Fuel in HGVs*. SAE International, 2014(2014-01-1948): p. 8.
51. Anand, R., et al., *Performance Emission and Combustion Characteristics of a Diesel Engine Fueled with Biodiesel Produced from Waste Cooking Oil*, 2010, SAE International.
52. Winfried, R., et al., *Usability of Food Industry Waste Oils as Fuel for Diesel Engines*. *Journal of Environmental Management*, 2008. **86**(3): p. 427-434.
53. Pandey, R.K., A. Rehman, and R.M. Sarviya, *Impact of Alternative Fuel Properties on Fuel Spray Behavior and Atomization*. *Renewable and Sustainable Energy Reviews*, 2012. **16**(3): p. 1762-1778.

54. Wakuri, Y., et al., *Studies on the Penetration of Fuel Spray in a Diesel Engine*. Bulletin of JSME, 1960. **3**(9): p. 129-130.
55. Singer, M., et al., *European Programme on Emissions, Fuels and Engine Technologies (EPEFE)*. SAE Technical paper 961074, 1996(961074).
56. Benson, R.S. and N.D. Whitehouse, *Internal Combustion Engines*. Vol. 1. 1979, London, UK: Pergamon Press Ltd. 201.
57. Ferguson, C.R., *Internal Combustion Engines; Applied Thermodynamics*. 1986, Canada: John Wiley & Sons, Inc. 543.
58. Heywood, J.B., *Internal Combustion Engine Fundamentals*. Vol. 930. 1988: Mcgraw-hill New York.
59. Hsu, B.D., *Practical Diesel-Engine Combustion Analysis*. 2002, USA: SAE International. 147.
60. United Kingdom, M.o.T., *Licensed Vehicles by Body Type at the End of Quarter, Great Britain, 1994 Q1 to 2015 Q3*, D. statistics, Editor 2015: UK.
61. United Kingdom, M.o.T., *Goods Moved, Goods Lifted and Vehicle Kilometres, Annual, 1990 - 2014 and Quarterly 2004 - 2014*, 2015, Department of Transport statistics.
62. United Kingdom, M.o.T., *Average Heavy Goods Vehicle Fuel Consumption: Great Britain, 1999-2014*, 2015, Department for Transport statistics: UK.
63. United Kingdom, M.o.T., *Carbon Dioxide Emissions by Transport Mode: United Kingdom, 1999-2013*, 2015, Department for Transport statistics: UK.
64. United Kingdom, M.o.T., *Air Pollutant Emissions by Transport Mode: United Kingdom, from 2000*, 2015, Department for Transport statistics: UK.
65. Johnson, K.C., et al., *Quantifying In-Use PM Measurements for Heavy Duty Diesel Vehicles*. Environmental Science and Technology, 2011. **45**: p. 6073-6079.
66. Wang, A., et al., *On-Road Pollutant Emission and Fuel Consumption Characteristics of Buses in Beijing*. Environmental Sciences, 2011. **23**(3): p. 419-423.
67. Moynahan, N., et al., *Development of a Vehicle Road Load Model for ECU Broadcast Power Verification in On-Road Emissions Testing*. SAE Int., 2006(2006-01-3392).
68. Koupal, J., et al., *Moves 2004 Energy and Emissions Inputs*, 2005, EPA: USA.
69. Kinsey, J.S., et al., *Evaluation of the Emissions from Low-Sulfur and Biodiesel Fuel Used in a Heavy-Duty Diesel Truck*

- During On-Road Operation*, 2009, Office of Research and Development, US EPA: Washington, DC.
70. Fraer, R., et al., *Operating Experience and Teardown Analysis for Engines Operated on Biodiesel Blends (B20)*, 2005, SAE International.
 71. Chase, C.L., et al., *A 322,000 kilometer (200,000 mile) Over the Road Test with HySEE Biodiesel in a Heavy Duty Truck*, 2000, SAE International.
 72. Nishimura, K., M. Miura, T. Hashimoto, K. Yari, M. Maruyama, N. Iseya, K. Takeoka, K. Yasuda, T. Yamazaki *Impacts on Engine Oil Performance by the Use of Waste Cooking Oil as Diesel Fuel*. SAE, 2011(2011-01-2115).
 73. Fazal, M.A., A.S.M.A. Haseeb, H. H. Masjuki, A.S.M.A. Haseeb, and H.H. Masjuki, *Degradation of Automotive Materials in Palm Biodiesel*. Energy 2012. **40**(2012): p. 76-83.
 74. Shahid, E.M. and Y. Jamal, *A Review of Biodiesel as a Vehicular Fuel*. Renewable and Sustainable Energy Reviews, 2008. **12**(9): p. 2484-2494.
 75. Hribernik, A. and B. Kegl, *Performance and Exhaust Emissions of an IDI Diesel Engine When Using Waste Cooking Oil as Fuel*. Energy and Fuels, 2009. **23**: p. 5.
 76. Broge, W.L., *Revving up for diesel*. SAE International, 2002. **110**(2): p. 40-49.
 77. Liu, Y. and R.D. Reitz, *Optimizing HSDI Diesel Combustion and Emissions Using Multiple Injection Strategies*. SAE Technical paper 2005-01-0212, 2005.
 78. Martinez, S. and F.A. Sanchez-Cruz, *Liquid Penetration Length in Direct Diesel Fuel Injection*. Applied Thermal Engineering, 2008. **28**: p. 1756-1762.
 79. Agarwal, A.K. and V.H. Chaudhury, *Spray Characteristics of the Biodiesel/Blends in a High Pressure Volume Spray Chamber*. Experimental Thermal and Fluid Science, 2012. **42**: p. 212-218.
 80. Lüft, M., et al., *Effect of Different Nozzle Geometries Using Pure Rapeseed Oil in a Modern Diesel Engine on Combustion and Exhaust Emissions*. SAE Int. J. Fuels Lubr., 2011. **5**(1): p. 180-189.
 81. Goosen, R., K. Vora, and C. Vona, *Establishment of the Guidelines for the Development of Biodiesel Standards in the APEC Region*, 2007, Hart Energy Consulting: Texas, USA. p. 136.

82. Kalam, M.A. and H.H. Masjuki, *Emissions and Deposit Characteristics of a Small Diesel Engine When Operated on Preheated Crude Palm Oil*. Biomass and Bioenergy, 2004. **27**: p. 289-297.
83. Rosca, R., et al., *Fuel and Injection Characteristics for a Biodiesel Type Fuel from Waste Cooking Oil*. SAE Int., 2005(2005-01-3674): p. 11.
84. Winfried, R., et al., *Usability of Food Industry Waste Oils as Fuel for Diesel Engines*. Journal of Environmental Management, 2008. **86**: p. 427-434.
85. Andrews, G.E., I.E. Ihezor-Ejiofor, and S.W. Pang, *Diesel Particulate SOF Emissions Reduction Using an Exhaust Catalyst*. SAE Int. Congress and Exposition, 1987(870251): p. 103-112.
86. Maricq, M.M., *Chemical Characterisation of Particulate Emissions from Diesel Engines: A review*. Journal of Aerosol Science, 2007. **38**: p. 39.
87. Tobias, H.J., et al., *Real Time Chemical Analysis of Organic Aerosols Using a Thermal Decomposition Particle Beam Mass Spectrometer*. Aerosol Science and Technology, 2000. **33**: p. 170-190.
88. Tan Pi-qiang, K. Deng, and J. Lu, *Analysis of Particulate Matter Composition from a Heavy-Duty Diesel Engine*. Journal of Automobile Engineering, 2004. **218**: p. 8.
89. Kittelson, D.B., *Engines and Nanoparticles: a review*. Journal of Aerosol Science, 1998. **29**(5–6): p. 575-588.
90. Kays, D. and S. Hochgreb, *Mechanisms for Particulate Matter Formation in Spark Ignition Engines. 3. Model of PM Formation*. Environmental Science and Technology, 1999. **33**(22): p. 3978-3992.
91. Glassman, I., *Soot Formation in Combustion Processes*. Proc. Combust. Inst., 1988. **22**: p. 295-311.
92. Lee, K.O., et al., *Detailed Characterization of Morphology and Dimensions of Diesel Particulates via Thermophoretic Sampling*, 2001, SAE International.
93. Dec, J.E., *A Conceptual Model of DI Diesel Combustion Based on Laser Sheet Imaging*. SAE Int. J. Engines, 1997(970873).
94. Kittelson, D.B., W.F. Watts, and J.P. Johnson, *On-Road and Laboratory Evaluation of Combustion Aerosols—Part1: Summary of Diesel Engine Results*. Journal of Aerosol Science, 2006. **37**(8): p. 913-930.

95. Barry, E.G., et al., *Heavy Duty Diesel Engine / Fuels Combustion Performance and Emissions*. SAE 852078, 1985(852078).
96. Miyamoto, N., et al., *Influence of the Molecular Structure of Hydrocarbon Fuels on Diesel Exhaust Emissions*, 1994, SAE International 940676.
97. Miyamoto, N., et al., *Smokeless, Low NO_x, High Thermal Efficiency, and Low Noise Diesel Combustion with Oxygenated Agents as a Main Fuel*, 1998, SAE International 980506.
98. Cheng, A.S., R.W. Dibble, and B.A. Buchholz, *The Effect of Oxygenates on Diesel Engine Particulate Matter*, 2002, SAE International 2002-01-1705.
99. Mueller, C.J., et al., *Effects of Oxygenates on Soot Processes in DI Diesel Engines: Experiments and Numerical Simulations*, 2003, SAE International 2003-01-1791.
100. Bardasz, E.A., et al., *The Impact of Lubricant and Fuel Derived Sulfur Species on Efficiency and Durability of Diesel NO_x Adsorbers*. SAE Technical paper 2004-01-3011, 2004(2004-01-3011).
101. Kweon, C., et al., *Detailed Chemical Composition and Particle Size Assessment of Diesel Engine Exhaust*. SAE Technical paper, 2002(2002-01-2670).
102. Goswami, A., et al., *Behaviour Study of Particulate Matter and Chemical Composition with Different Combustion Strategies*, 2013, SAE International.
103. Riddle, S.G., et al., *Size Distribution of Trace Organic Species Emitted from Heavy Duty Diesel Vehicles*. *Environmental Science and Technology*, 2007. **41**: p. 1962-1969.
104. Alander, T.J., et al., *Characterisation of Diesel Particulates: Effects of Fuel Reformulation, Exhaust Aftertreatment, and Engine Operation on Particle Carbon Composition and Volatility*. *Environmental Science and Technology*, 2004. **38**: p. 2707-2714.
105. Ullman, T.L., K.B. Spreen, and R.L. Mason, *Effects of Cetane Number, Cetane Improver, Aromatics, and Oxygenates on 1994 Heavy-Duty Diesel Engine Emissions*, 1994, SAE International.
106. Ladommatos, N., et al., *The Effect of Aromatic Hydrocarbons on Soot Formation in Laminar Diffusion Flames and in a Diesel Engine*. *Institute of Energy*, 1997. **70**: p. 84-94.

107. Kook, S. and L.M. Pickett, *Soot Volume Fraction and Morphology of Conventional, Fischer-Tropsch, Coal-Derived, and Surrogate Fuel at Diesel Conditions*. SAE Int. J. Fuels Lubr., 2012. **5**(2012-01-0678): p. 647-664.
108. Pickett, L.M., D.L. Siebers, and C.A. Idicheria, *Relationship Between Ignition Processes and the Lift-Off Length of Diesel Fuel Jets*, 2005, SAE International.
109. Li, T. and H. Ogawa, *Analysis of the Trade-off between Soot and Nitrogen Oxides in Diesel-Like Combustion by Chemical Kinetic Calculation*. SAE Int. J. Engines, 2011. **5**(2011-01-1847): p. 94-101.
110. Königsson, F., H. Dembinski, and H.-E. Angstrom, *The Influence of In-Cylinder Flows on Emissions and Heat Transfer from Methane-Diesel Dual Fuel Combustion*. SAE Int. J. Engines, 2013. **6**(4): p. 1877-1887.
111. Siebers, D. and B. Higgins, *Flame Lift-Off on Direct-Injection Diesel Sprays Under Quiescent Conditions*, 2001, SAE International.
112. Delacourt, E., B. Desmet, and B. Besson, *Characterisation of Very High Pressure Diesel Spray Using Digital Imaging Techniques*. Fuel, 2005. **84**: p. 859-867.
113. Galle, J., S. Defruyt, and C. Van de Maele, *Experimental Investigation Concerning the Influence of Fuel Type and Properties on the Injection and Atomization of Liquid Biodiesels in an Optical Combustion Chamber*. Biomass and Bioenergy, 2013. **57**: p. 13.
114. Martinez-Martinez, S., et al., *Liquid Penetration Length in Direct Diesel Fuel Injection*. Applied Thermal Engineering, 2008. **28**: p. 7.
115. Payri, F., et al., *Effect of Intake Oxygen Concentration on Particle Size Distribution Measurements from Diesel Low Temperature Combustion*. SAE Int. J. Engines 2011-01-1355, 2011. **4**(1): p. 1888-1902.
116. Shah, S.D., et al., *Emission Rates of Particulate Matter and Elemental and Organic Carbon from in-use Diesel Engines*. Environmental Science and Technology, 2004. **38**: p. 2544-2550.
117. Dembinski, H. and H.-E. Angstrom, *Swirl and Injection Pressure Effect on Post-Oxidation Flow Pattern Evaluated with Combustion Image Velocimetry, CIV, and CFD Simulation*, 2013, SAE International.

118. Jazair, W., et al., *Improvement of Emissions in a DI Diesel Engine Fuelled by Bio-diesel Fuel and Waste Cooking Oil*, 2007, SAE International.
119. Dec, J.E. and P.L. Kelly-Zion, *The Effects of Injection Timing and Diluent Addition on Late-Combustion Soot Burnout in a DI Diesel Engine Based on Simultaneous 2-D Imaging of OH and Soot*, 2000, SAE International.
120. Li, T., et al., *Characterization of Low Temperature Diesel Combustion with Various Dilution Gases*, 2007, SAE International.
121. Manin, J., et al., *Effects of Oxygenated Fuels on Combustion and Soot Formation/Oxidation Processes*. SAE Int. J. Fuels Lubr. 2014-01-2657, 2014. **7**(3).
122. Ladommatos, N., Z. Xiao, and H. Zhao, *The Effect of Piston Bowl Temperature on Diesel Exhaust Emissions*. Automobile Engineering, 2004. **219 Part D**: p. 1-18.
123. Hottenbach, P., T. Brands, and G. Grünefeld, *An Experimental Investigation of Combustion and Soot Formation of Sprays from Cluster Nozzles for DI Diesel Engines*, 2009, SAE International.
124. Oliveira, L., D. Savvidis, and M. Pecqueur, *Controlling Particulate Matter Emissions in Vehicles Using Different Strategies Under Heavy-Duty Test Cycle*. SAE International, 2012.
125. Boger, T., et al., *A Next Generation Cordierite Diesel Particulate Filter with Significantly Reduced Pressure Drop*. SAE International Journal of Engines, 2011. **4**(1): p. 902-912.
126. Hellier, P., et al., *The Impact of Saturated and Unsaturated Fuel Molecules on Diesel Combustion and Exhaust Emissions*. SAE Int. J. Fuels Lubr., 2011. **5**(2011-01-1922): p. 106-122.
127. Li, H., et al., *Comparison of Exhaust Emissions and Particulate Size Distribution for Diesel, Biodiesel and Cooking Oil from a Heavy Duty DI Diesel Engine*, 2008, SAE International.
128. Hossain, A.K. and P.A. Davies, *Combustion and Emission Characteristics of a Typical Biodiesel Engine Operated on Waste Cooking Oil Derived Biodiesel*, 2012, SAE International.
129. Sidibe, S., et al., *Use of Crude Filtered Vegetable Oil as a Fuel in Diesel Engines State of the Art: Literature review*. Renewable and Sustainable Energy Reviews, 2010. **14**: p. 2748-2759.

130. Saravanan, S., et al., *Correlation of Thermal NO_x Formation in a Compression Ignition (CI) Engine Fuelled with Diesel and Biodiesel*. Energy, 2012. **42**: p. 401-410.
131. Ramirez-Verduzco, L.F., J.E. Rodriguez-Rodriguez, and A. Jaramillo-Jacob, *Predicting Cetane Number, Kinematic Viscosity, Density and Higher Heating Value of Biodiesel from its Fatty Acid Methyl Ester Composition*. Fuel, 2011. **91**: p. 9.
132. Guo, G., et al., *Advanced Urea SCR System Study with a Light Duty Diesel Vehicle*. SAE Technical Paper, 2012(2012-01-0371).
133. Betelin, V.B., et al., *Evaporation and Ignition of Droplets in Combustion Chambers; Modeling and Simulation*. Acta Astronautica, 2012. **70**: p. 12.
134. Clarebout, G., et al., *Selective Catalytic Reduction of Nitric Oxide with Ammonia on Vanadium Oxide Catalysts Supported on Titania-Alumina*. Applied Catalysis, 1991. **76**(1): p. 9-14.
135. Cosseron, A.F., et al., *Study of Non-Regulated Exhaust Emissions Using Biodiesels and Impact on a 4 Way Catalyst Efficiency*, 2011, SAE International.
136. Keuper, A., et al., *Investigations to Achieve Highest Efficiencies in Exhaust Gas After-treatment for Commercial Vehicles using an SCR System*. SAE Int. J. Commer. Veh., 2011. **4**(1): p. 145-154.
137. Ardanese, M., et al., *Emissions of NO_x, NH₃ and Fuel Consumption Using High and Low Engine-Out NO_x Calibrations to Meet 2010 Heavy Duty Diesel Engine Emission Standards*. SAE International, 2009.
138. Naseri, M., et al., *Development of SCR on Diesel Particulate Filter System for Heavy Duty Applications*. SAE Int. J. Engines, 2011. **4**(1): p. 1798-1809.
139. Mizushima, N., et al., *Effect of Biodiesel on NO_x Reduction Performance of Urea-SCR System*. SAE Int. J. Fuels Lubr., 2010. **3**(2): p. 1012-1020.
140. Brookshear, D.W., et al., *Investigation of the Effects of Biodiesel-based Na on Emissions Control Components*. Catalysis Today, 2012. **184**(1): p. 205-218.
141. Obert, E.F., *Internal Combustion Engines and Air Pollution*. 1973, USA: Harper and Row publishers Inc.
142. Wu, F., et al., *Effects of Different Biodiesels and their Blends with Oxygenated Additives on Emissions from a Diesel Engine*, 2008, SAE International.

143. İřcan, B. and H. Aydın, *Improving the Usability of Vegetable Oils as a Fuel in a Low Heat Rejection Diesel Engine*. Fuel Processing Technology, 2012. **98**(0): p. 59-64.
144. Aydın, H., *Combined Effects of Thermal Barrier Coating and Blending with Diesel Fuel on Usability of Vegetable Oils in Diesel Engines*. Applied Thermal Engineering, 2013. **51**: p. 623-629.
145. Jaichandar, S., P. Senthil Kumar, and K. Annamalai, *Combined Effect of Injection Timing and Combustion Chamber Geometry on the Performance of a Biodiesel Fuelled Diesel Engine*. Energy, 2012. **47**: p. 388-394.
146. Stoffels, H., S. Quiring, and B. Pinggen, *Analysis of Transient Operation of Turbo-Charged Engines*. SAE Int. J. Engines, 2010. **3**(2010-32-0005): p. 438-447.
147. Cieslar, D., et al., *A Novel System for Reducing Turbo-Lag by Injection of Compressed Gas into the Exhaust Manifold*, 2013, SAE International.
148. Rao, G.A.P. and P.R. Mohan, *Effect of Supercharging on the Performance of a DI Diesel Engine with Cotton Seed Oil*. Energy Conversion and Management, 2003. **44**(6): p. 937-944.
149. Mueller, C.J., et al., *An Experimental Investigation of In-Cylinder Processes Under Dual-Injection Conditions in a DI Diesel Engine*, 2004, SAE International 2004-01-1843.
150. Pickett, L.M. and D.L. Siebers, *Non-Sooting, Low Flame Temperature Mixing-Controlled DI Diesel Combustion*, 2004, SAE International.
151. Fang, T., et al., *Combustion and Soot Visualization of Low Temperature Combustion within an HSDI Diesel Engine Using Multiple Injection Strategy*, 2006, SAE International.
152. Pidol, L., et al., *Ethanol as a Diesel Base Fuel-Potential in HCCI Mode*, 2008, SAE International.
153. Polonowski, C.J., et al., *An Experimental Investigation of Low-Soot and Soot-Free Combustion Strategies in a Heavy-Duty, Single-Cylinder, Direct-Injection, Optical Diesel Engine*. SAE Int. J. Fuels Lubr., 2011. **5**(2011-01-1812): p. 51-77.
154. Chhetri, A.B., W.F. Watts, and M. Rafiqul Islam, *Waste Cooking Oil as an Alternate Feedstock for Biodiesel Production*. Energies, 2008. **1**: p. 3-18.
155. Pastor, J.V., et al., *Fuel Effect on the Liquid-phase Penetration of an Evaporating Spray Under Transient Diesel-like Conditions*. Fuel, 2011. **90**: p. 3369-3381.

156. Kittelson, D.B., et al., *On-Road and Laboratory Evaluation of Combustion Aerosols-Part 2: Summary of Spark Ignition Engine Results*. Journal of Aerosol Science, 2006. **37**: p. 931-949.
157. *Touching Lives Product Guide*, W.p.o.G. Healthcare, Editor 2011, Whatman: United Kingdom.
158. Copley, M., *Cascade Impactors; Theory, Design, and Practical Information for Optimal Testing*, 2008, Copley Scientific.
159. Taylor, J.R., *An Introduction to Uncertainty Analysis; The Study of Uncertainties in Physical Measurements*. 1982, Mill Valley: University Science Books.
160. Langton, A.L., H. Li, and G.E. Andrews, *Comparison of Particulate PAH Emissions for Diesel, Biodiesel and Cooking Oil Using a Heavy Duty Diesel Engine*. SAE International, 2008(2008-01-1811).
161. Chan, S.H. and J. Zhu, *Exhaust Emissions Based Air-Fuel Ratio Model (I): Literature Review and Modelling*. SAE Technical Papers, 1996(961020).
162. Chan, S.H. and J. Zhu, *Exhaust Emissions Based Air-Fuel Ratio Model (II): Divergence Analysis and Emissions Estimations*. SAE International, 1996(961021).
163. Daham, B., G.E. Andrews, and H. Li, *Application of a Portable FTIR for Measuring On-Road Emissions*. SAE Technical Paper series, 2005(2005-01-0676).
164. Li, H., K. Ropkins, and G.E. Andrews, *Evaluation of the FTIR Emission Measurement System for Legislated Emissions Using a SI Car*. SAE Technical paper, 2006(2006-01-3368).
165. Andrews, G.E., et al., *Influence of Ambient Temperature on Cold-Start Emissions for a Euro 1 SI Car Using In-Vehicle Emissions Measurement in an Urban Traffic Jam Test Cycle*. SAE International, 2005(2005-1-1617).
166. Google maps, <http://www.doogal.co.uk/RouteElevation.php>, 2014.
167. Demirbas, A., *Relationships Derived from Physical Properties of Vegetable Oil and Biodiesel Fuels*. Fuel, 2008. **87**: p. 1743-1748.
168. Pickett, L.M., et al., *Comparison of Diesel Spray Combustion in Different High-Temperature, High-Pressure Facilities*. SAE International 2010-01-2106, 2010. **3**(2).
169. Horiba, A.T.S., *Engine Emissions Measurement Handbook*. 2014, Warrendale,PA, USA: SAE International. 173.

170. EPA, *Determination of Metals by Inductively Coupled Plasma (ICP) Methods*, 2006, SERAS: USA. p. 1~42.
171. *Nanoscience instruments*. Available from: www.nanoscience.com/products/sem/technology.
172. *Materials Evaluation and Engineering, I.*; Available from: www.mee-inc.com/hamm/energy-dispersive-x-ray-spectroscopyeds/.
173. Davis, C., *SPSS Step by Step*. 2013, Great Britain: The Policy Press, University of Bristol.
174. Schmuller, J., *Statistical Analysis with Excel*. 3rd ed. 2013, New Jersey, USA: John Wiley & Sons, Inc.
175. Tat M. E. and J.H. Van Gerpen, *Measurement of Biodiesel Speed of Sound and Its Impact on Injection Timing*, N.R.E. Laboratory, Editor 2003: Iowa, USA. p. 120.
176. Nikolic', B.D., et al., *Determining the Speed of Sound, Density, and Bulk Modulus of Rapeseed Oil, Biodiesel, and Diesel Fuel*. *Thermal Science*, 2012. **16**: p. 9.
177. Chherti A. B. and W.F. Watts, *Surface Tension of Petro-Diesel, Canola, Jatropha and Soupnut Biodiesel Fuels at Elevated Temperatures and Pressures*. *Fuel*, 2013. **104**: p. 6.
178. Aatola, H., et al., *Hydrotreated Vegetable Oil (HVO) as a Renewable Diesel Fuel: Trade-off between NO_x, Particulate Emission, and Fuel Consumption of a Heavy Duty Engine*. *SAE Int. J. Engines*, 2008. **1**(1): p. 1251-1262.
179. Monks, P., et al., *Fine Particulate Matter (PM_{2.5}) in the United Kingdom*, 2012, Defra.
180. Cormier, S.A., et al., *Origin and Health Impacts of Emissions of Toxic By-Products and Fine Particles from Combustion and Thermal Treatment of Hazardous Wastes and Materials*. *Environmental Health Perspectives*, 2006. **114**(6): p. 810-817.
181. Dizayi, B., et al. *Particulate Matter Emissions from a Heavy Duty Vehicle Fuelled by Petroleum Diesel and Used Cooking Oil Blends*. in *European Combustion Meeting*. 2015. Budapest, Hungary.
182. Lloyd, A.C. and T.A. Cackette, *Diesel Engines: Environmental Impact and Control*. Air and Waste Management Association, 2001. **51**: p. 809-847.
183. MacCarthy, J., et al., *UK Greenhouse Gas Inventory, 1990 to 2013*, in *Annual Report for Submission under the Framework Convention on Climate Change 2015*, Department of Energy and Climate Change: UK.

